Teneurins in vertebrate synapse formation
Investigating subcellular localisation and synaptogenic properties of Teneurins

Schachermayer, Greta

Awarding institution:
King's College London

Teneurins in vertebrate synapse formation: Investigating subcellular localisation and synaptogenic properties of Teneurins

Greta Schachermayer

MRC Centre for Developmental Neurobiology
Institute of Psychiatry, Psychology, and Neuroscience
King's College London

Thesis submitted for the degree of Doctor of Philosophy

June 2017

Supervisors: Dr Robert Hindges and Prof Juan Burrone
Examiners: Dr Joris de Wit and Prof Stephen R. Price

Abstract

A critical open question in neuroscience is how neurons distinguish one another and form precise synaptic connections with their appropriate partners. Synaptic cell-adhesion molecules have been postulated to contribute to the establishment, assembly and maintenance of synapses. One family of cell-adhesion molecules, the Teneurins, are highly conserved and expressed in interconnected regions of the brain during development. Teneurins have been shown to regulate appropriate synaptic partner matching and synaptic assembly in *Drosophila*. In vertebrates, which have four Teneurin paralogues (Tenm1-4), Teneurins have been shown to play important roles in the establishment of functional visual circuits. However, their exact role in the initial establishment and maintenance of synapses in vertebrates is not yet known. In this thesis I explored the role of Teneurins, in particular of Tenm3, in vertebrate synapse formation. I found that all four members of the Teneurin family are partially localised at synapses of hippocampal neurons. Tenm3, which is selectively expressed in CA1 in the hippocampus, was found to be enriched in dendritic spines and in the dendritic shaft directly below the spine neck in CA1 pyramidal neurons. To examine the role of Tenm3 in synapse formation *in vivo*, a Tenm3 gene trap mutant was crossed to a Thy1-GFP reporter line, which expresses green fluorescence protein (GFP) in sparse CA1 neurons in the hippocampus. Unexpectedly, I found that Tenm3 mutant mice had significantly increased dendritic spine densities compared to wild type litter mates. This effect was the result of a general increase in spine density across all spine categories, however the largest relative increase was observed for mushroom spines, which are considered the most mature spine type. The results suggest that Tenm3 acts as a negative regulator of spine development and maturation and define this protein as an important mediator of appropriate synaptic connectivity.

Statement of Declaration

The work presented in this thesis is the result of my own original research. Wherever contributions of others were involved, every effort was made to indicate this clearly in the text. However, I would like to use this space to highlight and thank the following people for their contributions:

Dr. Vladimir Grigoriev and Alina Letzel, for genotyping hundreds of mouse skin samples and showing me how to do PCRs.

Sarah Kemlo, for cloning and providing the PSD-95-FingR-TdTomato and Gephyrin-FingR-TdTomato as well as her help with *in utero* electroporations and her patience in showing me how to perform the procedure.

Mideia Kotsogianni, for the help with cell culture and for contributing some of the dissociated hippocampal cultures used in this work.

Dr. Guilherme Neves, for providing Igor Pro (wavemetrics) analysis software and showing me how to write and use functions.

Dr. Tatsuya Okafuji, for cloning and providing the Teneurin expression plasmids

Prof. Beatriz Rico, for giving me access to Imaris (Bitplane) image analysis software

Dr. Matthew Smithen, for contributing some of the cryosections stained with X-gal.

Dr. Andy Symonds, for contributing to the characterisation of the RRD180 mouse line through identification of the insertion site of the gene trap vector as well as the development of a PCR genotyping protocol.

Acknowledgements

Firstly, I would like to thank my primary supervisor Dr Robert Hindges for allowing me to undertake this PhD adventure in his lab. I am grateful for the trust he showed in me, when I first started this project as an inexperienced MSc graduate and for the scientific freedom and support I was given over the past three and a half years. I would also like to thank all the members of the Hindges lab, particularly Ankur Perry, Dr Katherine Trevers, Nadine Brassel and Dr Paride Antinucci, for being lovely colleagues and creating an enjoyable and cooperative work environment. Very special thanks also go to my secondary supervisor, Prof Juan Burrone, for his helpful and enthusiastic guidance as well as for his generosity with his lab's resources throughout this PhD. I am also very grateful for all the help I received from many members of the Burrone lab, particularly Dr Guilherme Neves for his generous input and help with image analysis, Mideia Kotsogianni for all her help with cell cultures, and Sarah Kemlo for being a great friend and all the hours she spent teaching and helping me with IUEs. I must also thank my PhD advisors, first Dr Esther Bell and Prof Ian Thompson, then Dr Matt Grubb and Prof Anthony Graham, for their useful guidance and advice throughout this PhD. Many thanks also go to the BSU staff for all their help with the mouse colonies used in this project. I should also emphasise that I consider myself blessed to have had the opportunity to spend the last years working in the MRC Centre, which is truly a great research environment, made special by all its wonderful and inspiring members.

I am very grateful to my family, especially my parents, for their generous support and unconditional love throughout my life and without whom I would not have been able to do this PhD. There is one person who I must especially thank, my husband Winny, who has taken care of all other aspects of our lives during the writing-up phase to allow me to focus on finishing my thesis, and who has been there for me with food, clean clothes, encouraging words and emotional support. I would also like to thank my second family, the Kalras, and all my friends for believing in me and for their motivational pep talks. Lastly, I would like to thank Denise, for companionship during the thesis-writing process and for being a great friend with whom to share tears and laughter.

Table of Contents

List of Figures

List of Tables

List of Abbreviations

aa	Amino acid
AFM	Atomic force microscopy
AIS	Axon initial segment
AMPA	α-amino-3-hydroxy-5-methyl-4-isoxazolepropionic acid
ApoE	Apolipoprotein E
APP	Amyloid precursor protein
ASD	Autism spectrum disorder
a.u.	Arbitrary unit
Brp	Bruchpilot
BSA	Bovine serum albumin
CA	Cornu ammonis
CaMKII	Calcium calmodulin-dependent protein kinase II
CAP	c-Cbl-associated protein
Cdh9	Cadherin 9
CDS	Coding DNA sequence
CNS	Central nervous system
Cntn5	Contactin 5
CRF	Corticotrophin release factor
DG	Dentate gyrus
DGC	Dentate granule cell
DIV	Days in vitro
dLGN	Dorsal lateral geniculate nucleus
DPBS	Dulbecco's phosphate-buffered saline
EBSS	Earle's balanced salt solution
EC	Entorhinal cortex
ECD	Extracellular domain
EGF	Epidermal growth factor
EM	Electron microscopy
ES	Embryonic stem cell
F-actin	Filamentous actin

FAK	Focal adhesion kinase
FBS	Foetal bovine serum
Ferrate II	Potassium hexacyanoferrate II trihydrate
Ferrate III	Potassium hexacyanoferrate III
FI	Fluorescence intensity
FingR	Fibronectin intrabody
FLRT	Fibronectin leucine-rich repeat transmembrane protein
G-actin	Globular actin
GABA	γ-aminobutyric acid
GBSS	Gey's balanced salt solution
GFP	Green fluorescent protein
GPCR	G-protein coupled receptor
HBSS	Hank's balanced salt solution
HEK293	Human embryonic kidney 293
HF	Hippocampal formation
ICD	Intracellular domain
IgSF	Immunoglobulin superfamily
IPB	Infrapyramidal bundle
IPL	Inner plexiform layer
IUE	In utero electroporation
Lasso	latrophilin-1-associated synaptic surface organiser
LEC	Lateral entorhinal cortex
LGN	Lateral geniculate nucleus
LRRTM	Leucine-rich repeat transmembrane neuronal protein
LTD	Long term depression
LTP	Long term potentiation
MBD1	methyl-CpG binding protein 1
MEC	Medial entorhinal cortex
MEM	Minimum essential medium
mGluR	metabotropic glutamate receptors
N-WASP	Neuronal Wiskott-Aldrich syndrome protein
NA	Numerical aperture
Nb2a	Neuroblastoma 2a

NGS	Normal goat serum
NHL	NCL-1, HT2A and Lin-41
NL1	Neuroligin 1
NL2	Neuroligin 2
NL3	Neuroligin 3
NL4	Neuroligin 4
NLS	Nuclear localisation signal
NMDA	N-methyl-D-aspartate
NMJ	Neuromuscular junction
ORN	Olfactory receptor neuron
PBS	Phosphate buffered saline
PCP4	Purkinje cell protein 4
PCR	Polymerase chain reaction
PFA	Paraformaldehyde
PML	Promyelocytic leukemia
PN	Projection neuron
PSD	Postsynaptic density
PSF	Point spread function
RGC	Retinal ganglion cell
RHS	Retrotransposon hot spots
RIP	Regulated intramembrane proteolysis
ROI	Region of interest
SAC	Starburst amacrine cell
SCFS	Single cell force spectroscopy
SER	Smooth endoplasmic reticulum
SH3	Src homology 3
SREBP	Sterol regulatory element binding protein
STED	Stimulated emission depletion
SynCAM	Synaptic cell-adhesion molecule
TCAP	Teneurin C-associated peptide
Tenm1	Teneurin1
Tenm2	Teneurin2
Tenm3	Teneurin3

Tenm4	Teneurin4
V1	Primary visual cortex
WASP	Wiskott-Aldrich syndrome protein
YD	Yyrosine and aspartate

1 Introduction

During development of the central nervous system (CNS) several events have to occur before a functional brain is formed. These developmental steps include formation and patterning of the neural tube, birth and differentiation of neurons and glial cells, growth and guidance of axons to their target areas, the formation of synapses and their (activity-dependent) maturation. The function of neural circuits critically depends on the precision of its connections, and the specificity with which these are formed represents a remarkable example of cellular and sub-cellular recognition. The generation of synaptic specificity is an intensively studied field, but a vast amount remains unexplained (Washbourne *et al.*, 2004; Waites, Craig and Garner, 2005; Dalva, McClelland and Kayser, 2007; Sanes and Yamagata, 2009; Shen and Scheiffele, 2010; Williams, de Wit and Ghosh, 2010; Missler, Südhof and Biederer, 2012; Yogev and Shen, 2014; de Wit and Ghosh, 2015).

There is consensus that the specificity of neuronal connections emerges gradually, through sequential processes, which successively restrict the availability of possible synaptic partners (Shen and Scheiffele, 2010; Yogev and Shen, 2014). A large body of research provides compelling evidence that transmembrane adhesion proteins play critical roles in the regulation of these processes and thus are critical for the specification of neuronal connectivity. Many of these proteins fulfil several roles, from guiding appropriate partner matching and providing structural adhesion, to conveying signals that coordinate the formation and function of synapses. The Teneurins are a family of conserved transmembrane proteins that have only recently been implicated in the specification of connectivity in the invertebrate and vertebrate nervous system. This thesis is dedicated to the investigation of the role of Teneurins in vertebrate synapse formation.

In this introduction, I begin by giving a brief overview of the role of synaptic cell adhesion molecules in regulating neuronal connectivity. I then introduce the Teneurin family of proteins and describe their roles in neuronal wiring. This is followed by a brief overview of the anatomy and connectivity of the chosen model system, the hippocampus, and of the structure and function of dendritic spines. Finally, I describe the aims of this thesis.

1.1 Cell-adhesion molecules in neuronal connectivity

1.1.1 Synapse formation

Synapses are highly specialised sites of contact between two neurons, which enable electrochemical signalling. Typically, synapses consist of an axonal presynaptic compartment that is in close apposition to a dendritic postsynaptic compartment (Waites, Craig and Garner, 2005). Both structures are separated by a small distance of ~20 nm, termed the "synaptic cleft" (Schikorski and Stevens, 1997). The presynaptic compartment within the axon contains an accumulation of synaptic vesicles, which fuse with the plasma membrane within a specialised domain called the active zone. The postsynaptic compartment within the dendrite is characterised by an electron-dense thickened membrane specialisation called the postsynaptic density (PSD), which serves to cluster a dense meshwork of proteins, including receptors, ion channels and cell-adhesion molecules, that extend from the cytoplasm of the postsynaptic cell into the synaptic cleft. The proteins that extend across the synaptic cleft are thought to hold together the pre- and postsynaptic compartment and ensure the apposition of the active zone and PSD.

These features are shared by synapses throughout the brain, however there are variations in size and organisation, which depend on the type and function of the underlying synapse. Indeed, excitatory synapses on principal spiny neurons are mainly formed on small dendritic protrusions called spines (Peters and Kaiserman-Abramof, 1970), whereas inhibitory synapses are mainly formed on dendritic shafts, cell bodies and axon initial segments (Gray, 1957). Excitatory and inhibitory synapses differ in both their content of neurotransmitter vesicles and receptors as well as in their morphology and molecular composition. Much more is known about the structure and synaptogenesis of excitatory, glutamatergic synapses due to their greater abundance and distinctive structure. Excitatory synapses are also referred to as "asymmetric" synapses because of their thickened postsynaptic densities, which are apposed to the active zone. The predominant excitatory neurotransmitter is glutamate and the PSD of excitatory synapses contains glutamate receptors as well as a host of scaffolding and signalling molecules (Sheng and Kim, 2011). There are approximately ~460 different PSD proteins present in excitatory synapses (Peng *et al.*, 2004; Collins *et al.*, 2006).

These include signalling proteins of the calcium calmodulin-dependent protein kinase II (CaMKII) family and scaffolding proteins of the PSD-95 family, which were amongst the most abundant molecules, as well as N-methyl-D-aspartate (NMDA), α-amino-3-hydroxy-5-methyl-4-isoxazolepropionic acid (AMPA), kainate and metabotropic glutamate receptors (mGluRs; Peng *et al.*, 2004). The ionotropic AMPA, NMDA and kainite receptors are ligand-gated ion channels and mediate rapid excitatory glutamate signalling at synapses (Traynelis *et al.*, 2010). Conversely, glutamate signalling mediated by mGluRs, which are G-protein coupled receptors (GPCRs), is indirect and thus results in a slower and longer-lasting postsynaptic response compared to ionotropic receptors. GPCRs are cell-surface receptors that use trimeric GTP-binding proteins (G-proteins) to relay signals inside the cell. Upon binding of a ligand to a GPCR, the receptor undergoes a conformational change which activates G-proteins in a GTP-dependent manner. This further leads to the dissociation of the α subunit from the β and γ subunit pair. Both subunits then interact with various downstream targets such as enzymes and ion channels. There are three groups of mGluR receptors and a total of eight mGluR subtypes have been identified thus far. Of these, only group I mGluRs, which comprise mGluR1 and mGluR5, are localised postsynaptically, whereas group II and group III mGluRs are mostly localised presynaptically. Group I mGluRs promote the release of Ca^{2+} from intracellular stores through the activation of $G\alpha_{q/11}$ proteins, which stimulate phospholipase Cβ1 (PLCβ1) and the formation of diacylghycerol (DAG) and inositol-1,4,5-triphosphate (IP3) (Hermans and Challiss, 2001). Inhibitory synapses only show a thin electron-dense thickening of the postsynaptic membrane and hence are described as symmetric synapses. The predominant inhibitory neurotransmitter is γ-aminobutyric acid (GABA) and the main postsynaptic components of symmetrical synapses are ionotropic $GABA_A$ receptors and the Gephyrin scaffolding proteins (Sheng and Kim, 2011).

Synapse formation is a complex and highly orchestrated process that occurs over an extended period of development, starting in the embryo and protracting well into early postnatal life. Synaptogenesis does not end during development but occurs throughout adult life, where it forms part of the processes underlying learning and memory. Synapse formation can conceptually be divided into three stages (Figure 1.1; Washbourne *et al.*, 2004; Waites, Craig and Garner, 2005; Missler, Südhof and

Biederer, 2012). After recognition of an appropriate postsynaptic partner neuron by a presynaptic growth cone, an initial contact is formed (synapse establishment). This is followed by the recruitment of molecular components, such as synaptic vesicles, active zone and PSD structures, and the assembly of the pre- and postsynaptic machinery (synapse assembly). At this stage, synapses acquire specific properties and are differentiated into distinct types of synapses (synapse assembly and specification), including inhibitory and excitatory synapses. Finally, synapses are subject to plasticity mechanisms, which can remodel the synapse and affect changes in its molecular assembly (synaptic plasticity), which is why this last step is often viewed as an extension of synapse formation.

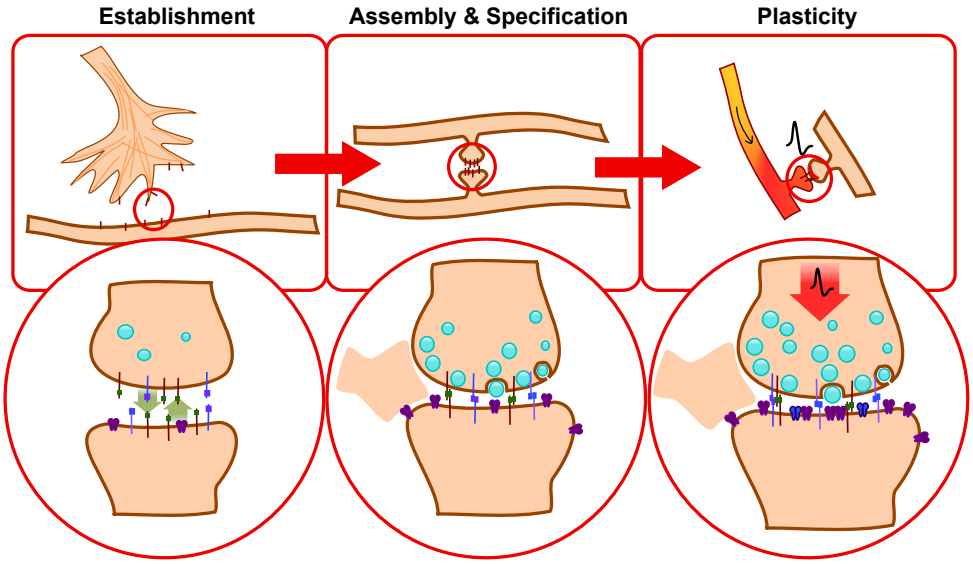

Figure 1.1. Schematic representation of the different stages of synapse formation. Synapse formation involves three partially overlapping stages. First, an axo-dendritic contact is established between appropriate pre- and postsynaptic partners. Homo- and heterophilic interactions between synapse-inducing cell-surface adhesion molecules contribute to this process. In a second stage, synapses are assembled and specified. During this stage synaptic cell-adhesion molecules mediate physical cell-cell adhesion and contribute to the clustering and recruitment of pre- and postsynaptic components such as synaptic vesicles, receptors and scaffolding molecules. At this stage synapses acquire distinct physiological properties. In the final stage, mature synapses are subject to activity-dependent structural and functional plasticity mechanisms and remodelling. Cell-surface adhesion molecules contribute to synaptic plasticity mechanisms such as long-term potentiation.

1.1.2 Molecular mediators of synaptogenesis

Synapse formation involves a myriad of secreted factors, receptors, signalling molecules and cell-surface adhesion molecules. The latter are likely required during all stages of synaptogenesis, from cell-cell recognition, to induction, assembly and maintenance of synaptic contacts. The role of adhesion in regulating the communication between the pre- and postsynaptic compartment became apparent early on, with the very first ultrastructural studies of synapses already hypothesising that the electron dense regions within the pre- and postsynaptic membranes have adhesive properties (Gray, 1957). Cryo-electron microscopy studies later showed the existence of dense, periodic, “trans-cleft complexes” and thus confirmed the existence of transmembrane adhesion proteins that bridge the synaptic cleft (Lučić *et al.*, 2005; Zuber *et al.*, 2005). A number of influential studies have demonstrated that cell-surface adhesion molecules not only “glue” the pre- an postsynaptic side together, but also induce synapse formation through direct axo-dendritic contact and drive structural and functional changes in developing synapses (Scheiffele *et al.*, 2000; Biederer *et al.*, 2002; Linhoff *et al.*, 2009). Many of these cell-surface adhesion molecules are sufficient to drive

synapse assembly to a remarkable extent and are accordingly considered synaptogenic proteins. These molecules were identified in coculture (or "mixed culture") assays, where the investigated cell-surface adhesion molecules were expressed in non-neuronal cells, such as human embryonic kidney 293 (HEK293) cells, and their ability to induce pre- or postsynaptic differentiation in neurons was examined (Biederer and Scheiffele, 2007).

The first synapse inducing cell-surface adhesion molecule to be identified was Neuroligin, a postsynaptic single-pass transmembrane protein. In a seminal study, Scheiffele *et al.* (2000) found that Neuroligins are capable of inducing presynaptic differentiation in neurons cocultured with Neuroligin-expressing HEK293 cells. These presynaptic specialisations, although artificial, are functional to the extent that they contain a pool of recycling synaptic vesicles, and are capable of spontaneous and evoked neurotransmitter release (Scheiffele *et al.*, 2000; Dean *et al.*, 2003; Sara *et al.*, 2005). Neuroligins act bidirectionally with their presynaptic receptors Neurexins, which elicit postsynaptic differentiation (Dean *et al.*, 2003; Graf *et al.*, 2004). Additionally, overexpression of Neuroligins *in vivo* and *in vitro* induces the formation of dendritic spines and promotes recruitment of postsynaptic scaffolding molecules and NMDA receptors (Gerrow *et al.*, 2006; Dahlhaus *et al.*, 2010). Furthermore, this effect is dependent on the presence of the presynaptic Neurexin (Graf *et al.*, 2004), which provides further evidence for the bidirectional action of the Neurexin-Neuroligin complex. Neuroligins are expressed from four genes in vertebrates and the four paralogues (NL1-4) are specifically localised to particular synapses. NL1 is only localised to excitatory synapses, NL2 and NL4 are only present at inhibitory synapses, and NL3 is localised to both excitatory and inhibitory synapses (Missler, Südhof and Biederer, 2012). In contrast, Neurexins are encoded by three vertebrate genes and pan-neuronally expressed (Missler, Südhof and Biederer, 2012). Neurexins exist in a shorter β-Neurexin and a longer α-Neurexin isoform, which are generated from two alternative promoters. Both Neurexins and Neuroligins are extensively spliced in their extracellular region, which regulates their ligand interactions and creates potentially thousands of isoforms. Studies of knockout mice revealed that the Neurexin-Neuroligin complex plays vital roles in synapse formation and organisation. This is evidenced by the fact that the combined knockout of all three α-Neurexins is lethal at birth due to strongly impaired neurotransmitter release (Missler *et al.*, 2003). Surprisingly, although

glutamatergic synaptic transmission is severely reduced in these mice, there is no reduction in excitatory synapses. However, these mice have fewer inhibitory synapses (Missler *et al.*, 2003). Triple NL1, NL2 and NL3 knockout mice also die shortly after birth due to respiratory failure. Similar to the α-Neurexin knockout, these mice show no major changes in synaptic density but severely reduced inhibitory and excitatory synaptic transmission (Varoqueaux *et al.*, 2006). In contrast to knockout studies, acute RNAi mediated loss-of function of a single Neuroligin isoform has been shown to result in loss of synapses in rodent neurons (Chih, Engelman and Scheiffele, 2005; Shipman *et al.*, 2011). However, not all studies that used RNAi mediated knockdown of Neurexins or Neuroligins found the same effect (Ko *et al.*, 2011; Soler-llavina *et al.*, 2011). It is possible that these discrepancies might partially be caused by off target effects of RNAi and developmental compensation in genetic knockouts. Conversely, overexpression of Neuroligins leads to a dramatic increase in synapse density (Boucard *et al.*, 2005; Chih, Engelman and Scheiffele, 2005), with differential upregulation of excitatory synapses by Neuroligin-1 and of inhibitory synapses by Neuroligin-2 (Chubykin *et al.*, 2007). This indicates that expression of different Neuroligin and Neurexin isoforms has different effects on synapse formation and thereby creates a transsynaptic signalling code. Despite the wealth of information available on Neurexins and Neuroligins, their precise roles remain incompletely understood. However, the data suggests that these proteins have a bidirectional organising function whereby Neurexins coordinate the recruitment of calcium channels and presynaptic release machinery and Neuroligins organise the postsynaptic terminal of select synapses. Neurexins were found to engage in heterophilic *trans* interactions with many other transmembrane proteins, including leucine-rich repeat transmembrane neuronal proteins (LRRTMs), Latrophilins and Dystroglycan (Sugita *et al.*, 2001; de Wit *et al.*, 2009; Boucard, Ko and Südhof, 2012). Of these, LRRTMS are synapse inducing proteins (de Wit *et al.*, 2009, 2013; Linhoff *et al.*, 2009) and one study found that Latrophilins were also able to induce postsynaptic specialisations (Silva *et al.*, 2011). LRRTMs are postsynaptic heterotypic cell-adhesion molecules that promote presynaptic differentiation of excitatory terminals upon transsynaptic binding to other ligands, including Neurexins (de Wit *et al.*, 2009) and Glypicans (de Wit *et al.*, 2013). Latrophilins are adhesion-G-protein coupled receptors (GPCRs) that were originally identified, together with Neurexins, as receptors for the black widow spider venom α-Latrotoxin (Ushkaryov *et al.*, 1992; Davletov *et al.*, 1996). In addition to Neurexin, Fibronectin leucine-rich

repeat transmembrane proteins (FLRTs) and Teneurins were identified as Latrophilin ligands (Silva *et al.*, 2011; O'Sullivan *et al.*, 2012; Boucard, Maxeiner and Südhof, 2013). Latrophilins function as presynaptic heterotypic cell-adhesion molecules and their interaction with Teneurins or FLRTs is thought to directly or indirectly contribute to the formation or maintenance of synapses (Boucard, Maxeiner and Südhof, 2013). However, the exact role of the interactions of Latrophilins, Teneurins and FLRTs at synapses remains to be established. Other well-known synapse inducing proteins are SynCAMs (synaptic cell-adhesion molecules). SynCAMs are members of the Immunoglobulin superfamily (IgSF) of adhesion molecules and induce presynaptic differentiation through homophilic interactions in *trans* (Biederer *et al.*, 2002).

Other classical adhesion molecules such as Cadherins do not initiate synapse formation (Sara *et al.*, 2005; Jüngling *et al.*, 2006), but are involved in synapse assembly, maintenance and plasticity. Cadherins are a large family of cell-adhesion molecules with at least six subclasses that interact mostly homophilically and establish calcium-dependent adhesion (Salinas and Price, 2005). Classical, or type I Cadherins are linked to the cytoskeleton through interactions with cytoplasmic Catenin molecules. Whilst Cadherins were initially perceived as simple adhesion scaffolds, it is now established that Cadherin complexes play important roles in synaptic signalling (Dalva, McClelland and Kayser, 2007; Missler, Südhof and Biederer, 2012; de Wit and Ghosh, 2015). Indeed, neuronal N-Cadherins accumulate at nascent synapses after axo-dendritic contacts are formed (Benson and Tanaka, 1998) and contribute to excitatory synapse assembly (Salinas and Price, 2005). Evidence for this came from a study, where the overexpression of a dominant negative N-Cadherin in hippocampal neurons resulted in the partial disassembly of dendritic spines, presumably due to disruption of endogenous N-Cadherin complexes (Togashi *et al.*, 2002). Synaptic perturbations manifested in the form of fewer and more diffuse presynaptic and postsynaptic puncta, fewer vesicle recycling sites and a shift from more mature mushroom-shaped spines to immature filopodia-like protrusions. N-Cadherin also associates with and regulates trafficking of AMPARs (Nuriya and Huganir, 2006). Furthermore, lack of αN-Catenin, a member of the α-Catenin family expressed in neurons, leads to similar spine defects with excessively motile filopodia-like protrusions, whereas overexpression of αN-Catenin increases spine density and stabilises spines (Abe *et al.*, 2004). Catenins are also required for correct assembly of presynaptic terminals. Indeed, mice with a loss of

β-Catenin exhibit smaller and mislocalised synaptic vesicle reserve pools and an increase in total synapse number, which is likely the result of a homeostatic response to decreased synaptic efficacy (Bamji *et al.*, 2003). Together, these findings show that the Cadherin-Catenin complex is required on both sides of the synaptic junction to regulate the stabilisation of the cytoskeleton and the assembly of pre- and postsynaptic terminals. Cadherins also play a role in activity-dependent structural and functional plasticity of synapses, as evidenced by the fact that N-Cadherin accumulates at synaptic sites during long term potentiation (LTP; Bozdagi *et al.*, 2000). Moreover, there is an increase in the synthesis and dimerisation of N-Cadherins, which is necessary for strong adhesion and this suggests increased transsynaptic homophilic interactions during LTP (Tanaka *et al.*, 2000). A study in which neuronal differentiation of pluripotent embryonic stem cells from N-Cadherin knockout mice was induced, showed that N-Cadherin is required for synaptic vesicle release and short term plasticity (Jüngling *et al.*, 2006). Neuronal activity also regulates the distribution of Cantenins; decreased activity reduces the levels of αN-Catenin at synaptic sites, whereas increased activity leads to an increase of αN-Catenin at synaptic sites and a translocation of β-Catenin from shafts to spines (Murase, Mosser and Schuman, 2002; Abe *et al.*, 2004). Furthermore, translocation of β-Catenin to spines upon depolarisation induces its association with N-Cadherin, and results in an increase in the frequency of miniature excitatory post-synaptic potentials as well as the size of PSD-95 and vesicle clusters (Murase, Mosser and Schuman, 2002). Thus, Cadherin-Catenin signalling contributes to the structural synaptic changes that occur during LTP. Finally, Cadherins are also important for long-term stability and maintenance of dendritic spines (Mendez *et al.*, 2010). This was evidenced by the fact that overexpression of N-Cadherin enhanced long-term stability and persistence of stimulated spines, whereas dominant negative N-Cadherin prevented the stabilisation of spines following LTP induction (Mendez *et al.*, 2010). It is important to note that different Cadherins have distinct synaptic functions. Indeed, Cadherin-11, which belongs to the Cadherin type II subgroup, decreases synaptic function. Loss of Cadherin-11 does not impair synaptic structure and leads to enhanced LTP (Manabe *et al.*, 2000).

Despite an accumulation of research on the cell-surface adhesion molecules discussed above, the synaptic signalling mechanisms downstream of these molecules remain poorly understood. However, the literature to date establishes that cell-surface adhesion

proteins are crucial regulators of all stages of synaptogenesis, from the initial contact establishment, to synapse assembly and plasticity (Washbourne *et al.*, 2004; Salinas and Price, 2005; Dalva, McClelland and Kayser, 2007; Missler, Südhof and Biederer, 2012; de Wit and Ghosh, 2015). There is an emerging theme whereby many of these proteins have the ability to interact with scaffolding proteins and the cytoskeleton and thereby can recruit receptors and signalling molecules necessary for the assembly of synapses (Waites, Craig and Garner, 2005; Shen and Scheiffele, 2010). The function and adhesive specificity of synaptic cell-adhesion molecules is based on the structural organisation of their extracellular domains. These domains often contain repeated units, which determine the interactions of cell-adhesion molecules with their ligands (Missler, Südhof and Biederer, 2012). Extracellular domains also protrude into the synaptic cleft, allowing cell-adhesion molecules to bind and form transsynaptic complexes, which provide mechanical stability for the synapse and enable bidirectional signalling. It is clear that the induction and assembly of synapses is a complex process that requires many molecules and signalling pathways, and it is thought that many cell-adhesion molecules with synaptic functions remain to be identified. Here, adhesion proteins that are evolutionarily conserved are of particular interest, since they might provide insights into universal events leading to synaptogenesis.

A hallmark of the brain is the precise pattern of synaptic connectivity, which is also crucial for the functional integrity of neural circuits. Indeed, neurons have the remarkable ability to select appropriate synaptic partners among a dense population of potential targets. Quantitative evidence of this property came from an anatomical study, where reconstruction of the arbour of a cat retinal ganglion cell (RGC) in the lateral geniculate nucleus (LGN) revealed that it only synapsed with 4 out of 43 contacting cells (Hamos *et al.*, 1987). The cellular and molecular mechanisms that ensure the formation of synapses between appropriate partner neurons and at particular subcellular locations are generally referred to as “synaptic specificity”.

1.1.3 How is synaptic specificity achieved?

The establishment of appropriate synapses relies on a number of mechanisms, which ensure that dendrites and axons are matched to their appropriate target cells. Axon guidance and topographic mapping mechanisms bring growing axons into their correct

target areas, where local mechanisms with increasing levels of specificity further regulate the establishment of appropriate connectivity (Sanes and Yamagata, 2009; Williams, de Wit and Ghosh, 2010; Yogev and Shen, 2014; de Wit and Ghosh, 2015). A prominent anatomical feature of the CNS is that many brain regions are divided into specific laminae that contain distinct populations of neurons, which form synapses within defined laminar borders. Thus, the choice of possible postsynaptic partners for incoming axons is restricted and gives rise to "laminar specificity" (Huberman, Clandinin and Baier, 2010). Another important mechanism that ensures the formation of appropriate wiring specificity is a neuron's ability to distinguish between neurites from appropriate partner neurons as well as its own. This process termed "self-avoidance" leads dendritic or axonal branches arising from the same neuron (also termed "isoneuronal" or "sister" branches) to repel each other. Once and axon reaches an appropriate target region, it will form contacts with distinct types of neurons, thus imparting "cellular specificity". The number of potential connections can further be limited to a specific domain of that cell, thus enabling "subcellular specificity". This step can be considered the last step of neuronal wiring, before the axonal growth cone undergoes a morphological transformation, which enables synapse formation. The differentiation of contacts between different neurons into specific types of synapses creates "synaptic diversity". Finally, neuronal connections are refined during the critical process of synapse elimination. Together, these mechanisms, which are closely related and overlapping, contribute to synaptic specificity and result in the formation of structurally and functionally distinct synapses.

1.1.4 Molecular mechanisms of synaptic specificity

The molecular mechanisms that regulate synaptic specificity in the vertebrate brain are only beginning to be understood. Historically, the "chemoaffinity hypothesis", which was first introduced by John Langley (1895), and later formulated by Roger Sperry (1963), postulated that recognition of appropriate partner neurons was mediated by "individual identification tags" present on cells and nerve fibres. Thus, molecular cues present on the cell surface generate synaptic specificity by a "lock and key" mechanism, where a cell is presented as being target or non-target based on its expression of specific molecules. In addition to contributing to the formation of synapses, the cell-surface

adhesion molecules discussed above also have the potential to provide molecular mechanisms for determining appropriate synaptic partner matching consistent with the surface tags envisioned by Langley and Sperry. Substantial progress has been made in identifying and characterising transmembrane adhesion proteins that regulate the different aspects of synaptic specificity discussed above. As for synapse formation, the most studied cell-surface proteins with such roles include the Cadherins, IgSF proteins, Neurexins/ Neuroligins, and leucine-rich repeat transmembrane proteins.

Laminar specificity is a major contributor to synaptic specificity in the vertebrate nervous system. This is particularly striking in the visual system, where synaptic connections are strictly segregated in specific laminae along the entire visual pathway. Lamina-specific connectivity also occurs in the dorsal horn of the spinal cord, the cerebral cortex and the hippocampus, however the underlying mechanisms differ between these regions. Indeed, laminar specificity in the vertebrate retina involves homophilic interactions between cell-surface proteins, whereas activity-dependent competitive interactions and subcellular specificity mechanisms govern lamination in the dLGN and the hippocampus respectively (Sanes and Yamagata, 2009). The vertebrate retina is organised into layers, notably the RGC layer and the inner plexiform layer (IPL), where dendrites of RGCs receive input from bipolar and amacrine cells (Figure 1.2). Within the IPL, specific connections are organised into distinct synaptic laminae. Three families of IgSF proteins have been shown to play pivotal roles in establishing sublaminar specificity in the chick retina: Dscams, Sidekicks and Contactins (Yamagata and Sanes, 2008, 2012). These cell-surface proteins are expressed by non-overlapping subsets of RGCs, amacrine and bipolar cells and concentrate at synaptic sites within the IPL. Crucially, pre- and postsynaptic cells that express the same IgSF proteins arborise in the same sublamina, suggesting that these cell-surface proteins promote homophilic layer-specific adhesion between select neurons. Functional studies support this model (Yamagata and Sanes, 2012), as each Dscam, Sidekick or Contactin adheres only to the same protein on other cells and thus engages in homophilic interactions. Furthermore, loss and gain of function of these proteins disrupts the targeting of RGC dendrites and afferent bipolar or amacrine cell axons to specific IPL laminae. Thus, expression patterns of Dscams, Sidekicks and Contactins create a laminar specificity code based on homophilic interactions in the chick retina, but the stages in which these proteins act remain to be determined. Indeed,

it is not yet clear whether IgSF proteins regulate laminar specificity by promoting laminar targeting or by directly matching synaptic partners within specific laminae. Moreover, the laminar specificity code has not yet been fully deciphered and it is likely that many other molecules that contribute to the specification of this code still remain to be discovered. One example of a novel protein with roles in specific laminar targeting of RGC dendrites in the IPL is Teneurin 3 (Tenm3). Indeed, knockdown of Tenm3 in zebrafish leads to arborisation defects of RGCs in the IPL and erroneous targeting of dendritic processes to outer portions of the retina (Antinucci *et al.*, 2013).

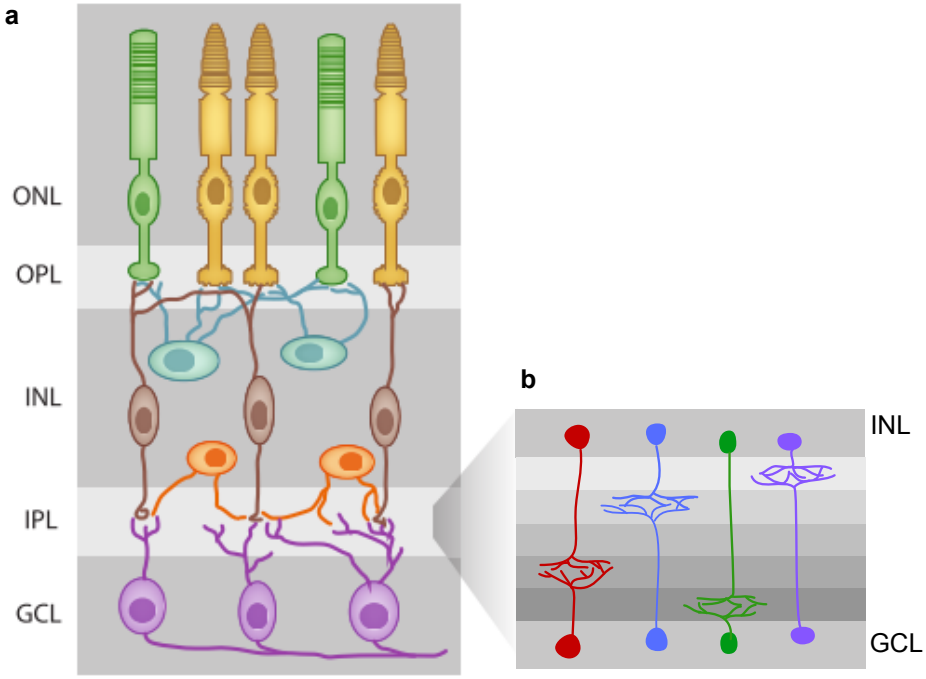

Figure 1.2. Schematic representation of the laminar organisation of the retina. **a.** Illustration of the different layers of the retina. The outer nuclear layer (ONL) contains rod (green) and cone (yellow) photoreceptors. Bipolar (brown) and horizontal cells (blue) reside in the inner nuclear layer (INL) and form synapses with photoreceptors in the outer plexiform layer (OPL). In the inner plexiform layer (IPL), ganglion cell (purple) dendrites ramify and form synapses with amacrine (orange) and bipolar cell axons in specific sublaminae. The schematic is reproduced from Yogev & Shen, 2014. **b.** Ganglion cells residing in the ganglion cell layer (GCL) synapse with amacrine and bipolar cells in specific sublaminae of the IPL. Laminar stratification is specified by homophilic interactions between differentially expressed adhesion molecules, including Sidekick, Dscam and Contactin (see text).

Transmembrane proteins can also mediate inhibitory signalling by promoting contact-mediated repulsion. Interestingly, whilst Dscams promote homophilic attraction in the chick retina, the same protein family mediates self-avoidance in individual sensory neurons in *Drosophila* and thus ensures the spreading of dendrites to cover the body-wall surface evenly (Zipursky and Sanes, 2010). Alternative splicing of the *Drosophila*

Dscam (Dscam1) generates up to ~38,000 potential isoforms and thus comprises a remarkable example of molecular diversity. Furthermore, Dscam1 isoforms bind exclusively homophilically and multiple distinct isoforms are stochastically expressed in neurons (Neves *et al.*, 2004). Consequently, every cell is left with a unique signature of Dscam1 isoforms and recognition code for self-avoidance (Chen *et al.*, 2006). In vertebrates, self-avoidance follows a similar mechanism and is mediated by clustered protocadherins, a protein family with great molecular diversity and unique adhesive interactions. Protocadherins are part of the Cadherin superfamily of transmembrane proteins and are subdivided into clustered and non-clustered protocadherins. Clustered protocadherins further comprise α-, β- and γ-clusters which undergo extensive alternative splicing. Furthermore, isoforms from the α-, β- and γ-gene clusters engage in highly specific homophilic *trans* interactions and can form multimers through *cis* binding, thus generating the potential for a large variety of isoform combinations and recognition specificity (de Wit and Ghosh, 2015). Deletion of all 22 γ-Protocadherin isoforms in mouse retinal starburst amacrine cells (SACs), which have radially symmetric dendrites that rarely cross, leads to extensive overlap and bundling of dendrites belonging to the same cell, the formation of autapses (synapses between neurites from the same cell) and results in severely impaired dendritic field coverage (Lefebvre *et al.*, 2012; Kostadinov and Sanes, 2015). This phenotype is caused by a loss of repulsive homotypic *trans* interactions between isoneuronal dendrites and thus a loss of self-avoidance. Consistent with this, rescue of a single γ-Protocadherin isoform in γ-Protocadherin knock out SACs rescues self-avoidance and leads to decreased co-fasciculation and connectivity between neighbouring SACs (Lefebvre *et al.*, 2012; Kostadinov and Sanes, 2015). This indicates that the diversity of clustered Protocadherins defines unique cell-surface identities that enable isoneuronal recognition and self-avoidance in vertebrates, similar to the Dscam1 in *Drosophila*. Protocadherins are not the only cell-surface proteins to mediate self-avoidance. Heterotypic repulsive signalling between the transmembrane protein Semaphorin 6A and its receptor Plexin A2 mediates self-avoidance in ON SACs through a similar mechanism (Sun *et al.*, 2013).

Cell-surface adhesion molecules also play important roles in cellular specificity. Interestingly, the nervous system appears to use the same cell-adhesion molecules in different mechanisms to achieve synaptic specificity at different levels and in various

systems. For example, whilst homophilic interactions between Contactins mediate laminar specificity in the retina as described above, Contactins mediate cellular specificity in the mouse spinal cord (Ashrafi *et al.*, 2014). Contactin 5 (Cntn5), a member of the Contactin subfamily of IgSF cell-surface adhesion proteins, is expressed in proprioceptive sensory neurons. Axonal terminals of these proprioceptive sensory neurons are selectively innervated by a class of presynaptic GABAergic interneurons, called "GABApre" neurons. The cellular recognition between these two types of neurons was shown to be mediated by Cntn5, which forms a receptor-complex with the Contactin-associated protein 4 (Caspr4) in proprioceptive sensory neurons, and interacts with a receptor complex of NrCAM and CHL1, two members of the L1 subfamily of IgSF cell-surface adhesion proteins, on GABApre neurons (Ashrafi *et al.*, 2014). Thus, in the spinal cord, heterophilic interactions between IgSF molecules ensure appropriate recognition of synaptic partners. In addition to the recognition provided by homophilic and heterophilic binding of cell surface proteins, the levels of expression of cell surface receptors can contribute to the appropriate wiring of synaptic partners. Such a mechanism was observed in the *Drosophila* antennal lobe, where Teneurins are highly expressed in matching olfactory receptor neurons (ORNs) and projection neurons (PNs) and regulate appropriate connectivity based on their relative expression levels (refer to 1.2.6; Hong, Mosca and Luo, 2012).

The above-mentioned example of the establishment of cellular specificity through Contactin interactions with L1 family proteins also presents an example of remarkable subcellular specificity. Indeed, this interaction not only results in matching of GABApre neurons with proprioceptive sensory neurons, but also in the selective subcellular targeting of axo-axonic synapses on proprioceptive sensory axonal terminals (Ashrafi *et al.*, 2014). This highlights the fact that the different stages of synaptic specificity are overlapping and the distinction between laminar, cellular and subcellular specificity is not always clear-cut. Most inhibitory neurons show high specificity in targeting specific subcellular compartments, which is critical for their ability to modulate the activity of their postsynaptic target neurons (Miles *et al.*, 1996). Perisomatic inhibition has a profound effect on action potentials elicited in postsynaptic neurons, whereas inhibitory synapses on distal dendrites mostly affect dendritic calcium-dependent spikes. Thus, subcelluar specificity has important functional consequences. Specific subcellular targeting is not restricted to interneurons, indeed

there are many examples of subcellular specificity that involve principal neurons. Similar to the mechanisms involved in generating cellular specificity, it is believed that subcellular specificity is generated by cell-adhesion molecules that are preferentially localised in specific regions of a neuron and thus create a molecular code at the subcellular level. One example of a brain area that exhibits striking segregation of different classes of excitatory inputs is the hippocampus. Here, Cadherin 9 (Cdh9), a member of the Cadherin family of transmembrane proteins, plays important roles in controlling the subcellular specificity of synaptic connections between dentate granule cells (DGCs) and CA3 pyramidal neurons (Williams *et al.*, 2011). Indeed, Cdh9 is expressed selectively in CA3 neurons and DGCs and bidirectionally regulates appropriate mossy fibre synapse formation via homophilic adhesion. Knockdown of Cdh9 in CA3 neurons only disrupts synaptic contacts from DGCs (mossy fibre synapses), but does not affect CA3 synapses from other sources. This shows that Cdh9 is required for the formation of mossy fibre synapses, which are restricted to apical CA3 dendrites in the *stratum lucidum* (refer to 1.3.1.1 and Figure 1.5), and is thus a molecular mediator of subcellular specificity.

Despite considerable advances in identifying cell-surface proteins that contribute to synaptic specificity, much remains to be determined about the precise mechanisms by which these molecules function. Although the number of cell-surface molecules implicated in establishing synaptic specificity is vast, they all share a few common denominators, which can be envisioned as criteria for the identification of further proteins: Such proteins should be expressed in distinct populations of neurons and localise to synapses at one or more stages of development. Furthermore, they should be capable of homo- and/ or heterophilic interactions in *trans*. Loss- or gain of function should alter wiring specificity and/ or synapse formation. Moreover, because of the complexity of synaptic connections, such proteins should provide great combinatorial diversity, which is why it has been proposed that genes encoding cell-surface adhesion molecules involved in synaptic specificity should also provide enough molecular diversity, for instance through alternative splicing (de Wit and Ghosh, 2015).

1.2 Teneurins as synaptic cell-adhesion molecules

Over recent years, new protein families have been implicated in axonal pathfinding and the establishment of synaptic specificity. One of these is the Teneurin protein family, members of which have been shown to have roles in neuronal wiring, particularly in the visual system (Leamey *et al.*, 2007; Dharmaratne *et al.*, 2012; Antinucci *et al.*, 2013, 2016; Merlin *et al.*, 2013; Young *et al.*, 2013; Carr *et al.*, 2014), as well as in appropriate synaptic partner matching and organisation (Hong, Mosca and Luo, 2012; Mosca and Luo, 2014). In the following sections, I will provide an overview of the literature on Teneurins to date and explore their roles as synaptic cell-adhesion molecules in neuronal connectivity.

1.2.1 A brief history of the discovery of Teneurins

Teneurins are a family of conserved cell-surface proteins that were independently discovered in *Drosophila* by two different laboratories in the early 1990s. A low-stringency cDNA screen for homology to the extracellular matrix protein Tenascin-C identified two novel proteins named Ten-m and Ten-a, for "Tenascin-like protein accessory" and "Tenascin-like protein major" (Baumgartner and Chiquet-Ehrismann, 1993; Baumgartner *et al.*, 1994). However, the sequence similarity was confined to the Tenascin-type epidermal growth factor (EGF) like sequences. Ten-m was independently discovered by another group at the same time, who called the protein "Odd oz" or "Odz", because of its expression in odd-numbered body segments of the fly embryo (Levine *et al.*, 1994). It was initially thought to be a pair-rule gene, because *Ten-m* mutants were found to exhibit segmentation defects and a phenotype similar to that of *odd-paired* (*opa*) mutants. However, it was later discovered that *Ten-m* is unrelated to segmentation defects (Zheng *et al.*, 2011). Both names persisted when the four vertebrate Teneurin homologues were identified, and these are often referred to as "Ten-m1-4", "Tenm1-4" as well as "Odz1-4". In 1999, the new name "Teneurin" was proposed for the protein family to honour the original name and in reference to the nervous system, where Teneurins are predominantly expressed in vertebrates and invertebrates (Minet *et al.*, 1999). Finally, while searching for Latrophilin-1 ligands, another group identified a protein, which they provisionally named latrophilin-1-associated synaptic surface organiser (Lasso; Silva *et al.*, 2011). Lasso was later

identified as a splice variant of the vertebrate Teneurin-2 (Tenm2). The term "Teneurin" is now widely used, however the literature is still full of references to Odz, Ten-m, Tenm, Ten-a, Ten-1 (which refers to the *C. elegans* Teneurin homologue) and Lasso. In this thesis, I will use the term "Teneurin" when referring to the protein family, "Tenm1-4" when referring to the four vertebrate Teneurin homologues, and "Ten-a" and "Ten-m" when referring to the two *Drosophila* homologues.

1.2.2 Teneurins are a family of proteins with an evolutionarily conserved structure

The Teneurins are evolutionarily ancient molecules, with an ancestral Teneurin homologue discovered in choanoflagellate *Monosiga brevicollis,* the living unicellular eukaryote most closely related to animals. The choanoflagellate Teneurin gene appears to have evolved as a complex hybrid fusion protein from a prokaryotic gene and a diatom or algal gene through horizontal gene transfer (Tucker *et al.*, 2012). Teneurins are conserved across invertebrate and vertebrate species. Most invertebrates have a single Teneurin gene, with the exception of insects, where a gene duplication event led to two Teneurin homologues Ten-a and Ten-m. Two further duplication events in vertebrates resulted in four Teneurins, where Tenm1 and Tenm4 appear to share one common ancestor, as do Tenm2 and Tenm3. The fact that Teneurins are conserved between invertebrates and vertebrates indicates that these proteins may be required for fundamentally important mechanisms.

1.2.2.1 Basic protein structure

Across phyla, these type II transmembrane proteins retain the same basic structure and domain organisation with some small inter-species and intra-species variations (Figure 1.3). All Teneurin homologues are large proteins, composed of 2500 to 2800 amino acids (aa) and with a molecular weight just over 300kDa. The N-terminal intracellular domain (ICD) is small compared to the size of the protein with 300 to 400 aa and attached to a single, short, hydrophobic transmembrane region of 34 aa. The C-terminal extracellular domain (ECD) comprises the largest part of the protein with about 2400 aa. Teneurins can be cleaved at several putative furin cleavage sites and are thought to undergo a process called regulated intramembrane proteolysis (RIP; see 1.2.4.1). One

furin cleavage site was proposed to be within the cytosolic N-terminal domain and leads to the release of the ICD, which translocates to the nucleus and participates in transcription control (Bagutti *et al.*, 2003). A second furin cleavage site is thought to exist in the transmembrane domain and to enable release of the ectodomain (Vysokov *et al.*, 2016). A third furin cleavage site has been found within a linker region of about 200aa in the C-terminal, immediately after the transmembrane domain (Rubin *et al.*, 1999; Tucker *et al.*, 2001; Vysokov *et al.*, 2016). It has been suggested that only Tenm2 and Tenm3 have a furin cleavage site in this region (Tucker *et al.*, 2012), which serves as a proteolytic processing site, allowing the ECD to be shed. Finally, the far C-terminal end of Teneurins contains a putative furin cleavage site, which can generate a bioactive neuropeptide called Teneurin C-associated peptide (TCAP; Qian *et al.*, 2004). This peptide is 40-41 aa long and highly conserved in all vertebrates. TCAP shows some structural homology with the corticotrophin release factor (CRF) family of peptides and studies using a synthetic version of TCAP found that it can modulate CRF-mediated behaviours relating to stress and anxiety *in vivo* (Wang *et al.*, 2005; Al Chawaf *et al.*, 2007; Lovejoy, Rotzinger and Barsyte-Lovejoy, 2009; Tan *et al.*, 2009; Erb *et al.*, 2014). Furthermore, TCAP was found to promote neurite and axonal outgrowth and increase β-Tubulin and β-actin protein expression *in vitro* (Al Chawaf *et al.*, 2007). The fact that some Teneurins can release both their ICD and ECD indicates that in addition to acting as cell-surface receptors, these proteins might also serve as extracellular and intracellular signalling factors.

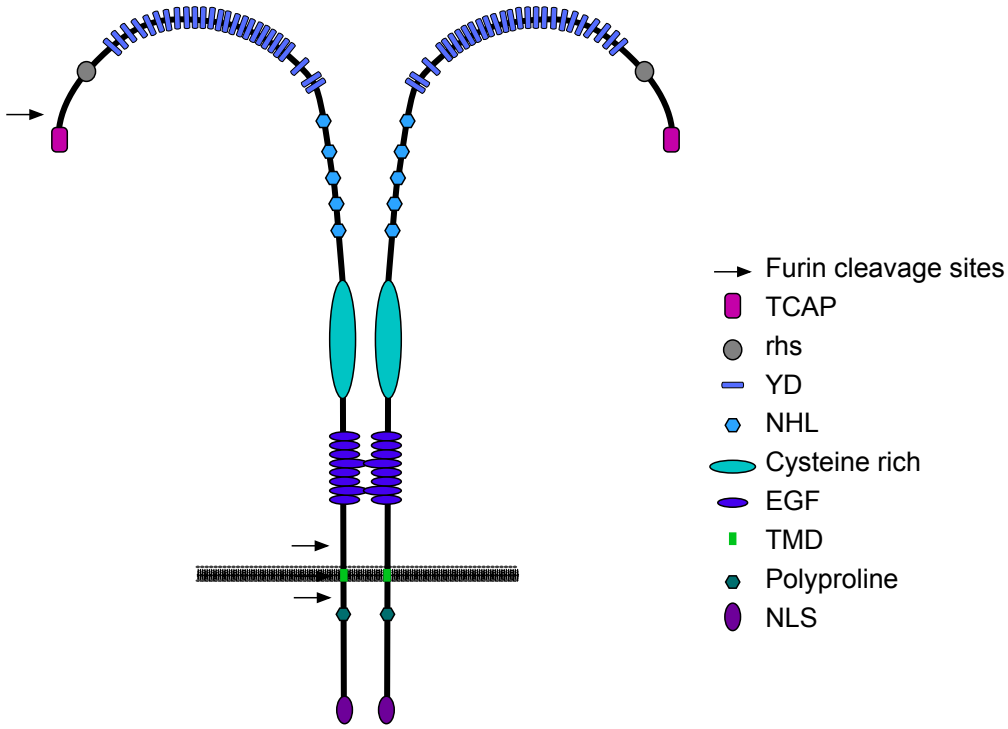

Figure 1.3. Schematic diagram illustrating the structure and major domains of Teneurins. A pair of globular, dimerised Teneurins is shown. Note that not all features are common to all Teneurins.

1.2.2.2 Basic domain organisation

The ICDs of Teneurins are highly conserved in vertebrates and contain nuclear localisation signals (NLSs), putative tyrosine phosphorylation sites, two EF-hand-like calcium-binding motifs and one or two proline-rich motifs, characteristic of Src homology 3 (SH3) binding domains (Tucker *et al.*, 2012). Using a yeast-two-hybrid screen, the ICD of Tenm1 has been shown to bind to the SH3-domains containing adapter protein c-Cbl-associated protein (CAP)/ ponsin as well as the transcriptional repressor methyl-CpG binding protein MBD1 (Nunes *et al.*, 2005). The phylogenetically conserved ECD contains eight EGF repeats, a cysteine-rich region, five NHL (from NCL-1, HT2A and Lin-41) domains, tyrosine and aspartate (YD) repeats, and a region similar to the core-associated domain of retrotransposon hot spots (RHS). The second and fifth EGF repeats each miss one cysteine residue, which is replaced with a tyrosine and phenylalanine residue respectively, resulting in five instead of six cysteines. This is thought to facilitate homo- and hetero-dimerisation of

Teneurins in *cis* through covalent, disulfide bonds (Feng *et al.*, 2002). Using rotary shadowing electron microscopy, one group found that ECDs of all four mouse Teneurin members form "cherry-like" structures, consisting of two globular domains connected by two extended rods. The cysteine-rich region following the EGF domain is thought to aid the folding of these globular domains (Oohashi *et al.*, 1999; Feng *et al.*, 2002). In vertebrates, Teneurins are encoded by four genes. The ability of all four Teneurins to form homo- as well as heterodimers (Feng *et al.*, 2002) implies that these proteins may be able to form up to ten distinct *cis*-dimers. Further distally in the ECD is the NHL domain consisting of five NHL repeats in vertebrates and four repeats in invertebrates (Tucker *et al.*, 2012). An elegant study, that used atomic force microscopy (AFM)-based single cell force spectroscopy (SCFS) combined with genetic engineering, found that the NHL domain mediates homophilic recognition and binding of Teneurins in *trans* (Beckmann *et al.*, 2013). NHL domains are known to form β-propellers (Edwards *et al.*, 2003), which have been shown to mediate interactions between other cell surface receptors such as Semaphorins and Plexins (Janssen *et al.*, 2010; Liu *et al.*, 2010). The C-terminal two thirds of Teneurins contain a domain composed of twenty-six YD repeats, which had only been described in bacteria, before being found in Teneurins (Minet and Chiquet-Ehrismann, 2000). The fact that Teneurins have a conserved domain organisation and the ability to interact homo- and heterophilically in *trans,* positions these molecules as good candidates to act as transmembrane adhesion proteins in the specification of connectivity. Furthermore, it is conceivable that Teneurins achieve molecular diversity through homo- and heterodimerisation and alternative splicing. However, this is an issue that has not been investigated to date.

1.2.3 Teneurins are highly expressed during development

Teneurins are strongly expressed in the nervous system of vertebrates and invertebrates. Additional areas of expression of Teneurins, with the exception of Tenm2, include non-neuronal tissue, particularly at sites of pattern formation (Ben-Zur *et al.*, 2000). *Drosophila* Ten-m is segmentally expressed in stripes in the cellular blastoderm and at later stages in the cardiac mesoderm, ventral nerve cord and epidermis of the fly embryo (Baumgartner *et al.*, 1994). Ten-a and Ten-m were also found to be expressed in select

matching pairs of PNs and ORNs of the antennal lobe (Hong, Mosca and Luo, 2012; Mosca and Luo, 2014). The same group also found that Ten-a and Ten-m are expressed in both motor neurons and muscles, but that Ten-m is found at higher levels in the postsynaptic muscle, whereas Ten-a is found at higher levels in the pre-synaptic motor-axon (Mosca *et al.*, 2012).

In mice, Teneurins are expressed at early developmental stages, with Tenm3 and Tenm4 being present as early as E7.5, Tenm2 at E10.5 and Tenm1 at E15.5 (Zhou *et al.*, 2003). Tenm3 and Tenm4 expression starts in the neural plate and gradually extends to distinct but partially overlapping areas throughout the forebrain, midbrain and diencephalon as well as the periocular area. Tenm2 is mainly expressed in the midbrain and the spinal cord and gradually extends to the forebrain and nasal cavity. By late embryonic and neonatal stages all four Teneurins are strongly expressed in the thalamus, cortex, hippocampus and cerebellum (Zhou *et al.*, 2003). The different Teneurin members are present in distinct patterns in these regions. In the neocortex, Tenm1 is notably expressed at higher levels in the rostral part, whereas caudal areas exhibit higher levels of Tenm2, Tenm3 and Tenm4 (Figure 1.4, Li, Bishop and O'Leary, 2006). In the cerebellum, Teneurins are confined to distinct neuronal populations; Tenm3 and Tenm4 are exclusively expressed in Purkinje cells, Tenm1 is restricted to the granular layer and Tenm2 can be found in the granular and molecular layer (Zhou *et al.*, 2003). In the hippocampus Teneurins are expressed in the two main neuronal layers, the *stratum pyramidale* and the granular layer of the dentate gyrus (DG; Li, Bishop and O'Leary, 2006), and the expression patterns are mostly maintained into adulthood (Figure 1.4, Figure 3.1). Tenm1 is expressed in the CA1 subfield of the *stratum pyramidale* and in the DG in the neonatal brain and in the adult. Tenm2 is clearly present throughout the layers of pyramidal and granule cells in neonates. In adults, Tenm2 expression becomes restricted to the pyramidal layer, where it is weakly expressed in CA3, CA2 and more strongly in CA1. Tenm3 is only expressed in CA1, where it is present in a strong gradient with high proximal (close to CA2) and low distal levels. Tenm3 expression is often reported to be in CA2, however, data from the Hindges lab using a Purkinje cell protein 4 (PCP4) antibody, which delineates CA2 from CA3 and CA1 (San Antonio *et al.*, 2014), shows that it is restricted to CA1 (Appendix 1). Interestingly, Tenm3 is also found in a corresponding gradient in the subiculum, with low proximal (closer to CA1) and high distal levels, suggesting that

these proteins might be involved in topographic mapping in this region. This complementary expression pattern is maintained from the neonatal brain into adulthood. Tenm4 is expressed throughout pyramidal and granule cell layers in neonates but becomes restricted to CA3 and CA1 in the adult.

The expression pattern of Teneurins, especially of Tenm3, has been very well characterised in the visual system. Tenm3 is found in complementary gradients in interconnected regions of the visual pathway and this expression pattern seems to be conserved across mammalian species. Indeed, Tenm3 is found in the retina, the dorsal lateral geniculate nucleus (dLGN), superior colliculus and visual cortex of the mouse (Leamey *et al.*, 2007, 2008) and the marsupial wallaby (Carr *et al.*, 2014). Importantly, Tenm3 is consistently found in a gradient, which is highest in areas along the ventral visual pathway. In zebrafish, Tenm3 is expressed in a subset of RGCs and their presynaptic amacrine cells and postsynaptic tectal target neurons (Antinucci *et al.*, 2013). Furthermore, Tenm3 expression is higher in the ventral region of the retina of zebrafish. Tenm2 has also been found to be expressed throughout the visual pathway of the mouse, although this expression pattern is uniform and does not follow visual topography gradients (Young *et al.*, 2013). Tenm1 is expressed in interconnected regions of the avian tectofugal pathway, including RGCs, the optic tectum and the nucleus rotundus (Kenzelmann *et al.*, 2008). Tenm4 is strongly expressed in the dLGN and visual cortex in mice (Li, Bishop and O'Leary, 2006). Altogether, this shows that Teneurins tend to be expressed in partially overlapping and interconnected regions of the brain and thus further positions these proteins as strong candidates to regulate neuronal wiring. Furthermore, the life-long expression suggests that Teneurins may play roles not only in the early specification of neural circuits but also in the maintenance and plasticity of synaptic connections.

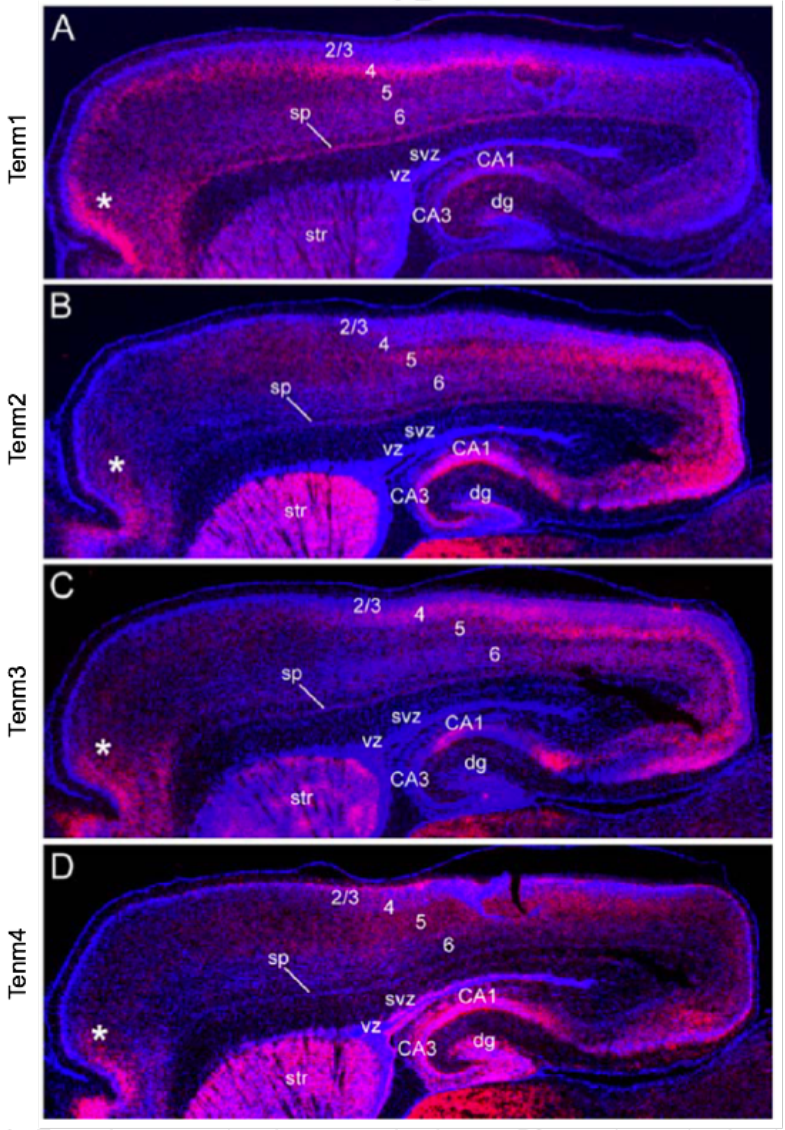

Figure 1.4. Teneurin expression in neonatal mice at P2 as shown by in situ hybridisation and DAPI counterstaining. **A.** Tenm1 is mostly expressed in layer 4 in a decreasing gradient from rostral to caudal in the cortex, as well as in the subplate and the orbital and insular area. In the hippocampus Tenm1 is expressed in the DG and CA1. **B.** Tenm2 is expressed in an increasing gradient from rostral to caudal and in layer 5 of the visual cortex. Tenm2 is also strongly expressed in the orbital and insular area and in the striatum. In the hippocampus Tenm2 is expressed throughout the DG and CA3, CA2, CA1. **C.** Tenm3 is expressed similarly to Tenm2 in the cortex, in an increasing gradient from rostral to caudal, in layer 5 of the visual cortex but also in layer 4 of the somatosensory area. Tenm3 is also strongly expressed in the orbital and insular area. In the hippocampus Tenm3 is expressed in a gradient along CA1 and in the subiculum. **D.** Tenm4 is expressed more diffusely in the cortex and in an increasing gradient from rostral to caudal. Tenm4 is also strongly expressed in the orbital and insular area and in the striatum as well as the ventricular and subventricular zone. In the hippocampus, Tenm4 is expressed in the DG and along CA3, CA2 and CA1. dg, dentate gyrus; sp, subplate; str, striatum; svz, subventricular zone; vz, ventricular zone, asterisks indicate the orbital and insular area. Adapted from Li, Bishop & O'Leary, 2006.

1.2.4 Teneurin processing, downstream interactions and signalling

1.2.4.1 Interactions of Teneurin ICDs with signalling pathways, transcriptional regulators and the cytoskeleton

Teneurins have been reported to be processed in multiple ways. As mentioned earlier, Teneurins have the potential to be cleaved at several furin cleavage sites (Figure 1.3). A number of studies have found that Tenm1 and Tenm2 are proteolytically cleaved within the N-terminal and that their ICDs translocate to the nucleus (Bagutti *et al.*, 2003; Nunes *et al.*, 2005; Kenzelmann *et al.*, 2008). The Tenm1 ICD was found to have a NLS which is necessary for translocation to the nucleus *in vitro* and *in vivo* (Kenzelmann *et al.*, 2008). Nuclear translocation of the ICD of Tenm2 *in vitro* was triggered by homophilic interactions of its ECD in *trans* (Bagutti *et al.*, 2003). Human Teneurins were found to have a NLS in Tenm1, Tenm3 and Tenm4 but not Tenm2. In mice, only Tenm1 and Tenm3 were found to have NLSs (Tucker *et al.*, 2012). This was surprising given that Tenm2 was found to translocate to the nucleus *in vitro*. Furthermore, Teneurin ICDs were found to interact with various transcriptional regulators and signalling molecules; the ICD of Tenm1 was found to interact with CAP/Ponsin and MBD1 (Nunes *et al.*, 2005), whereas the ICD of Tenm2 was found to colocalise with promyelocytic leukemia (PML) proteins and downregulate the transcription of apolipoprotein E (ApoE; Bagutti *et al.*, 2003). CAP/Ponsin is an adapter protein with a function in insulin signalling (Baumann *et al.*, 2000) as well as cell-cell and cell-matrix adhesions (Ribon *et al.*, 1998; Mandai *et al.*, 1999). MBD1 binds to methylated DNA in heterochromatin and acts as a transcriptional repressor (Wade, 2001). PML proteins are involved in a number of functions associated with transcriptional control (Zhong, Salomoni and Pandolfi, 2000). These interactions suggest that Teneurins can participate in specific signalling pathways and transcriptional regulation via their ICDs. In addition to possible roles in gene transcription, Teneurin ICDs might mediate interactions with the cytoskeleton (Rubin *et al.*, 2002; Nunes *et al.*, 2005). Indeed, CAP/Ponsin interacts with several regulators of the actin cytoskeleton and cell adhesion, and as mentioned above, binds to the Tenm1-ICD. Adapter proteins link protein-binding partners together and facilitate the creation of larger complexes. Thus, it is conceivable that CAP/Ponsin links the ICD of Tenm1, which was found to bind to the last SH3 domain of Ponsin, with Vinculin, an F-actin binding protein that binds to the first and second SH3 domains (Mandai *et al.*,

1999). CAP has also been shown to bind to the focal adhesion kinase (FAK; Ribon *et al.*, 1998) raising the possibility that CAP/Ponsin might create a large signalling complex involving vinculin, Tenm1 and FAK. Additionally, Tenm2 overexpression in mouse neuroblastoma (Nb2a) cells leads to the accumulation of actin at sites of Tenm2-rich cell-cell contacts and the Tenm2-ICD was found to colocalise with actin (Rubin *et al.*, 2002). Taken together, these results suggest that Tenm1 and Tenm2 interact with the actin cytoskeleton through their cytoplasmic domains. However, a direct interaction with actin has not yet been shown and it is unknown whether the ICDs of Tenm3 and Tenm4 are involved in similar mechanisms.

The release of the ICD has been proposed to happen via a mechanism described as regulated intramembrane proteolysis (RIP; Bagutti *et al.*, 2003; Kenzelmann *et al.*, 2008). RIP is a two-step mechanism, whereby a first cleavage and release of the ECD is a prerequisite for a second cleavage, which results in the separation of the ICD from the cell membrane, its translocation to the nucleus and participation in transcriptional regulation. RIP was first proposed as a signalling model by which the sterol regulatory element binding protein (SREBP) regulates lipid metabolism and is now known to control the processing of several transmembrane signalling molecules such as Notch-1 and amyloid precursor protein (APP; Brown *et al.*, 2000). Such a processing mechanism would be consistent with a dual role, where Teneurins act as extracellular adhesion molecules as well as signalling molecules (Vysokov *et al.*, 2016).

Interactions of Teneurins with the cytoskeleton have also been shown in *Drosophila*. Using a yeast two-hybrid screen and GST pull down, it was shown that Ten-m physically interacts with Filamin, an actin binding protein, and both proteins are believed to act together to influence appropriate growth cone progression of motor neurons (Zheng *et al.*, 2011). Teneurin mutations were also found to cause cytoskeletal disruption at the neuromuscular junction (NMJ; Mosca *et al.*, 2012) with catastrophic disorganisation of presynaptic microtubules as well as less pronounced disruption of the postsynaptic spectrin cytoskeleton. Furthermore, Ten-m was shown to directly interact with α-spectrin and to regulate Wiskott-Aldrich syndrome protein (WASP) and Adducin, which are themselves actin-regulating proteins. These findings led to the hypothesis that Teneurins may regulate appropriate synapse formation by organising the cytoskeleton (Mosca, 2015).

1.2.4.2 Homophilic and heterophilic Teneurin interactions

Work in *Drosophila* has demonstrated that transsynaptic homophilic interactions between Teneurins promote matching specificity between synaptic partners (Hong, Mosca and Luo, 2012). The same group also investigated whether Teneurins interact *in vitro* and performed coimmunoprecipitations from lysates of two populations of Drosophila S2 cells transfected with tagged Teneurin constructs. They found that Ten-m, and to a lesser extent, Ten-a formed strong homophilic complexes. Additionally, heterophilic interactions between Ten-a and Ten-m also occurred.

A number of transfection studies, mostly performed *in vitro*, have also observed homophilic binding between Teneurins in *trans* (Rubin *et al.*, 2002; Leamey *et al.*, 2008; Beckmann *et al.*, 2013; Boucard, Maxeiner and Südhof, 2013). Human fibrosarcoma (HT1080) cells permanently transfected with Tenm2 were found to aggregate and Tenm2 was heavily enriched at sites of cell-cell adhesion in transiently transfected Nb2a (Rubin *et al.*, 2002), indicating that Tenm2 promotes homophilic adhesion between cells. The EGF domain, which is required for the dimerisation of Teneurins in *cis* (Oohashi *et al.*, 1999; Feng *et al.*, 2002), did not play a role in cell aggregations, demonstrating that homophilic binding in *trans* is not mediated by this domain but instead by a part of the Teneurin ECD distal to the EGF domain. Moreover, Tenm2 was found to induce the formation of filopodia, which was dependent on the ICD (Feng *et al.*, 2002). One group identified Tenm3 as a differentially expressed molecule in the visual system of mice during formation of afferent and efferent projections using microarray analysis and found that Tenm3 is highly expressed along axonal tracts of projection neurons of the developing visual pathway (Leamey *et al.*, 2008). Upon further investigation, they found that hippocampal neurons transfected with Tenm3 *in utero* at E14 formed large clumps of clustered cells with intertwined processes and delayed migration at P8. The authors of this study interpreted these findings as evidence that Tenm3 promotes homophilic adhesion *in vivo* and that the delay in migration is a consequence of overexpression of an adhesive molecule. Another study was dedicated to deciphering the domains and mechanisms that facilitate the formation of homophilic Teneurin bonds (Beckmann *et al.*, 2013). This was investigated using a sophisticated experimental approach with a variety of Tenm1 and Tenm2 constructs with deleted and swapped domains. These constructs were

transfected into HEK293 cells, which were brought into contact to allow cells to form adhesive contacts. After an initial contact time ranging from 1 to 120 seconds both cells were separated and their maximal adhesion force was measured using AFM-based SCFS. AFM-based SCFS assays allow the quantification of the adhesive forces of single receptor-ligand bonds on the surface of living cells (Müller *et al.*, 2009). As mentioned previously, the NHL domain was shown to be responsible for homophilic recognition and binding of Teneurins (Beckmann *et al.*, 2013). Furthermore, the strength of the NHL domain-mediated cell−cell adhesion was found to be critically dependent on the ICD, which is thought to anchor to the actin-cytoskeleton. This was further supported by the fact that disruption of the actin cytoskeleton using latrunculin A compromised adhesion strengthening. Moreover, longer contact times between cells resulted in significantly increased adhesion strength, which led the authors to hypothesise that adhesion strengthening may be facilitated by a clustering of Teneurins anchored to the actin cytoskeleton. Similar mechanisms have been observed for other cell adhesion receptors such as Cadherins, Nectins and SynCAMs, which also cluster at interaction sites to increase the adhesion strength (Pokutta and Weis, 2007; Fogel *et al.*, 2011; Kurita, Ogita and Takai, 2011). Using a neurite outgrowth assay, the group also found that homophilic adhesion inhibits outgrowth (Beckmann *et al.*, 2013). This finding led to the postulation of a model for the actions of Teneurins, whereby homophilic adhesion between Teneurins expressed on growth cones and appropriate target structures causes a cessation of neurite outgrowth and presumably leads to synapse formation.

However, some controversy exists as to whether homophilic Teneurin interactions are sufficiently strong to support cell-cell adhesion. This concern was raised after an independent study found that homophilic Teneurin interactions were not sufficiently strong to promote intercellular cell-adhesion, but instead required heterophilic binding of Teneurins to Latrophilins (Boucard, Maxeiner and Südhof, 2013). More specifically, the authors of the study identified all four Teneurins as ligands of Latrophilin 1 by mass-spectrometry and confirmed specific binding of Tenm2 and Tenm4 to Latrophilin 1 in subsequent pull-down experiments. Tenm3 was not assayed during the pull-down experiments and the lack of Tenm1 binding to Latrophilins in this assay may be due to decreased affinity of this isoform (Boucard, Maxeiner and Südhof, 2013). The authors then showed that Tenm2 and Tenm4 (Tenm1 and Tenm3 were not further assayed)

bound to Latrophilin 1 on the cell surface of HEK cells in a surface-binding assay. Moreover, HEK cells expressing Latrophilin 1, 2, and 3 formed large cell aggregates with cells expressing Tenm2 and Tenm4 in a cell-aggregation assay. This demonstrated a high binding affinity between Teneurins and Latrophilins that was sufficiently strong to promote intercellular adhesion. Contrary to this, no cell aggregation was observed between Tenm2 or Tenm4 expressing cells, either alone or in combination, even though soluble Tenm2 specifically bound to HEK cells expressing Tenm2 or Tenm4 in the surface binding assay (Boucard, Maxeiner and Südhof, 2013). These findings suggested that although Teneurins homophilically and heterophilically bind to other Teneurins, these interactions do not mediate intercellular cell-adhesion. The authors of this study argued that the apparent discrepancy between their findings and those of Beckmann *et al.* (2013) stems from the fact that they analysed spontaneous aggregates whereas the latter brought transfected HEK cells into contact to induce the formation of adhesive contacts. While additional confirmation will be needed to resolve this discrepancy, this study highlighted the fact that Teneurins can heterophilically interact with Latrophilins and that this binding is able to support stable intercellular cell-adhesion. This is further supported by other studies. Indeed Tenm2 was initially identified as a high-affinity, endogenous ligand of Latrophilin 1 and provisionally named Lasso, until molecular cloning and peptide sequencing identified the ligand as a splice variant of Tenm2 (Silva *et al.*, 2011). A different study, which investigated interactions between Latrophilin 3 and FLRT proteins, revealed that all four Teneurins are strong candidate ligands of Latrophilin 3 by affinity chromatography and mass spectrometry, however this interaction was not further assayed by pull-downs (O'Sullivan *et al.*, 2012). A subsequent investigation of the role of Latrophilin 3 in synaptic transmission, development and abundance confirmed that Tenm1 binds to Latrophilin 3 using a surface binding assay (O'Sullivan *et al.*, 2014). Interestingly, the Olfactomedin and Lectin domains in the globular extracellular domain of Latrophilin 3 were found to mediate binding of Tenm1 (O'Sullivan *et al.*, 2014). Finally, Olfactomedin 1 itself was found to bind to Tenm4 (Nakaya *et al.*, 2013).

There is some ambiguity as to the binding affinity between different Latrophilin and Teneurin members. Using affinity chromatography and mass spectrometry, all four Teneurins were identified as Latrophilin 1 and Latrophilin 3 ligands in two of the aforementioned studies (O'Sullivan *et al.*, 2012; Boucard, Maxeiner and Südhof, 2013),

whilst another study only identified Tenm2 as a ligand of Latrophilin 1 (Silva *et al.*, 2011). Furthermore, only Tenm2 and Tenm4 were confirmed as high-affinity ligands of Latrophilin 1 in subsequent pull down experiments (Boucard, Maxeiner and Südhof, 2013), and Tenm1 was confirmed as a ligand of Latrophilin 3 using a surface binding assay (O'Sullivan *et al.*, 2014). Additional information is needed to identify further heterophilic Teneurin binding partners and how these proteins interact with each other.

1.2.5 Teneurins in development

Since the discovery of Teneurins many studies have attempted to characterise the endogenous function of Teneurins and have provided evidence of their fundamental importance in basic developmental events. For instance, knockdown of Teneurin in *C. elegans* with RNAi was found to lead to a broad range of phenotypes that include fundamental developmental processes such as cell migration and axon pathfinding (Drabikowski, Trzebiatowska and Chiquet-Ehrismann, 2005). Teneurin deletion mutants had an abnormal nervous system and gonadal disintegration (Drabikowski, Trzebiatowska and Chiquet-Ehrismann, 2005). An independent study found that Teneurin *C.elegans* mutants display enhanced lethality as well as gross defects in epidermal development and body wall musculature (Trzebiatowska *et al.*, 2008). These phenotypes arise from the disruption of the interaction of Teneurin with the Integrin and Dystroglycan homologues *ina-1* and *dgn-1*, which together are thought to regulate collagen IV and maintain basement membranes during embryonic development. In *Drosophila*, the picture is less clear, since conflicting evidence was presented about Teneurin function in early developmental events. Whilst Ten-m was initially thought to be a pair-rule gene (Baumgartner *et al.*, 1994; Levine *et al.*, 1994), it was later found that it is not responsible for segmentation defects, but rather important for appropriate motor axon guidance (Zheng *et al.*, 2011). Knockdown of Ten-m and Ten-a was found to lead to loss of photoreceptors in addition to defects in the size, shape and rotation of ommatidia, the *Drosophila* eyes, suggesting a role in cell proliferation and/ or survival as well as cellular specification (Kinel-Tahan *et al.*, 2007). Furthermore, Teneurins have been shown to instruct appropriate synaptic partner matching between select pairs of pre- and postsynaptic olfactory neurons as well as presynaptic motorneurons and

postsynaptic muscles via homophilic transsynaptic interactions (Hong, Mosca and Luo, 2012; Mosca *et al.*, 2012; Mosca and Luo, 2014).

1.2.6 Teneurins in neuronal wiring

Whilst Boucard *et al* (2014) argue that Teneurins cannot function as homophilic synaptic adhesion molecules because their interaction is insufficient to establish intercellular adhesion, evidence from *in vivo* studies that support a role for Teneurins in neuronal wiring through homophilic adhesion has accumulated over the past years. The most convincing evidence showing that Teneurins play a role in target selection has been delivered by the two aforementioned studies conducted in *Drosophila*. These studies directly demonstrated that Teneurins form homophilic, bidirectional, transsynaptic signalling complexes that regulate synaptic partner matching (Hong, Mosca and Luo, 2012; Mosca *et al.*, 2012). Using a genetic screen, Hong *et al* (2012) identified Teneurins as the only proteins out of 410 candidate cell-recognition molecules to cause mismatching defects in the antennal lobe when overexpressed. Further investigation revealed that Ten-m and Ten-a are each highly expressed in distinct, but partially overlapping, subsets of matching ORNs and PNs. Additionally, Teneurins were expressed at a low level in all glomeruli. Teneurin overexpression caused PN dendrites to lose endogenous connections with ORNs expressing lower levels of Teneurin and mismatch with high-Teneurin expressing ORNs. On the other hand, loss of Teneurins caused PNs to mismatch with low-Teneurin expressing ORNs. Knocking down Ten-m and Ten-a individually caused mild mismatching defects, whilst simultaneous knockdown of both Teneurins greatly enhanced mismatching. Finally, they detected strong homophilic interactions between Ten-m and Ten-a respectively using coimmunoprecipitations from lysates of Drosophila S2 cells transfected with Teneurins. The results of this study showed that Teneurins instruct connection specificity through homophilic attraction, by matching Ten-m or Ten-a levels in PN and ORN partners. The same group also showed that homophilic attraction between Ten-m in motor axons and postsynaptic muscles is required for appropriate target selection (Mosca *et al.*, 2012). Indeed, RNAi mediated knockdown of Ten-m in either muscles or motor neurons resulted in a loss of muscle innervation, whereas overexpression of Ten-m in either muscles or neurons biased target choice and resulted

in ectopic connections. These results provided further evidence to show that Teneurins exert homophilic transsynaptic attraction at the NMJ and in the olfactory system. Interestingly, both studies found that synaptic partner matching involves homophilic interactions, however, synapse organisation appears to preferentially involve heterophilic interactions (Mosca *et al.*, 2012).

In vertebrate systems, Teneurins are likely responsible for analogous processes and their roles have been best characterised in the visual pathway. Mice with targeted deletion in Tenm2 and Tenm3 exhibit phenotypes which affect different aspects of ipsilateral connections from the retina to the brain and result in impaired binocular vision (Leamey *et al.*, 2007; Dharmaratne *et al.*, 2012; Young *et al.*, 2013). As noted above, Tenm3 is expressed in topographically corresponding gradients in interconnected regions of the visual pathway. This, together with the homophilic adhesion properties of Teneurins, suggested that Tenm3 may play a role in instructing connectivity along the visual pathway in the manner of a homophilic chemoaffinity molecule, as hypothesised by Langley and Sperry (Langley, 1895; Sperry, 1963). This hypothesis was tested by anterograde tracing in a Tenm3 knockout mouse, which revealed aberrant mapping of ipsilateral retinal projections to the dLGN and superior colliculus (Leamey *et al.*, 2007; Dharmaratne *et al.*, 2012; Chun & Hindges, unpublished). Specifically, axons from ventrotemporal RGCs, which exclusively project to the ipsilateral dorsomedial dLGN and rostromedial superior colliculus in wild type mice, were found to send aberrant projections to ventrolateral dLGN and caudomedial superior colliculus in Tenm3 knockout mice (Leamey *et al.*, 2007; Dharmaratne *et al.*, 2012). This resulted in profound visual deficits, such as loss of stereoscopic depth perception, likely due to interocular mismatch. Furthermore, it was shown that mismapped ipsilateral input is conveyed to the primary visual cortex (V1), where binocular stimulation is suppressed (Merlin *et al.*, 2013). Deletion of Tenm2 also resulted in changes to the ipsilateral visual pathway, however these changes did not affect topographic mapping but instead manifested in the form of reduced projections from the retina to the dLGN and superior colliculus (Young *et al.*, 2013). Interestingly, even though Tenm2 expression is uniform across the RGC layer, loss of Tenm2 only affected ipsilateral projections, which originate from the ventral retina. This suggests that Tenm2 may exert an important part of its function through interactions with other molecules that are yet to be identified. Behavioural assessment showed that the

reduction in ipsilaterally projecting neurons was associated with a loss of visual acuity, especially in the dorsal visual field (Young *et al.*, 2013). In the wallaby, Tenm3 is expressed in a similar pattern as in mice, and retinal overexpression of Tenm3 was found to result in an extension of the ipsilateral projection area in the dLGN and superior colliculus (Carr *et al.*, 2013, 2014). In zebrafish, Tenm3 was found to be required for appropriate functional and morphological connectivity of the visual system. Knockdown of Tenm3 resulted in stratification and mistargeting defects of RGC dendrites in the IPL as well axonal arborisation defects in the tectum (Antinucci *et al.*, 2013). Moreover, functional analysis of these fish revealed a selective deficit in orientation selectivity, suggesting that Tenm3 plays a role in wiring subsets of functionally defined visual circuits. Together, these studies demonstrate that altered expression of Tenm3 and Tenm2 leads to loss of axonal targeting specificity in the vertebrate visual circuit. This is consistent with the proposed homophilic synaptic partner-matching role of Teneurins described above for *Drosophila*.

1.2.7 Teneurins in synapse formation

In addition to having important roles in neuronal wiring, Teneurins have also been implicated in synapse formation. However, the synaptic role of Teneurins has only just begun to be investigated and is not yet clear. To date, the only direct role of Teneurins in synapse assembly has been elegantly demonstrated in *Drosophila* (Mosca *et al.*, 2012; Mosca and Luo, 2014). While homophilic Ten-m interactions were found to regulate target selection between motor neurons and muscles, additional roles were reported for heterophilic interactions between Ten-m and Ten-a. Low, basal levels of presynaptic Ten-a and postsynaptic Ten-m were found to be present at all neuromuscular connections, and knockdown of either component at the NMJ caused a broad range of phenotypes consistent with failures of synaptic assembly. The formation of heterophilic, transsynaptic receptor pairs at the NMJ was demonstrated through immunohistochemistry as well as coimmunoprecipitation of Ten-a and Ten-m from larval synaptosomes. Thus, Ten-a and Ten-m function as bidirectional transsynaptic signalling molecules to organise neuromuscular synapses. This role was distinct from the homophilic transsynaptic interactions shown to regulate synaptic partner matching, which is the last step of neuronal wiring before morphological shifts enable synapse

formation, and drew a critical distinction between Teneurins in synaptic partner matching versus synapse assembly. Observed changes to synapses following disruption of heterophilic Teneurin interactions included: fewer synaptic boutons, failed active zone apposition, changes in vesicle organisation and defects in synaptic transmission. Changes to the cytoskeleton were also observed; these included severe disorganisation of presynaptic microtubules and, to a lesser extent, of post-synaptic spectrin. The interaction of postsynaptic Ten-m with muscle α-spectrin suggested that Teneurins could, at least in part, exert their effects on synapse assembly by organising the cytoskeleton and linking it to the neuronal membrane. The same group then showed that Teneurins mediate appropriate density and structure of synapses in ORNs in the antennal lobe (Mosca and Luo, 2014). Using a fluorescently tagged, short, non-functional version of Bruchpilot (Brp), the main structural component of active-zone T-bars, they were able to fluorescently label the active zone of a subpopulation of ORNs. The authors of this study showed that presynaptic Ten-a and postsynaptic Ten-m regulate central synapse number and active zone structure, thus demonstrating that heterophilic Teneurin interactions also mediate CNS synapse assembly. These findings further confirmed that Ten-a functions upstream of spectrin, supporting the model whereby Teneurins regulate appropriate synaptic assembly by organising the cytoskeleton. Together, these studies identified Teneurins as novel, critical components of the suite of transsynaptic signals, whose function is conserved between peripheral and central nervous system processes.

The synaptic role of Teneurins in vertebrates is much less clear and has only been investigated *in vitro* or indirectly *in vivo*. As described above, cocultured Nb2a cells expressing Tenm2 and Latrophilin 1 were found to aggregate and form junctions that were enriched in both proteins (Silva *et al.*, 2011). Additionally, using a mixed culture assay, the authors of this study showed that Tenm2 expressed on the surface of HEK cells was able to induce strong axonal attraction and artificial presynaptic contacts from hippocampal neurons, but not postsynaptic contacts. On the other hand, Latrophilin 1 was able to recruit synaptic contacts from passing dendrites, but not from axons. Furthermore, immunoelectron microscopy of synaptosomes and immunostaining of cultured hippocampal neurons showed that Latrophilin 1 and Tenm2 are enriched at synapses. In both systems Latrophilin 1 was presynaptic and Tenm2 postsynaptic. These results demonstrate that Tenm2 and Latrophilin 1 form high-affinity intercellular

receptor pairs and suggest that they might interact across synapses to induce synapse formation. Moreover, the extracellular domain of Tenm2 binds to Latrophilin 1 and induces presynaptic calcium signalling (Silva *et al.*, 2011; Vysokov *et al.*, 2016). In an independent study, Latrophilin 1 was found to bind to Tenm2 and Tenm4 and application of the recombinant extracellular domain of Latrophilin 1 to hippocampal cultures decreased excitatory and inhibitory synaptic density (Boucard, Maxeiner and Südhof, 2013). While this showed that Latrophilin 1 contributes to synapse formation and/ or maintenance, it is unclear whether this occurs via the Teneurins or by sequestration of FLRT3, which is also a Latrophilin 1 ligand (O'Sullivan *et al.*, 2012). Latrophilin 3 is required to bind to FLRT3 but not to Tenm1 to maintain its role in synaptic development (O'Sullivan *et al.*, 2014), and it is possible that similar mechanisms might take place for Latrophilin 1. However, it is possible that Teneuerin interactions with Latrophilins act at different synapses, for instance in different layers of the cortex or in the hippocampus. Further studies examining the function of FLRT and Teneurin expression with markers for cortical sublayers may characterise the expression of these proteins in specific subpopulations of neurons and offer insights into the full range of locations in the CNS where Latrophilin and Teneurin interactions may occur. Moreover, because Latrophilin 3 binds to FLRT3 via its Olfactomedin domain and to Tenm1 via its Olfactomedin and Lectin domains, binding of FLRT3 and Tenm1 might be mutually exclusive and implies that Latrophilin 3 may interact with both ligands in different contexts.

In summary, it has been established that Teneurins play important roles in the wiring of vertebrate neural circuits and Tenm3 in particular is required for ensuring correct connectivity in the visual system. Drosophila Ten-m and Ten-a have also been shown to play crucial roles in regulating the abundance and proper organisation of synapses in the olfactory system and NMJ via interactions with the cytoskeleton. While Tenm3 plays important roles in neuronal wiring, no studies have been performed to date investigating Tenm3 at a synaptic level. Findings from *in vitro* studies indicate that Tenm2 may form a heterophilic transsynaptic receptor complex with Latrophilin 1 and induce synapse formation. However, a direct synaptic role for Teneurins in vertebrates has not yet to be shown. Thus, the role of Teneurins at vertebrate synapses remains unknown and an exciting question of great importance for future work.

1.2.8 Teneurins and their relevance for human disorders

Consistent with a critical role in the assembly of neural circuits, Teneurin mutations have been linked to disorders in humans. Tenm1 and Tenm2 genes map onto loci linked to intellectual disability and mutations in these regions are associated with visual and auditory deficits as well as craniofacial and limb abnormalities (Malmgren *et al.*, 1993; Minet *et al.*, 1999; Abuelo, Ahsanuddin and Mark, 2000). Furthermore, several variants of Tenm1 were identified in one family with autism spectrum disorders (ASD; Nava *et al.*, 2012). Mutations of Tenm3 are linked to severe eye and visual defects, including microphthalmia (Aldahmesh *et al.*, 2012), as well as spinocerebellar ataxia (Storey *et al.*, 2009). Tenm3 was also recently identified as a candidate gene for epileptic seizure resistance in a large-scale screen in zebrafish (Hortopan, Dinday and Baraban, 2010), which may have implications for epileptogenesis in humans. Tenm4 has been identified as a susceptibility region for bipolar disorder (Sklar and Group, 2011; Heinrich *et al.*, 2013) and mutations in Tenm4 were implicated in essential tremor (Hor *et al.*, 2015).

In recent years, the synaptic basis of many psychiatric and neurological disorders has received more interest, as many conditions have synaptic aetiologies. These synaptic diseases, or "synaptopathies", are caused by mutations in genes pertaining to the synapse proteome and include ASD, intellectual disability, schizophrenia, bipolar disorder and many other disorders (Grant, 2012). Synaptic cell-adhesion molecules in particular have been strongly linked to synaptopathies. One such example is the Neurexin-Neuroligin complex, which has been linked to schizophrenia and ASD, but the mechanisms by which these proteins contribute to the aetiology of these disorders have proven difficult to ascertain (Südhof, 2008). Because of the genetic association of Teneurins with many synaptopathies and their potential roles in synapse formation and/ or maintenance it is tempting to hypothesise that mutations in Teneurins may contribute to the aetiology of these disorders through synaptic defects. However, understanding of the complete synaptic role of Teneurins is in its infancy. Further work is needed to understand the mechanisms by which Teneurins are regulated and processed *in vivo* and to identify their binding partners and downstream signalling pathways. A recent surge of interest in Teneurins will hopefully resolve some of these issues and offer insights into how Teneurins affect human brain function.

1.3 Hippocampal neurons as a model system

The hippocampus is one of the most intensely studied structures of the brain. The reasons for this are manifold. Firstly, the hippocampus is critical for learning and memory, spatial navigation and major disease states (Andersen, 2007). Secondly, it is a readily recognisable brain structure that can be targeted *in vivo* in a rodent model system or easily isolated for *in vitro* preparations. Thirdly, it has a relatively simple and well-established cytoarchitecture and circuitry, making it an ideal model system for neurobiology. Furthermore, the hippocampus provides the basis for widely used *in vitro* and *in vivo* systems to investigate synapse formation, function and plasticity and thus an extensive database that provides the starting point for new experiments has been generated over the past decades.

The hippocampus also lent itself as an ideal model system to explore the synaptic role of Teneurins. In this thesis, I used an *in vitro* system of dissociated hippocampal cultures and organotypic hippocampal slice cultures, as well as morphological analysis of dendritic spines in CA1 neurons from adult mice. In the following sections I will briefly describe the neuroanatomy and connectivity of the hippocampus followed by an introduction into the structure and function of dendritic spines.

1.3.1 The hippocampus

1.3.1.1 Nomenclature and anatomy

The neuroanatomy of the hippocampus has been studied for more than a century and tens of thousands of research articles on the hippocampus have been produced over the decades (Andersen, 2007). Despite this, there is still no consensus over certain facets of its nomenclature. The nomenclature adapted in this thesis defines the hippocampus as one of several related brain regions that together comprise the hippocampal formation (HF). The HF comprises the dentate gyrus (DG), the hippocampus proper, which consist of CA3, CA2 and CA1 (CA stands for *cornu ammonis*), the subiculum, presubiculum and parasubiculum, as well as the entorhinal cortex (EC; Andersen, 2007; Cutsuridis *et al.*, 2010). The subregions of the HF have three layers with a highly organised laminar distribution (Figure 1.5-a), with the exception of the EC, which has

six layers. In the hippocampus proper, the deepest polymorph layer is called the *stratum oriens* and contains basal dendrites of principal cells, afferent and efferent fibres as well as interneurons. The second layer is the *stratum pyramidale* and contains principal neurons and interneurons. The most superficial layer, the *stratum radiatum*, contains apical dendrites of principal neurons and afferent inputs. In the DG these three layers are, respectively, referred to as the *hilus*, the granular cell layer and the *stratum moleculare*. In the CA region, the *cornu ammonis*, the superficial layer is divided into further sub-layers. In CA3, the following three sublayers are distinguished; most superficially, the *stratum lacunosum moleculare* comprises the apical tufts of CA3 dendrites, followed by the *stratum radiatum*, which contains the apical dendrites of CA3 neurons, and most deeply the *stratum lucidum*, which receives mossy fibre input from the DG. The lamination in CA2 and CA1 is similar to that in CA3, with the exception that the *stratum lucidum* is missing. In the subiculum, the superficial molecular layer is sometimes subdivided into an outer and inner portion. Below that lie the pyramidal cell layer, the *stratum pyramidale*, and the deepest layer, the *stratum oriens*. The EC is commonly divided into a medial (MEC) and lateral (LEC) part. The six layers of the EC are referred to as molecular layer I, stellate cell layer II, superficial pyramidal cell layer III, lamina dissecans, which is the cell-sparse layer IV, deep pyramidal cell layer V and finally the polymomorph cell layer VI.

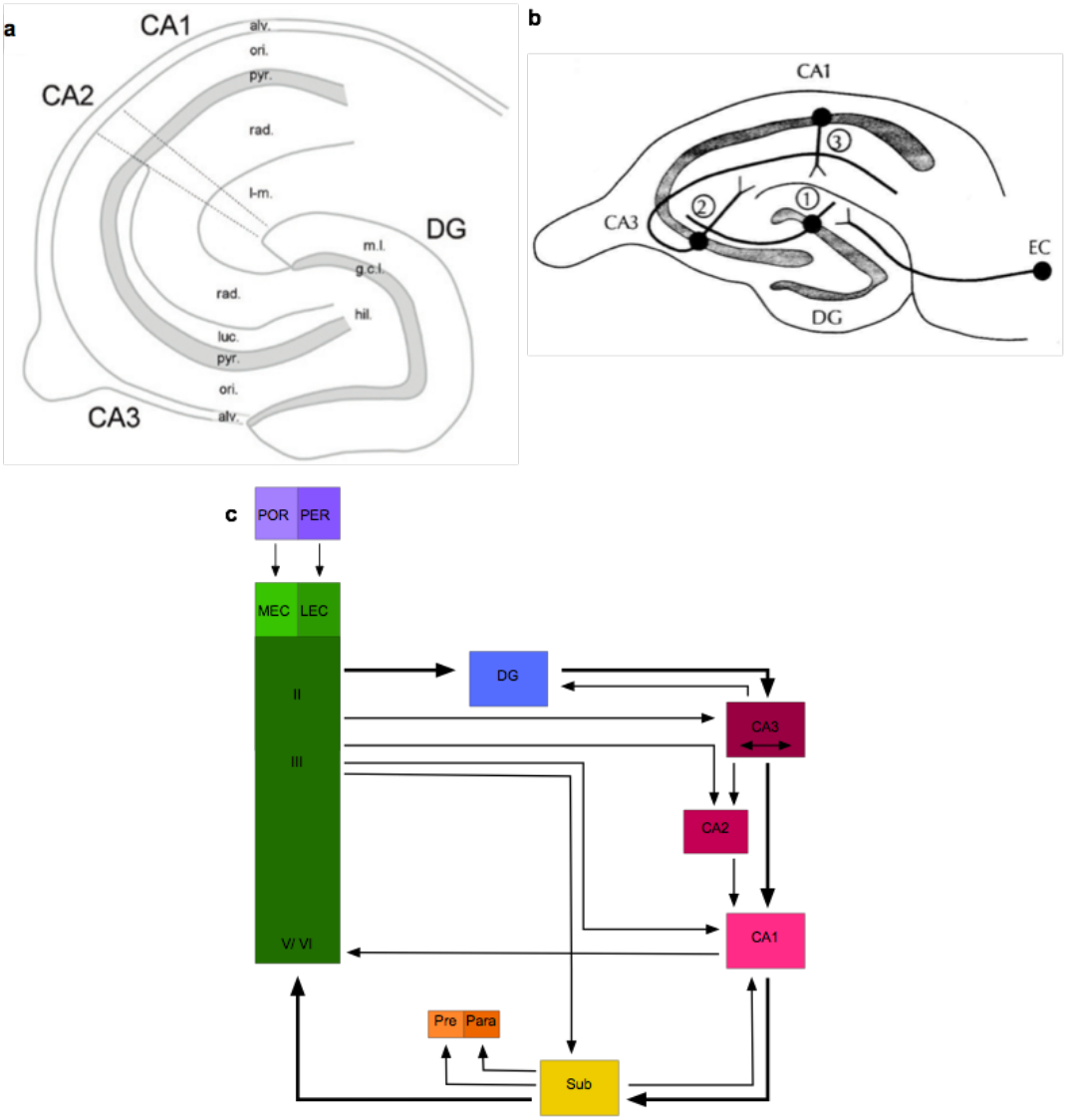

Figure 1.5. Hippocampal anatomy and circuitry. **a.** Areas and layering of the hippocampus depicted in a schematic transverse section of the ventral mouse hippocampus. Dashed lines indicate borders between CA areas. Abbreviations: alv., alveus; ori., stratum oriens; pyr. pyramidal layer; rad., stratum radiatum; l-m., stratum lucidum-moleculare; luc., stratum lucidum; g.c.l., granular cell layer, hil., hilus; m.l., molecular layer. Adapted from Cutsuridis et al. 2010. **b.** The classic tri-synaptic pathway: Neurons from the EC project to the DG through the perforant pathway. The granule cells of the DG project to the CA3 field via mossy fibre projections. Pyramidal neurons in the CA3 field project to CA1 via Schaffer collaterals. Pyramidal cells in CA1 project to the subiculum. Adapted from Amaral, 1993. **c.** Summary of the serial, parallel and back projections through the hippocampal formation. The classic tri-synaptic pathway is represented with thicker arrows.

1.3.1.2 Circuit organisation in the Hippocampus

The organisation of the intrinsic connections in the hippocampus differs from the common features governing connections in the neocortex, in that it is not reciprocal. Indeed, as first described by Ramón y Cajal (1893) the hippocampus has a unique set of unidirectional pathways and is traditionally viewed as having a trisynaptic excitatory feedforward circuit organisation (Figure 1.5-b, Andersen *et al.*, 1971; Andersen, 2007). The majority of the neocortical input reaching the HF passes through the EC, which is why the EC can be considered the first step in the hippocampal circuit. The LEC receives projections from the perirhinal cortex, whereas the MEC receives projections from the postrhinal cortex. Cells in the superficial layer II of the LEC and MEC give rise to axons that project to the DG and form the major hippocampal input pathway called the *perforant pathway*. The granule cells of the DG in turn give rise to axons called mossy fibres, which connect to the pyramidal neurons of CA3, thus forming the *mossy fibre pathway*. Pyramidal CA3 neurons provide the major input to pyramidal neurons of the CA1 field through the *Schaffer collateral* axons, which target both the *stratum oriens* and *stratum radiatum* of CA1. The CA1 field projects to the subiculum, providing its major excitatory input as well as to the deep layers of the EC (Naber, Lopes Da Silva and Witter, 2001). The strong CA1-subiculum projection shows a marked topology, with cells in the proximal one-third of CA1 projecting to the distal one-third of the subiculum and vice versa, cells in distal CA1 target cells in the proximal part of the subiculum (Amaral, 1993). The most prominent cortical projection of the subiculum is directed towards the EC, however it also projects to the presubiculum and the parasubiculum. The output connections of the CA1 field and the subiculum close the hippocampal processing loop, which starts in the superficial layers of the EC and ends in its deep layers.

Over the decades, these pathways were corroborated and additional pathways were described and appended to the trisynaptic model, thus resulting in a more complex, circuit with parallel and back-projections (Figure 1.5-c, Cutsuridis *et al.*, 2010). The projections from the EC to the DG for instance have been extended through tracing studies that drew attention to additional projections from the EC to various areas in the HF. Indeed, the entorhinal layer II also connects to CA3, whereas additional projections, referred to as the *temporoammonic pathway*, connect the entorhinal layer

III to the *stratum lacunosum-moleculare* of CA1 and the subiculum (Figure 1.6; Amaral, 1993). There is also a pathway connecting the superficial layers of the EC as well as axons from CA3 with CA2 pyramidal neurons (San Antonio *et al.*, 2014). CA2 axons in turn project to the *stratum oriens* and, to a lesser extent, the *stratum radiatum* of CA1 (Chevaleyre and Siegelbaum, 2010). Furthermore, CA3 axon collaterals were found to connect to interneurons and other CA3 pyramidal neurons, thus forming an autoassociative network (Le Duigou *et al.*, 2014). In addition to these unidirectional circuits, back projecting pathways have been discovered in the HF. For instance, the DG and CA3 were found to be synchronised via backprojections from CA3 to the DG (Shi *et al.*, 2014). There is also evidence that a significant backprojection exists between the subiculum and CA1 (Xu *et al.*, 2016). This projection is not yet well understood and anatomical studies that have investigated these projections were affected by technical limitations. However, it appears as though the backprojection from the subiculum to CA1 is likely to include excitatory and inhibitory input (Sun *et al.*, 2014; Craig and McBain, 2015). No detailed information is available as to the spread of the projection along the longitudinal axis, but the data indicates no marked topography. In terms of laminar organisation, different studies have found that projections from the subiculum terminate in all three layers of the CA1 field (Xu *et al.*, 2016).

In light of the differential Teneurin expression patterns in the hippocampus and their homophilic and heterophilic binding abilities, some interesting interactions can be envisaged. Notably, Tenm2 and Tenm4 are expressed in the DG, CA3 and CA1 early in development (Figure 1.4) and may be involved in homophilic guidance of axons within the trisynaptic pathway. The graded expression of Tenm3 is particularly interesting because it corresponds to the topology of CA1 projections to the subiculum, suggesting that Tenm3 may be involved in instructing connectivity along this pathway via homophilic attraction. Tenm3 is also expressed in the EC, which indicates that it may be involved in guiding connections from the subiculum and CA1 to the deep entorhinal layers. Furthermore, the distinct but partially overlapping expression patterns of all four Teneurin paralogues raise the possibility of heterophilic Teneurin interactions along the hippocampal circuit.

1.3.1.3 Synaptic organisation in CA1 pyramidal neurons

As the focus of this thesis was mainly on CA1 neurons, in this section I will briefly review their local connectivity, morphological characteristics and synaptic organisation. It is worth noting that although nowadays mice are more commonly used due to the large variety of genetic mutants available, the majority of data on the anatomical structure of pyramidal neurons is still from the rat hippocampus.

Principal neurons in the *cornu ammonis* are tightly aligned and form the well-defined *stratum pyramidale*. The *stratum oriens* is beneath the cell body layer and contains the basal dendrites, whereas the *stratum radiatum* is above the cell body layer and contains the apical dendrites. Both these layers are the innervation zones for the commissural and associational axons respectively originating from the ipsilateral and contralateral CA3 as well as CA2 areas. The CA1 *stratum lacunosum moleculare,* which contains the distal apical tuft, receives input from the EC through the temporoammonic path as well as from the thalamus (Andersen, 2007). CA1 pyramidal neurons are one of the most investigated types of neurons in the brain. They have pyramidal cell bodies, from the apex of which one large-calibre apical dendritic trunk emerges (Figure 1.6). The axon typically originates from the base of the soma, but it can also emerge from a proximal basal or apical dendrite. The main axonal collaterals are found in the *alveus* and are directed towards the subiculum and the EC. Some axonal collaterals are also present in the *stratum oriens* and, to a lesser extent, in the *stratum radiatum,* however local axonal arborisation is limited. The main apical trunk ascends until the *stratum lacunosum-moleculare* and emits many secondary thinner oblique branches in the *stratum radiatum*. There are between nine to thirty oblique branches per neuron, each typically bifurcating just once close to its origin from the apical trunk (Bannister and Larkman, 1995). The apical trunk bifurcates in the *stratum radiatum* or in the stratum *lacunosum moleculare* before forming a dendritic tuft with many thin branches. In the *stratum oriens*, between three to five primary basal dendrites emerge from the base of the soma and bifurcate repeatedly close to the cell body (Megías *et al.*, 2001).

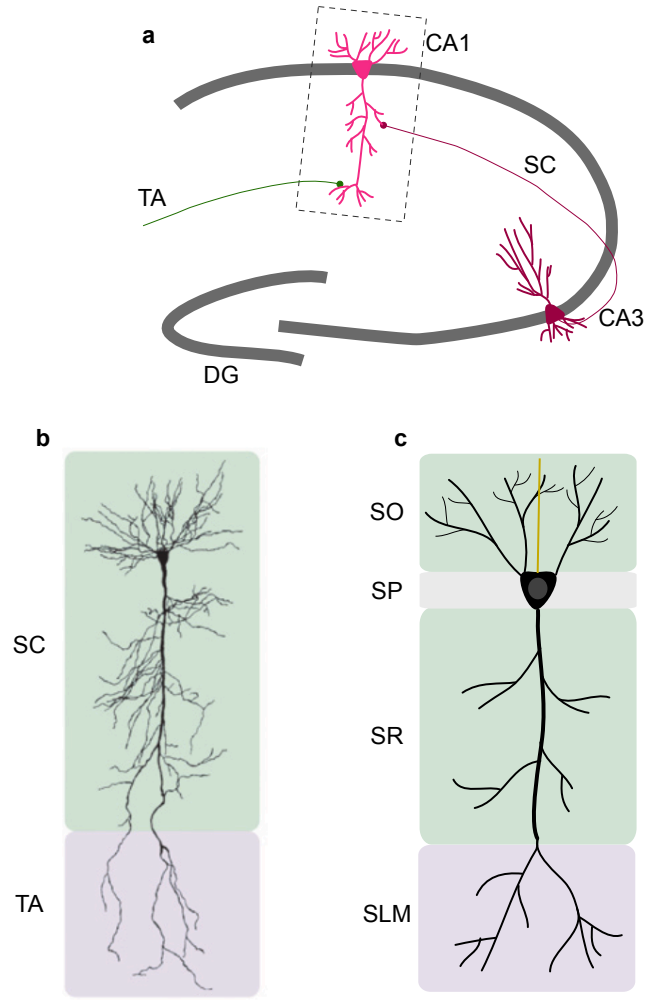

Figure 1.6. CA1 pyramidal neuron structure and domains of synaptic input. **a.** CA1 pyramidal neurons receive input on their proximal dendrites from CA3 pyramidal neurons through the Schaffer collaterals (SC), as well as input on their distal dendrites originating from the entorhinal cortex through the temporoammonic pathway (TA). **b.** Morphological reconstruction of a CA1 pyramidal neuron. The apical tuft, (highlighted in purple) receives excitatory synaptic input through the temporoammonic pathway, the proximal basal and apical dendrites (highlighted in green) receive excitatory synaptic input through the Schaffer collaters. Image reproduced from Spruston, 2008. **c.** Schematic representation of a CA1 pyramidal neuron and its dendritic domains in hippocampal layers. *The stratum oriens* (SO) contains the basal dendrites, the cell body lies in the *stratum pyramidale* (SP), the *stratum radiatum* (SR) contains the apical dendrites and the *stratum lacunosum moleculare* (SLM)

Dendrites of pyramidal neurons are densely covered in spines, which constitute the postsynaptic site of asymmetric glutamatergic synapses. The total number of spines in one rat CA1 neuron has been estimated to average ~32,000 in a detailed morphological study (Megías *et al.*, 2001). The authors of this study found that the distribution of synapses is not homogenous on the dendritic surface of CA1 pyramidal neurons. In the *stratum oriens* thick primary basal dendrites close to the cell body have few or no spines, however thinner, more distal dendrites are covered with numerous spines, averaging a density around 3.4 μm^{-1}. The apical trunk is largely devoid of spines close to the soma but is studded with increasing numbers of spines in the more distal part, reaching a spine density ranging from 2.3 μm^{-1} in the mid-distal and 6.9 μm^{-1} in the far distal area. Oblique apical dendrites are densely covered in spines with a density around 3.5 μm^{-1}. Finally, the apical tuft is sparsely spiny with spine densities ranging from 0.4 to 1.7 μm^{-1}. Whilst typically over 99% of excitatory glutamatergic synapses are estimated to be formed on dendritic spines, in the *stratum lacunosum-moleculare* up to 17% of excitatory synapses are thought to form on dendritic shafts. The number of inhibitory synapses is much lower and CA1 neurons are estimated to receive an average of ~ 1,700 GABAergic inputs, which corresponds to 5.3% of the total synaptic population. Whilst pyramidal cell bodies are devoid of excitatory synapses, a large proportion of inhibitory synapses are found in the perisomatic region, with 7% of inhibitory synapses contacting the soma and the axon initial segment (AIS) and 33% contacting proximal dendrites. Inhibitory synapses are sparse in basal and apical dendrites, where they make up 4-5% of all synaptic input, but more abundant in the apical tuft, where this proportion increases to 16%. The majority (98%) of inhibitory synapses are formed on dendritic shafts, however in the *stratum lacunosum moleculare* between 10-20% of inhibitory terminals have been found to contact spines (Megías *et al.*, 2001).

1.3.2 Dendritic spines

Electron microscopic (EM), immunocytochemical and physiological analyses have all converged to the conclusion that the vast majority of dendritic spines receive excitatory glutamatergic input and that spine density can be used as a reasonable measure of excitatory synapse density (Harris, Jensen and Tsao, 1992; Megías *et al.*, 2001;

Andersen, 2007). In this thesis, dendritic spine density was analysed to evaluate the effect of a loss of Tenm3 on synapse formation. In the next sections, I will briefly describe the morphology, main components and plasticity mechanisms of dendritic spines.

Dendritic spines are tiny dendritic protrusions that typically consist of a bulbous head that contacts the axon, a constricted neck in the middle, and a delta-shaped base that connects the spine with the dendritic shaft (Figure 1.8). Spines exhibit a diverse range of sizes, lengths and shapes and, based on their morphology, they are typically categorised into four different classes identified in EM studies (Figure 1.7); "stubby spines", "sessile spines", "long thin spines" and "mushroom spines" (Peters and Kaiserman-Abramof, 1970; Harris and Stevens, 1989; Harris, Jensen and Tsao, 1992; Kater and Harris, 1994; McKinney *et al.*, 1999; Sorra and Harris, 2000; Hering and Sheng, 2001). These types of spines are not restricted to any particular region of the CA1 dendritic tree, but can be found in close proximity on any dendritic branch. Different spine morphologies can reflect different inputs. For example, in the lateral nucleus of the amygdala cortical inputs synapse exclusively onto thin spines, whereas thalamic inputs synapse onto mushroom spines (Humeau *et al.*, 2005). However, different synaptic inputs don't always translate into different spine shapes, as illustrated by CA1 neurons, which can receive CA3 inputs onto both thin and mushroom spines (Harris and Stevens, 1989).

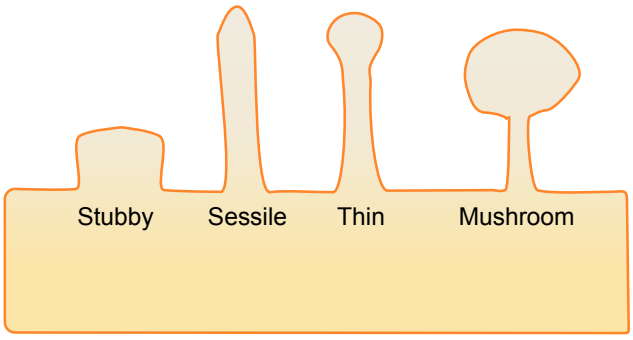

Figure 1.7. Morphological classification of dendritic spines. Spines can be grouped into four different types according to their morphology; stubby, sessile, thin and mushroom spines.

1.3.2.1 Molecular composition of dendritic spines

Dendritic spines contain numerous organelles. One prominent feature of spines is the PSD, an electron-dense thickening of the postsynaptic membrane. The PSD is located at the tip of the spine head, directly opposed to the presynaptic active zone and can either be perforated or non-perforated. Perforated PSDs have complex shapes and are more enriched in AMPA receptors than non-perforated PSDs, which are smaller and disk-like (Nusser *et al.*, 1998). Functionally, the PSD is a biochemical specialisation that enables numerous molecules, such as ion channels, receptors, adhesion molecules, scaffolding proteins, and kinases, to be associated in a structural array at the synapse (Feng and Zhang, 2009; Sheng and Kim, 2011). The three types of glutamate receptors hosted by the PSD are: NMDA, AMPA and metabotropic glutamate receptors (mGluR). Spines also contain smooth endoplasmic reticulum (SER), which is found in about half of all spines in CA1 and mostly present in large, complex spines (Spacek and Harris, 1997). Occasionally, the SER elaborates into a spine apparatus, which consists of stacks of SER and polyribosomes and its function is unknown. Free polyribosomes and mRNA are also contained in spines, indicating that proteins can be synthesised in individual spines. The main cytoskeleton component of spines is actin, which also facilitates spine motility (Hotulainen and Hoogenraad, 2010). Spines notably lack microtubules and neurofilaments, which are restricted to the dendritic shaft (Figure 1.8). The presence of large numbers of molecules in spines together with the separation from the dendritic shaft provided by the neck, have led to the hypothesis that spines represent isolated compartments which segregate postsynaptic chemical responses and enable synapse-specific changes in synaptic-strength (Kater and Harris, 1994). The geometry of the spine neck is thought to regulate postsynaptic calcium diffusion between dendrite and spine.

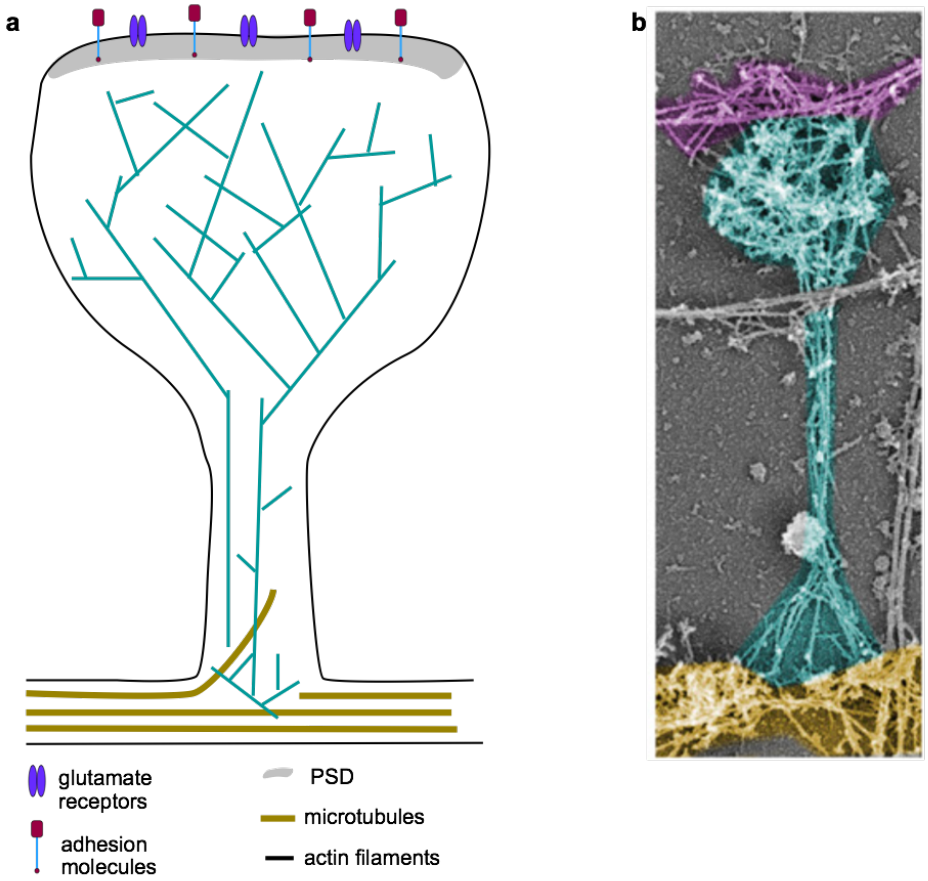

Figure 1.8. Cytoskeletal organisation of dendritic spines. **a.** Schematic diagram of a mature mushroom type spine. Microtubules are restricted to the dendritic shaft, the actin-cytoskeleton is formed of a continuous network of branched and straight actin filaments. The actin cytoskeleton is spread in the spine base, constricted in the spine neck and extensively branched in the spine head. **b.** A mature mushroom spine visualised by platinum replica EM. The axonal cytoskeleton is highlighted in purple, the dendritic shaft in yellow and the spine head and neck in cyan. Adapted from Korobova & Svitkina, 2010.

1.3.2.2 Actin organisation in dendritic spines

The distinctive architecture of dendritic spines is created by a specialised cytoskeletal structure. Actin was identified as the major cytoskeletal component of dendritic spines in early electron microscopy studies (Matus *et al.*, 1982) and extensive research showed that the actin cytoskeleton controls the formation, dynamics and structure of spines (Halpain, 2000; Ethell and Pasquale, 2005; Tada and Sheng, 2006; Hotulainen and Hoogenraad, 2010). Both globular (G-actin) and filamentous actin (F-actin) are present in spines and the ratio of G-actin to F-actin reflects the dynamics of actin polymerisation. Actin in the spine head forms a network of short and branched

filaments with longer bundles in the core region and finer fibres at the periphery (Figure 1.8). The spine neck contains long linear as well as branched actin filaments (Korobova and Svitkina, 2010). In addition, actin filaments at the tip of spine heads were shown to be highly dynamic with very short turnover rates (~ 40 seconds; Star, Kwiatkowski and Murthy, 2002), whereas actin filaments at the base of the spine head are much more stable with long turnover rates (~ 17 minutes; Honkura *et al.*, 2008). Based on these distinct turnover rates, the existence of two F-actin pools that dynamically regulate the structure and plasticity of spines has been proposed (Kuriu *et al.*, 2006; Wang and Zhou, 2010); a dynamic actin pool, which controls movement of the spine, and a stable pool, which maintains the size, shape and PSD components of spines. However, a third calmodulin-dependent actin pool was recently discovered. This pool of actin filaments with a turnover time of 2-15 minutes, termed the "enlargement pool", appears at the tip of the spine head during spine enlargement and generates an expansive force, which is likely to control spine volume (Honkura *et al.*, 2008).

1.3.2.3 Dendritic spine motility

Dendritic spines were traditionally assumed to be relatively immobile structures, however in the past two decades advances in imaging techniques have revealed that spines are dynamic and constantly changing their shape. Time-lapse two photon microscopy studies, and more recently super resolution stimulated emission depletion (STED) microscopy (Nägerl *et al.*, 2008), have shown that spines are inherently motile, constantly undergoing rapid (seconds to minutes) changes in shape and size ("morphing") without permanently altering either parameter (Fischer *et al.*, 1998; Dunaevsky *et al.*, 1999, 2001). These changes, which are macroscopically observed as "dancing" of spines (Halpain, 2000), are in fact mediated by a dynamic movement of the actin cytoskeleton. This movement results from the addition (polymerisation) and removal (depolarisation) of monomeric G-actins at the barbed and pointed ends of F-actin respectively. This process termed 'actin treadmilling' leads to a dynamic turnover of actin filaments without altering the length of F-actin. Spine morphing seems more prominent in dissociated cultured neurons (Fischer *et al.*, 1998; Korkotian and Segal, 2001; Star, Kwiatkowski and Murthy, 2002), likely due to fewer structural constraints and reduced glial contact. However, spine morphing has also been reported in cultured and acute brain slices (Dunaevsky *et al.*, 1999) as well as *in vivo* (Lendvai *et al.*, 2000;

Oray, Majewska and Sur, 2004), thus dispelling the idea that spines surrounded by neuropil are static and do not move. Furthermore, spine motility decreases with age (Dunaevsky *et al.*, 1999; Lendvai *et al.*, 2000; Oray, Majewska and Sur, 2004) and is inversely correlated with the activity of the synapse (Korkotian and Segal, 2001). The functional significance of spine morphing remains unclear, but it may fulfil a searching function during synaptogenesis (Bonhoeffer and Yuste, 2002) and facilitate the diffusion of molecules through the plasma membrane into spines (Richards *et al.*, 2004).

Dendritic spines are also capable of larger amplitude movements, especially early during development. Early in postnatal life, dendritic spines show dramatic structural changes and can even appear or disappear over minutes to hours (Lendvai *et al.*, 2000). Spines are continuously formed and eliminated during postnatal life, however the rates of net turnover are developmentally regulated and decrease as synaptic circuits mature (Alvarez and Sabatini, 2007; Holtmaat and Svoboda, 2009). Several studies have investigated the morphological plasticity of dendritic spines in the mature brain and showed an age-dependent decline in spine turnover. In different regions of the cortex dendritic spines are largely stable and persist for weeks to months. The percentage of stable spines during a one month period in young adult mice (1-2 months old) ranged from ~55% in the somatosensory cortex (Trachtenberg *et al.*, 2002; Holtmaat *et al.*, 2005) to ~75% in the visual cortex (Grutzendler, Kasthuri and Gan, 2002; Majewska and Sur, 2003) and this proportion increased to ~70% to ~90% respectively in mature adult mice (4-5 months old; Trachtenberg *et al.*, 2002; Holtmaat *et al.*, 2005; Zuo *et al.*, 2005). Increased spine stability in mature brains occurs through a decline in the rate of spine elimination (Zuo *et al.*, 2005).

1.3.2.4 Functional plasticity of dendritic spines

Dendritic spines also change their structure in response to receptor activation or hormonal signals. An impressive body of research conducted over the past decades, evidenced by the large number of review articles published on the subject has investigated the role of dendritic spine remodelling in the context of synaptic plasticity (Sorra and Harris, 2000; Hering and Sheng, 2001; Nimchinsky, Sabatini and Svoboda, 2001; Yuste and Bonhoeffer, 2001; Segal, 2005; Hotulainen and Hoogenraad, 2010;

Wang and Zhou, 2010; Sala and Segal, 2014). Growth of new spines and changes to the structure of existing spines are indeed believed to provide a substrate for synaptic plasticity in the hippocampus. Synapses can undergo bidirectional changes in response to stimuli, which cause either long-lasting increases, or decreases in synaptic strength. The first form of synaptic plasticity is termed LTP and thought to underlie memory formation and storage, whereas the latter is termed long term depression (LTD) and considered to be a parallel and opposite process to the more common LTP. LTP and LTD are widely used as helpful paradigms to study the cellular and molecular mechanisms underlying synaptic plasticity and the function and mechanisms of spine remodelling have been extensively studied in this context. Findings from early EM studies (Van Harreveld and Fifkova, 1975; Fifková and Anderson, 1981; Desmond and Levy, 1986; Geinisman, deToledo-Morrell and Morrell, 1991), which were later confirmed by time-lapse fluorescence imaging studies (Lang *et al.*, 2004; Matsuzaki *et al.*, 2004; Yang *et al.*, 2008), have shown that an expansion of the spine head occurs with the induction of LTP. Some, but not all studies also found that LTP resulted in an increase in spine density and de-novo spine formation (Engert and Bonhoeffer, 1999; Toni *et al.*, 1999). However, it remains unclear whether this effect is selective to developing neurons in culture, as *in vivo* studies in adult animals and studies using acute slice preparations have failed to observe increases in spine numbers (Sorra and Harris, 1998; Lang *et al.*, 2004; Popov *et al.*, 2004; Zhang *et al.*, 2015). Enlargement of spine heads is also proportional to an increase in the PSD area (Desmond and Levy, 1986; Nusser *et al.*, 1998; Popov *et al.*, 2004), the number of postsynaptic receptors (Nusser *et al.*, 1998) and the number of presynaptic docked vesicles (Schikorski and Stevens, 1997). Conversely, LTD has been shown to lead to retraction and shrinkage of spines (Na *et al.*, 2004; Okamoto *et al.*, 2004; Zhou, Homma and Poo, 2004). Thus, synapse strength is strongly correlated with spine size.

LTP- and LTD-induced synaptic modifications that are associated with morphological changes in dendritic spines are driven by modulation of actin dynamics in the cytoskeleton (Matus, 2000; Cingolani and Goda, 2008; Hotulainen and Hoogenraad, 2010). Both, LTP- and LTD- inducing activity patterns result in a reduction in the turnover rate of dynamic actin and consequently a reduction in spine motility (Star, Kwiatkowski and Murthy, 2002; Honkura *et al.*, 2008). In the stable actin pool, LTP induction shifts the ratio of G-actin/F-actin toward F-actin, resulting in increased actin

polymerisation and spine volume, whereas LTD shifts this ratio towards G-actin, resulting in depolymerisation and spine shrinkage (Matsuzaki *et al.*, 2004; Okamoto *et al.*, 2004; Yang *et al.*, 2008).

1.3.2.5 Morphological categorisation of dendritic spines

Although the exact contribution of spine remodelling to synaptic plasticity remains unclear, it is evident today that structural modifications (on a morphological and cytoskeletal level) are necessary to support persistent synaptic modifications. In order to identify changes in spine morphology following experimental manipulations, it has proven useful to classify spines according to their shape. The morphology of spines varies over a continuum of shapes from short to long, spines featuring no head to large bulbous heads and thin to thick necks (Figure 1.7). *Stubby spines* are short, wide, lack a clear head or neck and their morphology is best described as a small swelling or protuberance on the dendritic shaft. *Sessile spines* are longer than their diameter but have no discernible head. *Thin spines* have an elongated neck and a small bulbous head. Finally, the most readily distinguishable are *mushroom spines*, which feature a short, constricted neck and a characteristic large bulbous head. It is important to note that there are different nomenclatures and the oldest, most common classification schemes distinguish only between stubby, thin and mushroom spines (Peters and Kaiserman-Abramof, 1970; Harris and Stevens, 1989; Harris, Jensen and Tsao, 1992). In this thesis, a morphological classification of spines was performed to determine whether a loss of Tenm3 leads to a shift in spine morphology.

1.4 Aims

Teneurins are good candidate molecules for controlling interactions between neurons belonging to specific circuits in the brain. They have established roles in neuronal wiring where they are believed to regulate partner matching through homophilic interactions. Furthermore, they have been implicated in synaptic organisation in *Drosophila*, but it remains unclear whether Teneurins have similar synaptic roles in vertebrates. Thus, these proteins remain enigmatic and much remains to be discovered about their roles in synapse formation.

The aims of this thesis were (1) to characterise the subcellular localisation pattern of all four Teneurins *in vitro*, and (2) to explore whether Tenm3 plays a synaptic role *in vivo* by analysing the effect of a loss of Tenm3 in the hippocampus.

In chapter 3, I investigate the subcellular localisation of all four vertebrate Teneurin paralogues *in vitro*.

In chapter 4, I characterise the subcellular localisation pattern of Tenm3 in pyramidal CA1 neurons in detail.

In chapter 5, I explore the functional consequences of a loss of Tenm3 *in vivo* by analysing the density and morphology of CA1 dendritic spines in a mutant mouse line.

Finally, in the discussion I will elaborate on the significance and limitations of the results presented in this thesis.

2 Materials and methods

2.1 Hippocampal cultures

2.1.1 Dissociated hippocampal cultures

Dissociated hippocampal neurons were grown on 18mm diameter glass coverslips (Menzel Glaser, Germany). The coverslips were washed three times in 100% Ethanol, rinsed in distilled H_2O and air-dried. Dry coverslips were sterilised at 220ºC for 3 hours and kept in a sterile glass Petri dish until required. Prior to culturing, coverslips were treated with Poly-L-lysine (50 µg/ml in PBS, Sigma) at 37ºC for one hour, washed three times with distilled water, three times with Dulbecco's phosphate-buffered saline (DPBS, Life Technologies) and then incubated with Laminin (50 µg/ml in PBS, Sigma) at 4ºC over night.

Cultures were prepared from 18 day-old Wistar rat embryos (embryonic day 18, E18) of either sex (Charles River Laboratories). Pregnant Wistar rats were humanely killed using a CO_2 chamber, following the UK Home Office Schedule 1 protocol. The hippocampi of the embryos were rapidly dissected in ice-cold Hank's balanced salt solution (HBSS, Thermo Fisher Scientific). Two hippocampi per tube were digested with 2.5% Trypsin (Thermo Fisher Scientific) for 15 min at 37ºC, then washed three times in HBSS. The hippocampi were triturated through fire polished Pasteur pipettes with increasingly narrow diameter in Neurobasal media (Thermo Fisher Scientific), supplemented with 2% foetal bovine serum (FBS, Life Technologies), 0.5mM GlutaMAX (Thermo Fisher Scientific), 100U/ml Penicillin and 100µg/ml Streptomycin (Invitrogen). The cells were counted using a haemocytometer (Neubauer) and the suspension medium was adjusted to a density of 100,000 cells/ml). 500µl of cell suspension was added per 18mm coverslip (12 well plate, 1ml medium) for a final density of 50,000 cells/ coverslip, and topped up with 500µl Neurobasal media supplemented with 2% B-27 (Thermo Fisher Scientific), 0.5mM GlutaMAX and 100U/ml Penicillin and 100µg/ml Streptomycin. Plates were placed in a tissue culture incubator at 35.5°C with humidified, 5% CO_2. At 7 days in vitro (7DIV) and 14 DIV one third of the media was replaced with fresh Neurobasal plus 2% B-27, 0.5mM GlutaMAX and 100U/ml Penicillin and 100µg/ml Streptomycin.

2.1.2 Organotypic hippocampal cultures

Organotypic hippocampal slices were acquired from 7 day old CD1 mice of either sex (provided by the biological service unit at KCL). The pups were humanely killed through cervical dislocation, following the UK Home Office Schedule 1 protocol. After decapitation, the brains were removed and placed in a petri dish with ice-cold dissecting solution containing 23mM D-glucose (Sigma) in Gey's balanced salt solution (GBSS, Sigma). The hippocampi were dissected and placed on the Teflon stage of a tissue cutter. Coronal slices of 400μm were cut and separated from each other by addition of dissecting solution and gentle mixing in a falcon tube. Well defined and undamaged slices were selected under the microscope and transferred onto sterile, porous (0.4μm) Millicell-CM membranes (Millicell, Millipore) in six well tissue culture plates at a density of 4 slices per membrane. The slices were incubated at 35.5ºC, 5% CO_2 in 1.2ml slice culture medium containing 49% Minimum essential medium (MEM, Gibco), 25% Earle's balanced salt solution (EBSS, Gibco), 25% heat inactivated horse serum (Gibco), 1% B-27 and 35.4mM D-glucose. At 1DIV and every two days thereafter a full media change was done.

2.2 Plasmids and transfections

2.2.1 Expression constructs

The four mammalian expression vectors for Tenm1, Tenm2, Tenm3 and Tenm4 were kindly provided by Tatsuya Okafuji. The full coding sequences of Tenm1 (Figure 2.1), Tenm2 (Figure 2.2), Tenm3 (Figure 2.3) and Tenm4 (Figure 2.4) respectively, were inserted into a pCAGGS4 expression vector. A Myc and His tag were inserted at the end of the coding sequences for detection and purification.

The NCBI Reference Sequence accession number of Tenm1 is NM_011855 and can be viewed at https://www.ncbi.nlm.nih.gov/nuccore/NM_011855. The full coding DNA sequence (CDS) inserted in the Tenm1 expression vector corresponds to 1758 - 9956 bp in the NCBI Reference Sequence accession number NM_011855.

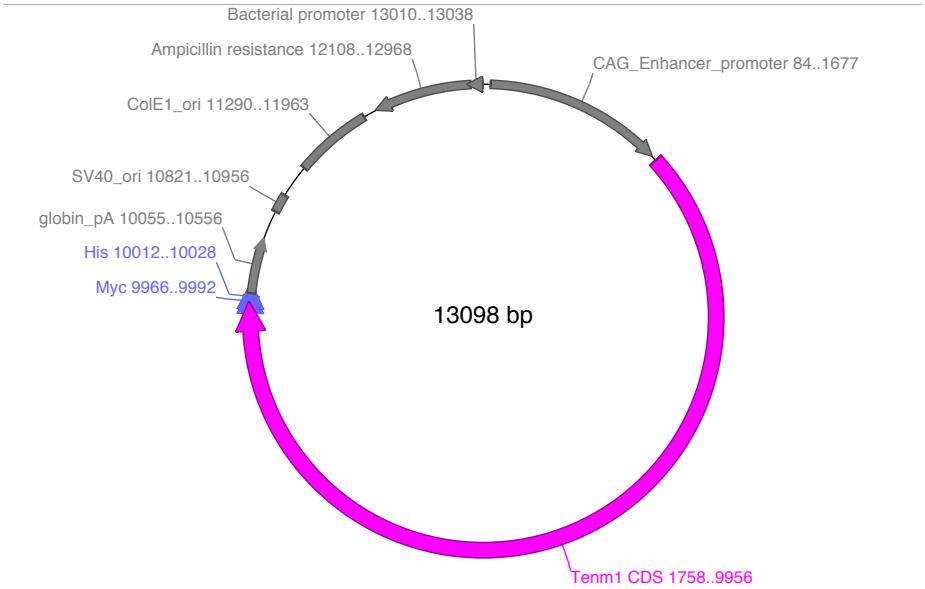

Figure 2.1. Tenm1 expression plasmid map. The expression vector contains a pCAG promoter, the full Tenm1 coding sequence as well as a Myc and His tag

The NCBI Reference Sequence accession number of Tenm2 is NM_011856 and can be viewed at https://www.ncbi.nlm.nih.gov/nuccore/NM_011856. The full CDS inserted in the Tenm2 expression vector corresponds to 50 – 8367 bp in the NCBI Reference Sequence accession number NM_011856.

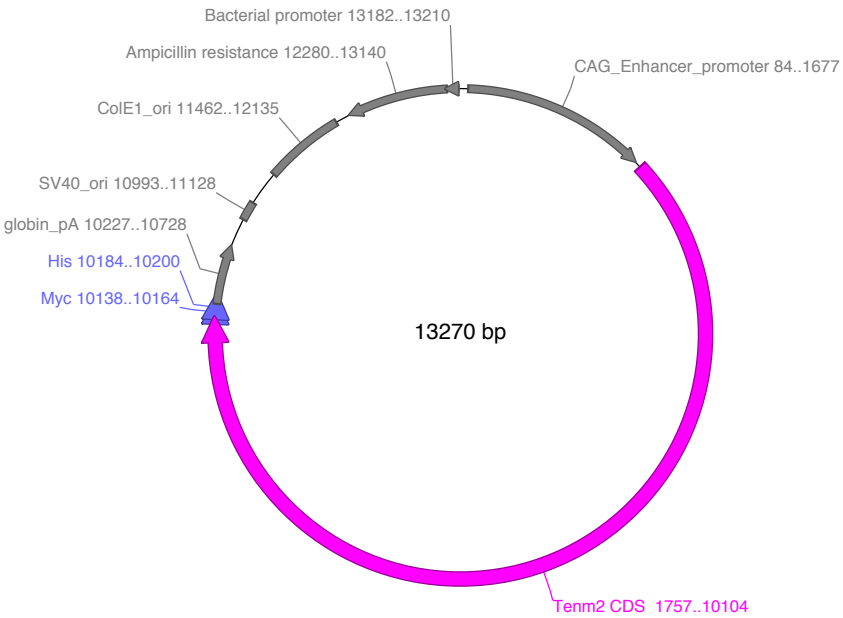

Figure 2.2. Tenm2 expression plasmid map. The expression vector contains a pCAG promoter, the full Tenm2 coding sequence as well as a Myc and His tag.

The NCBI Reference Sequence accession number of Tenm3 is NM_011857 and can be viewed at https://www.ncbi.nlm.nih.gov/nuccore/NM_011857. The full CDS inserted in the Tenm3 expression vector corresponds to 44 – 8194 bp in the NCBI Reference Sequence accession number NM_011857.

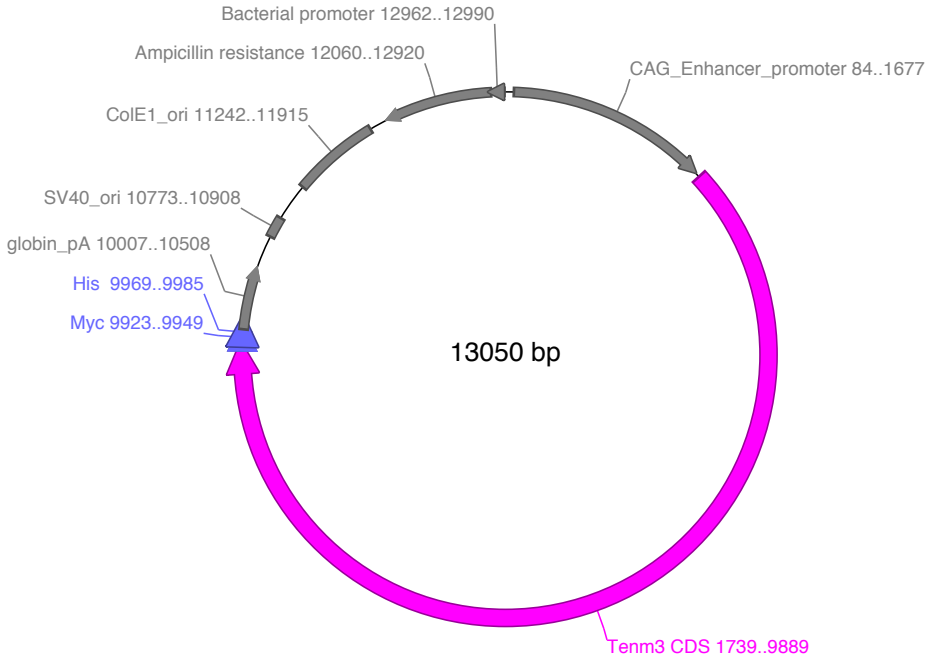

Figure 2.3. Tenm3 expression plasmid map. The expression vector contains a pCAG promoter, the full Tenm3 coding sequence as well as a Myc and His tag.

The NCBI Reference Sequence accession number of Tenm4 is NM_011858 and can be viewed at https://www.ncbi.nlm.nih.gov/nuccore/NM_011858. The full CDS inserted in the Tenm4 expression vector corresponds to 270 – 8668 bp in the NCBI Reference Sequence accession number NM_011858.

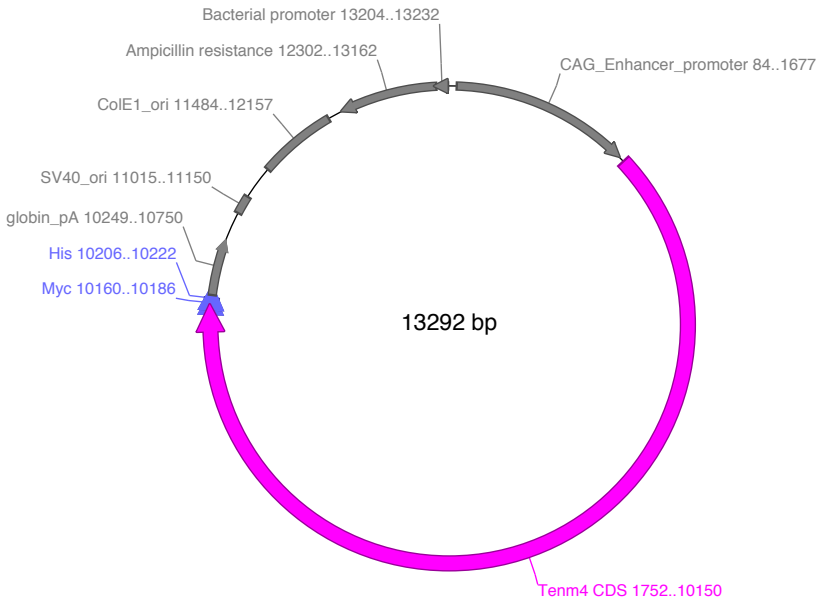

Figure 2.4. Tenm4 expression plasmid map. The expression vector contains a pCAG promoter, the full Tenm4 coding sequence as well as a Myc and His tag.

The membrane-bound GFP plasmid was constructed by Takahiko Matsuda and purchased from addgene. The vector sequence and map can be viewed at http://www.addgene.org/14757/.

The PSD95-TdTomato-FingR and Gephyrin-TdTomato-FingR expression vectors were kindly cloned and provided by Sarah Kemlo (Burrone Laboratory). Gphn-FingR-GFP, PSD-FingR-GFP, Gphn-FingR-mKate and PSD-FingR-mKate constructs was kindly donated by Don B. Arnold (Gross *et al.*, 2013) and vector sequences and maps can be viewed at https://www.addgene.org/Don_Arnold/. Gphn-FingR and PSD-FingR intrabodies with an optimised tdTomato marker in place of GFP or mKate marker were sub-cloned by removing the Gphn-FingR-mKate insert from its vector and replacing it with either a Gphn-FingR-tdTomato (optimised) or a PSD-FingR-tdTomato

(optimised) insert purchased from GeneArt. Gphn-FingR-tdTomato and PSD-FingR-tdTomato constructs were provided in plasmid form from GeneArt.

Plasmid DNA for all the used expression vectors was purified with a Qiagen Midi-prep kit according to manufacturer's protocols. Plasmid DNA was diluted in autoclaved double distilled H_2O to a concentration of 1µg/µl for *in vitro* applications and to 3µg/µl for *in utero* electroporation.

2.2.2 Transfection of neurons

After optimising the transfection protocol as detailed in 3.2.1., the dissociated hippocampal neurons were transfected two days prior to fixation using Lipofectamine 2000 (Thermo Fisher Scientific). One day prior to transfection, the entire cell culture media was replaced with 1ml fresh culture media without antibiotics (Neurobasal media supplemented with 2% B-27 and 0.5 mM GlutaMAX) and the removed conditioned media was stored at 4ºC for later use. For transfection of a single 18 mm coverslip, 0.7 µg of either of the four Teneurin expression vectors, together with 0.2 µg membrane-bound GFP, was diluted in 25 µl Opti-MEM (Thermo Fisher Scientific) and 0.5µl of Lipofectamine 2000 reagent was diluted in a separate tube with 25 µl Opti-MEM. Both were left to incubate for 5 minutes at room temperature. Then, the diluted DNA and Lipofectamine 2000 were added at a 1:1 ratio, mixed very gently and incubated for 25 minutes at room temperature. The DNA-lipid complex was added drop-wise to the coverslip and incubated at 35.5ºC and 5% CO_2 for 15 minutes. After this time, the DNA-lipid complex was entirely removed and replaced with pre-warmed culture media, which contained the reserved conditioned media supplemented 1:1 with fresh cell culture media with antibiotics.

2.2.3 DNA Bullets and biolistic transfection of neurons with a gene gun

To make DNA bullets for biolistic transfection with a gene gun, 0.015g of 1.6µm gold microcarriers (BioRad) were mixed with 100 µl spermidine (0.05 M) and sonicated for 3 seconds. Either 35 µg of Tenm3 expression vector and 10µg of membrane-bound GFP expression vector or 25 µg of membrane-bound GFP expression vector (control

condition), were added to the gold solution and vortexed. Then 100 µl of 1 M calcium chloride was added drop-wise to each of the gold-DNA solutions whilst vortexing. The gold microcarriers were left to precipitate for 10 minutes at room temperature and then centrifuged for 15 seconds. The supernatant was removed and 1ml 100% ethanol was added to the gold microcarriers, vortexed and centrifuged four times. Finally, 3ml of 100% ethanol was added to the gold microcarriers and the gold-DNA solutions were vortexed and sonicated again for 3 seconds. Then the gold-DNA solutions were injected into 70 cm of tubing, which was previously rinsed with 100% ethanol and dried with nitrogen gas at 3-4 LPM flow for 20 minutes in a tubing prep station (BioRad). The gold microcarries were left to settle in the tube for 4 minutes. The ethanol was removed carefully and the tubing was rotated by 180º and left for 4 seconds. Then, nitrogen was passed through the tubing at 5 psi, 3 LPM whilst spinning for 5 minutes. The tubing was chopped using a clean razor blade and the DNA bullets were stored at 4ºC in tubes with silica gel.

Organotypic slices from P7 CD1 mice were transfected at 1DIV. A Helios gene gun was used to shoot organotypic hippocampal slices with a helium pressure of ~140 PSI (~9.5 Bar). After transfection the slices were placed back in the incubator. Gene expression and cell survival was checked after 24 and 48 hours.

2.3 Animals and genotyping

2.3.1 RRD180

The Tenm3 mutant mouse line used in this thesis is a gene trap line called RRD180, named after the embryonic stem cell line used to generate the mutants. The mutation was generated by insertion of the GT1Lxf genetrap vector into the genomic Tenm3 locus. The gene trap vector sequence can be found under http://www.genetrap.org/cgi-bin/vector.py?type=cellline&value=RRD180. The gene trap vector is inserted ~680bp downstream of exon 3, within intron 3-4. The gene trap vector contains a splice acceptor signal at the 5' end, a β-galactosidase selectable reporter tag, and a polyadenylation signal at the 3' end. The splice acceptor should interrupt normal splicing and attach the gene trap cassette, including the β-galactosidase reporter, to the previous exon during the splicing process. The polyadenylation site in the gene trap cassette should cause a premature stop in translation and thus lead to the production of a truncated Tenm3-β-galactosidase fusion protein.

In order to determine the genotype of RRD180 mice used in this thesis, pups were ear clipped either around P14 or prior to transcardial perfusion. To extract the DNA from the tissue, 100 µl NaOH (50 mM) was added to the samples and mixed for 50 minutes at 95°C, 750rpm in a thermomixer (Eppendorf). 10 µl TRIS (1 M, pH 8) were then added to the samples and vortexed. Tubes were then centrifuged at 13.000 rpm for 5 minutes.

Mice were genotyped using primer sequences within intron 3-4 and the genetrap vector as shown in Figure 2.5. To determine whether the mice had a wild type allele, a "wild type" polymerase chain reaction (PCR) was carried out with the "Tenm3 up" primer (from 5' to 3': CTG TCG CCT CCG TGA TAC) and the "Tenm3 low" primer (from 5' to 3': CAG ATG AGC AGA CAG CCA C) leading to a main band at 648bp with strong laddering. Homozygous Tenm3 mutant mice ($Tenm3^{-/-}$ mice that do not have the wild type allele) exhibit no band at 648bp and strong laddering. To determine whether the mice had the mutated allele with the gene trap vector insertion, a "gene trap" PCR reaction was carried out with the "Tenm3 up" primer and the "gene trap low" primer

(from 5' to 3': CAC TCC AAC CTC CGC AAA CTC) leading to a strong band at 474bp with no laddering.

For the PCR, 1 µl of DNA was mixed with 0.5 µl of the appropriate forward and reverse primers respectively, 0.5 µl dNTPs (10mM), 0.2 µl Taq DNA Polymerase, 2 µl 10X PCR Buffer (Roche) and 15.3 µl double distilled, autoclaved H_2O. The PCR tubes were transferred to a pre-heated thermocycler. The conditions for the PCR were set to and initial denaturation cycle of 2 minutes at 94°C, an annealing step of 1 minute at 59°C and an extension step of 45 seconds at 72°C. Thirty cycles with a 30 second denaturation at 94°C were carried out as well as a final hold step of 7 minutes at 72°C.

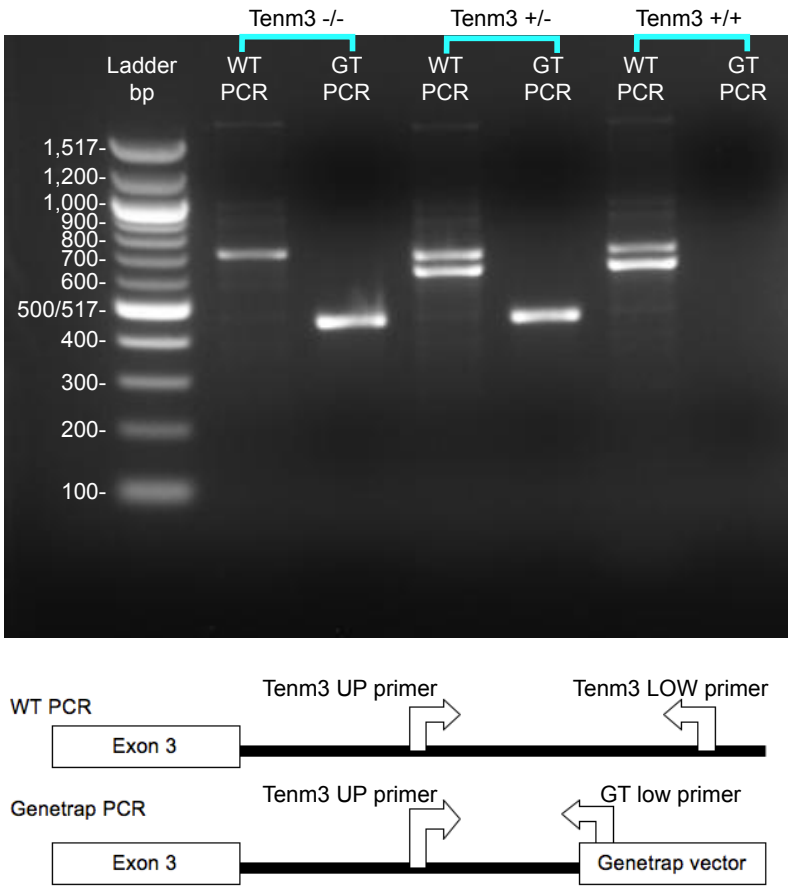

Figure 2.5. Primers used for genotyping RRD180 mice. The genetrap vector is inserted ~680 bp downstream of exon 3, within intron 3-4. Wild type animals exhibit a band at 648 bp with strong laddering in the wild type (WT) PCR reaction. Tenm3-/- mice exhibit no band at 648 bp but strong laddering. Genetrap vector insertion in Tenm3 mutant mice leads to a strong band at 474 bp in the genetrap (GT) PCR reaction. A 100 bp ladder from New England Biolabs was used.

2.3.2 Thy1-GFP

The RRD180 mouse line was crossed to a reporter mouse line, which strongly but sparsely expresses GFP in specific neuronal populations including CA1 neurons. The reporter line used was the Thy1-GFP M-line (Feng *et al.*, 2000).

2.4 Surgical procedures and tissue preparation

2.4.1 *In utero* electroporation

Plasmid DNA solutions were prepared by adding Fast Green (final concentration 0.05%) to Tenm3, PSD95-TdTomate-FingR or Gephyrin-TdTomato-FingR (final concentration 2.25µg/µl) and membrane bound GFP (final concentration 0.75µg/µl). Glass capillaries (1.5mm) were pulled using a Micropipette needle puller (Stutter Instruments) and the tips were cut off under the microscope to achieve a sharp end with a thickness of ~ 0.3-0.4 µm. The pregnant mouse was subcutaneously injected with 0.1mg/kg Vetergesic, and after 20 minutes deeply anaesthetised with Isofluorane in oxygen carrier (oxygen 1.3 L/min) in an induction chamber until loss of righting reflex. The animal was then transferred to a surgery mask on a heating pad and a drop of eye gel was placed on each eye. The abdomen was shaved, cleaned and covered with a sterile drape. The surgery was started after the pedal reflex was lost. The uterine horns were exposed and kept hydrated with sterile, pre-warmed phosphate buffered saline (PBS). Using a mouth pipette, ~0.5µl of DNA solution was injected through the uterus into the lateral ventricle of the embryonic forebrain (E14.5) through the glass micropipette. A drop of PBS was used to wet the paddles of the electrode (Nepagene), which were then placed on either side of the head of the embryo, with the positive paddle on the opposite side to the injected ventricle and angled slightly towards the top of the head. Then five 35V electrical pulses (50 msec duration) were applied with 950 msec intervals using a square pulse generator (CUY21-EDIT, Nepagene). The embryos in the uterus were placed back into the abdominal cavity and the abdomen wall was sutured using Vicryl absorbable sutures. The skin was stapled together using autoclips. The animal was placed in a recovery chamber for 15-20 minutes and then checked 24 and 48 hours after the surgery. The autoclips were removed 4 days after the surgery. The electroporated pups were collected at P21.

2.4.2 Perfusion and tissue collection

Postnatal day 21 mice were deeply anaesthesised by intraperitoneal injection with sodium pentobarbital (Nembutal, 50mg/kg). The procedure was started after the pedal reflex was lost. The thoracic cage was cut open and the heart was exposed. A small

incision in the right atrium was made and the animals were transcardially perfused through the left ventricle with 15 ml PBS followed by 15 ml 4% paraformaldehyde (PFA, Sigma), pH 7.5.

After decapitation, the brains were collected and post-fixed for 24 hours in 4% PFA, pH 7.5. Then brains were stored in 0.05% sodium azide (MP Biomedicals) and PBS until further processing.

2.4.3 Vibratome sectioning

Post-fixed brains were rinsed 3 times in PBS for 5 minutes each. Brains were sectioned in PBS using a Vibratome (Leica) in 100μm serial, coronal sections, from the level of the hippocampus through the entorhinal cortex. Sections were placed in PBS in 24-well plates.

2.4.4 Cryosections

Post-fixed brains were rinsed three times in PBS for 5 minutes and then cryoprotected in 30% sucrose in PBS over night at 4ºC (until the brains sunk to the bottom of the bijou tube). The cerebellum and brainstem were cut off to provide an even surface. Then, the brains were coated with OCT compound in an OCT bath and transferred to a cryomold filled with OCT. The tissue was oriented vertically, with the caudal side at the bottom and the rostral side facing up. The crymold was carefully placed on dry ice. When the OCT compound became solid white, the frozen tissue was stored at -80ºC until further processing.

Brains were cryosectioned (Bright instruments) in 30 μm coronal sections from the level of the entorhinal cortex through the hippocampus, slices were kept at -80ºC until further processing.

2.5 Stainings

2.5.1 Immunocytochemistry

Dissociated hippocampal neurons were fixed for 10 minutes in 2% PFA followed by 10 minutes in 4% PFA (both pH 7.5). Cells were then washed three times in PBS for 10 minutes, permeabilised for 5 minutes in 0.25% Tween 20 (Sigma) in PBS and blocked for 1 hour in 10% normal goat serum (NGS, Sigma) in PBS. Primary antibody incubation was done in 2% NGS, 0.1% Tween 20 in PBS with the appropriate antibodies (Table 1) for minimum 5 hours or over night in a humidified chamber. This was followed by three 20-minute washes in PBS and incubation with the appropriate secondary Alexa Fluor antibodies (Table 1) for 2 hours, protected from light. After further three 20-minute washes in PBS, the coverslips were mounted on glass slides in Fluoromount G (Cambridge Bioscience) and stored at 4ºC, protected from light. All the steps were carried out at room temperature.

2.5.2 Immunohistochemistry

The following protocol was used to stain vibratome slices collected from electroporated P21 Tenm3$^{+/+}$, Tenm3$^{+/-}$ and Tenm3$^{-/-}$ mutant mouse brains and organotypic hippocampal slices. Before staining, organotypic hippocampal slices were fixed for 1 hour at room temperature in 1% PFA, 4% sucrose in PBS, pH 7.5. Organotypic and vibratome slices were washed three times for 10 minutes in PBS. Slices were then permeabilised for 1 hour in 1% Triton X-100 (Sigma), 0.05% sodium azide in PBS. Slices were blocked for two hours in 1% bovine serum albumin (BSA, Sigma), 10% NGS, 0.1% Triton X-100, 0.05% sodium azide in PBS. At this stage, organotypic slices were removed from the cell culture inserts by cutting the membrane around the slice and placed in eppendorf tubes. The blocking solution was removed and the slices were incubated in the primary antibody solution, containing 1% NGS, 0.1% BSA, 0.1% Triton X-100, 0.05% sodium azide and the appropriate antibodies (Table 1), for two days on a rocker plate. Following the primary antibody incubation, slices were washed three times for 20 minutes in 0.1% Triton X-100 in PBS. Then, slices were incubated with the appropriate secondary Alexa Fluor antibodies (Table 1) for 2-3 hours. The slices were washed again three times for 20 minutes in 0.1% Triton X-100 in PBS,

mounted in Fluoromount G and stored at 4ºC, protected from light. All steps were carried out at room temperature and protected from light.

Vibratome slices collected from P21 Tenm3$^{-/-}$/Thy1-GFP, Tenm3$^{+/-}$/Thy1-GFP and Tenm3$^{+/+}$/Thy1-GFP mice were not stained because the GFP signal did not require any amplification. Slices were rinsed in PBS, mounted in Vectashield antifade mounting medium (Vector labs) and stored at 4ºC, protected from light.

Detection of β-galactosidase was attempted in both cryosections and fixed hippocampal slices from RRD180 mice. The same protocol as for organoytpic and vibratome slices was used for hippocampal slices. For β-galactosidase detection in cryosections, slices were thawed at room temperature for 20 minutes and then rehydrated for 10 minutes in PBS. Slides were then incubated in blocking solution, containing 1% NGS in PBS, for 30 minutes at room temperature. The primary antibody solution containing 1% BSA, 1% NGS, 0.3% Triton X-100, 0.01% sodium azide and different concentration of β-galactosidase (1:100, 1:500, 1:1000, 1:2000) antibodies (Table 1) in PBS, was applied to the slices in a humidified chamber and left to incubate over night at 4ºC. Slides were washed three times for 15 minutes in PBS before the appropriate secondary antibody solution was applied to the slices and left to incubate in a humidified dark chamber for 2 hours at room temperature. Slides were washed again three times for 15 minutes in PBS, mounted in Fluoromount G and stored at 4ºC, protected from light.

Table 1. Antibodies used in this project.

Antibody	Supplier	Dilution	Host and isotype
Polyclonal anti-GFP	Abcam	1:1000	Chicken
Monoclonal anti-Myc	New England Biolabs	1:1000	Mouse IgG2a
Polyclonal anti-Synapsin I	Millipore	1:500	Rabbit
Monoclonal anti-Bassoon	Abcam	1:500	Mouse
Monoclonal anti-Shank2	Neuromab	1:500	Mouse
Polyclonal anti-DsRed	Takara Bio Clontech	1:2000	Rabbit
Antibodies that were tested but not used for experiments in this thesis			
Polyclonal anti- vGlut1	Synaptic Systems	1:100 to 1:2000	Rabbit

Monoclonal anti-Gephyrin	Synaptic Systems	1:100 to 1:2000	Rabbit
Polyclonal anti-Gephyrin	Abcam	1:100 to 1:2000	Rabbit
Polyclonal anti-Map2	Millipore	1:500	Rabbit
Polyclonal anti-Tau	Daco	1:2000	Rabbit
Monoclonal anti-Ankyrin G	Neuromap	1:100 to 1:2000	Mouse IgG2b
Polyclonal anti-β-galactosidase	Abcam, ab9361	1:100 to 1:2000	Chicken
Polyclonal anti-β-galactosidase	Abcam, ab616	1:100 to 1:2000	Rabbit
Polyclonal anti-β-galactosidase	Abd serotect, ahp 1292	1:100 to 1:2000	Rabbit
Polyclonal anti-β-galactosidase	MP Biomedicals, 559761	1:100 to 1:2000	Rabbit
Secondary antibodies			
Anti-chicken Alexa Fluor 488	Life Technologies	1:1000	Goat
Anti-mouse IgG2a Alexa Fluor 594	Life Technologies	1:1000	Goat
Anti-rabbit Alexa Fluor 405	Life Technologies	1:1000	Goat
Anti-rabbit Alexa Fluor 568	Life Technologies	1:1000	Goat

2.5.3 X-gal staining

Cryosections were air-dried for 30 minutes at room temperature and then washed in PBS for 10 minutes. The staining solution, containing 2mM magnesium chloride (Sigma), 0.02% NP-40 (Calbiotech), 0.01% sodium deoxycholate, 5mM potassium hexacyanoferrate III (Ferrate III, Sigma), potassium hexacyanoferrate II trihydrate

(Ferrate II, Sigma), was pre-warmed to 37ºC and 40mg/ml X-gal in DMSO was added to the staining solution (final concentration 1.33mg/ml). The X-gal staining solution was applied to the slides in a humidified chamber and incubated at 37ºC. The signal was left to develop for 16 to 20 hours. Slides were washed three times for 10 minutes in PBS at room temperature and counterstained with Hoechst (1:10,000 in ddH_20, Molecular Probes) for 5 minutes. Slides were washed three times for 10 minutes in ddH_2O and then air dried protected from light. Finally, the slides were mounted in Fluoromount G and stored at 4ºC.

2.6 Image acquisition and analysis

2.6.1 Confocal imaging

Organotypic hippocampal slices and coverslips with transfected hippocampal neurons were visually scanned in search of healthy transfected cells using a Zeiss Axioskop and Volocity acquisition software. The same equipment was used to visually scan vibratome slices from RRD180/Thy1-GFP and electroporated RRD180 mouse brains in search for sparse GFP-expressing CA1 neurons. Higher resolution image stacks of selected neurons were then acquired using confocal microscopy.

For confocal imaging of dendritic spines in organotypic slices, vibratome slices and synaptic puncta in dissociated neurons, microscope slides were mounted on a Nikon A1R inverted confocal microscope with a 40× water immersion objective (NA 1.15) and 408-, 488- and 561- nm laser lines. Images were taken at 1x zoom for whole neuron morphology and 3x zoom for spine morphology and synaptic puncta (1x zoom =0.31µm/pixel, 3x zoom = 0.10µm/pixel) and as a z-stack with 0.3µm steps. Images were acquired using the NIS Elements software. Image stacks were exported as raw 16-bit ND2 files.

2.6.2 Brightfield imaging

Brightfield imaging of cryosections after X-gal staining was performed with a Zeiss Axioskop connected to a cooled RGB CCD camera (Retiga EXi Blue) and Volocity acquisition software.

2.6.3 Analysis of colocalisation between Teneurins and a synaptic marker

To analyse the level of colocalisation between Teneurins and Synapsin, images were analysed in ImageJ using the Analyse Particles and Measurements functions. Z-stack images were converted into maximum intensity projections and the Teneurin (imaged in the 561nm laser) and Synapsin (imaged in the 408nm laser) channels were split. The threshold was manually adjusted for every image so that all Synapsin and Teneurin puncta were detected with minimal background. Both thresholded images were

converted into binary images and particles were detected for the binary Teneurin image. The particle analyser was configured to detect particles ranging from 0.1 to 10μm in size and 0 to 1 in circularity ($circularity = 4\pi \times (area/perimeter)^2$) and particles were saved as regions of interest (ROIs). Before proceeding, the Teneurin particle ROIs ($Tenm_{ROIs}$) were overlaid on the original Teneurin image to ensure an accurate depiction of Teneurin puncta and edited if necessary. Then $Tenm_{ROIs}$ were added to the binary Synapsin image and the area and area fraction for each particle were measured. The area fraction measures the percentage of black pixels (thresholded Synapsin puncta) in each $Tenm_{ROI}$ and thus gives a measure of the overlap between Teneurin and Synapsin for every $Tenm_{ROI}$. In the control condition, the same procedure was adopted, except that the Teneurin image was rotated 90º to the right and Teneurin-control particle ROIs ($CtrlTenm_{ROI}$) were detected from the rotated image. All measurements were exported into Igor Pro (Wavemetrics) and analysed using custom–written functions.

In Igor Pro, all Teneurin puncta that overlapped with Synapsin ($Tenm_{ROIs}$ *with fraction area >1*) were extracted for each image in order to calculate the proportion of Teneurin puncta colocalised with Synapsin. Furthermore, all the measurements for every phenotype (Tenm1, Tenm2, Tenm3, Tenm4, Shank2, Bassoon and corresponding controls) were compiled and exported into Prism (GraphPad) for statistical analysis.

2.6.4 Analysis of subcellular Tenm3 localisation in hippocampal CA1 neurons

ImageJ and IgorPro were used to analyse the subcellular localisation pattern of Tenm3 in CA1 neurons in organotypic hippocampal slices. Before carrying out different measurements and analyses detailed in separate sections below, all images were processed as follows; Z-stack images were imported into ImageJ and the Tenm3 (imaged in the 561nm laser) and GFP (imaged in the 488nm laser) channels were split. To reduce noise in the fluorescence intensity measure, a 3D median filter of 2x2x2 pixel was applied to both z-stacks. ROIs were traced in the GFP channel, blind to the Tenm3 channel, and always in the correct focal plane for every spine. Each spine was assigned four different, non-overlapping ROIs: $Spine_{ROI}$, $Shaft_{ROI}$), $Dendrite_{ROI}$ and $Background_{ROI}$ (Figure 4.1) The $Spine_{ROI}$ enclosed the spine head and part of the neck, but did not include pixels within the radius of the dendritic backbone. The $Shaft_{ROI}$ was

traced along the backbone line and radius of the dendrite, centred on each spine. The $Dendrite_{ROI}$ was traced like the $Shaft_{ROI}$ but ~0.5µm more distally on the dendrite. The $Background_{ROI}$ was traced nearby the spine, in a region of the image that was representative of the background fluorescence. To measure the spine intensity for the GFP and the Tenm3 channel the same four ROIs were applied to the GFP and Tenm3 channel respectively and maximum intensity values were measured. The data was then exported into Igor Pro for further analysis.

2.6.4.1 Analysis of Tenm3 localisation in dendritic spines

To analyse the localisation of Tenm3 in dendritic spines only the $Spine_{ROI}$ were used. Due to the variation in fluorescence intensity (FI) between images, the FI value of every spine (FI_{Spine}) was normalised to the median FI of all spines in the image. $Spine_{ROI}$ fluorescence intensity measures were normalised to the median. After this step, the measurements for all spines were compiled for the GFP and Tenm3 channel and the ratio ($Ratio_{Spine}$) of normalised $Tenm3FI_{Spine}$ to $GFPFI_{Spine}$ was calculated in order to asses whether spines had high or low levels of Tenm3 signal.

$$\text{normalised Tenm3FI}_{\text{Spine}} = \frac{\text{Tenm3FI}_{\text{Spine}}}{median(\text{Tenm3FI}_{\text{Spine}})}$$

$$\text{normalised GFPFI}_{\text{Spine}} = \frac{\text{GFPFI}_{\text{Spine}}}{median(\text{GFPFI}_{\text{Spine}})}$$

$$\text{Ratio}_{\text{Spine}} = \frac{\text{normalised Tenm3FI}_{\text{Spine}}}{\text{normalised GFPFI}_{\text{Spine}}}$$

All spines with a $Ratio_{Spine}$ above a certain cut-off value were considered Tenm3-positive spines. The cut-off value was calculated as follows:

$$cut\ off = mean(\text{Ratio}_{\text{Spine}}) + 5 * SEM$$

Next, the proportion of Tenm3 positive spines out of all counted spines was calculated.

2.6.4.2 Analysis of Tenm3 in dendritic shafts

To analyse the levels of Tenm3 in dendritic shafts, intensity values in $Shaft_{ROI}$, $Spine_{ROI}$ and $Background_{ROI}$ were measured in both the Tenm3 and GFP channel. Intensity values for $Shaft_{ROI}$ and $Spine_{ROI}$ were background subtracted ($Tenm3BkFI_{Spine}$, $Tenm3BkFI_{Shaft}$, $GFPBkFI_{Spine}$, $GFPBkFI_{Shaft}$). To avoid division through 0 in subsequent steps, all intensity measures below 30 were reset to 30, which was considered background fluorescence. Then, $Tenm3BkFI_{Spine}$, $Tenm3BkFI_{Shaft}$, $GFPBkFI_{Spine}$, $GFPBkFI_{Shaft}$ were normalised to the median.

$$\text{normalised } Tenm3BkFI_{Spine} = \frac{Tenm3FI_{Spine} - Tenm3FI_{Background}}{median\ (Tenm3FI_{Spine}, Tenm3FI_{Shaft})}$$

$$\text{normalised } Tenm3BkFI_{Shaft} = \frac{Tenm3FI_{Shaft} - Tenm3FI_{Background}}{median\ (Tenm3FI_{Spine}, Tenm3FI_{Shaft})}$$

$$\text{normalised } GFPBkFI_{Spine} = \frac{GFPFI_{Spine} - GFPFI_{Background}}{median\ (GFPFI_{Spine}, GFPFI_{Shaft})}$$

$$\text{normalised } GFPBkFI_{Shaft} = \frac{GFPFI_{Shaft} - GFPFI_{Background}}{median\ (GFPFI_{Spine}, GFPFI_{Shaft})}$$

The measurements from all images were compiled and the ratios of FI_{Shaft} to FI_{Spine} ($Ratio_{Shaft}$) were calculated from the normalised values in each channel.

$$Tenm3Ratio_{Shaft} = \frac{\text{normalised } Tenm3BkFI_{Shaft}}{\text{normalised } Tenm3BkFI_{Spine}}$$

$$GFPRatio_{Shaft} = \frac{\text{normalised } GFPBkFI_{Shaft}}{\text{normalised } GFPBkFI_{Spine}}$$

The $Tenm3Ratio_{Shaft}$ and $GFPRatio_{Shaft}$ were exported into Prism for statistical analysis and to determine whether shafts had high or low intensity levels of Tenm3.

2.6.4.3 Analysis of Tenm3 localisation in dendrites

To analyse the level of Tenm3 clustering in dendritic shafts below the spines, intensity values in $Dendrite_{ROI}$, $Shaft_{ROI}$ and $Background_{ROI}$ were measured in both the Tenm3 and GFP channel. The same steps as for the analysis of Tenm3 in shafts described in 2.6.4.2 were followed, except that $Spine_{ROI}$ was replaced by $Dendrite_{ROI}$. Intensity values for $Dendrite_{ROI}$ were background subtracted ($Tenm3BkFI_{Dendrite}$, $GFPBkFI_{Dendrite}$). To avoid division through 0 in subsequent steps, all intensity measures below 30 were again reset to 30, which was considered background fluorescence. Then, $Tenm3BkFI_{Dendrite}$ and $GFPBkFI_{Dendrite}$ were normalised to the median.

$$\text{normalised Tenm3BkFI}_{\text{Dendrite}} = \frac{\text{Tenm3FI}_{\text{Dendrite}} - \text{Tenm3FI}_{\text{Background}}}{median\ (\text{Tenm3FI}_{\text{Dendrite}}, \text{Tenm3FI}_{\text{Shaft}})}$$

$$\text{normalised GFPBkFI}_{\text{Dendrite}} = \frac{\text{GFPFI}_{\text{Dendrite}} - \text{GFPFI}_{\text{Background}}}{median\ (\text{GFPFI}_{\text{Dendrite}}, \text{GFPFI}_{\text{Shaft}})}$$

The measurements from all images were compiled and the ratios of $FI_{Dendrite}$ to FI_{Shaft} ($Ratio_{Dendrite}$) were calculated from the normalised values in each channel.

$$\text{Tenm3Ratio}_{\text{Dendrite}} = \frac{\text{normalised Tenm3BkFI}_{\text{Shaft}}}{\text{normalised Tenm3BkFI}_{\text{Dendrite}}}$$

$$\text{GFPRatio}_{\text{Dendrite}} = \frac{\text{normalised GFPBkFI}_{\text{Shaft}}}{\text{normalised GFPBkFI}_{\text{Dendrite}}}$$

The $Tenm3Ratio_{Dendrite}$ and $GFPRatio_{Dendrite}$ were exported into Prism for statistical analysis and to determine whether Tenm3 clustered within the shaft.

2.6.5 Quantification and analysis of dendritic spine density and morphology in CA1 neurons in Tenm3 mutant mice

Vibratome slices from RRD180/Thy1-GFP mice were imaged as described in 2.6.1. Z-stacks were imported into Imaris (Bitplane) and dendrites and spines were

reconstructed semi-automatically in the surpass mode. Dendrites were manually traced in the *xy*-plane using the AutoDepth function of the FilamentTracer module. The trace was automatically centred, smoothed, and the reconstruction of the diameter of the dendrite was done in the rebuild dendrite diameter function. The signal threshold for the detection of the dendrites was set automatically using the shortest distance from distance map algorithm and then adjusted manually to ensure accurate reconstruction of the dendrite diameter. For the detection of spines, the thinnest spine head diameter was set to 0.2µm and the maximal spine length was set to 2.5µm. The threshold for spine head detection was set automatically and then adjusted manually to ensure an accurate representation of spines. The signal threshold for the quantification of the spine diameter was set automatically using the shortest distance from distance map algorithm and then adjusted manually to ensure an accurate reconstruction of the spine volume. All dendrite and spine reconstructions were done blind to genotype.

Spine classifications of stubby, filopodial, long thin and mushroom spines were automatically completed through the classify spines wizard within the Imaris software package. Previously published classification schemes were used to distinguish four different types of spines on the basis of the size of their necks and heads (McKinney *et al.*, 1999; Staffend, Loftus and Meisel, 2011; Jung *et al.*, 2013; Gupta *et al.*, 2015). Spines were classified as *thin* if the width of the head and neck were similar (*mean width head* ≥ *mean width neck*). Very short spines were classified as *stubby* (*spine length* <1µm). Spines were classified as *mushroom* if the diameter of the head was much greater than the diameter of the neck (*spine length* <2.5µm and *maximum width head* >*mean width neck**2). All other spines were classified as *sessile*. Because, the maximum spine length was set to 2.5µm, sessile spines had to have no head and a length between 1-2.5µm. Statistics were exported into IgorPro for further processing and then into Prism for statistical analysis.

Spine densities were calculated per dendritic segment. The total number of spines in one dendritic segment was summed and divided by the length of that segment to give the average spine density/10µm. Total spine population and counts of each spine class (stubby, sessile, thin, and mushroom) were summed for each genotype.

2.7 Statistical analysis

Statistical analysis was carried out with Prism (GraphPad). Sample distributions were first assessed for normality with the D'Agostino and Pearson omnibus test. Details regarding the specific parametric or non-parametric tests carried out are reported in the results sections. Alpha values were set to 0.05 and tests were two-tailed for all experiments.

3 Characterisation of subcellular Teneurin localisation in dissociated hippocampal neurons

3.1 Introduction

One of the hallmarks of the brain is the precision with which synaptic connections are formed to become part of complex networks. Synapse formation is a process that has been extensively studied (Mcallister, 2005; Waites, Craig and Garner, 2005; Craig, Graf and Linhoff, 2006; Garner, Waites and Ziv, 2006; Shen, K., Scheiffele, 2010; Siddiqui and Craig, 2011; Chia, Li and Shen, 2013) and an important conceptual framework for understanding the molecular basis of connectivity has been laid down by elegant experiments using invertebrate model organisms like *Aplysia*, *C. elegans* and *Drosophila* (Mast *et al.*, 2006; Margeta, Shen and Grill, 2008). Still, the mechanisms regulating synaptic specificity and synapse formation in the vertebrate brain are incompletely understood. What has become clear, however, is that cell-surface adhesion molecules play a key role in the regulation of distinct aspects of neuronal connectivity, including laminar specificity, cellular specificity, subcellular specificity, synaptic differentiation and synaptic maintenance (Sanes, J.R. & Yamagata, 1999; Washbourne *et al.*, 2004; Dalva, McClelland and Kayser, 2007; Williams, de Wit and Ghosh, 2010; Missler, Südhof and Biederer, 2012; de Wit and Ghosh, 2015).

While Teneurins have established roles in conferring wiring specificity in the vertebrate CNS (Leamey *et al.*, 2007; Dharmaratne *et al.*, 2012; Antinucci *et al.*, 2013, 2016; Merlin *et al.*, 2013; Young *et al.*, 2013; Carr *et al.*, 2014) it remains to be determined whether they also have a synaptic role. Two influential studies in the field of Teneurin research (Hong, Mosca and Luo, 2012; Mosca *et al.*, 2012) revealed that both *Drosophila* Teneurins, Ten-a and Ten-m, interact homo- as well as heterophilically and transsynaptically between select pairs of pre- and postsynaptic partners in the olfactory bulb and the neuromuscular junction. The high degree of conservation across *phyla* (Tucker *et al.*, 2012) indicates that Teneurins might well regulate synaptic specificity through similar mechanisms in vertebrates. As cell-adhesion molecules, Teneurins are ideal candidates to interact across the synaptic cleft, however, with the exception of Tenm2 (Silva *et al.*, 2011), no synaptic localisation of Teneurins in vertebrates has been

reported to date and to our knowledge, the subcellular localisation of the different Teneurins has not yet been examined.

In this chapter I describe my investigation of the subcellular localisation pattern of all four Teneurin paralogues in cultured hippocampal neurons. Due to the lack of an antibody to specifically label individual Teneurins, the subcellular localisation of an epitope tagged Teneurin fusion protein was examined. Synaptic localisation was determined as a measure of colocalisation between Teneurins and the synaptic marker protein Synapsin. I begin by briefly describing the model system followed by the optimisation steps that preceded the establishment of the experimental protocol used in this chapter. Subsequently, I examine the subcellular localisation patterns of Tenm1, Tenm2, Tenm3 and Tenm4 in cultured hippocampal neurons.

3.2 Optimisation of subcellular Teneurin localisation analysis

The subcellular localisation pattern of Teneurins was investigated using dissociated hippocampal cultures. Rodent hippocampal cultures have been extensively used for visualising the subcellular localisation of endogenous or overexpressed proteins and for defining the molecular mechanisms underlying synapse formation (Friedman *et al.*, 2000; Bresler, 2004; Garner, Waites and Ziv, 2006; Gerrow *et al.*, 2006; Grabrucker *et al.*, 2009). One of the most important advantages of this model system is that it makes living neurons immediately accessible to manipulations such as transfection with expression constructs and immunocytochemistry. In addition, the low density and two-dimensional arrangement of neurons in culture is far less complex than neural tissue and thus provides an ideal preparation for imaging the subcellular localisation of neuronal proteins. Primary cultures from the rodent hippocampus lent themselves particularly well for the analysis of subcellular Teneurin expression for two reasons; (1) all four Teneurin paralogues, Tenm1, Tenm2, Tenm3 and Tenm4, are endogenously expressed in pyramidal neurons of the hippocampus (Figure 3.1), which account for the vast majority of the neuronal population in hippocampal cultures. (2) Cultured pyramidal hippocampal neurons pass through well-defined stages of maturation (Dotti, Sullivan and Banker, 1988; Craig and Banker, 1994) and express many of their key morphological features, including the formation of well-developed dendrites and axons, extensive synaptically connected networks (Bartlett and Banker, 1984; Fletcher, De Camilli and Banker, 1994; Grabrucker *et al.*, 2009) and an expression pattern of neuronal proteins that seems to be essentially identical to that of neurons that develop within the intact brain (Garner, Waites and Ziv, 2006).

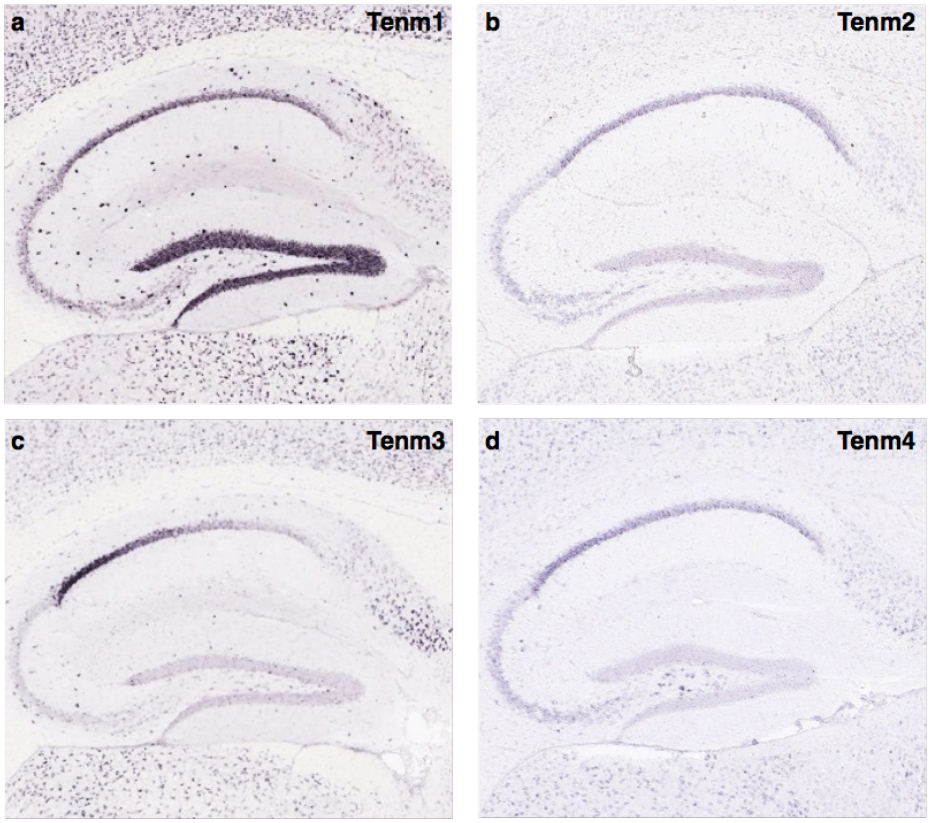

Figure 3.1. Teneurin expression in the hippocampus of adult mouse brains **a.** In situ hybridisation (ISH) for Tenm1 shows that Tenm1 is strongly expressed in the DG and in CA1. **b.** ISH for Tenm2 shows that Tenm2 is weakly expressed in CA3, CA2 and more strongly in CA1. **c.** ISH for Tenm3 shows that Tenm3 is expressed in a strong gradient along CA1. Tenm3 is also exressed in a complementary gradient in the subiculum. **d.** ISH for Tenm4 shows that Tenm4 is expressed in CA3 and CA1. All images are of sagittal sections from adult mouse brains (P56) and were reproduced from the Allen Brain Atlas.

We were not able to obtain antibodies that reliably recognise specific vertebrate Teneurin paralogues (Tenm1-4) without cross-reactivity. Therefore, it was not possible to analyse the subcellular expression pattern of Teneurins using immunohistochemical methods. One common approach to investigate intracellular protein trafficking (Burack, Silverman and Banker, 2000; Perestenko and Henley, 2003; Jensen *et al.*, 2014) and localisation (Arnold and Clapham, 1999; Bresler *et al.*, 2001) has been to exogenously express GFP-tagged proteins in sparse neurons. This method is particularly useful when there are limitations to the use of immunohistochemical approaches either because the application of antibodies to tissue results in too dense labeling to extract information about the localisation of proteins within individual cells, or the lack of an antibody to recognise the protein of interest. Although there are many

reports of GFP-tagged proteins faithfully recapitulating the endogenous protein localisation (Arnold and Clapham, 1999; Craven, El-Husseini and Bredt, 1999; Bresler *et al.*, 2001; Perestenko and Henley, 2003; Jensen *et al.*, 2014), the introduction of exogenous proteins can also have dramatic morphological and functional effects on cells (El-Husseini, Schnell and Chetkovich, 2000; Passafaro *et al.*, 2003). In this project, I used full-length expression plasmids for Tenm1, Tenm2, Tenm3 and Tenm4. The Teneurin expression plasmids all contained a Myc tag inserted after the Teneurin ECD, located on the protein's C-terminus, making it possible to visualise the Teneurin-Myc fusion proteins through subsequent immunohistochemical localisation with antibodies against Myc. The exogenous DNA was introduced into neurons via a cationic lipid-mediated transfection using Lipofectamine 2000, because this method had previously been reported to achieve satisfactory levels of expression (Kaech and Banker, 2006).

3.2.1 Finding the optimal conditions to transfect Teneurins into cultured neurons

Whilst introducing epitope-tagged proteins into sparsely distributed cells can be a useful method to study the subcellular localisation of the protein, overexpression of constructs is also inherently associated with the risk of altering the structure and function of cells and can lead to cytotoxicity. Therefore, it was necessary to establish the optimal transfection conditions for Teneurins in culture before studying their subcellular localisation pattern.

Post-mitotic primary neurons are notoriously more difficult to transfect than cell lines and the size of the vector is a major factor influencing the efficiency of plasmid DNA transfection. Indeed, nuclear delivery of large plasmids is compromised compared with smaller plasmids. Low nuclear delivery of large plasmids is probably due to a limited rate of intracellular transit, whereas smaller plasmids evade degradation by rapid transit through the cytoplasm (Lukacs *et al.*, 2000; McLenachan, Sarsero and Ioannou, 2007). Because Teneurins are large transmembrane proteins and the expression plasmids were of according size (Tenm1: ~13kb, Tenm2: ~13.3kb, Tenm3: ~13kb, Tenm4: ~13.3kb), it was difficult to transfect hippocampal neurons and it was necessary to start by

establishing the appropriate plasmid DNA concentrations to achieve acceptable transfection efficiencies whilst keeping cytotoxicity low (Table 2).

I started by transfecting cells at different ages with different concentrations of plasmid DNA to evaluate the transfection efficiency, cytotoxicity and possible adverse effects on cellular structure. Teneurin expression plasmids were always cotransfected with a separate plasmid encoding mGFP to detect transfected cells more easily and visualise the complete dendritic and axonal arborisations of cells. Initially, this optimisation step was carried out only with Tenm3 and Tenm4. Every condition was tested in 1-5 independent experiments and in each 12-well plate, 3 coverslips were cotransfected with either Tenm3 and mGFP, Tenm4 and mGFP or only transfected with mGFP (control condition). Cells were always plated at a density of ~50.000 cells per 18 mm coverslip.

In the first condition, cells were cotransfected with 0.45µg Teneurin plasmid and 0.25µg mGFP per coverslip at 4 days in vitro (DIV) and fixed at 7DIV. Interestingly, Tenm3 and Tenm4 clustered in puncta along both the axon and dendrites (Figure 3.2). Axons and dendrites were distinguished by their morphology, which was possible for most neurons. Dendrites can generally be recognised because of their characteristic taper, radial orientation and shorter length compared to axons. The axon can be distinguished thanks to its thinner origin and no taper over distance as well as a meandering course, which generally extends over long distances in the coverslip. The transfection efficiency was very low with an average of ~9 Teneurin-GFP cotransfected cells per coverslip (n = 3 independent cultures, cells were plated at density of ~50.000 cells per 18mm coverslip). In the control condition, cells were transfected with GFP only and in average there were ~15 GFP transfected control cells per coverslip. Furthermore, there seemed to be a high degree of cytotoxicity with many transfected cells displaying fragmented neurites, bulging cell bodies (Figure 3.2) and transfected neurons rarely surviving past 7DIV. In an attempt to reduce cytotoxicity, the transfection time was reduced to 10 minutes instead of 15 minutes. However, this led to even lower transfection efficiency with an average of ~2 cotransfected cells per coverslip (n = 1 culture) and no detectable Teneurin expression in GFP expressing cells, whilst there was no considerable improvement in cytotoxicity.

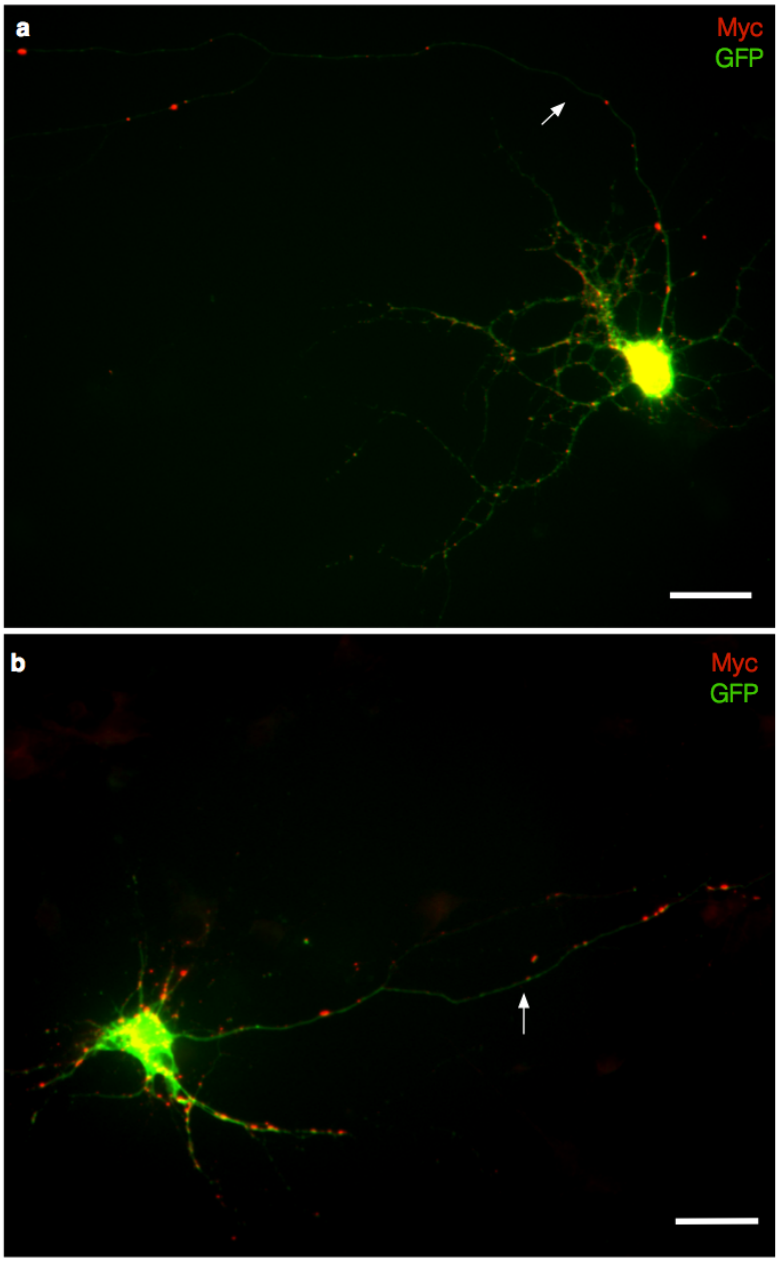

Figure 3.2. Representative images of punctate Teneurin-Myc distribution at 7DIV in dissociated hippocampal neurons. **a.** Image of DIV7 hippocampal neuron transfected with GFP and Tenm3-Myc. The arrow indicates the axon. Punctate Tenm3-Myc can be detected in axon and dendrites. **b.** DIV7 hippocampal neuron transfected with GFP and Tenm4-Myc. Punctate Tenm4-Myc can be detected in axon and dendrites. Both neurons seem unhealthy, which indicates possible toxicity or morphological changes as a result of Teneurin overexpression at 7DIV. Scale bar: 50µm.

We were interested to see whether the observed clustering of Teneurins would be present at an earlier developmental time point. I cotransfected hippocampal neurons with 0.45µg Teneurin plasmid and 0.25µg mGFP per coverslip at 2DIV and fixed neurons one day later at 3DIV (Figure 3.3). Tenm3 and Tenm4 were found diffusely throughout the soma and neurites. However, the transfection was accompanied by some cell death and the efficiency was very low with an average of ~5 cotransfected cells per coverslip (n = 2 independent cultures). Under normal conditions, by 3DIV most neurons in our culture system have broken their symmetry, with a clearly outgrowing axon and dendrites exhibiting some initial branching. The development of cells transfected with Tenm3 and Tenm4 seemed to be restricted, with some cells not exhibiting a clear polarity at 3DIV. Therefore, I could not exclude the possibility of morphological changes as a result of Tenm3 and Tenm4 overexpression, especially at early developmental stages.

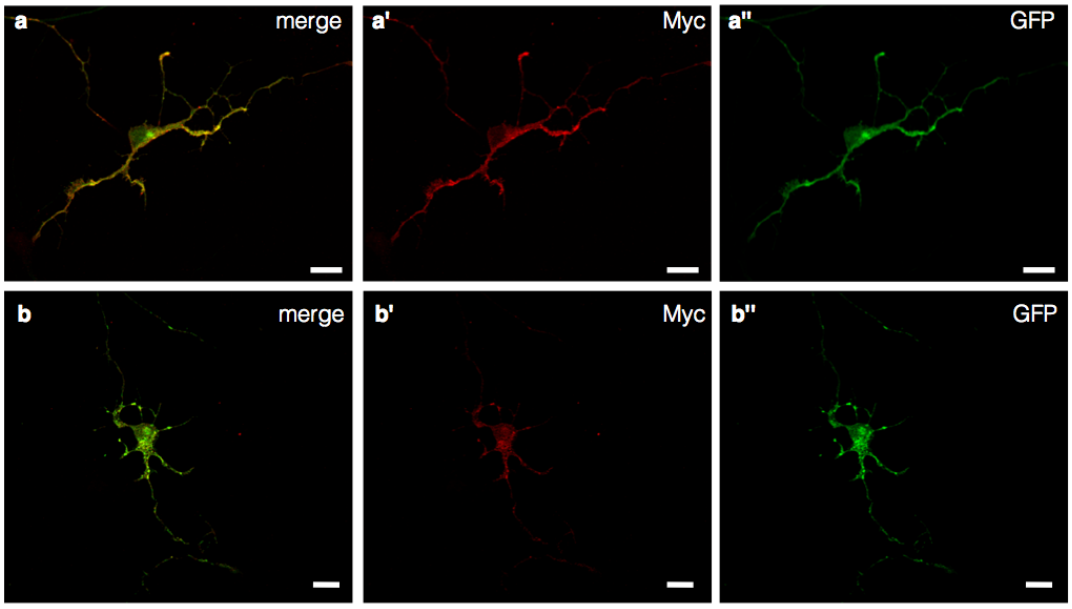

Figure 3.3. Representative images of diffuse Teneurin-Myc distribution at 3DIV in dissociated hippocampal neurons. **a.** Image of DIV3 hippocampal neuron transfected with GFP and Tenm3-Myc. **a** shows the merged image, **a'** the Tenm3-Myc channel and **a''** the GFP channel. **b.** Image of DIV3 hippocampal neuron transfected with GFP and Tenm4-Myc. **b** shows the merged image, **b'** the Tenm4-Myc channel and b'' the GFP channel. Scale bar: 20µm.

The observed punctate Teneurin localisation pattern at 7DIV was reminiscent of that of synaptic proteins and thus the first indicator that Teneurins could indeed be synaptic proteins. In order to evaluate whether Teneurins are synaptic proteins, expression had

to be analysed at a developmental stage at which synapses are a prominent feature of cultured neurons. In dissociated hippocampal cultures, the first synapses are formed around 7DIV and the first dendritic spines, which signal the formation of mature excitatory synapses, can be detected from 10DIV (Grabrucker *et al.*, 2009). Synaptogenesis only slowly increases during the second week of culture before steeply accelerating in the third week. Therefore, 12DIV was selected as a time point when there should be a steady amount of synapses but before the peak of synaptogenesis around 14DIV. In an attempt to reduce the observed cytotoxicity, the time between transfection and fixation was reduced. Neurons were cotransfected at 10DIV with 0.5µg Teneurin plasmid and 0.2µg mGFP per coverslip and fixed at 12DIV. Similar to the previous findings, Teneurins clustered in puncta along dendrites and axons and the transfection efficiency seemed to have improved slightly with an average of ~11 transfected cells per coverslip (n = 2 independent cultures). However, many GFP expressing cells did not express any Teneurin or expressed Teneurin only in the cell body. Cytotoxicity remained high with many cells exhibiting fragmented neurites. Furthermore, many transfected neurons seemed to have either restricted arbors compared to wild type neurons or abundant filopodia-like structures emanating from neurites resulting in a "bushy" look (Figure 3.4). Thus, I could not exclude that Teneurin overexpression might lead to morphological and/ or functional changes at this stage. Because many "cotransfected" neurons seemed to lack Teneurin expression, I increased the Teneurin plasmid concentration to cotransfect neurons at 10DIV with 0.7µg and 0.2µg mGFP before fixation at 12DIV. The increased Teneurin cDNA concentration led to a slight increase in the number of GFP expressing cells that also expressed Teneurin (~14 transfected cells per coverslip, n = 2 independent cultures), however cytotoxicity and morphological aberrations remained the same.

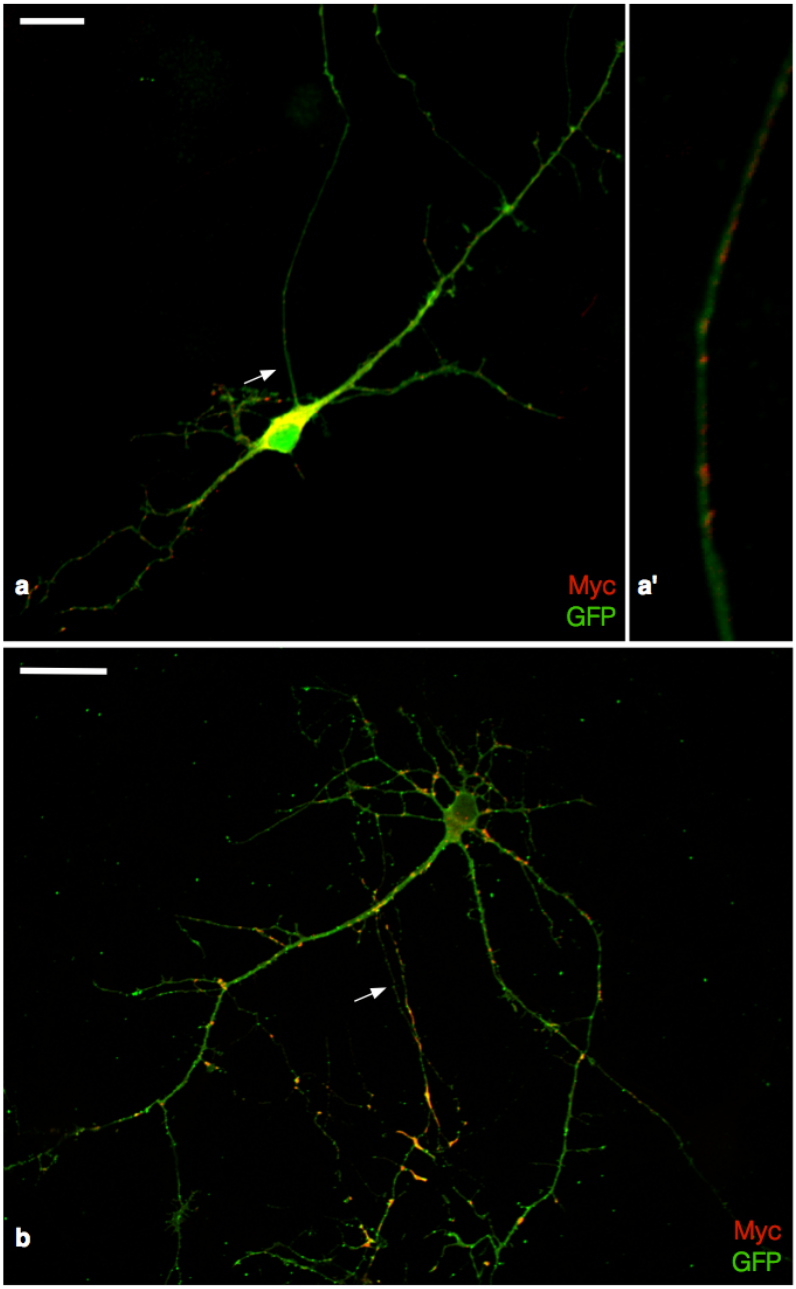

Figure 3.4. Representative images of punctate Teneurin-Myc distribution at 12DIV in dissociated hippocampal neurons. **a.** Image of DIV12 hippocampal neuron transfected with GFP and Tenm3-Myc. The arrow indicates the axon. Scale bar: 30µm. Punctate Tenm3-Myc can be detected in axon and dendrites. **a'** Magnified view of axonal segment indicated with arrow in **a.** clearly shows punctate Tenm3-Myc in axon. Scale bar: 10µm. **b.** DIV12 hippocampal neuron transfected with GFP and Tenm4-Myc. Punctate Tenm4-Myc can be detected in axon and dendrites. The axon is indicated with the arrow. This neuron has a fragmented axon and thus seems to be affected by cytotoxicity deriving from Tenm4-Myc overexpression.

Next, I wanted to test whether the cytotoxicity and possible morphological effects emanating from Teneurin overexpression could be reduced if neurons were transfected at a more mature stage, when extensive axonal and dendritic branching has been established. Neurons at 15DIV were cotransfected with two different concentrations of Teneurin plasmid, 0.7µg and 0.2µg mGFP (n = 5 independent cultures, Figure 3.5) or 0.5µg and 0.2µg mGFP (n = 1 culture), left to grow for two days and fixed at 17DIV. As for 7DIV and 12DIV, Teneurins clustered in puncta along both axons and dendrites. Both plasmid concentrations led to Teneurin expression in cotransfected neurons, however in neurons transfected with 0.5µg Teneurin plasmid there were more instances of GFP expressing neurons with no Teneurin expression. Transfection efficiency was similarly low at both concentrations with an average of ~8 transfected cells per coverslip. While some cytotoxicity was still apparent with some fragmented cells, most neurons did not display any obvious morphological abnormalities and had extensively arborised neurites as expected for this developmental stage.

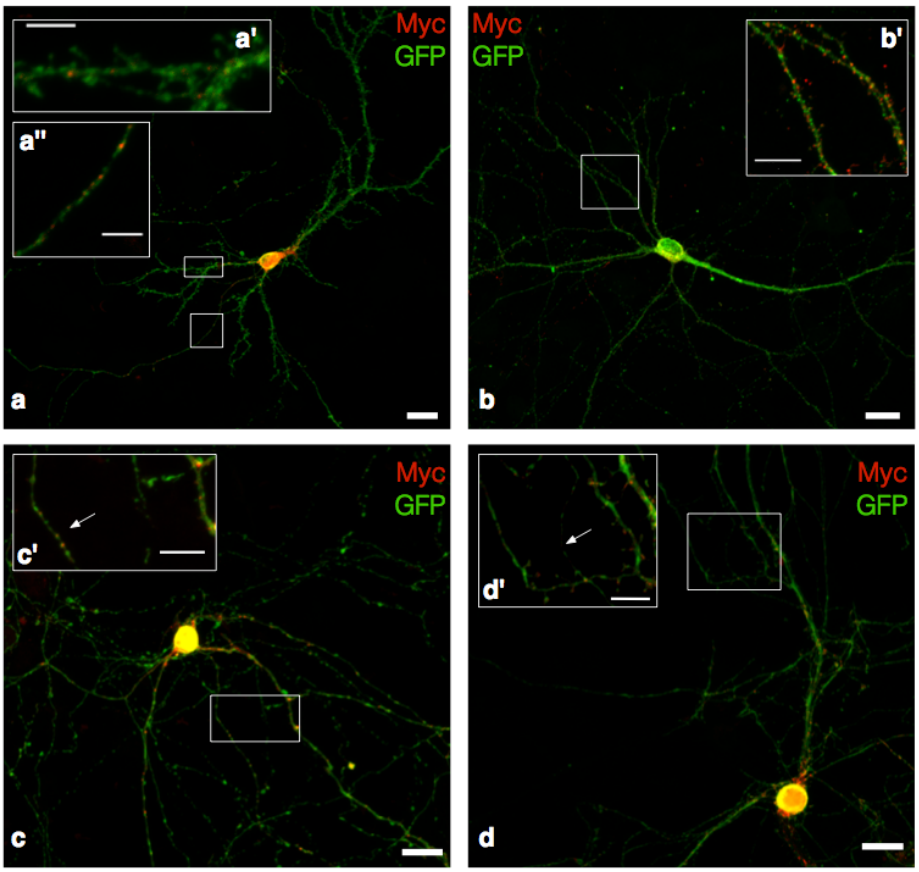

Figure 3.5. Representative images of punctate Teneurin-Myc distribution at 17DIV in dissociated hippocampal neurons. **a.** Image of 17DIV hippocampal neuron transfected with GFP and Tenm1-Myc. Scale bar: 20µm. Strong punctate Tenm1-Myc can be detected in the axon (**a"**) and weaker in dendrites (**a'**). The scale bar in **a'** and **a"** is 5µm. **b.** 17DIV hippocampal neuron transfected with GFP and Tenm2-Myc. Scale bar: 20µm. **b'.** Magnified view of the dendritic segment indicated in **b** shows strong punctate Tenm2-Myc in dendrites. Scale bar: 10µm. **c.** 17DIV hippocampal neuron transfected with GFP and Tenm3-Myc. Scale bar: 20µm. **c'.** Magnified view of white square indicated in **c**, showing punctate Tenm3-Myc in both axon (arrow) and dendrites. Scale bar: 10µm. **d.** 17DIV hippocampal neuron transfected with GFP and Tenm4-Myc. Scale bar: 20µm. **d'.** Magnified view of white square indicated in **d**, showing weak punctate Tenm4-Myc in axon (arrow) and stronger clustering in dendrites. Scale bar: 10µm.

These results indicated that Teneurin overexpression led to the least amount of cytotoxicity and morphological changes when neurons were transfected at mature stages. In an attempt to increase transfection efficiency, I cotransfected neurons with 0.7µg Teneurin plasmid and 0.2µg mGFP at 12DIV and left them to develop for 5 days before fixation at 17DIV (n = 1 culture). This led to Teneurins being expressed in puncta along neurites of most GFP expressing cells. However, cytotoxicity was very high with many fragmented neurons and transfection efficiency was even lower than for transfection at 15DIV with an average of only ~4 transfected cells per coverslip, likely due to cell-death of transfected neurons. Because most transfected neurons seemed apoptotic it was difficult to assess whether the longer overexpression time also had morphological or functional effects.

Finally, to test whether cytotoxicity would be decreased in mature cultures if the time between transfection and fixation was reduced, neurons were transfected with 0.7µg Teneurin plasmid and 0.2µg mGFP at 16DIV and fixed one day later at 17DIV (n = 1 culture). This led to very low transfection efficiency with an average of only ~3 transfected cells per coverslip. Furthermore, most GFP transfected cells either did not express Teneurin or expressed Teneurin only in the cell body and there was no noticeable improvement in cytotoxicity.

Table 2. Optimisation of Teneurin transfection in hippocampal neurons.

Teneurin cDNA concentration /coverslip	Cell age transfection - fixation	Transfection time at 37ºC	Teneurin expression	Normal neuronal morphology	Cytotoxicity	Transfection efficiency
0.45µg	2-3DIV	15 min	Yes in most transf. cells	No	some	low
0.45µg	4-7DIV	10 min	No	Mostly no	High	very low
0.45µg	4-7DIV	15 min	Yes	Mostly no	High	average
0.5µg	10-12DIV	15 min	Yes in few transf. cells	Mostly no	High	average
0.7µg	10-12DIV	15 min	Yes in most transf. cells	Mostly no	High	high
0.5µg	15-17DIV	15 min	Yes in very few transf. cells	Yes	Some	low - average
0.7µg	15-17DIV	15 min	Yes in most transf. cells	Yes	Some	low - average
0.7µg	16-17DIV	15 min	No	Yes	Some	very low
0.7µg	12-17DIV	15 min	Yes in most transf. cells	?	High	very low

From this first set of experiments (Table 2), I concluded that the best conditions for Teneurin expression were achieved when neurons were transfected at 15DIV and fixed at 17DIV. Teneurin expression was most reliable when 0.7µg Teneurin plasmid were cotransfected with 0.2µg mGFP. Whilst Teneurin overexpression seemed to have little to no effect on neuronal morphology at this developmental stage, cytotoxicity was still relatively high. Therefore, for all subsequent experiments, only the healthiest transfected neurons, exhibiting the least neurite fragmentation, normally shaped cell bodies and widely arborised dendrites and axons, were selected for further analysis. Synaptogenesis in cultured neurons peaks between the second and third week in culture and thus, the choice of 17DIV provided a good time point to further explore whether Teneurins are localised at synapses.

3.2.2 Finding the appropriate conditions to analyse the synaptic localisation of Teneurins

3.2.2.1 Choosing a synaptic marker

Having established that Teneurins cluster in puncta along axons and dendrites, I proceeded to investigate whether those puncta were localised at synapses. Initially, I used several different antibodies to identify synapses (refer to Table 1 for antibody

manufacturers). Rabbit anti-Synapsin I, rabbit anti-Syntaxin, rabbit anti-vGlut1 and mouse anti-Bassoon were used to label the presynaptic compartment. However, only rabbit anti-Synapsin and mouse anti-Bassoon yielded a consistent and strong labelling of synapses. Therefore, rabbit anti-Synapsin was used to analyse the colocalisation between Teneurin puncta and synapses, as it was compatible with the use of mouse anti-Myc and chicken-anti GFP antibodies also used in these experiments. Mouse anti-Bassoon was used as a control to evaluate the amount of colocalisation between Synapsin and Bassoon. Synapsins are abundant phosphoproteins associated with the membranes of synaptic vesicles. Specifically, they are thought to maintain the synaptic vesicle reserve pool at excitatory synapses and regulate the size of the readily releasable pool of GABAergic vesicles (Gitler *et al.*, 2004). Bassoon is a protein that is involved in cytomatrix organisation at the site of neurotransmitter release (tom Dieck *et al.*, 1998) of both excitatory glutamatergic and inhibitory GABAergic synapses (Richter *et al.*, 1999). Therefore, Bassoon and Synapsin are good synaptic marker proteins to label both inhibitory and excitatory presynaptic compartments.

A mouse anti-Shank2 antibody, which yielded a consistently strong staining of the postsynaptic compartment, was used as a control to evaluate the colocalisation between presynaptic Synapsin and postsynaptic Shank2. Shank2 is a scaffolding protein of the PSD of excitatory synapses (Naisbitt *et al.*, 1999; Tu *et al.*, 1999). Two different rabbit anti-Gephyrin antibodies were also tested to label the postsynaptic compartment of inhibitory synapses, however the immunoreactivity of these antibodies was inconsistent and therefore they were not used for further experiments.

3.2.2.2 Choosing a colocalisation analysis method

It is generally accepted that the location and physiological function of proteins are closely related. Assessing the colocalisation of novel proteins with well-characterised markers in order to understand their role in biological processes has become a routine approach in cell biology. However, despite the importance of these studies, there is surprisingly little standardisation in colocalisation analysis methods and this field is indeed one of contention and enigma (Bolte and Cordelières, 2006). In order to analyse the colocalisation between Synapsin and Teneurins, it was necessary to select an

appropriate analysis method. In the next paragraphs, I will describe methods that were considered and their limitations.

Most colocalisation analyses in the literature are reported on a simple visual basis and rarely quantified, i.e. it is commonly accepted that proteins depicted in the green and red channel will give rise to yellow hotspots where they are present in the same pixels. However, this approach is riddled by obvious limitations; (1) The presence of yellow spots is highly dependent on the relative signal intensity collected in the green and red channel, (2) These overlay methods are not appropriate for quantification purposes. In summary, this method was deemed unsuitable for our purpose.

The most readily available colocalisation analysis methods are based on intensity correlation scores and are provided in most standard image-analysis software packages. They are easy to implement and as the name suggests, statistical analysis of the correlation of pixel intensity values in dual-channel images is performed. This is done using correlation coefficients, such as the Pearson's coefficient, which give a measure of the linear relationship between the fluorescence intensities of both channels. Intensity correlation based methods can be useful to point out colocalisation when it is complete, however they are unsuitable to measure partial colocalisation. As the colocalisation of Teneurins with Synapsin was clearly not complete, the use of correlation coefficients was not appropriate for our experimental condition.

The most viable alternative for our experiments was to use an object-based colocalisation analysis method. In this method, protein clusters are segmented and identified as regions of interest. Three different methods were tested. An increasing number of automated object based methods have lately been developed and are publically available (Costes *et al.*, 2004; Bolte and Cordelières, 2006; Ippolito and Eroglu, 2010; Lagache, Meas-Yedid and Olivo-Marin, 2013). I started by testing an automated method based on Ripley's K function (Lagache, Meas-Yedid and Olivo-Marin, 2013) and which could be downloaded as a plugin into ICY, an open community platform for bioimage informatics. This method resulted as inadequate for our experiments, because it assumes normal distribution of data points. Due to the nature of neurons, the distribution of proteins within the cytoplasm is spatially restricted by the narrow diameter of neurites. As a result, the level of colocalisation was falsely

overestimated. Next, colocalisation analysis was attempted using the spots detection and colocalisation function in Imaris (Appendix 2). Unfortunately, this method was not appropriate for our analysis due to inadequate spot detection, i.e. it was not possible to generate an adequate representation of Teneurin and Synapsin protein clusters using spot detection despite many efforts to optimise the parameters for detection. The colocalisation analysis in Imaris (Bitplane) resulted in either a clear overestimation or underestimation of the number of Teneurin and Synapsin clusters, and consequently an over- or underestimation of colocalisation depending on the chosen spot detection parameters. Finally, ImageJ was used to semi-automatically detect regions of interest (ROI) representing Synapsin or Teneurin protein clusters. Thresholding of images was done manually and followed by automatic particle detection. This step was completed automatically, in order to avoid experimenter bias. Finally, the fraction area of Teneurin particles (ROIs) overlapping with thresholded Synapsin was calculated (refer to 2.6.3 for a detailed description of the analysis process). Due to the obvious differences in protein distribution between Synapsin and Teneurin it was not possible to blindly select thresholds. However, the analysis was conducted blind in relation to the four Teneurin paralogues. Even though this method comes with some limitations, it was deemed the most suitable for our purpose.

3.2.3 Validation of colocalisation analysis with Synapsin, Bassoon and Shank2 controls

The chosen colocalisation analysis method was assayed in a control condition, where the overlap between presynaptic Synapsin with presynaptic Bassoon and postsynaptic Shank2 was quantified. Neurons were transfected with GFP at 15DIV and fixed at 17DIV and stained with antibodies directed against Synapsin as well as Bassoon and Shank2 respectively. Each colocalisation analysis (Synapsin and Bassoon vs. Synapsin and Shank2) was performed on 5 neurons from 3 independent transfections. Two non-overlapping z-stacks of neuronal segments of every neuron were taken and fluorescence intensities of both the Synapsin channel and Bassoon or Shank2 channel were thresholded to identify protein clusters. The level of colocalisation was quantified as a measure of either Bassoon or Shank2 cluster overlap with Synapsin (fraction area) and compared to a negative control. The negative control was created by rotating the

Bassoon or Shank2 channel image 90° clockwise and assessing the colocalisation between clusters in the Synapsin channel and clusters in the rotated channel. Normality testing was performed for every data set followed by the appropriate parametric and non-parametric tests.

Bassoon and Synapsin expression could be detected in the soma and in discrete puncta along neurites. In order to segment individual protein puncta, both channels were thresholded and Bassoon and Synapsin particles were automatically detected. Synapsin puncta were larger (0.91 μm^2 ± 0.1 SEM, ± 1.47 SD, $p < 0.0001$, Mann-Whitney test) than Bassoon puncta (0.39 μm^2 ± 0.04 SEM, ± 0.49 SD). The colocalisation between both proteins was determined as a percentage of Bassoon cluster area overlapping with Synapsin for every Bassoon cluster. The data was not Gaussian ($p < 0.0001$ by D'Agostino & Pearson omnibus normality test), which is why the non-parametric Mann-Whitney rank-sum test was used for significance testing. As expected Bassoon and Synapsin significantly colocalised (n= 933, 40.87 % ± 1.38 SEM, ± 42.32 SD, $p < 0.0001$, Figure 3.6-k) compared to the negative Bassoon-control (n= 933, 0.89 % ± 0.22 SEM, ± 6.61 SD). The high degree of variability in the data was due to the fact that only 56.52% of Bassoon puncta (± 4.26 SEM, ± 9.52 SD) either fully or partially colocalised with Synapsin (Figure 3.6-l), whilst the other half did not colocalise at all. In the negative control condition 3.06% (± 1.18 SEM, ± 2.63 SD) of Bassoon puncta fully or partially colocalised with Synapsin, whilst the vast majority, as expected, did not colocalise. In colocalised Bassoon puncta, the overlap with Synapsin (Figure 3.6-m) tended to cover the majority of the Bassoon cluster area (71.14 % ± 1.34 SEM, ± 31.02 SD, $p < 0.0001$, Mann-Whitney Test). These results were consistent with previously reported findings, where Synapsin and Bassoon only partially colocalise at high magnification (tom Dieck *et al.*, 1998).

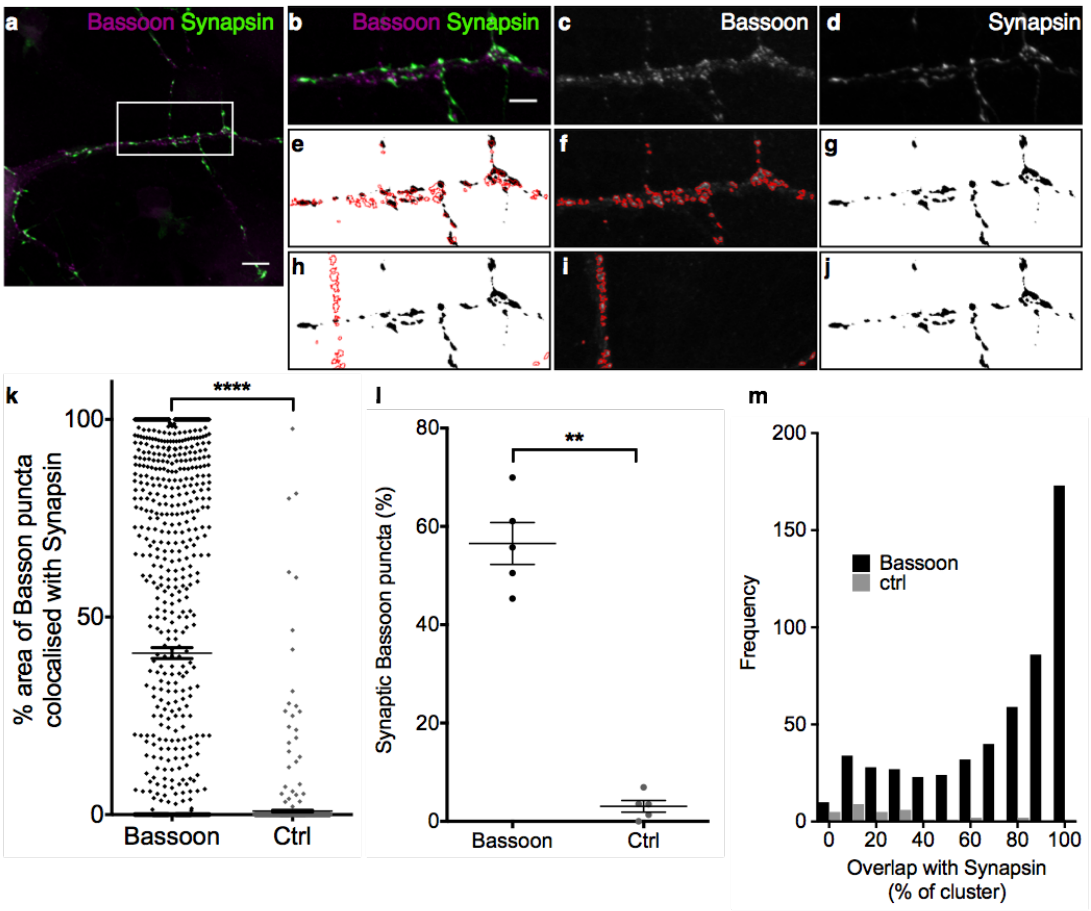

Figure 3.6. Colocalisation analysis between Bassoon and Synapsin in dissociated hippocampal neurons. **a.** Image of a representative hippocampal neuron stained for Bassoon and Synapsin. Scale bar: 10 µm. **b.** Dendritic segment of the neuron shown in **a**. Scale bar 5 µm. **c.** Dendritic segment stained for Bassoon. **d.** Dendritic segment stained for Synapsin. **e.** Colocalisation between Bassoon and Synapsin after image analysis. **f.** ROIs around bassoon puncta after image analysis. **g.** Binary image of Synapsin puncta after image analysis. **h.** Control colocalisation between Bassoon and Synapsin after 90° rotation of the Bassoon image channel (**c, f**). **i.** ROIs around Bassoon puncta after image channel was rotated 90°. **j.** Binary image of Synapsin puncta after image analysis. **k.** Colocalisation between Bassoon and Synapsin (black) and Synapsin and Bassoon-control (grey), ****P< 0.0001. **l.** Proportion of Bassoon clusters (black) and Bassoon-control clusters (grey) colocalised with Synapsin per neuron, **p= 0.0079. **m.** Frequency of full or partial Bassoon overlap with Synapsin in colocalised puncta. Data is from 933 Bassoon puncta and five hippocampal neurons. Two-tailed Mann-Whitney Test. Bars and error bars represent mean and SEM.

Next, the colocalisation between postsynaptic Shank2 and Synapsin was assessed. Staining for Shank2 showed that the protein was strongly expressed in the soma and formed discrete puncta along neurites. Diffuse low-level Shank2 expression along dendrites was very low and puncta could be clearly detected following thresholding. Synapsin puncta were larger (0.74 µm^2 ± 0.13 SEM, ± 1.06 SD, p=0.0013, Mann-Whitney test) than Shank2 puncta (0.25 µm^2 ± 0.02 SEM, ± 0.14 SD). The colocalisation between Shank2 and Synapsin was determined as above. The data was not Gaussian ($p < 0.0001$ by D'Agostino & Pearson omnibus normality test), and the non-parametric Mann-Whitney rank-sum test revealed that Shank2 and Synapsin

significantly colocalised (n= 1103, 22.41 % ± 1.07 SEM, ± 35.47 SD, p< 0.0001, Figure 3.7-k) compared to the negative Shank2-control (n= 1103, 0.92 % ± 0.23 SEM, ± 7.72 SD). The level of colocalisation between Shank2 and Synapsin was lower compared to Bassoon and Synapsin ($p < 0.0001$, Kruskal-Wallis test with Dunn's multiple comparison). This was expected, since Shank2 is a postsynaptic protein of excitatory synapses, whereas both Synapsin and Bassoon are presynaptic proteins of excitatory and inhibitory synapses. However, it was interesting to notice that 39.24% of Shank2 puncta (± 6.341 SEM, ± 14.18 SD, $p = 0.0079$, Mann-Whitney test) either fully or partially colocalised with Synapsin (Figure 3.7-l). In colocalised Shank2 puncta, the overlap with Synapsin (Figure 3.7-m) on average covered 60% of the Shank2 cluster area (± 1.64 SEM, ± 33.35 SD).

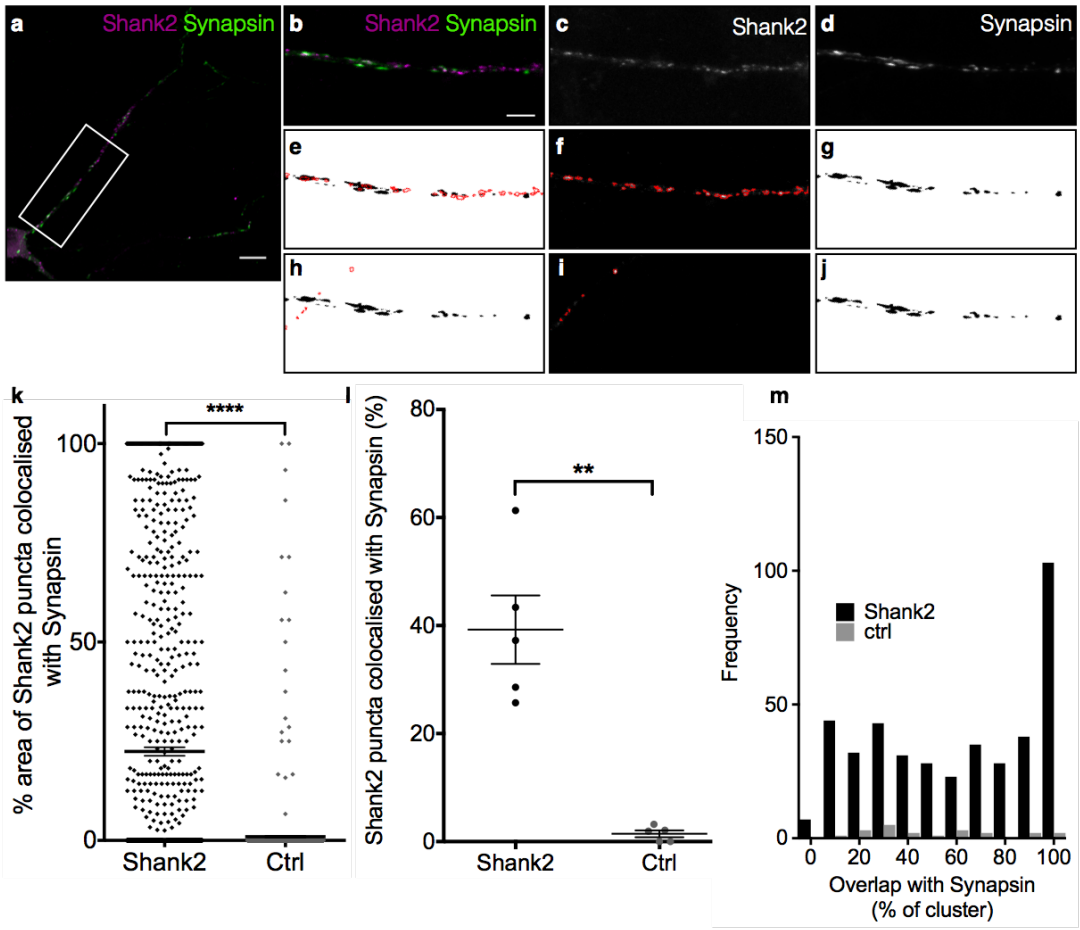

Figure 3.7. Colocalisation analysis between Shank2 and Synapsin in dissociated hippocampal neurons. **a.** Image of a representative hippocampal neuron stained for bassoon and synapsin. Scale bar: 10 µm. **b.** Dendritic segment of the neuron shown in **a**. Scale bar: 5 µm. **c.** Dendritic segment stained for Shank2. **d.** Dendritic segment stained for Synapsin. **e.** Colocalisation between Shank2 and Synapsin after image analysis. **f.** ROIs around Shank2 clusters after image analysis. **g.** Binary image of Synapsin clusters after image analysis. **h.** Control colocalisation between Shank2 and Synapsin after 90° rotation of the Shank2 image channel (**c, f**). **i.** ROIs around bassoon clusters after image was rotated 90°. **j.** Binary image of synapsin clusters after image analysis. **k**. Colocalisation between Shank2 and Synapsin (black) and Synapsin and Shank2-control (grey), ****P< 0.0001. **l.** Proportion of Shank2 clusters (black) and Shank2-control clusters (grey) colocalised with Synapsin per neuron, **p= 0.0079. **m**. Frequency of full or partial Shank2 overlap with Synapsin in colocalised puncta. Data is from 1103 Shank2 puncta and five hippocampal neurons. Two-tailed Mann-Whitney Test. Bars and error bars represent mean and SEM.

These findings validated the chosen colocalisation analysis method as an unbiased approach for the detection of synaptic protein puncta and the quantification of the level of overlap between two different proteins. Furthermore, the results from the colocalisation analyses of Synapsin with Bassoon and Shank2 provided a measure of the expected level of colocalisation between established pre- and postsynaptic proteins and could be used as positive control condition against which to compare Teneurins.

3.3 Subcellular localisation pattern of Teneurins in hippocampal neurons

In order to assess whether Teneurins are localised at synapses, the colocalisation between Tenm1-4 with Synapsin was measured. Quantification was performed on 5 neurons from three independent transfections for each condition (Tenm1, Tenm2, Tenm3, Tenm4). Neurons were transfected at 15DIV and fixed at 17DIV as described above. The level of colocalisation was quantified as a measure of Teneurin cluster overlap with Synapsin (fraction area) and compared to a negative control. As for the negative Shank2- and Bassoon-controls, the negative Teneurin-control was created by rotating the Teneurin channel image 90° clockwise and assessing the colocalisation between clusters in the Synapsin channel and clusters in the rotated Teneurin channel. Normality testing was performed for every data set followed by the appropriate parametric and non-parametric tests.

3.3.1 Tenm1

After immunocytochemical staining with antibodies directed against GFP, Synapsin and Myc, Tenm1 expression at 17DIV could be detected strongly in the soma as well as in puncta along dendrites and axons. Some low-level diffuse Tenm1 expression was also detected along most neurites. In order to quantify the level of colocalisation between Tenm1 and Synapsin both image channels were individually thresholded and Synapsin and Teneurin particles were automatically detected as described above. In 10 images representing 2 areas of neuronal segments of 5 hippocampal neurons, a total of 1399 Tenm1 clusters were detected. Tenm1 (0.36 μm^2 ± 0.04 SEM, ± 0.36 SD) and Synapsin clusters (0.39 μm^2 ± 0.02 SEM, ± 0.38 SD) did not significantly differ in size ($p=0.064$, Mann-Whitney test). The colocalisation of Tenm1 with Synapsin was determined as a percentage of Tenm1 cluster area overlapping with Synapsin for every Tenm1 cluster. Due to the non-normality of the data ($p < 0.0001$ by D'Agostino & Pearson omnibus normality test), the non-parametric Mann-Whitney rank-sum test was used to compare colocalisation between Synapsin and Tenm1 in the normal and negative Tenm1-control condition. As expected, Tenm1 significantly (n= 1399, 9.32 % ± 0.66 SEM, ±24.88 SD, $p< 0.0001$) colocalised with Synapsin compared to the negative Tenm1-control (n= 1399, 1.74 % ± 0.28 SEM, ±11.08 SD). However, it is

important to note the high variability of the data (Figure 3.8-l). This was due to the fact that only a subset of Tenm1 clusters either fully or partially colocalised with Synapsin (17.85 % ± 3.12 SEM, ± 6.99 SD), whereas the majority did not colocalise at all. Equally, the high variability in the negative control condition was due to some Tenm1-control clusters fully or partially colocalising with Synapsin (4.41 % ± 1.34 SEM, ± 2.99 SD; Figure 3.8-m) purely by chance, whilst the vast majority, as expected, did not colocalise. In colocalised Tenm1 puncta, the overlap with Synapsin (Figure 3.8-n) tended to be partial (49.56 % ± 2.2 SEM, ± 36.07 SD).

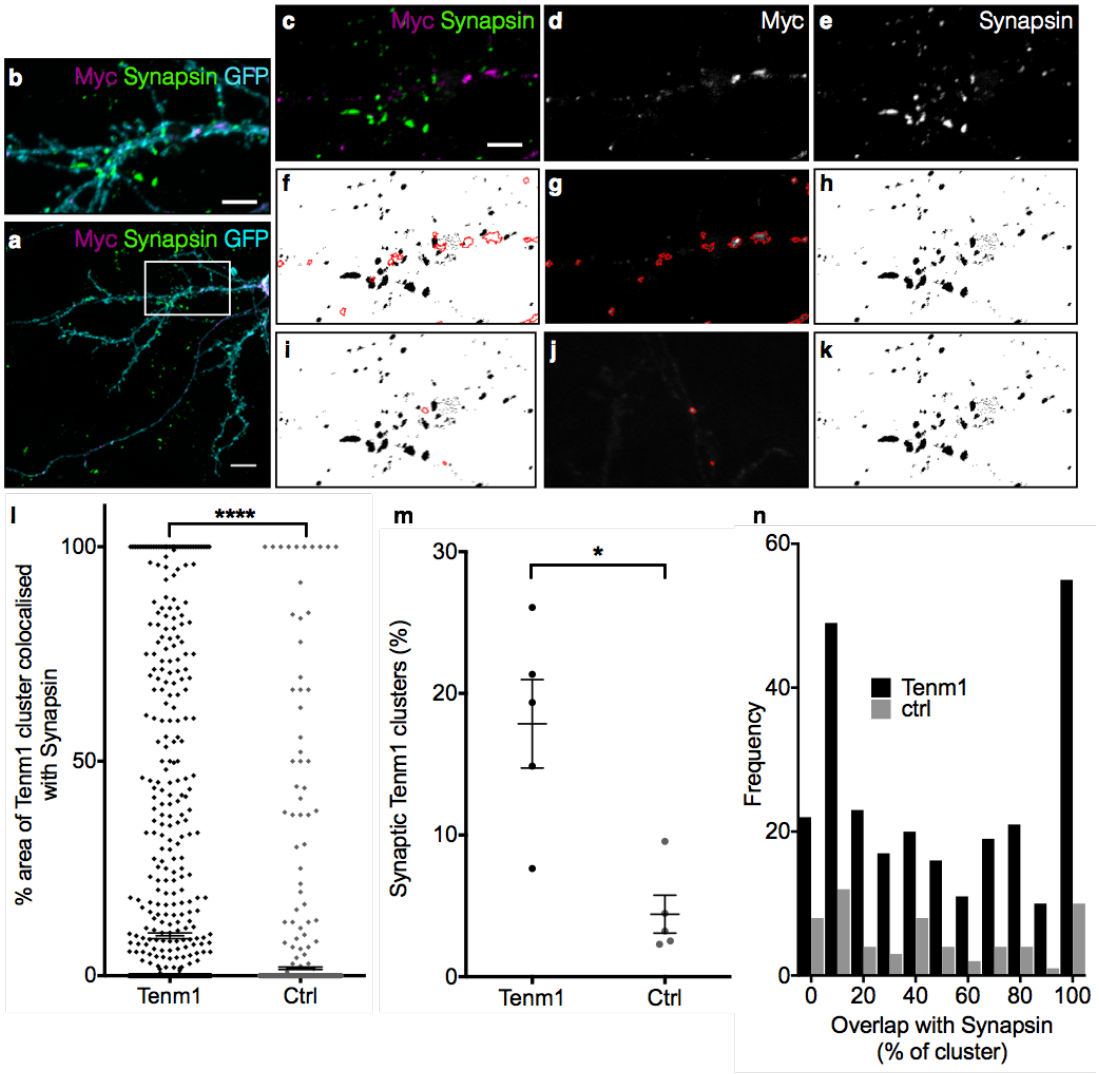

Figure 3.8. Colocalisation analysis between Tenm1-Myc and Synapsin in dissociated hippocampal neurons. **a.** Image of a representative hippocampal neuron, transfected with Tenm1-Myc and GFP, and stained for Synapsin. Scale bar: 10 µm. **b-c.** Dendritic segment of the neuron shown in **a**. Scale bar 5 µm. **d.** Tenm1-Myc localisation in dendritic segment. **e.** Dendritic segment stained for Synapsin. **f.** Colocalisation between Tenm1-Myc and Synapsin after image analysis. **g.** ROIs around Tenm1-Myc puncta after image analysis. **h.** Binary image of Synapsin puncta after image analysis. **i.** Control colocalisation between Tenm1-Myc and Synapsin after 90° rotation of the Tenm1-Myc image channel (**d, g**). **j.** ROIs around Tenm1-Myc puncta after image channel was rotated 90°. **k.** Binary image of Synapsin puncta after image analysis. **l**. Colocalisation between Tenm1 and Synapsin (black) and Synapsin and Tenm1-control (grey), ****P< 0.0001. **m**. Proportion of Tenm1 clusters (black) and Tenm1-control clusters (grey) colocalised with Synapsin per neuron, *p= 0.016. **n**. Frequency of full or partial Tenm1 overlap with Synapsin in colocalised puncta. Data is from 1399 Tenm1-Myc clusters and five hippocampal neurons. Two-tailed Mann-Whitney Test. Bars and error bars represent mean and SEM.

3.3.2 Tenm2

Strong Tenm2 expression at 17DIV could be detected in clusters along dendrites and axons as well as Tenm2 trapping in the soma. Similarly to Tenm1, there was a low basal level of diffuse Tenm2 expression along most neurites. The fluorescence intensity was thresholded in order to identify single Tenm2 clusters and their colocalisation with Synapsin puncta. A total of 1565 Tenm2 clusters were detected in 10 images representing 2 areas of neuronal segments of 5 hippocampal neurons. Tenm2 (0.34 μm^2 ± 0.02 SEM, ± 3.2 SD) and Synapsin clusters (0.47 μm^2 ± 0.03 SEM, ± 0.60 SD) did not significantly differ in size (p= 0.068, Mann-Whitney test). The colocalisation of Tenm2 with Synapsin was determined as a percentage of Tenm2 cluster area overlapping with Synapsin for every Tenm2 cluster. The data was not Gaussian ($p < 0.0001$ by D'Agostino & Pearson omnibus normality test), therefore the non-parametric Mann-Whitney rank-sum test was applied to compare colocalisation between Synapsin and Tenm2 in the normal and negative Tenm2-control condition. Tenm2 significantly (n= 1565, 8.16 % ± 0.56 SEM, ±22.2 SD, $p< 0.0001$) colocalised with Synapsin (Figure 3.9-l) compared to the negative control (n= 1565, 0.84 % ± 0.18 SEM, ± 7.1 SD). Only a proportion of 19.26 % (± 2.9 SEM, ± 6.49 SD) of Tenm2 clusters either fully or partially colocalised with Synapsin (Figure 3.9-m), whereas the majority did not colocalise at all. In the control condition a minor fraction of 2.12 % (± 1.11 SEM, ± 2.47 SD) Tenm2-control clusters fully or partially colocalised with Synapsin by chance. In colocalised Tenm2 puncta, the overlap with Synapsin (Figure 3.9-n) tended to be partial (42.7 % ± 1.92 SEM, ± 33.28 SD).

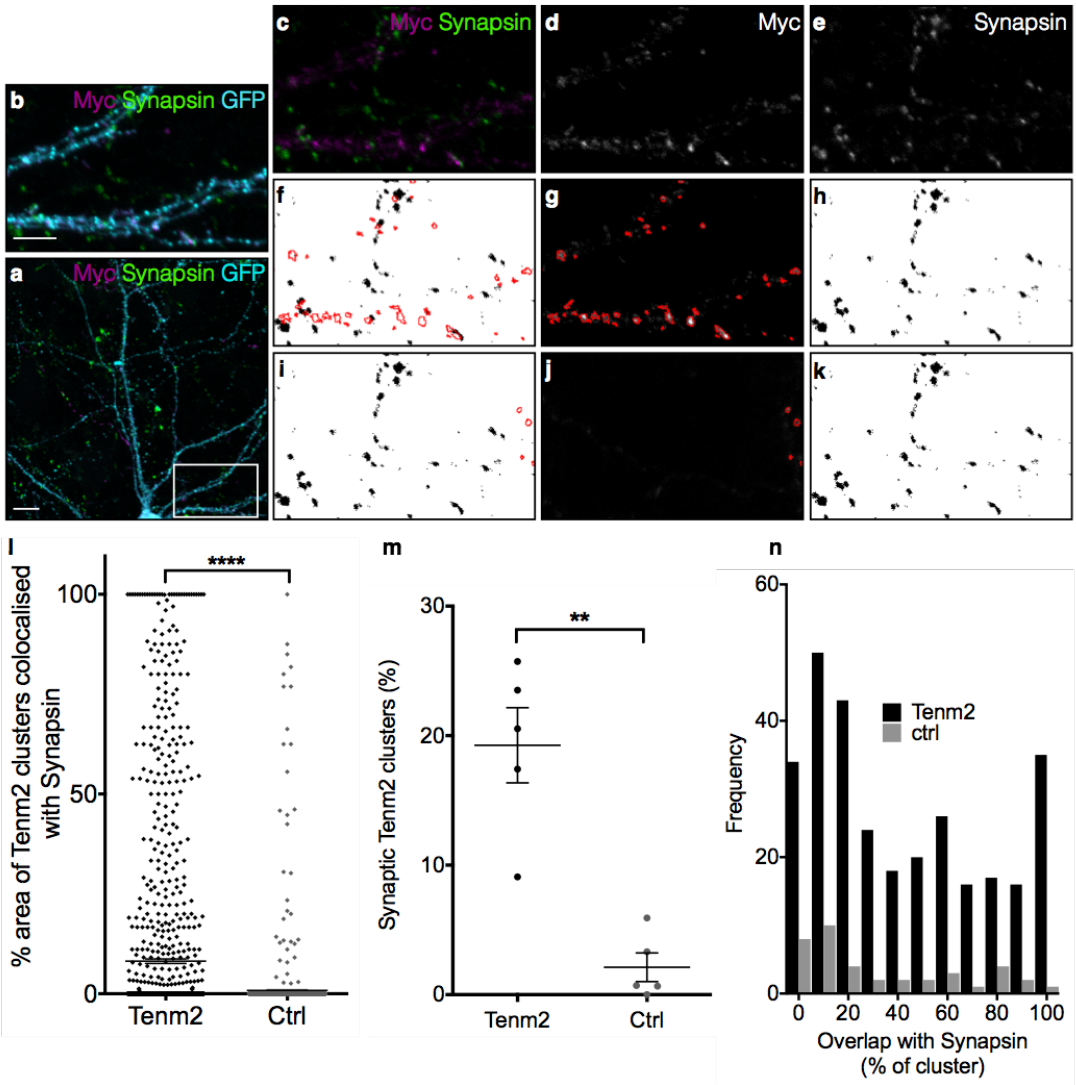

Figure 3.9. Colocalisation analysis between Tenm2-Myc and Synapsin in dissociated hippocampal neurons. **a.** Image of a representative hippocampal neuron, transfected with Tenm2-Myc and GFP, and stained for Synapsin. Scale bar: 10 µm. **b-c.** Dendritic segment of the neuron shown in **a**. Scale bar 5 µm. **d.** Tenm2-Myc localisation in dendritic segment. **e.** Dendritic segment stained for Synapsin. **f.** Colocalisation between Tenm2-Myc and Synapsin after image analysis. **g.** ROIs around Tenm2-Myc puncta after image analysis. **h.** Binary image of Synapsin puncta after image analysis. **i.** Control colocalisation between Tenm2-Myc and Synapsin after 90° rotation of the Tenm2-Myc image channel (**d, g**). **j.** ROIs around Tenm2-Myc puncta after image channel was rotated 90°. **k.** Binary image of Synapsin puncta after image analysis. **l**. Colocalisation between Tenm2 and Synapsin (black) and Synapsin and Tenm2-control (grey), ****P< 0.0001. **m**. Proportion of Tenm2 clusters (black) and Tenm2-control clusters (grey) colocalised with Synapsin per neuron, **p= 0.008. **n**. Frequency of full or partial Tenm2 overlap with Synapsin in colocalised puncta. Data is from 1565 Tenm2-Myc clusters and five hippocampal neurons. Two-tailed Mann-Whitney Test. Bars and error bars represent mean and SEM.

3.3.3 Tenm3

Tenm3 clusters along dendrites and axons could be detected at 17DIV as well as trapped Tenm3 in the soma. As previously, the fluorescence intensity was thresholded in order to pick out single Tenm3 clusters from low-level diffuse Tenm3 expression along neurites. Tenm3 expression seemed generally lower and less punctate than for Tenm1 and Tenm2, however no analysis of fluorescence intensities was performed as the general variability in transfection efficiency, expression and cell types generates a dataset that is not comparable. The decreased Tenm3 clustering and expression resulted in a lower number of Tenm3 puncta (n= 813, from 10 images representing 2 areas of neuronal segments of 5 hippocampal neurons). Tenm3 (0.77 μm^2 ± 0.17 SEM, ± 1.28 SD) and Synapsin clusters (0.45 μm^2 ± 0.04 SEM, ± 0.55 SD) did not significantly differ in size (p=0.43, Mann-Whitney test). The colocalisation between Tenm3 with Synapsin was determined as above. Normality testing revealed that the data was not Gaussian ($p < 0.0001$ by D'Agostino & Pearson omnibus normality test), hence the non-parametric Mann-Whitney rank-sum test was applied to compare colocalisation between Synapsin and Tenm3 in the normal and negative Tenm3-control condition. Tenm3 significantly (n= 813, 8.33 % ± 0.78 SEM, ±22.36 SD, $p< 0.0001$) colocalised with Synapsin (Figure 3.10-l) compared to the negative Tenm3-control (n= 813, 0.84 % ± 0.31 SEM, ± 8.77 SD). Out of all Tenm3 clusters, 23.04 % (± 3.39 SEM, ± 7.57 SD) either fully or partially colocalised with Synapsin (Figure 3.10-m). The random colocalisation of Tenm3 with Synapsin in the negative control condition amounted to 2.76 % (± 1.57 SEM, ± 3.5 SD). In colocalised Tenm3 puncta, the overlap with Synapsin (Figure 3.10-n) in average covered 39.62 % of the Tenm3 cluster area (± 2.58 SEM, ± 33.77 SD).

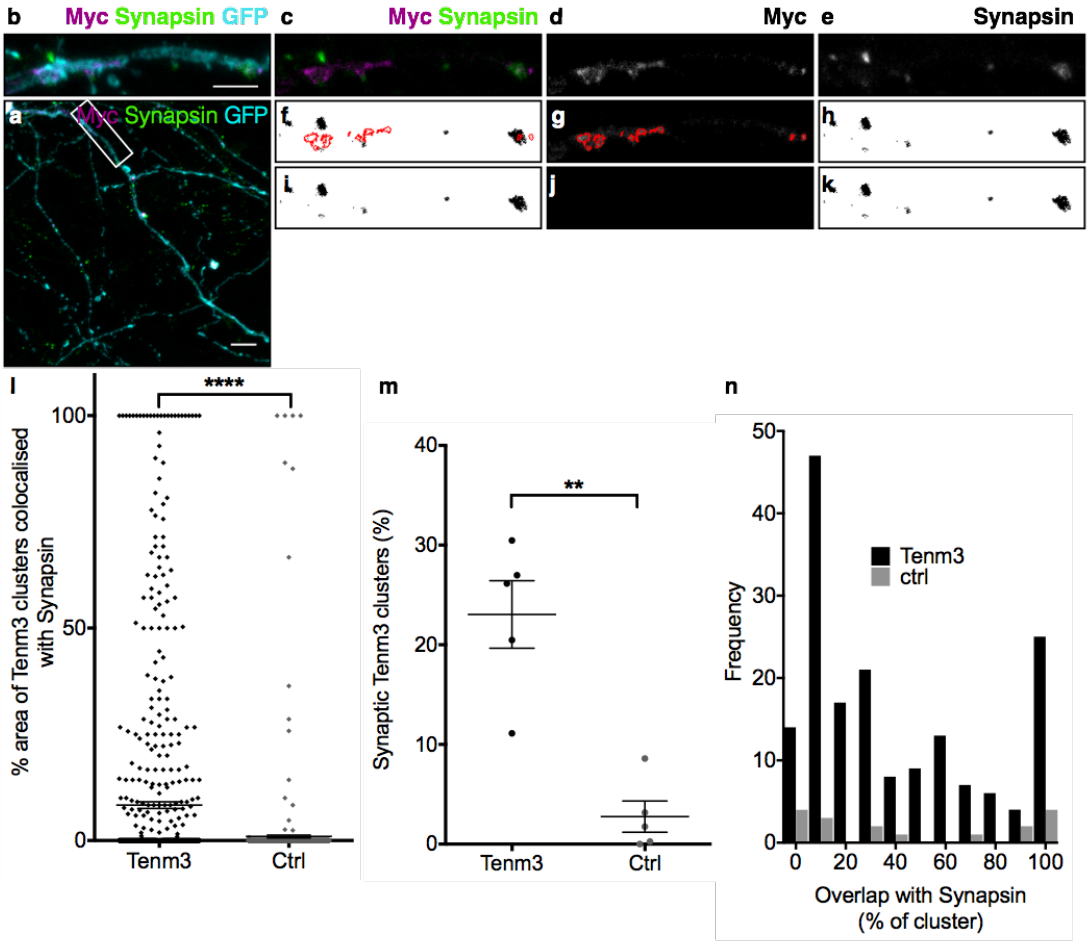

Figure 3.10. Colocalisation analysis between Tenm3-Myc and Synapsin in dissociated hippocampal neurons. **a.** Image of a representative hippocampal neuron, transfected with Tenm3-Myc and GFP, and stained for Synapsin. Scale bar: 10 µm. **b-c.** Dendritic segment of the neuron shown in **a**. Scale bar 5 µm. **d.** Tenm3-Myc localisation in dendritic segment. **e.** Dendritic segment stained for Synapsin. **f.** Colocalisation between Tenm3-Myc and Synapsin after image analysis. **g.** ROIs around Tenm3-Myc puncta after image analysis. **h.** Binary image of Synapsin puncta after image analysis. **i.** Control colocalisation between Tenm3-Myc and Synapsin after 90° rotation of the Tenm3-Myc image channel (**d, g**). **j.** ROIs around Tenm3-Myc puncta after image channel was rotated 90°. **k.** Binary image of Synapsin puncta after image analysis. **l**. Colocalisation between Tenm3 and Synapsin (black) and Synapsin and Tenm3-control (grey), ****P< 0.0001. **m**. Proportion of Tenm3 clusters (black) and Tenm3-control clusters (grey) colocalised with Synapsin per neuron, **p= 0.008. **n**. Frequency of full or partial Tenm3 overlap with Synapsin in colocalised puncta. Data is from 813 Tenm3-Myc clusters and five hippocampal neurons. Two-tailed Mann-Whitney Test. Bars and error bars represent mean and SEM.

3.3.4 Tenm4

Punctate Tenm4 expression at 17DIV could be detected along dendrites and axons as well as strong Tenm4 expression in the soma. Tenm4 expression also seemed lower and more diffuse than for Tenm1 and Tenm2. Following thresholding of the fluorescence intensity, a total of 1034 Tenm4 clusters were detected in 10 images representing 2 areas of neuronal segments of 5 hippocampal neurons. Tenm4 puncta were smaller (0.57 $\mu m^2 \pm 0.06$ SEM, $\pm$ 0.94 SD, $p < 0.0001$, Mann-Whitney test) than Synapsin puncta (0.74 $\mu m^2 \pm 0.04$ SEM, $\pm$ 0.85 SD). The colocalisation between Tenm4 with Synapsin was determined as above. Because the data was not normally distributed ($p < 0.0001$ by D'Agostino & Pearson omnibus normality test), the non-parametric Mann-Whitney rank-sum test was used. Tenm4 was significantly (n= 1034, 6.0 % $\pm$ 0.57 SEM, $\pm$ 18.51 SD, $p < 0.0001$) colocalised with Synapsin (Figure 3.11-l) compared to the negative Tenm4-control (n= 1034, 0.94 % $\pm$ 0.23 SEM, $\pm$ 7.38 SD). The proportion of Tenm4 clusters (Figure 3.11-m) that either fully or partially colocalised with Synapsin amounted to 22.37 % ($\pm$ 6.13 SEM, $\pm$ 13.7 SD). The proportion of random Tenm4 colocalisation with Synapsin in the negative control condition amounted to 3.53 % ($\pm$ 1.18 SEM, $\pm$ 2.64 SD). In colocalised Tenm4 puncta, the overlap with Synapsin (Figure 3.11-n) in average covered 32.81 % of the Tenm4 cluster area ($\pm$ 2.3 SEM, $\pm$ 31.59 SD).

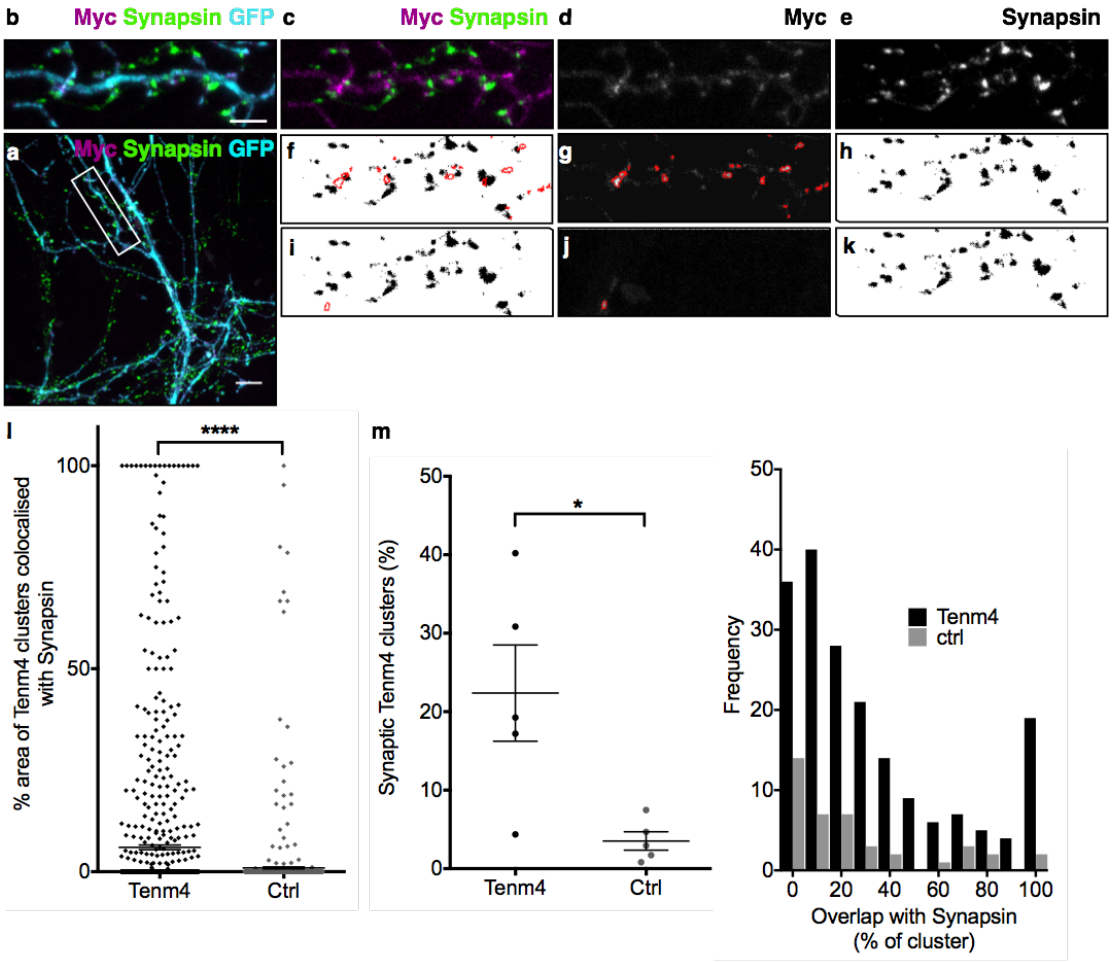

Figure 3.11. Colocalisation analysis between Tenm4-Myc and Synapsin in dissociated hippocampal neurons. **a.** Image of a representative hippocampal neuron, transfected with Tenm4-Myc and GFP, and stained for Synapsin. Scale bar: 10 µm. **b-c.** Dendritic segment of the neuron shown in **a**. Scale bar 5 µm. **d.** Tenm4-Myc localisation in dendritic segment. **e.** Dendritic segment stained for Synapsin. **f.** Colocalisation between Tenm4-Myc and Synapsin after image analysis. **g.** ROIs around Tenm4-Myc puncta after image analysis. **h.** Binary image of Synapsin puncta after image analysis. **i.** Control colocalisation between Tenm4-Myc and Synapsin after 90° rotation of the Tenm4-Myc image channel (**d, g**). **j.** ROIs around Tenm4-Myc puncta after image channel was rotated 90°. **k.** Binary image of Synapsin puncta after image analysis. **l**. Colocalisation between Tenm4 and Synapsin (black) and Synapsin and Tenm4-control (grey), ****P< 0.0001. **m**. Proportion of Tenm4 clusters (black) and Tenm4-control clusters (grey) colocalised with Synapsin per neuron, *p= 0.0317. **n**. Frequency of full or partial Tenm4 overlap with Synapsin in coloclaised puncta. Data is from 1034 Tenm4-Myc clusters and five hippocampal neurons. Two-tailed Mann-Whitney Test. Bars and error bars represent mean and SEM.

3.3.5 Comparison of the subcellular localisation of Teneurins with synaptic proteins

In order to assess the level of synaptic localisation of Teneurins compared to known synaptic proteins, the differences between Teneurin, Bassoon and Shank2 colocalisation with Synapsin were tested for statistical significance. As the datasets were not normally distributed, the non-parametric Kruskal-Wallis and Dunn's multiple comparisons tests were performed. The average fraction area of clusters overlapping with Synapsin was significantly lower for all four Teneurin paralogues compared to both Bassoon and Synapsin ($p < 0.0001$, Kruskal-Wallis and Dunn's multiple comparisons test Figure 3.12-a). However, the fraction area measures the degree of overlap between Synapsin and Teneurins (or Bassoon and Shank2 controls) for every individual cluster and thus takes into account whether there is full, partial or no overlap. Therefore, the proportion of colocalisation of Synapsin with Teneurins was compared to that of Shank2 and Bassoon (Figure 3.12-b). Only Tenm1 (17.85 % ± 3.12 SEM, ± 6.99 SD, $p=0.0143$, Dunn's multiple Comparisons test) and Tenm2 (19.26 % ± 2.9 SEM, ± 6.49 SD, $p=0.0267$, Kruskal-Wallis and Dunn's multiple Comparisons test) had a significantly lower proportion of clusters colocalising with Synapsin compared to Bassoon (56.52 % ± 1.07 SEM, ± 35.47 SD). The lower proportions of colocalised Tenm3 (23.04 % ± 3.39 SEM, ± 7.57 SD, $p = 0.2415$) and Tenm4 (22.37 % ± 6.13 SEM, ± 13.7 SD, $p = 0.0851$) clusters compared to Bassoon were not statistically significant. Furthermore, the proportion of colocalisation of all four Teneurins with Synapsin was not significantly different from Shank2 (39.24 % ± 6.341 SEM, ± 14.18 SD) for any of the Teneurin paralogues (Tenm1: $p = 0.3226$, Tenm2: $p = 0.5109$, Tenm3: $p > 0.9999$, Tenm4: $p > 0.9999$, Kruskal-Wallis and Dunn's multiple comparisons test).

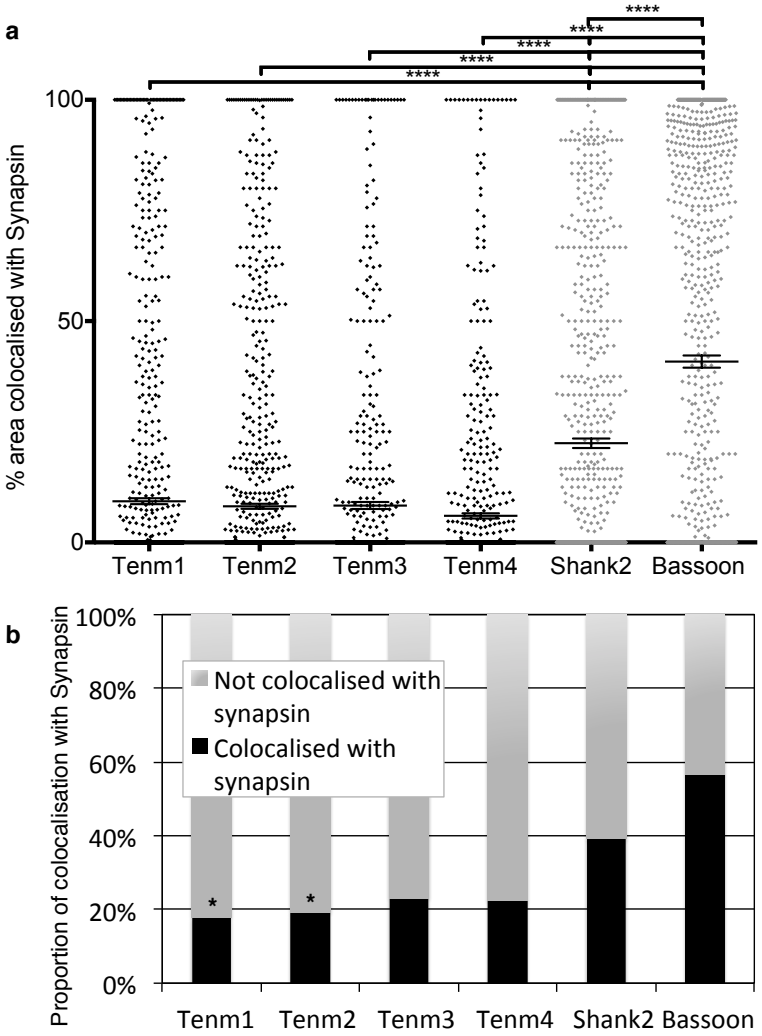

Figure 3.12. Colocalisation between Teneurins, Shank2 and Bassoon with Synapsin. **a**. Comparison of colocalisation between clusters of Tenm1 to Tenm4 (black), Shank2 and Bassoon (grey) with Synapsin, ****P< 0.0001, Dunn's multiple comparisons test. Bars and error bars represent mean and SEM **b**. Proportion of Teneurins, Shank2 and Bassoon colocalisation with Synapsin (black). Only Tenm1 (p= 0.0143) and Tenm2 (p= 0.0267) have a significantly lower proportion of clusters colocalising with Synapsin compared to Bassoon. Dunn's multiple comparisons test.

3.4 Summary and discussion

In this chapter, I investigated the subcellular localisation of Teneurins in cultured hippocampal neurons. Tenm3 and Tenm4 formed puncta along dendrites and axons as early as 7DIV. At 3DIV, both proteins were diffusely expressed throughout the cytoplasm. At 17DIV, expression of all four Teneurin homologues could be detected in puncta along dendrites and axons. The finding that Teneurins aggregated in puncta along neurites after 7DIV was the first indicator that the protein might indeed behave as a synaptic protein, since the punctate localisation pattern was reminiscent of that of other synaptic proteins. For instance, Shank2, which is amongst the first molecules of the PSD (Boeckers *et al.*, 2001), is evenly distributed in neurites and somata at 3DIV, but from 7DIV onwards it forms dot-like structures in dendrites and at later stages it is found in dendritic spines (Grabrucker *et al.*, 2009). It is important to note that it is currently unclear whether the observed Teneurin puncta are at the cell-surface or intracellular. This issue could be resolved in future experiments by omitting the use of a permeabilisation step during the immunocytochemical detection of Myc-tagged Teneurins.

In order to assess whether Teneurins are localised at synapses, the level of colocalisation between Teneurins and the presynaptic marker protein Synapsin was analysed at 17DIV using an unbiased approach. All four Teneurin paralogues significantly colocalised with Synapsin in comparison to the negative control condition. The negative control condition consisted of the colocalisation between Synapsin and the Teneurin channel rotated by 90º, thereby resulting in random, non-sense colocalisation. This result allowed us to conclude that Teneurins colocalise with Synapsin to an extent that is significantly higher than chance. However, comparing Teneurin-Synapsin codistribution with a random control has its problems. Indeed, this comparison does not allow for an unambiguous answer to the question whether Teneurins are synaptically localised. Hence, it was important to compare the Synapsin-Teneurin colocalisation to that of Synapsin with other known synaptic proteins such as Shank2 and Bassoon. All four Teneurins significantly differed from Shank2 (Tenm1: 9.32 %, Tenm2: 8.16 %, Tenm3: 8.33 %, Tenm4: 5.99 %, Shank2: 22.4 %) and Bassoon (40.87 %) in the mean percentage of cluster overlap with Synapsin (Figure 3.12-a). However, the proportion of Teneurin clusters overlapping with Synapsin (Tenm1:

17.85 %, Tenm2: 19.26 %, Tenm3: 23.04 %, Tenm4: 22.37 %) was not significantly different from Shank2 (38.24 %). In comparison to Bassoon (56.52 %), only Tenm1 and Tenm2 had a significantly lower proportion of clusters colocalising with Synapsin. It is important to note, however, that this analysis had low statistical power due to the small sample size and therefore it is possible that these differences may become significant with larger sample numbers. Indeed, the comparison of the proportions of clusters overlapping with Synapsin was calculated per neuron and therefore there were only 5 data points per condition.

The partial colocalisation of Synapsin with Bassoon and Shank2 reported in this chapter might seem surprising at first, however incomplete colocalisation within presynapses has previously been reported for Synapsin and Bassoon (tom Dieck *et al.*, 1998). Indeed, Synapsin and Bassoon appear largely codistributed at intermediate magnification, whereas at high magnification the two proteins only show partial colocalisation. Synapsin is homogenously distributed throughout presynaptic terminals, whereas Bassoon immunoreactivity appears in distinct little spots and is subsynaptically more restricted compared to Synapsin (tom Dieck *et al.*, 1998). The imaging performed in this chapter was at high magnification (0.10 µm/ pixel) and visualised large Synapsin puncta that only partially overlapped with small Bassoon puncta, which was consistent with these findings. Moreover, incomplete colocalisation between Shank2 and Synapsin was expected, because Shank2 is an excitatory postsynaptic protein, whereas Synapsin is a presynaptic protein found in both inhibitory and excitatory synapses. Indeed, it has been previously reported that about a quarter of all Shank2 signal does not colocalise with presynaptic Bassoon (Grabrucker *et al.*, 2009), most likely due to Bassoon labelling of inhibitory synapse active zones. When taking into account the high magnification used in the experiments in this chapter, an even lower degree of colocalisation between Shank2 and Synapsin is to be expected, as both proteins are localised in apposed synaptic compartments. It is important to note, however, that the colocalisation analysis method used in this chapter indiscriminately takes into account all protein clusters, regardless of whether they are in the axon, dendrites or dendritic spines. Therefore, even though most transport of synaptic proteins takes place in young neurons during early stages of synapse formation, it cannot be excluded that some of the non-colocalised Bassoon, Shank2 and Synapsin are not functional synapses, but instead may represent protein clusters that are

transported along dendrites and axons. Piccolo-Bassoon transport vesicles (or dense core vesicles), for instance, are most frequent in young neurons, where they carry active zone material to nascent presynapses (Shapira *et al.*, 2003), but they have also been observed in mature synapses (Grabrucker *et al.*, 2009).

There are several possible interpretations to explain the partial colocalisation of Teneurins with Synapsin. Firstly, it is likely that many detected Teneurin puncta may be in the process of being transported along axons and dendrites. Indeed, the transfection optimisation experiments showed that at least two days were needed post-transfection to observe punctate expression of Teneurins, indicating that intracellular trafficking of this large protein is slow and large amounts of the protein might have been in the process of being transported in neurites at the time of analysis. Another explanation for the high level of partial Teneurin-Synapsin overlap could suggest that Teneurins are more abundantly expressed on the postsynaptic site and therefore only partially colocalise with presynaptic Synapsin. However, this hypothesis needs to be further examined via a colocalisation analysis of Teneurin with a postsynaptic marker protein. Unfortunately, it was not possible to perform this analysis due to the time constraints of this PhD project. Lastly, it is possible that the low level of colocalisation with Synapsin stems from the fact that Teneurins may only be partially localised at Synapses, whilst a larger proportion might cluster within the dendritic shaft. Furthermore, it is important to note that some Teneurin puncta that overlapped with Synapsin may not be synaptic, since it is possible that not all Synapsin puncta are functional synapses.

An important drawback of the experiments presented in this chapter is that we have no way of verifying that the observed Teneurin localisation pattern corresponds to the endogenous pattern. Indeed, subcellular localisation was investigated through the use of tagged Teneurin expression constructs. As mentioned above, this is a common approach to investigate the subcellular localisation and transport of proteins and there are many reports of faithful localisation of GFP-tagged synaptic proteins (Arnold and Clapham, 1999; Craven, El-Husseini and Bredt, 1999; Bresler *et al.*, 2001; Perestenko and Henley, 2003; Jensen *et al.*, 2014). However, there is a risk that the tagged Teneurin proteins may fail to localise properly due to saturation of the targeting machinery. The endogenous subcellular localisation of Tenm2 in hippocampal neurons was

investigated in only one study, which showed that Tenm2 was mostly localised in dendrites, where it concentrated in dendritic spines and shafts (Silva *et al.*, 2011). The authors of this study elicited anti-Tenm2 antibodies in mice, but it is unclear whether these antibodies cross-react with other Teneurins. The endogenous Tenm2 localisation reported in this study is consistent with the subcellular localisation pattern of Tenm2 described in the present chapter. However, to our knowledge, this is the only study that investigated the subcellular localisation of a Teneurin and therefore no data on the localisation of Tenm1, Tenm3 and Tenm4 is available to compare to our findings. Unfortunately, it will not be possible to confirm that the Teneurin localisation reported here recapitulates the endogenous pattern until reliable antibodies are produced that specifically recognise the four Teneurin paralogues. Alternatively, one could generate transgenic mice with GFP knocked into the Teneurin loci responsible for synaptic localisation.

Primary cultures are a valuable system that has been instrumental for the field of neuroscience since it was first established (Banker and Cowan, 1977), however it comes with limitations. Due to the dissociated nature of the cultures, subtle structural changes are harder to detect than in intact brain tissue, where the morphology of neurons is better preserved. For this reason, despite the great care taken in the selection of analysed neurons, we cannot exclude that the morphology or function of neurons might have been affected following Teneurin overexpression. Indeed, overexpression of proteins is associated with the inherent risk of disrupting the normal function and morphology of neurons. Protein overexpression can lead to a wide variety of phenotypes, including de novo synapse formation and increased synaptic size and maturation, but it can also result in synapse reduction (El-Husseini, Schnell and Chetkovich, 2000; Passafaro *et al.*, 2003).

Another limitation was that in dissociated cultures, identification of different cell types on a morphological basis is almost impossible. Indeed, the accurate distinction of different neurons requires the use of cell type-specific antibodies. Hippocampal cultures consist of a heterogeneous population of neurons. The largest proportion of neurons (70-90 %) consists of excitatory DGCs and pyramidal cells from the CA1, CA2 and CA3 areas. Inhibitory neurons, of which basket cells are the most common, constitute no more than 30% of all the cells. To reduce the variability within the

hippocampal population, attempts were made to focus on one single cell type. The first choice was the CA1 pyramidal neuron, because all four Teneurin paralogues are expressed in CA1 (Figure 3.1). However, the identification of CA1 neurons in culture requires the combined use of antibodies against CTIP2, which labels CA1 pyramidal neurons and most DG neurons, and Prox1, which specifically labels DG neurons (Williams *et al.*, 2011). This would have raised the number of required antibodies to five, which would have been prohibitive both in terms of potential cross-reactivity and fluorophore detection. In contrast, it was possible to selectively label DG neurons as this only required the use of an anti-Prox1 antibdody. Focusing exclusively on DG neurons led to two problems; (1) a generally low transfection efficiency at 17DIV meant an even lower transfection efficiency for one specific cell type. (2) While Tenm1 is endogenously expressed in DG, it is likely that heterologous expression of Tenm2, Tenm3 and Tenm4 had cytotoxic effects, because DG neurons looked underdeveloped and exhibited apoptotic symptoms. For these reasons, I decided not to focus on only one cell type in this chapter. Instead I included all transfected hippocampal cells in the analysis, under the condition that neurons showed no obvious morphological changes as a result of Teneurin overexpression. As a result, it was not possible to assess whether different cell types exhibit different subcellular Teneurin localisation pattern, or indeed whether the analysed neurons endogenously expressed Teneurin (in addition to exogenously transfected Teneurin).

The findings presented in this chapter show that Teneurins cluster in puncta along axons and dendrites and partially colocalise with the presynaptic protein Synapsin, indicating that Teneurins are partially localised at synapses. However, there were some drawbacks with the experiments presented in this chapter. Notably, the use of Synapsin as a proxi for synapses is problematic and raises the need for a more reliable method of identifying synapses, such as a morphologically distinguishable feature as in the case of dendritic spines. Additionally, the use of epitope-tagged Teneurin to analyse the protein's expression pattern is not ideal, however in light of the lack of alternatives, this was the only viable method to use. As described in chapter 1, Teneurins have many similarities with established synaptic cell-adhesion molecules such as N-Cadherins, Neurexins and Neuroligins. Notably, Teneurins are transmembrane adhesion molecules that have the ability to bind homo- and heterophilically (Rubin *et al.*, 2002; Silva *et al.*, 2011; Mosca *et al.*, 2012; Beckmann *et al.*, 2013; Boucard, Maxeiner and Südhof, 2013; Mosca and

Luo, 2014; O'Sullivan *et al.*, 2014), and they have established roles in neuronal wiring (Leamey *et al.*, 2007; Hong, Mosca and Luo, 2012; Antinucci *et al.*, 2013). Despite the limitations in this chapter, this is the first study to analyse the subcellular localisation pattern of all four Teneurin paralogues and to show that they are - at least partially - localised at synapses. Thus, these findings provide further support for a role of Teneurins in mediating transsynaptic adhesion in vertebrates. However, Teneurins also strongly clustered within dendritic shafts and non-synaptic parts of axons and therefore are likely to fulfil additional roles, which are yet to be identified. As such, the results presented in this chapter, provide a good starting point to further explore the nature of the role of Teneurins in synapse formation.

4 Subcellular Tenm3 localisation in CA1 neurons

4.1 Introduction

In the previous chapter I investigated the subcellular localisation of the four vertebrate Teneurin paralogues, Tenm1, Tenm2, Tenm3 and Tenm4, in dissociated hippocampal neurons. In the present chapter, I will focus specifically on the subcellular localisation pattern of Tenm3 in CA1 neurons.

Teneurin 3 is expressed in a strong gradient in the CA1 region of the hippocampus (Figure 3.1). The subcellular localisation pattern of Tenm3 in CA1 neurons was investigated using organotypic hippocampal cultures. Organotypic cultures were the ideal model system to perform a detailed analysis of Tenm3 localisation in CA1 neurons, as they retain many of the advantages associated with *in vitro* systems whilst also offering a more naturalistic context than the dissociated culture system. Indeed, organotypic cultures make neurons immediately accessible to manipulations such as transfection using a biolistic particle delivery system. This method was originally created to transfect plant cells (Klein *et al.*, 1987) and has since been used as an effective tool to transfect a variety of animal tissue (Cheng, Ziegelhoffer and Yang, 1993). It is a physical method of transfection where micron-sized gold particles coated with plasmid DNA are accelerated to high velocity through pressurised helium and thus penetrate deep inside the organised tissue of organotypic slices. Single particles can be coated with multiple plasmids to allow simultaneous expression of several genes. Once the DNA has crossed the membrane, cells transcribe the DNA as after other transfection procedures. One significant drawback of biolistic gene delivery is that it often leads to tissue damage, something mammalian neurons are very sensitive to. For the experiments in this chapter, organotypic hippocampal slices were prepared from 7 day-old mice and cultured for further 7 days. After one day in culture, slices were biolistically transfected with DNA bullets coated in Tenm3 and mGFP expression plasmids using a helios gene gun (BioRad). The gene bullets were prepared from the same expression plasmids used in work described in the previous chapter; i.e. the full length, myc-tagged Tenm3 vector and the mGFP vector. As for cationic-lipid mediated transfection described in the previous chapter, biolistic transfection of neurons with

Tenm3 remained a considerable challenge due to the size of the plasmid and the efficiency was very low.

Organotypic hippocampal cultures are characterised by a well preserved three-dimensional organisation of the nervous tissue (Stoppini, Buchs and Muller, 1991) and exhibit similar morphological properties to those found in adult hippocampal slices (Zimmer and Gähwiler, 1984). The fact that organotypic cultures maintain structural and synaptic organisation was particularly useful for our experiments, making it possible to anatomically visualise and distinguish different cell types, notably CA1 neurons. Furthermore, pyramidal neurons are covered with thousands of dendritic spines, which constitute the postsynaptic site for most asymmetric excitatory glutamatergic synapses, thus providing a morphologically distinguishable feature of synapses. Dendritic spines are better preserved in organotypic slices compared to dissociated neurons and thus asymmetric synapses could be identified without the use of immunohistochemistry against synaptic marker proteins. Pyramidal neurons receive synaptic inputs at the soma, axon and dendrites. In this chapter the focus is on excitatory synapses on the dendrites and not on the inhibitory input onto axon, soma and dendrites, as the identification of symmetrical synapses requires the use of inhibitory synaptic markers. The dendritic tree of pyramidal neurons has two domains; the basal dendrites, descending from the base of the soma, and the apical dendrites, descending from the apex. Different dendritic domains receive distinct synaptic inputs. As described in chapter 1, the distal apical tuft of CA1 neurons receives input from the entorhinal cortex and from the thalamus through the temporoammonic pathway, whereas proximal apical dendrites and basal dendrites receive input from CA3 through the Schaffer collaterals (Figure 1.6; Andersen, 2007). Furthermore, proximally located CA3 neurons (closer to the hilus of the DG) project primarily to apical dendrites, whereas distally located CA3 neurons (closer to CA2) project more to basal dendrites (Ishizuka, Weber and Amaral, 1990; Li *et al.*, 1994). However, there is a rationale for subdividing dendritic trees even further (Spruston, 2008), as several observations have suggested that synapses at different dendritic locations perform different specialised functions. In CA1 neurons for instance, mid apical dendrites have higher AMPAR densities and more perforated synapses than proximal apical dendrites (Nicholson *et al.*, 2006). Conversely, dendrites in the apical tuft have large numbers of perforated synapses but with lower AMPAR densities (Nicholson *et al.*, 2006) as well as large numbers of excitatory synapses on

the dendritic shaft and inhibitory inputs onto spines (Megías *et al.*, 2001). The high AMPAR densities and proximal location of synapses from CA3 onto apical dendrites suggest their inputs are integrated differently from inputs from the entorhinal cortex, which are restricted to the distal tuft. But even inputs from the same source onto various dendritic regions are likely to have distinct properties. This is exemplified by the observations that inputs onto the main apical dendrite and the oblique apical dendrites are integrated differently, although they both originate from CA3 through the Schaffer collaterals (Gasparini, Migliore and Magee, 2004; Losonczy and Magee, 2006). This provides further justification for distinguishing between populations of synapses on the basis of their location on different dendritic domains. In this chapter, oblique apical dendrites of the *stratum radiatum* as well as basal dendrites of the *stratum oriens* were analysed (Figure 1.6). Even though both domains receive input from Schaeffer collaterals, they are likely to integrate it differently. For this reason, I report results from apical and basal measurements individually in this chapter.

In this chapter, the aim was to thoroughly investigate the subcellular localisation pattern of Tenm3 in CA1 neurons and to establish whether Tenm3 is localised at excitatory synapses. I begin by characterising Tenm3 localisation in dendritic spines, followed by an investigation of the broader Tenm3 distribution along the dendritic backbone.

4.2 Results

CA1 neurons in organotypic hippocampal cultures were biolistically cotransfected with expression vectors for Tenm3 and mGFP at a ratio 3.5:1. Due to the well-preserved architecture of cells, morphological aberrations following transfection could be more confidently identified than in dissociated culture and all CA1 neurons analysed here had no obvious arborisation defects. Still, overexpression of Tenm3 was likely to have some cytotoxic or functional effects on a subcellular level, as small bumps could be detected along dendrites and axons making them appear "blebbed" and probably indicating the beginning of apoptotic processes. In average, there were <1 transfected excitatory hippocampal cells (pyramidal neuron of CA1, CA2 or CA3 or dentate granule neuron) per slice (0.72 ± 1.8 SD), with some slices exhibiting up to 6 transfected pyramidal neurons but the majority of slices exhibiting no transfected excitatory cells. Additionally, there were many off-target transfections of astrocytes expressing GFP (Figure 4.2-b). Moreover, some transfected pyramidal neurons expressed only GFP and no detectable Tenm3. The low numbers of transfected pyramidal neurons were undoubtedly also a result of cell death, since slices exhibited larger numbers of GFP-positive neurons one day after transfection (2.1 ± 1.5 SD) compared to 6 days post transfection (slices were transfected at 1DIV and fixed at 7DIV). Furthermore, control CA1 neurons transfected with GFP only (1.12 ± 0.64 SD) survived better after 7DIV than neurons cotransfected with GFP and Tenm3, indicating that some cytotoxicity emanated from Tenm3 overexpression. Because of the very low transfection efficiency, only 7 cotransfected CA1 neurons from 5 slices from 5 independent cultures could be selected for imaging and further analysis.

4.2.1 Tenm3 in dendritic spines

To analyse the localisation of Tenm3 in spines, two to three image-stacks at a resolution of 0.104 μm were taken of every analysed CA1 neuron; one to two image-stacks of the basal dendrites and one of the apical dendrites. Unfortunately, the signal to noise ratio in slices was very low and it was therefore not possible to analyse all the dendrites in every image. For every image two to three dendrites with the best resolution were selected and regions of interest were manually traced in ImageJ around spines ($Spine_{ROI}$, Figure 4.1, Figure 4.2-d). Spines were traced in the focal plane and only in

the GFP channel to avoid bias. Fluorescence intensity in every spine was then measured in the GFP channel and Tenm3 channel separately. Spine fluorescence intensity values ($Tenm3FI_{Spine}$, $GFPFI_{Spine}$) were normalised to the median fluorescence intensity of all spines in every image. For a more detailed description of the analysis refer to 2.6.4.1

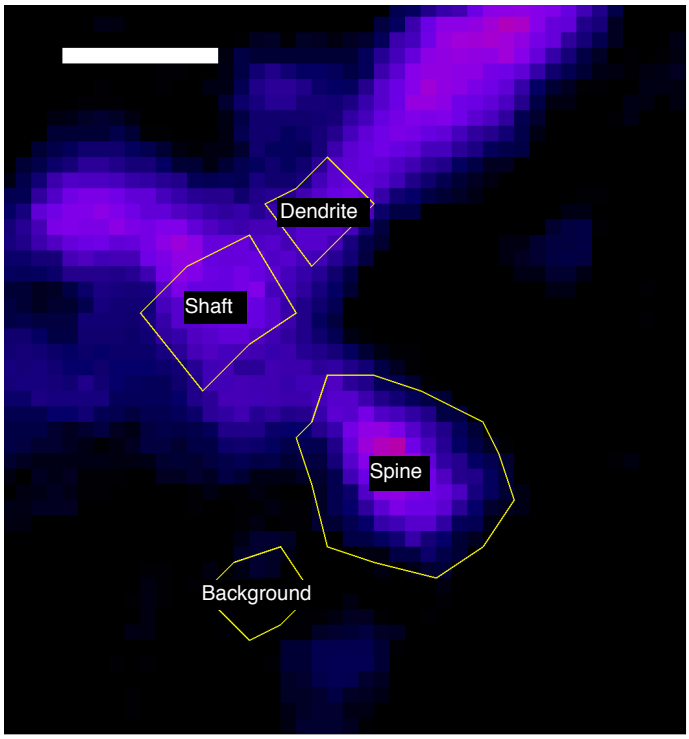

Figure 4.1. ROI selection for Tenm3 localisation analysis in CA1 neurons. For each spine, four ROIs were selected: SpineROI, ShaftROI, DendriteROI, BackgroundROI. Scale bar: 1µm.

Cotransfected CA1 neurons expressed GFP and Myc-tagged Tenm3, which was visualised with an anti-Myc antibody. Following immunostaining Tenm3 could be detected at relatively low levels throughout dendritic arbours. Interestingly, the protein aggregated in discrete clusters (Figure 4.2-e), consistent with our observations in dissociated cultures. For all of the analyses below, non-parametric tests were used because normality testing revealed that $Tenm3FI_{Spine}$ values did not follow a normal distribution (basal: n = 444, 1.306 a.u. ± 0.065 SEM, ± 1.372 SD, $p < 0.0001$; apical: n = 200, 1.253 a.u. ± 0.077 SEM, ± 1.089 SD, $p < 0.0001$, D'Agostino & Pearson normality test).

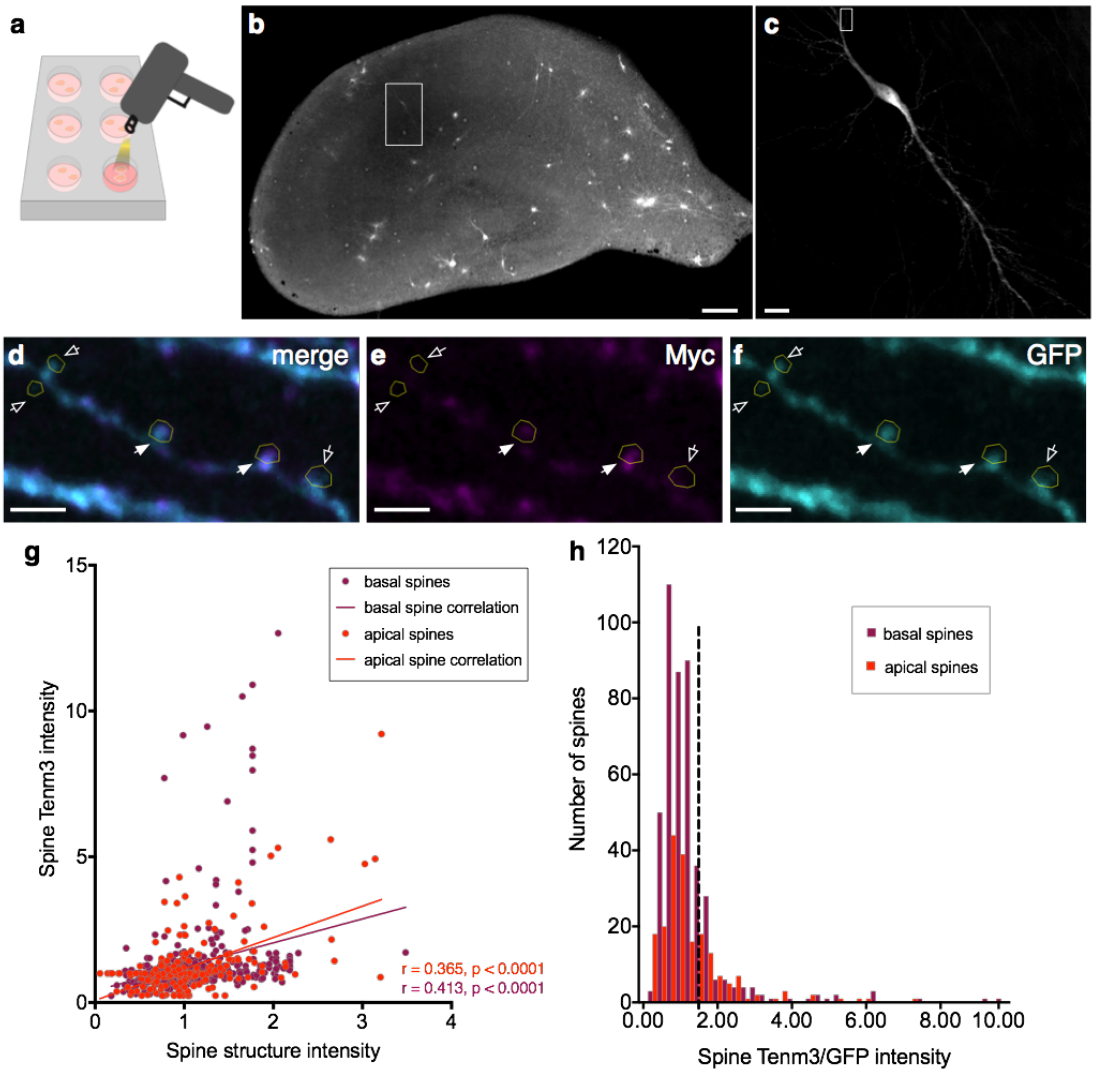

Figure 4.2. Tenm3 localisation in dendritic spines of CA1 neurons. **a-b.** Organotypic hippocampal slice biolistically transfected with Tenm3-Myc and GFP. The white square in **b** indicates a positively transfected CA1 neuron. Pyramidal neurons of CA3 and the subiculum as well as astrocytes were also transfected in this slice. The scale bar is 200μm. **c.** Magnified view of transfected CA1 neuron. The scale bar is 20μm. **d-f.** Representative image showing localisation of Tenm3-Myc in a basal dendritic segment of the CA1 neuron indicated with the white square in **c**. Dendritic spines are indicated by yellow ROIs. Note the different Tenm3-Myc levels in neighboring spines, with Tenm3-Myc localisation in some spines (filled arrows) and some other spines devoid of Tenm3-Myc (empty arrows). The scale bar is 10μm. **g.** Correlation between basal (purple) and apical (red) spine-Tenm3 intensity and spine-GFP intensity (spine structure). r, non-parametric Spearman correlation coefficient. **h.** Histogram of basal (purple) and apical (red) spine Tenm3 intensity, where Tenm3 intensity is determined as the ratio Tenm3/GFP intensity. The dotted black line indicates the threshold above which spines are considered to express Tenm3 (1.531). Spines below this threshold are considered to express only backgrund levels of Tenm3 (see text).

Tenm3 intensity in spines was positively correlated with spine size (Figure 4.2-g) in basal (Spearman r = 0.413, p < 0.0001) and apical dendrites (Spearman r = 0.365, p < 0.0001). Spine size was estimated using the GFP fluorescence intensity, because the fluorescence intensity of homogenously distributed proteins is correlated with spine size and therefore larger spines display higher fluorescence intensity levels (Zhang *et al.*, 2015). This finding was also confirmed through a different measure (basal: Spearman r = 0.249, p < 0.0001; apical: Spearman r = 0.245, p = 0.0005), where spine size was estimated using the $Spine_{ROI}$ area (Figure 4.3). However, as spines were traced manually, this measure was less reliable than GFP intensity. Interestingly, there were dramatic differences in Tenm3 signal in spines within a few micrometres of each other along the same dendrite; some spines had high levels of Tenm3 while neighbouring spines had barely detectable levels (Figure 4.2-e).

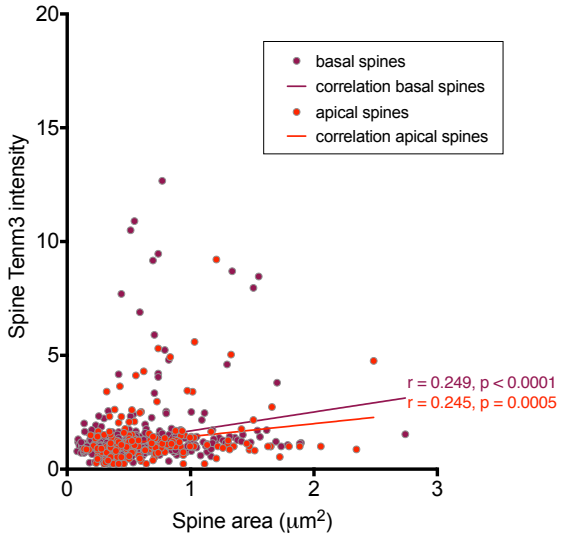

Figure 4.3. Correlation between Tenm3 intensity and spine size. Tenm3 fluorescence intensity in basal (purple) and apical (red) spines is correlated with spine size. r, non-parametric Spearman correlation coefficient.

As Tenm3 was overexpressed in CA1 neurons, a fraction of the protein was expected to homogenously spread throughout the cytoplasm. Consequently, the resulting background Tenm3 fluorescence was expected to correlate with spines size. In order to compensate for changes in spine size, the ratio of $Tenm3FI_{Spine}$ to $GFPFI_{Spine}$ ($Ratio_{Spine}$; 1.291 ± 0.048 SEM, ± 1.024 SD) was calculated. An intensity threshold was then set to

identify the spines for which Tenm3FI$_{Spine}$ was higher than expected by an increase in spine volume. The threshold value was calculated as *Mean(Ratio$_{Spine}$) + 5 * SEM*, which amounted to the threshold value 1.531. Spines that had a Ratio$_{Spine}$ above this threshold were considered to have high levels of Tenm3 (termed "Tenm3-positive spines"), whereas spines below that threshold were considered to only have background Tenm3 signal (termed "Tenm3-sub-threshold spines"; Figure 4.2-h). This data indicates that only a subpopulation of 17.34 % of all basal spines and 25.5 % of all apical spines were Tenm3-positive. When apical and basal spines were pooled together, the total proportion of Tenm3-positive CA1 spines amounted to 19.87 %. Tenm3 fluorescence intensity at Tenm3-positive spines (Figure 4.4) was not significantly different between basal (n = 77, 2.723 a.u. ± 0.199 SEM, ± 1.745 SD) and apical dendrites (n = 51, 2.572 a.u. ± 0.179 SEM, ± 1.277 SD, p > 0.9999, Kruskal-Wallis & Dunn's multiple comparisons test).

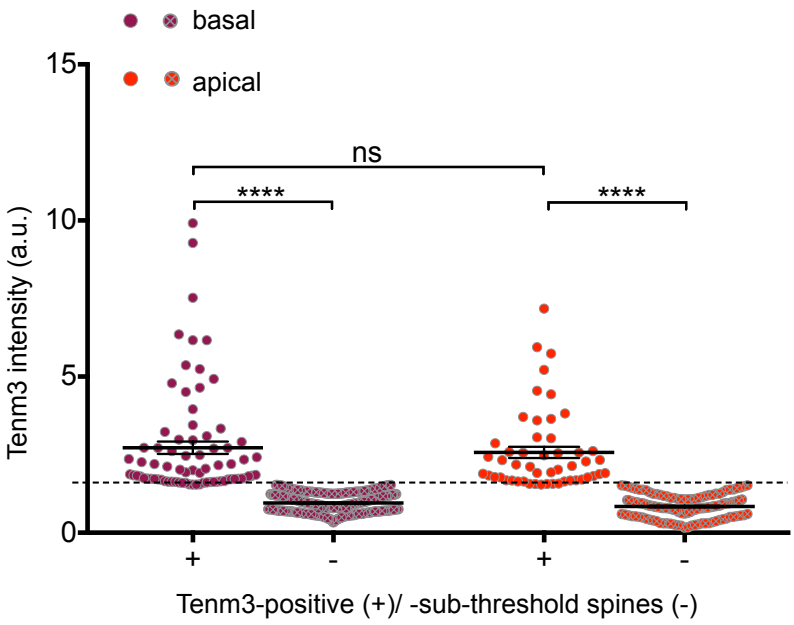

Figure 4.4. Tenm3 fluorescence intensity in Tenm3 positive spines. Tenm3 intensity did not significantly differ between basal (purple) and apical (red) Tenm3-positive spines, p > 0.9999 or between Tenm3-sub-threshold spines, p = 0.0845. The low-level background fluorescence intensity that was present in Tenm3-sub-threshold spines, was significantly lower compared to Tenm3-positive spines. The dotted black line represents the cut-off value of 1.531, above which spines were considered to be Tenm3-positive. Kruskal-Wallis test with Dunn's multiple comparisons test, ns for non-significant, ****p < 0.0001. Error bars represent sem.

4.2.2 Tenm3 in the dendritic shaft

Whilst analysing Tenm3 localisation in spines, it became apparent that many Tenm3 clusters seemed to form in the dendritic shaft below the spine. In order to analyse Tenm3 localisation in shafts, $Shaft_{ROIs}$ were traced in the dendritic backbone encompassing the radius of the dendrite, centred on each spine and in the same focal plane as spines (Figure 4.1, Figure 4.5-c). ROIs were always traced in the GFP channel to avoid bias. Due to the noise in these images, a $Background_{ROI}$ was translated in x/y to a region of the image nearby the spine that was representative of the background fluorescence. Next, fluorescence intensities were measured for every $Shaft_{ROI}$ and its corresponding $Spine_{ROI}$ and $Background_{ROI}$ in the GFP channel and Tenm3 channel respectively. Background-subtracted values were generated by subtracting the intensity measured in $Background_{ROI}$ from the intensity measured in every $Shaft_{ROI}$ and $Spine_{ROI}$. In order to avoid division by 0 in subsequent steps, background-subtracted intensity values below 30 were reset to 30 (considered background fluorescence) and normalised. For a more detailed description of the analysis refer to 2.6.4.2.

Tenm3 was strongly localised in shafts. Normality testing revealed that shaft-Tenm3 intensity values in basal and apical dendrites did not follow a Gaussian distribution (basal: 2.01 a.u. ± 0.101 SEM ± 2.123 SD, $p < 0.0001$; apical: 3.208 a.u. ± 0.257 SEM ± 3.597 SD, $p < 0.0001$, D'Agostino & Pearson omnibus normality test), therefore non-parametric tests were used in the subsequent analyses. Shaft-Tenm3 fluorescence intensity weakly correlated with spine size in basal (Spearman $r = 0.197$, $p < 0.0001$, Figure 4.5-d) and apical (Spearman $r = 0.145$, $p < 0.042$) dendrites. I was interested in the relationship between spine-Tenm3 and shaft-Tenm3 and found that Tenm3 intensity levels between those two areas did correlate in both basal (Spearman $r = 0.237$, $p < 0.0001$) and apical dendrites (Spearman $r = 0.192$, $p = 0.0075$, Figure 4.5-e). Further analysis of this relationship (Figure 4.5-f) revealed that shafts below Tenm3-positive spines (these spines were identified as described above in 4.2.1) had significantly higher levels of Tenm3 (basal: 2.61 a.u. ± 0.286 SEM, ± 2.576 SD, $p = 0.0405$; apical: 4.423 a.u. ± 0.696 SEM, ± 4.511 SD, $p = 0.0416$, Mann-Whitney test) compared to shafts below spines with sub-threshold Tenm3 levels (basal: 1.875 a.u. ± 0.105 SEM, ± 1.987 SD; apical: 2.99 ± 0.283 SEM, ± 3.529 SD). However, it is important to note that this difference only narrowly reached statistical significance. This highlights the fact that

Tenm3 is not only localised at shafts below Tenm3-positive spines, but also at shafts below spines with sub-threshold levels of Tenm3, albeit at slightly lower levels. As expected, there were no significant differences between GFP intensity levels at shafts below Tenm3-positive (basal: 1.224 a.u. ± 0.053 SEM, ± 0.484 SD, p = 0.0568; apical: 1.493 a.u. ± 0.096 SEM, ± 0.633 SD, p = 0.1245, Mann-Whitney test) and Tenm3-sub-threshold spines (basal: 1.402 a.u. ± 0.035 SEM, ± 0.659 SD; apical: 1.289 a.u. ± 0.04 SEM, ± 0.5 SD).

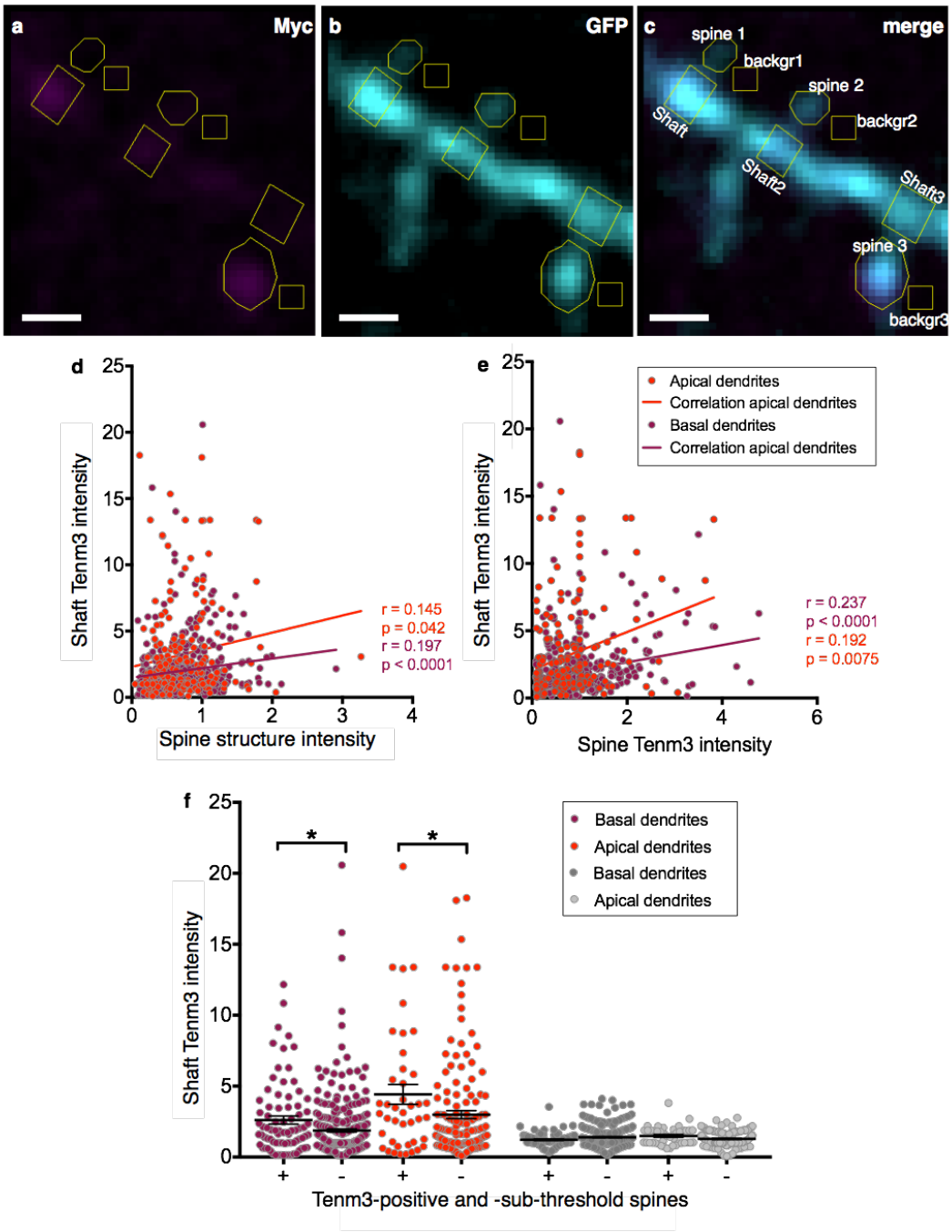

Figure 4.5. Tenm3 localisation in dendritic shafts of CA1 neurons. **a-c.** Representative image showing localisation of Tenm3-Myc in a basal dendritic segment. For every spine, three ROIs were traced: SpineROI, ShaftROI and BackrgoundROI (**c**). The scale bar is 1μm. **d.** Correlation between Shaft-Tenm3 intensity and spine size (spine-GFP intensity) in basal (purple) and apical (red) dendrites. **e.** Correlation of Shaft- and spine-Tenm3 intensity in basal (purple) and apical (red) dendrites. r, non-parametric Spearman correlation coefficient. **f.** Shaft-Tenm3 intensity at basal (purple) and apical (red) spines with high levels of Tenm3 (+) and spines with sub-threshold levels of Tenm3 (-). Basal and apical Tenm3-positive spines have significantly higher levels of Shaft-Tenm3 compared to spines with sub-threshold Tenm3 levels. The control expression of GFP did not significantly differ between Tenm3-positive and -sub-threshold spines. Non-parametric Mann-Whitney test. *p<0.05. Error bars represent sem.

In order to evaluate the proportion of shafts below Tenm3-positive and –sub-threshold spines with high levels of Tenm3 intensity, the ratio of $Tenm3FI_{Shaft}$ to $Tenm3FI_{Spine}$ was calculated ($Tenm3Ratio_{Shaft}$). Because Tenm3-positive spines have high Tenm3 intensity, shafts that had a $Tenm3Ratio_{Shaft} \geq 1$ were considered to have high levels of Tenm3, with either equal or higher $Tenm3FI_{Shaft}$ compared to $Tenm3FI_{Spine}$ (Figure 4.6-b, d). 71.95% of basal and 93.02% of apical shafts below Tenm3-positive spines had high levels of $Tenm3FI_{Shaft}$ (Figure 4.6-a). Spines with sub-threshold levels of Tenm3 only exhibit background Tenm3fluorescence, thus $Tenm3FI_{Spine}$ in Tenm3-positive spines was in average 1.76 times higher in basal (1.516 a.u. ± 0.129 SEM, ± 1.172 SD, $p < 0.0001$, Mann-Whitney test) and 2.96 times higher in apical (1.91 a.u. ± 0.399 SEM, ± 2.617 SD, $p < 0.0001$, Mann-Whitney test) spines compared to Tenm3-sub-threshold spines (basal: 0.862 a.u. ± 0.028 SEM, ± 0.53 SD; apical: 0.645 a.u. ± 0.034 SEM, ± 0.428 SD). Therefore, only shafts below Tenm3-sub-threshold spines with a $Tenm3Ratio_{Shaft} \geq 1.76$ in basal dendrites and ≥ 2.96 in apical dendrites were considered to have high levels of Tenm3 (Figure 4.6-c, e). Interestingly, 46.41 % of shafts below Tenm3-sub-threshold spines in basal dendrites and 56.33 % in apical dendrites had high levels of $Tenm3FI_{Shaft}$. This indicates that Tenm3 clusters at the base of the majority of Tenm3-positive spines, but it is also found at the shaft of about half the spines that do not have Tenm3 signal. In total, 51.13 % of all basal shafts and 64.18% of all apical shafts have high levels of Tenm3 intensity. This surprising finding indicated that Tenm3 is more frequently localised at the shaft than at the spine.

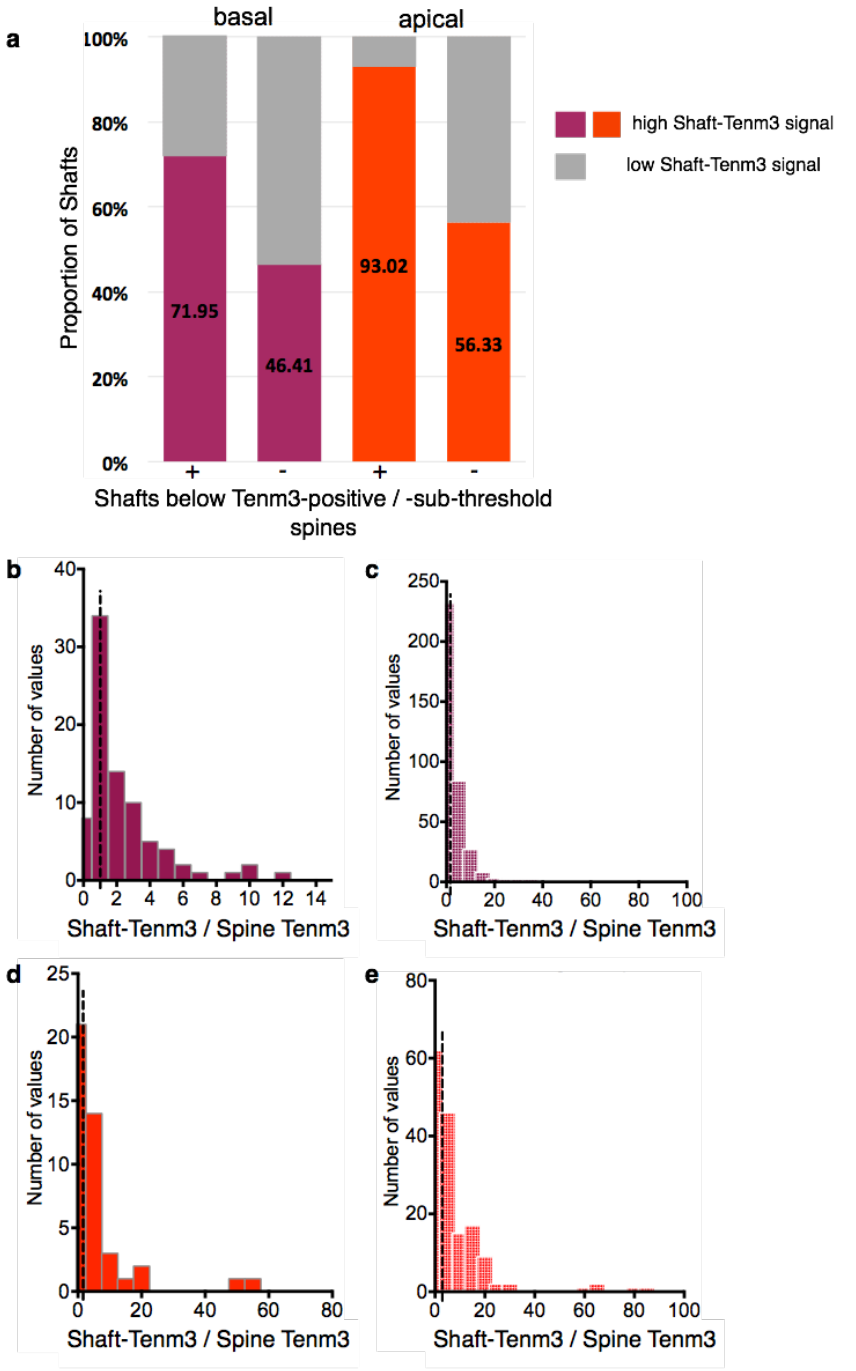

Figure 4.6. Proportions of shafts with high Tenm3 intensity below Tenm3-positive and -sub-threshold spines. **a.** Proportions of shafts with high and low Tenm3 signal below basal (purple) and apical (red) Tenm3-positive (+) and -sub-threshold (-) spines. **b-d.** Histograms of the ratio Shaft-Tenm3/Spine-Tenm3 in Tenm3-positive basal spines (**b**), in Tenm3-sub-threshold basal spines (**c**), in Tenm3-positive apical spines (**d**) and in Tenm3-sub-threshold apical spines (**e**). Dotted black lines represent the thresholds above which Tenm3 signal is considered to be strong in shafts. For Tenm3-positive spines (**b, d**) the threshold is 1, for basal Tenm3-sub-threshold spines (**c**) the threshold is 1.76 and for apical Tenm3-sub-threshold spines (**e**) the threshold is 2.96.

As it became apparent that Tenm3 occurs at the shaft more often than at the spines, I proceeded to investigate which of the two had the higher Tenm3 signal. As spines are smaller than the dendritic backbone the fluorescence intensity in spines is naturally lower. In order to get a measure of the differential fluorescence intensity in spines and shafts of a homogenously cytosolic distributed protein, the ratio of $GFPFI_{Shaft}$ to $GFPFI_{Spine}$ was calculated ($GFPRatio_{Shaft}$; Figure 4.7). In basal dendrites, $GFPFI_{Shaft}$ was in average 3.196 (± 0.252 a.u. SEM, ± 3.609 SD) times higher than $GFPFI_{Spine}$ and 2.556 times higher in apical dendrites (± 0.176 a.u. SEM, ± 1.394 SD). $Tenm3FI_{Shaft}$ was in average 3.572 times higher $TenmFI_{Spine}$ (± 0.325 a.u. SEM, ± 6.855 SD) in basal dendrites, whereas in apical dendrites it was 7.148 (± 0.745 a.u. SEM, ± 10.52 SD) times higher. In both basal and apical dendrites, the $Tenm3Ratio_{Shaft}$ was significantly higher compared to $GFPRatio_{Shaft}$ (basal: $p < 0.0001$; apical: $p = 0.0121$, Mann-Whitney test; Figure 4.7). This indicates that Tenm3, unlike GFP, is not a homogenously distributed protein, but rather, it is disproportionately targeted to the shaft. Thus, Tenm3 localisation is higher in the shaft relative to the spine.

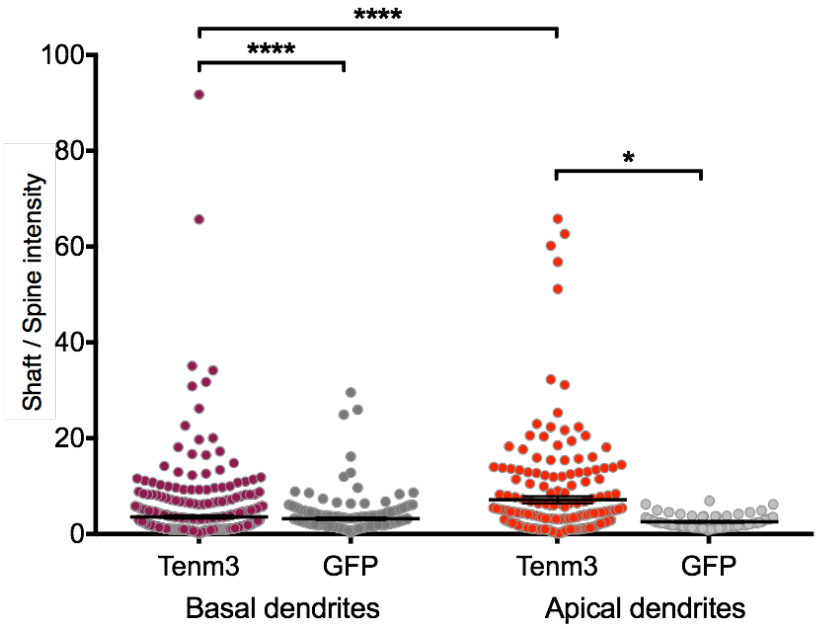

Figure 4.7. Tenm3 signal in Shafts compared to spines. The ratio shaft/spine fluorescence intensity was calculated for Tenm3 and GFP. In both apical and basal dendrites, the ratio shaft/spine is significantly higher for Tenm3 than for GFP. ****$p < 0.0001$, *$p = 0.0121$, Mann-Whitney test. The Tenm3 ratio is also significantly higher in apical dendrites compared to basal dendrites. ****$p < 0.0001$, Kruskal-Wallis test with Dunn's multiple comparisons test.

Finally, I wanted to investigate how restricted Tenm3 clustering was in the dendritic shaft. In order to investigate this, Tenm3 intensity was measured both in the shaft below the spine and at adjacent points on the dendrite. These points were called $Dendrite_{ROI}$ and were traced on the dendrite approximately ~0.5µm distally to the $Shaft_{ROI}$ (Figure 4.1, Figure 4.8-a). As previously, $Dendrite_{ROI}$ and $Shaft_{ROI}$ values were background-subtracted and normalised. For a detailed description of this, refer to 2.6.4.3.

In basal dendrites, $Tenm3FI_{Shaft}$ was in average 2.293 times higher than $Tenm3FI_{Dendrite}$ (± 0.139 a.u. SEM, ± 2.931 SD), in apical dendrites it was 2.893 (± 0.246 a.u. SEM, ± 3.482 SD) times higher (Figure 4.8-d). The ratio of $GFPFI_{Shaft}$ to $GFPFI_{Dendrite}$ ($GFPRatio_{Dendrite}$) was 1.521 (± 0.066 a.u. SEM, ± 1.388 SD) in basal dendrites and 1.485 (± 0.094 a.u. SEM, ± 1.338 SD) in apical dendrites. The difference between Tenm3 and GFP was significantly different in both basal ($p < 0.0011$, Mann-Whitney test) and apical ($p < 0.0002$, Mann-Whitney test) dendrites, indicating that Tenm3 does indeed cluster in the shaft in a spatially restricted manner and is not diffusely localised along dendrites.

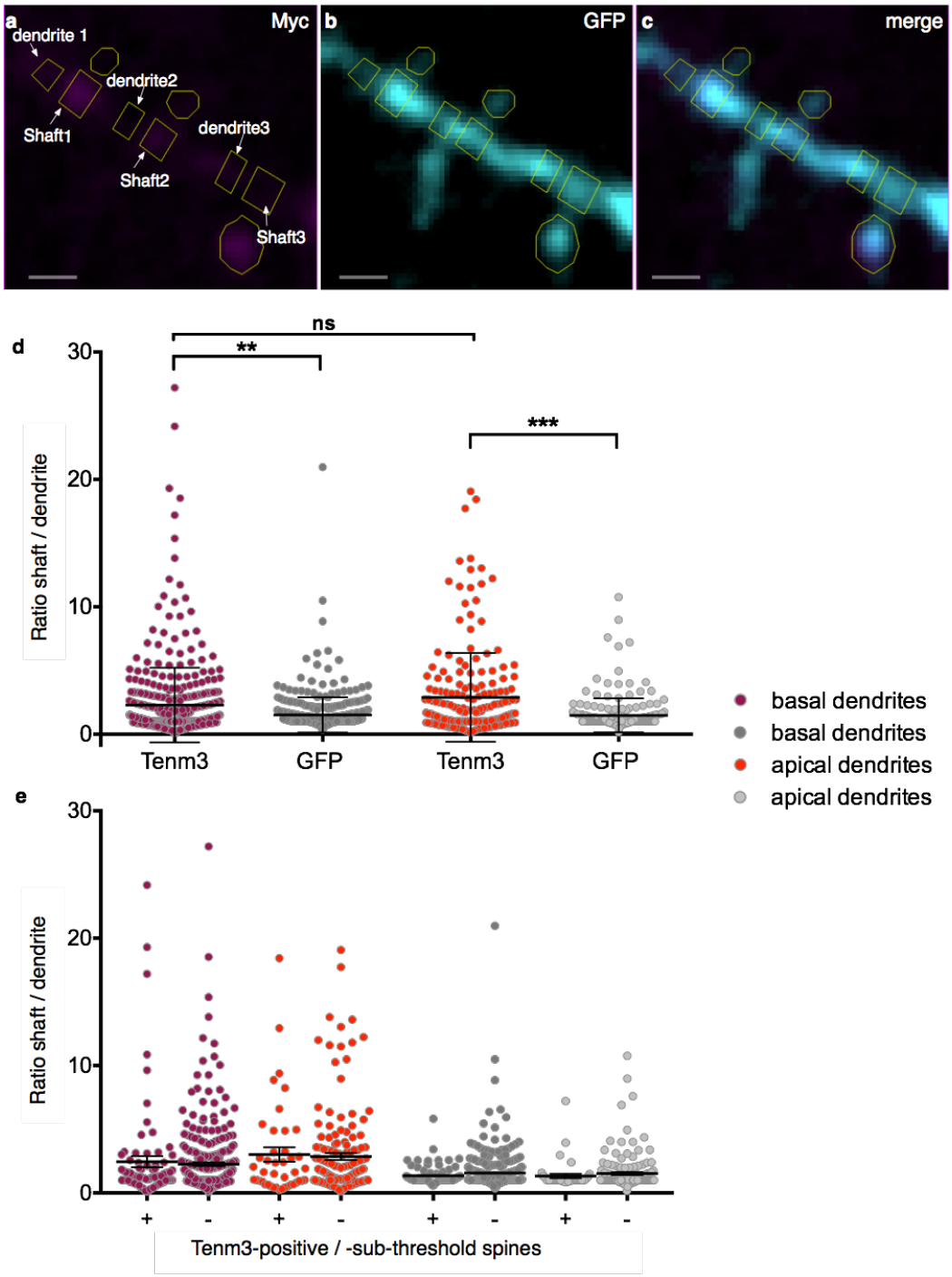

Figure 4.8. Clustering of Tenm3 at shafts **a-c.** Representative image showing localisation of Tenm3-Myc in a basal dendritic segment. DendriteROIs and ShaftROIs were traced. The scale bar is 1μm. **d.** The ratio shaft/dendrite fluorescence intensity was calculated. In both apical and basal dendrites the shaft/dendrite ratio is significantly higher for Tenm3 compared to uniformly distributed GFP. Mann-Whitney test. **p = 0.0011, ***p < 0.0002. There is no significant difference between the shaft/dendrite ratio for Tenm3 intensity in basal and apical spines, p > 0.9999, Kruskal-Wallis test. **e.** There is no significant difference between shaft/dendrite Tenm3 ratios in Tenm3-positive and -sub-threshold spines. There also were no significant differences in the GFP control condition. Kruskal-Wallis test. Error bars represent sem.

Spatially restricted clustering of Tenm3 prevailed at both Tenm3-positive and –sub-threshold spines (Figure 4.8-e), as the $Tenm3Ratio_{Dendrite}$ did not differ between the two in either basal (Tenm3-positive: 2.451 a.u. ± 0.438 SEM, ± 3.966 SD; Tenm3-sub-threshold: 2.257 a.u. ± 0.139 SEM, ± 2.647 SD, p = 0.1906, Mann Whitney test) nor apical dendrites (Tenm3-positive: 3.015 a.u. ± 0.569 SEM, ± 3.731 SD; Tenm3-sub-threshold: 2.859 a.u. ± 0.273 SEM, ± 3.422 SD, p = 0.7071, Mann-Whitney test). In the GFP control condition, as expected, there were no significant differences in $GFPRatio_{Dendrite}$ between Tenm3-positive and -sub-threshold spines (basal: Tenm3-positive: 1.346 a.u. ± 0.083 SEM, ± 0.749 SD; Tenm3-sub-threshold : 1.56 a.u. ± 0.078 SEM, ± 1.494 SD p = 0.2928; apical: Tenm3-positive: 1.331 a.u. ± 0.165 SEM, ± 1.084 SD; Tenm3-sub-threshold : 1.527 a.u. ± 0.111 SEM, ± 1.4 SD p = 0.4424, Mann-Whitney test). These results confirm that Tenm3 forms discrete puncta in the shaft and that this spatially restricted clustering prevails at shafts below both Tenm3-positive and -sub-threshold spines. A summary of the most important statistical test results reported in this chapter can be viewed in Table 3.

Table 3. Summary of statistical tests used to analyse subcellular Tenm3 localisation in CA1 neurons.

Measurement	Basal	Significance Test	Apical	Significance Test	Significance Test, basal vs apical	Figure
Tenm3 FI in SpineROIs	n = 444, 1.306 ± 0.065 SEM	p < 0.0001, AP	n = 200, 1.25 ± 0.08 SEM	p < 0.0001, AP		4.2
Spine-Tenm3 correlation with spine-GFP	r = 0.413	p < 0.0001	r = 0.365	p < 0.0001		4.2-g
Spine-Tenm3 correlation with spine area	r = 0.249	p < 0.0001	r = 0.245	p = 0.0005		4.3
Proportion of Tenm3-pos spines	17.34%		25.5%			4.2-h
Tenm3 FI in Tenm3-pos spines	n = 77, 2.723 ± 0.199 SEM		n = 51, 2.572 ± 0.179 SEM		p > 0.9999, KW	4.4
Tenm3 FI in Tenm3-sub-threshold spines	n = 367, 0.949 ± 0.015 SEM		n= 149, 0.84 ± 0.027 SEM		p > 0.9999, KW	4.4
Tenm3 FI in shaftROIs	2.01 ± 0.101 SEM	p < 0.0001, AP	3.208 ± 0.257 SEM	p < 0.0001, AP		4.5
Shaft-Tenm3 correlation with spine-GFP	r = 0.197	p < 0.0001	r = 0.145	p = 0.042		4.5-d
Shaft-Tenm3 correlation with spine-Tenm3	r = 0.237	p < 0.0001	r = 0.192	p = 0.0075		4.5-e
Tenm3 FI in shafts below Tenm3-pos spines vs. Tenm3-sub-threshold spines	2.61 ± 0.286 SEM vs 1.875 ± 0.105 SEM	p = 0.0405, MW	4.423 ± 0.696 SEM vs 2.99 ± 0.283 SEM	p = 0.0416, MW	p = 0.2566, KW p = 0.0251, KW	4.5-f
Proportion high-Tenm3 shafts below Tenm3-pos spines	71.95%		93.02%			4.6-a
Proportion high-Tenm3 shafts below Tenm3-sub-threshold spines	46.41%		56.33%			4.5-a
Proportion of all shafts with high Tenm3 FI	51.13%		64.18%			4.5-a
Ratio shaft / spine FI in Tenm3 vs GFP	3.572 ± 0.745 SEM vs 3.196 ± 0.252 SEM	p < 0.0001, MW	7.148 ± 0.745 SEM vs 2.556 ± 0.176 SEM	p = 0.0121 MW	p < 0.0001, KW p > 0.9999, KW	4.7
Ratio shaft / dendrite in Tenm3 vs GFP	2.293 ± 0.139 SEM vs 1.521 ± 0.066 SEM	p < 0.0011, MW	2.893 ± 0.246 SEM vs 1.485 ± 0.094 SEM	p < 0.0002, MW	p > 0.9999, KW p = 0.4293, KW	4.8-d
Tenm3 Ratio shaft / dendrite below Tenm3-positive spines vs Tenm3-sub-threshold spines	2.451 ± 0.438 SEM vs 2.257 ± 0.139 SEM	p = 0.1906, MW	3.015 ± 0.569 SEM vs 2.859 ± 0.273 SEM	p = 0.7071, MW	p > 0.9999, KW p > 0.9999, KW	4.8-e

Abbreviations:
FI: fluorescence intensity
AP: D'Agostino & Pearson normality test
r: Spearman r, non-parametric correlation coefficient
KW: Kruskal-Wallis test, non-parametric ANOVA followed by Dunn's multiple comparisons test.
MW: Mann-Whitney test, non-parametric t-test
ns: not significant
P values: 0.05 (*), 0.01 (**), 0.001 (***), 0.0001 (****)

4.3 Summary and discussion

In this chapter, I describe my investigation of the subcellular localisation of Tenm3 in CA1 neurons using organotypic hippocampal cultures. Consistent with our observations in dissociated neurons, Tenm3 formed distinct clusters in dendrites. To investigate whether Tenm3 is localised at synapses, dendritic spines were manually selected and Tenm3 fluorescence intensity was measured. My results show that Tenm3 was indeed localised at dendritic spines and that the total proportion of Tenm3-positive spines in CA1 neurons was 19.87 % (when apical and basal spines were pooled together). Strikingly, neighbouring spines had very varied Tenm3 levels, with some spines exhibiting high Tenm3 levels within just a few micrometres of spines with barely detectable Tenm3 levels. During the analysis of Tenm3 localisation in spines, I noticed that Tenm3 seemed to cluster in the dendritic shaft below spines. In order to quantitate this, shafts were manually traced and Tenm3 intensity was measured in these areas. High levels of Tenm3 were measured in shafts, which correlated only weakly with spines size but more strongly with the presence of Tenm3 protein in the spine itself (spine-Tenm3). Additionally, Tenm3 was more frequently found in shafts than in spines, with 51.13% of all shafts below basal spines and 64.18% in apical spines exhibiting high Tenm3 signal. Furthermore, Tenm3 signal intensity was stronger in shafts relative to spines, indicating that Tenm3 might be more important for processes happening at the shaft underlying spines (see below). Shaft-Tenm3 intensity was then analysed in relation to an adjacent point further distally on the dendrite. This revealed that Shaft-Tenm3 does indeed cluster in discrete puncta that are spatially restricted to the area below the spine.

These findings suggest that shaft-Tenm3 may serve as a reserve pool for synaptic recruitment to the spine, as has been observed for other proteins such as the Cadherin-associated β-Catenin and Profilin, a regulator of actin polymerisation (Murase, Mosser and Schuman, 2002; Ackermann and Matus, 2003). However, despite the positive correlation between shaft- and spine-Tenm3 intensity, Tenm3 localisation in these two regions was distinct; the majority but, not all Tenm3-positive spines had high Tenm3 signal in their shafts, and around half of all shafts below Tenm3-sub-threshold spines also had high Tenm3 signal. Thus, shaft-Tenm3 localisation can be independent of spine-Tenm3. Therefore, it is unlikely that acting as a reserve pool is the only function

fulfilled by shaft-Tenm3. One hypothesis may be that spine-Tenm3 has a role in synaptic maintenance. Indeed, as a cell-surface adhesion molecule Tenm3 is ideally poised to bridge the synaptic cleft and physically link the pre- and postsynaptic compartments. Such a role would be consistent with previous studies, which demonstrated that transsynaptic interactions between Teneurins are required for appropriate synapse formation (Mosca *et al.*, 2012; Mosca and Luo, 2014). However, these studies were done in *Drosophila*, a model organism without pyramidal neurons, and therefore we can only speculate that similar mechanisms might take place at the level of dendritic spines in mammals. Furthermore, it is important to note that it is currently unclear whether the observed Tenm3 is intracellular or at the cell-surface, since a detergent was used during the immunocytochemical detection of Tenm3-Myc. Conversely, the more abundant levels of shaft-Tenm3 and its location at the base of spines suggest a more general role. Disruption of Teneurins in invertebrates has previously been shown to lead to phenotypes consistent with broad failures of synaptic organisation, including failed active zone apposition, disorganisation of synaptic proteins and failed pre- and postsynaptic differentiation (Mosca *et al.*, 2012). Therefore, we can hypothesise that shaft-Tenm3 may be involved early in synaptic assembly. Indeed, it has been established that Teneurins interact with the cytoskeleton (Nunes *et al.*, 2005; Zheng *et al.*, 2011; Mosca *et al.*, 2012; Suzuki *et al.*, 2014) and therefore it is plausible that shaft-Tenm3 may exert its effects on synapse formation and assembly by arranging a cytoskeletal meshwork to ensure spatial organisation. Furthermore, Teneurins have been shown to interact with Latrophilins (Silva *et al.*, 2011; Boucard, Ko and Südhof, 2012; Vysokov *et al.*, 2016) and they are thought to interact with other signalling molecules such as the Neurexin/Neuroligin complex (Mosca *et al.*, 2012). Therefore, another reasonable hypothesis may be that shaft-Tenm3 coordinates cytoskeletal organisation through the recruitment of signalling molecules and complexes.

There were no striking differences between Tenm3 localisation in basal and apical dendrites (Table 3), but it is worth noting that the proportions of spines and shafts with high Tenm3 signal tended to be larger in apical dendrites. Tenm3 intensity in spines and shafts below Tenm3-positive spines were not significantly different in apical and basal dendrites, and the spatial restriction of shaft-Tenm3 clusters was the same in both dendritic compartments. Apical dendrites did have significantly higher levels of Tenm3

at shafts below Tenm3-sub-threshold spines as well as significantly higher shaft-Tenm3 relative to spine-Tenm3. Altogether, these differences suggest that Tenm3 is more strongly targeted to shafts and spines in apical dendrites and this might have implications for synapse organisation and maintenance.

The use of organotypic hippocampal cultures had many advantages in comparison to dissociated hippocampal cultures, including the fact that this system enabled the easy identification of different cell types. Indeed, using this approach it was possible to focus the analysis exclusively on CA1 neurons. Since CA1 neurons endogenously express Tenm3, transfected Tenm3 is more likely to reproduce the endogenous localisation pattern within this cell type. However, due to the endogenous Tenm3 already present in these neurons, transfected cells are also more likely to reach overexpression levels of the protein, which might lead to cytotoxicity. Another advantage of organotypic hippocampal cultures over dissociated neurons was that they simulate a more *in vivo*-like situation. Indeed, structural and synaptic organisation of the hippocampus are better preserved and neurons in this system are studded with dendritic spines, the post-synaptic protrusions of excitatory synapses. Thus, dendritic spines allow the visualisation and identification of excitatory synapses without the use of antibodies targeting synaptic proteins. However, it is important to note that the number of dendritic spines represents an estimate of the number of synapses on a neuron. Indeed most dendritic spines contain a single synapse but some spines contain multiple synapses (Yankova, Hart and Woolley, 2001) and there are instances of excitatory synapses being formed on shafts (Megías *et al.*, 2001). Furthermore, functional studies have shown that larger spines have more AMPARs (Matsuzaki *et al.*, 2001), suggesting that small spines might contain weaker, and in some cases silent synapses (Malenka and Nicoll, 1997; Voronin and Cherubini, 2004). The results presented here, showed that Tenm3 was only localised in a subpopulation of spines and correlated with spine size, whereas shaft-Tenm3 was present below more spines but correlated more weakly with spine size and more in basal dendrites. This fits with the hypothesis that spine-Tenm3 may be involved in spine maturation, whereas shaft-Tenm3 would contribute to earlier synapse organisation events at the base of smaller or de novo spines.

Despite the advantages associated with the use of organotypic hippocampal cultures, there were some limitations with the experiments presented in this chapter. First,

gathering enough data for these experiments was challenging, due to the very low transfection efficiency and cell death following transfection. One of the major disadvantages of the slice culture system is that it is an axotomised system, thus many neurons lose their target innervation and die as a result of this (Humpel, 2015). Furthermore, biolistic transfection inevitably causes some tissue damage and therefore cell death. Moreover, it is likely that some cytotoxicity and cell death of transfected neurons was also partly caused by Tenm3 overexpression. Whilst none of the analysed CA1 neurons exhibited any obvious structural or morphological changes on the cellular scale, there were some subcellular signs of cytotoxicity, notably some dendrites and axons appeared "blebby". Thirdly, the problems associated with the use of an overexpression system to analyse the subcellular localisation of an epitope-tagged protein remained. Consequently, due to the lack of Teneurin paralogue-specific antibodies, it also remained impossible to verify whether the subcellular Tenm3 localisation pattern observed here corresponds to the endogenous Tenm3 localisation pattern. However, the fact that we found very similar Tenm3 subcellular localisation patterns using two different culture systems, substantiates these findings. Another drawback of using organotypic slices was that images had a lot of background and identifying spines was difficult due to the low signal to noise ratio. The noisiness of these images was likely caused during immunostaining with anti-Myc antibodies, since control slices, where the signal of neurons transfected with GFP was amplified only with anti-GFP, did not have such high levels of background. Finally, the analysis was done in ImageJ and IgorPro software and functions used to analyse the data were custom written for each specific analysis. This enabled a very detailed analysis of the acquired imaging data. However, experimenter error cannot be fully excluded due to the fact that ROIs were traced manually and the identification of spines was made difficult by the noise in the images.

In summary, the results presented in this chapter confirmed that Tenm3 is localised to a subpopulation of synapses. Additionally, the results also revealed a new and surprising finding, which was that Tenm3 is more frequently and more strongly localised in the vicinity of synapses, at the shaft. Similar subcellular localisation patterns have been observed for other proteins such as β-Catenin and Profilin. Both these proteins translocate from the shaft to the spine in response to synaptic stimulation,

where they contribute to synaptic stabilisation through interactions with the cytoskeleton (Murase, Mosser and Schuman, 2002; Ackermann and Matus, 2003). The fact that Tenm3 was enriched at shafts, broadened the possible roles of this protein to an involvement in events associated with synaptic assembly, notably through interactions with the cytoskeleton at the base of spines. The functional significance of synaptic Tenm3 is further explored in the next chapter.

5 Excitatory synapse formation in CA1 neurons in Tenm3 mutant mice

5.1 Introduction

In the previous chapter I showed that Tenm3 is localised in a subpopulation of dendritic spines and shafts. Dendritic spines form the postsynaptic component of most excitatory synapses and the function and plasticity of synapses depends on the physical structure of spines. This chapter is aimed at further exploring the functional significance of Tenm3 occurrence at spines and shafts. More specifically, I investigate how the absence of Tenm3 affects the structural integrity of synapses *in vivo*.

5.1.1 Dendritic spines and their classification

5.1.1.1 Dendritic spine structure

Dendritic spines are micrometre sized protrusions of dendritic membrane, whose primary function it is to compartmentalise local synaptic signalling pathways and to restrict the diffusion of postsynaptic signals (Hering and Sheng, 2001). This function is facilitated by the structure of spines, which typically have a spherical head and a narrow neck (Harris and Stevens, 1989). However, spines considerably vary in shape and size (Harris, Jensen and Tsao, 1992). Indeed, when spines are subject to patterns of activity that induce functional plasticity mechanisms such as LTP or LTD, structural plasticity mechanisms take place, which respectively lead to either an enlargement or shrinkage of spines (Wang and Zhou, 2010; Sala and Segal, 2014). Spines also constantly undergo very rapid changes, which make spines appear as if they were “dancing” (Halpain, 2000).

The formation, maturation and plasticity of dendritic spines depends on the remodelling of its cytoskeleton (Ethell and Pasquale, 2005; Cingolani and Goda, 2008; Hotulainen and Hoogenraad, 2010), which was found to be highly enriched in actin (Matus *et al.*, 1982). Dendritic spine changes that accompany alterations of synaptic strength are also driven by actin dynamics and include processes such as organisation of the PSD and fast delivery of receptors into the synapse (Allison *et al.*, 1998; Richards *et al.*, 2004;

van Zundert *et al.*, 2004; Kuriu *et al.*, 2006). The cytoskeleton of dendritic spines exhibits a continuous network of branched and straight actin filaments. The spine head contains a network of highly branched filaments, which get constricted in the neck, before spreading out again in the spine base, where it cross-links to the array of microtubules present in the dendritic shaft (Korobova and Svitkina, 2010).

The large variability of spine shapes observed in early EM studies led to the establishment of different nomenclatures that classify spines into different types according to their morphology (Figure 1.7). The three main types of spines are short "stubby" spines without well-defined necks, long "thin" spines with small spherical heads, and characteristic "mushroom" spines with large heads and constricted necks (Peters and Kaiserman-Abramof, 1970; Harris and Stevens, 1989; Harris, Jensen and Tsao, 1992). Distinct nomenclatures differ slightly in their characterisation of spine morphology and some include further types, such as "sessile", "filopodial" "cup-shaped" and "branched" spines. Filopodial spines are believed to be spine-like projections that only occasionally bear synaptic contacts and whose existence subsides after development (Fiala *et al.*, 1998; McKinney *et al.*, 1999). Sessile spines were initially described by Jones and Powell (1969) for the categorisation of stubby spines, however they are also ascribed to spines that are longer than their diameter but lack a bulbous head (Sorra and Harris, 2000). Branched spines are defined as having two heads emerging from one dendritic shaft, however their classification sometimes overlaps with that of cup-shaped spines. Furthermore, cup-shaped spines are sometimes categorised as mushroom spines. This brings to light some issues with spine classification schemes. First, spines come in a vast variety of shapes and are continuously motile, therefore assigning them to arbitrary categories underestimates the great heterogeneity of spine morphologies and can, at best, only be a rough classification. Furthermore, spine categories vary between nomenclatures and have loosely defined criteria, which can lead to overlaps between classes and makes it difficult to correctly assign spine types. In this thesis spines were classified into stubby, sessile, thin and mushroom categories in order of increasing maturity and according to previously described criteria (McKinney *et al.*, 1999; Staffend, Loftus and Meisel, 2011; Jung *et al.*, 2013; Gupta *et al.*, 2015).

Whilst the molecular and structural processes leading to morphological changes in spines remain a standing issue, it is generally agreed that morphological differences between spines are likely to reflect functional differences (Sala and Segal, 2014). Therefore, despite its shortcomings, spine categorisation is a useful and relevant tool to investigate functional changes following experimental manipulations and was used in this thesis to evaluate dendritic spine morphology in CA1 neurons of Tenm3 mutant mice.

5.1.2 Tenm3 mouse mutant

To investigate the functional role of Tenm3 in synapse formation, a Tenm3 mutant mouse was generated. This mouse was generated prior to the start of this project using the gene trap method, which is an efficient system to simultaneously characterise gene function and expression (Stanford *et al.*, 2001).

5.1.2.1 Gene trap mutagenesis

Gene trap mutations are randomly generated in embryonic stem (ES) cells and characterised *in vitro* before germ-line transmission. A gene trap vector containing a splice acceptor site at the 5' end, a reporter gene and a polyadenylation signal at the 3' end, is randomly inserted into an intronic region of genomic DNA. The splice acceptor site interrupts normal splicing and causes the vector sequence to be spliced into the mRNA, whereas the polyadenylation signal causes a stop in translation and thus premature truncation of the mRNA. The gene trap vector is promoterless, since this system takes advantage of the endogenous transcription and splicing apparatus and therefore the reporter cassette is under the control of and endogenous upstream promoter. On transcriptional activation of the endogenous *cis*-acting promoter, a fusion transcript is generated from the upstream coding sequence and the reporter gene, thus simultaneously mutating the trapped gene and reporting its expression pattern (Figure 5.1-a). The insertion of a gene trap vector in a genic region typically results in a complete inactivation of the trapped gene, thus leading to a null-mutation. However, alternative splicing can sometimes take place and because the gene trap insertion occurs in an intron, it can fail to fully inactivate the gene, leading to lower levels of wild-type transcripts and resulting in hypomorphic or dominant negative phenotypes. The

characterisation of the vector insertion site is necessary to design a PCR-based genotyping strategy. A large number of ES cell clones with are variety of trapped genes is available through the International Gene Trap Consortium and can be ordered for the generation of mutant mice through blastocyst injection and breeding of chimaeric mice for germline transmission.

5.1.2.2 Generation and characterisation of a Tenm3 gene trap mutant

The Tenm3 mutant mouse used in this thesis was generated through blastocyst injection of a targeted ES cell line by BayGenomics. The resulting mouse mutant line was called RRD180 in reference to the gene trap ES cell line. This Tenm3 mutant has an insertion of the pGT1Lxf gene trap vector. This vector is frequently used by BayGenomics for their gene trapping project and contains a β-geo reporter gene, a fusion of the *lacZ* gene, which encodes the marker β-galactosidase, and the *neo* gene, which encodes neomycin phosphotransferase II and confers neomycin resistance.

The characterisation of the RRD180 mouse line, identification of the insertion site of the gene trap vector as well as the development of a PCR genotyping protocol were carried out by Dr. Andy Symonds (Hindges Laboratory). The gene trap insertion was found to be within intron 3-4, approximately ~680bp downstream of exon 3. In theory, this insertion leads to a premature truncation of the Tenm3 protein directly after exon 3 and results in a Tenm3-β-galactosidase fusion transcript. This fusion transcript contains only the intracellular domain, since transcription is interrupted before Exon 4, which encodes the transmembrane domain (Figure 5.1-a). The generation of a truncated Tenm3 protein was not verified by sequencing, however X-gal staining of brain tissue from RRD180 mice revealed that β-galactosidase is expressed in these mice and perfectly recapitulates the endogenous expression pattern of Tenm3 (Figure 5.1-c-d; refer to 2.5.3 for method). There are two validated Tenm3 isoforms, which both include exon 3 and 4, and therefore would be truncated in the RRD180 mouse mutant. NCBI predicts eighteen further splice variants (Appendix 3), which would also all be affected by the gene trap insertion. Ensembl predicts only six further splice variants (Appendix 4), however one of those transcripts would not be affected by the gene trap insertion as it is predicted to include only the first two exons and terminate transcription before intron 2-3.

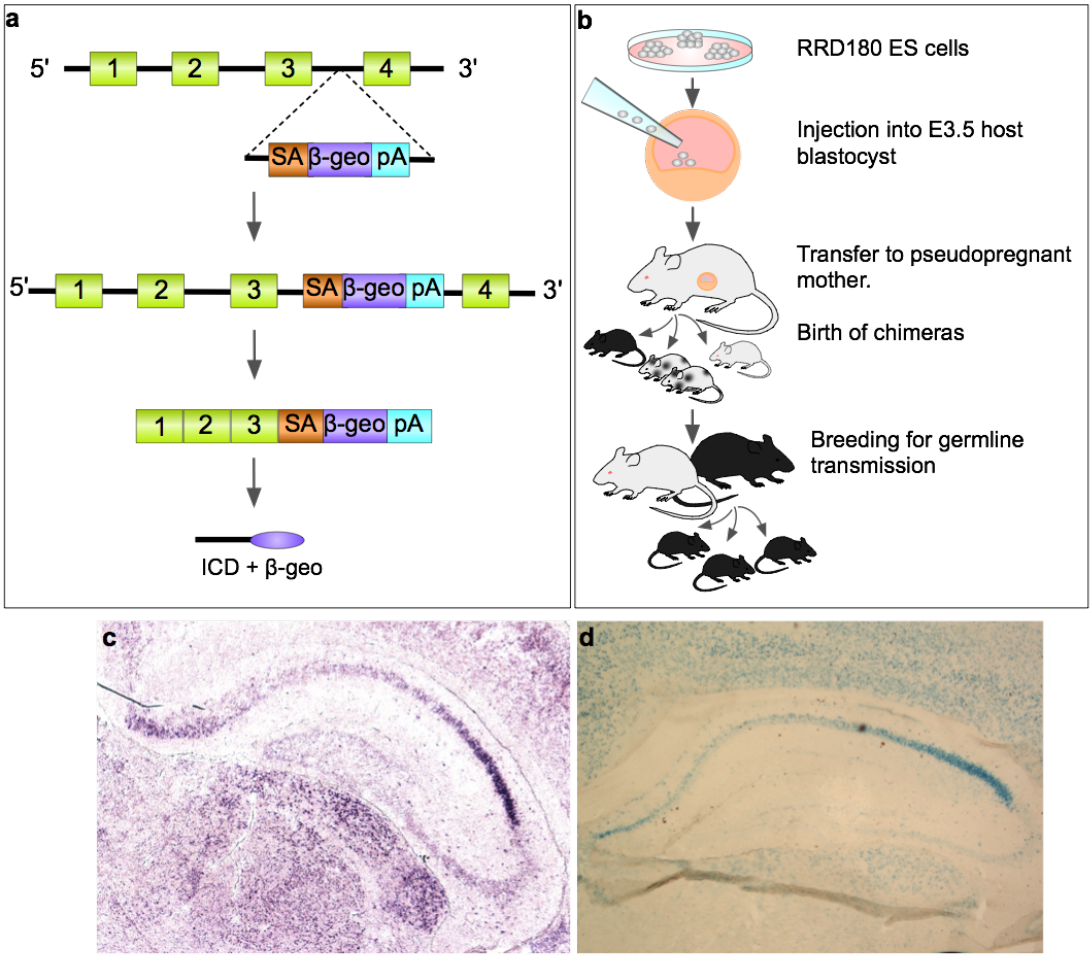

Figure 5.1. The Tenm3 mutant mouse line RRD180. **a.** The gene trapping process. The gene trap cassette with the splice acceptor (SA), β-geo gene and polyadenylation signal (pA) is inserted downstream of Tenm3 Exon 3, in intron 3-4. The gene trap vector interrupts normal transcription and produces a truncated fusion protein consisting of the Tenm3 intracellular domain and β-galactosidase. **b.** Generation of Tenm3 mutant mous line through blastocyst injection. **c.** In situ hybridisation of Tenm3 in a coronal section of the hippocampus. This image was obtained from Denise van Nieuwenhuize. **d.** X-gal staining in a hippocampal coronal section o of a Tenm3 mutant mouse brain reveals that β-galactosidase expression recapitualtes the endogenous Tenm3 expression pattern along CA1.

The success of the gene trap method is dependent on several factors. For example, the insertion site of the vector is an important determinant for the efficiency of gene disruption. In the RRD180 line, the vector insertion is near the 5' end of the Tenm3 gene, preventing a large proportion of exons from being transcribed, and thus is likely to result in a complete Tenm3 inactivation. Another concern with gene trapping is inactivation of multiple genes. This is an issue in cases where the coding regions of multiple genes overlap or if genes are coding on the opposite strand. In the case of the RRD180 line, the genomic region surrounding the vector insertion was carefully investigated and it is unlikely that other genes than Tenm3 are inactivated as a result of

the gene trap insertion, since (1) no genes code on the opposite strand of the genomic region and (2) the Tenm3 coding region does not overlap with that of any other genes.

Homozygous Tenm3 RRD180 mutants ($Tenm3^{-/-}$) are viable and survive into adulthood. However, they form less than 25% of litters from heterozygote breedings, indicating some embryonic lethality. Furthermore, $Tenm3^{-/-}$ females plug less frequently than C57BL/6 females, suggesting reduced fertility, and they appear more nervous, frequently over-grooming their offspring (naked coat) or killing it in the first 48 hours post-partum. Tenm3 mutant pups tend to be a little smaller than wild type littermates during early postnatal development but display otherwise no obvious developmental delays. Histological observations of Tenm3 mutant mouse brains did not reveal any major changes in brain structure or organisation.

Tenm3 is expressed in the retina and its target regions, the dLGN and superior colliculus. Interestingly, Tenm3 is found in corresponding gradients in these three regions; i) in the retina, Tenm3 is expressed in high ventral and low dorsal levels, ii) in the dLGN Tenm3 is expressed in high dorsal and low ventral levels, iii) in the superior colliculus, Tenm3 is expressed in high medial and low lateral levels. As described in the introduction, a study performed on Tenm3 knockout mice found that these mice showed abnormalities in mapping of ipsilateral projections from the retina to the dLGN. These abnormalities result from aberrant projections of RGC axons from the ventral retina to the ventrolateral dLGN (instead of dorsomedial dLGN; Leamey *et al.*, 2007). In a pilot study from the Hindges lab (Chun & Hindges, unpublished), which investigated retinal projections in the RRD180 Tenm3 mouse mutant line, a similar phenotype was observed, confirming the loss of function of Tenm3 in the RRD180 line. Based on these results, we are confident that β-galactosidase expression indeed reports the disruption of Tenm3 in cells in this mouse line.

5.1.3 Aim

In this chapter I explore the functional consequences of the absence of Tenm3 in CA1 neurons *in vivo*. The aim was to investigate what effect a lack of Tenm3 has on excitatory and inhibitory synapse formation. However, due to technical difficulties detailed below (5.2), only excitatory synapses were analysed. Specifically, I

investigated dendritic spine density and morphology in the Tenm3 mouse mutant line. I begin by taking the reader through the attempts made at investigating inhibitory and excitatory synapse density in Tenm3 mutant mice. Secondly, I examine the density of dendritic spine types in Tenm3 mutant mice crossed to a Thy1-GFP reporter mouse line (Feng *et al.*, 2000).

5.2 Investigation of inhibitory and excitatory synapse density in Tenm3 mutant mice using *in utero* electroporation

5.2.1 In *utero* electroporation

In utero electroporation (IUE) was used in this chapter to fluorescently label sparse CA1 neurons of the hippocampus in Tenm3 mutant mice. IUE is a powerful tool to transfect and manipulate neuronal precursor cells in numerous brain areas *in vivo* (Saito and Nakatsuji, 2001; Saito, 2006). Embryos were electroporated at E14.5, as this is the time point when pyramidal neurons of the *cornu ammonis* are born (Nakahira and Yuasa, 2005), and mice were collected as adolescent pups at P21. In addition to GFP, either genetically encoded antibody-like proteins (Fibronectin intrabodies or FingRs; Gross *et al.*, 2013), or the Tenm3 expression plasmid, used in the previous chapters, were coelectroporated. Intrabodies are recombinant antibody-like proteins that bind endogenous PSD-95 or Gephyrin and are fused to TdTomato to visualise excitatory and inhibitory synapses. These FingRs are designed with a transcriptional regulation system, which matches the expression of the intrabody to that of the target protein, thus accurately reporting endogenous PSD-95 and Gephyrin expression without affecting their function (Gross *et al.*, 2013). The intrabodies used for these experiments were PSD95-TdTomato-FingR and Gephyrin-TdTomato-FingR and were cloned by Sarah Kemlo (Burrone Laboratory) with an optimised Td-Tomato marker in place of the GFP or mKate marker, which were made available by the Arnold Laboratory.

5.2.2 Synaptic density in mice with loss or overexpression of Tenm3

In a first step, I set up heterozygous/ homozygous and heterozygous/ heterozygous Tenm3 mutant breedings and electroporated embryos of Tenm3 homozygous and heterozygous mutant females. The resulting 50% homozygous, 50% heterozygous or 25% homozygous, 50% heterozygous, 25% wild type embryos were electroporated with GFP and Gephyrin-TdTomato-FingR or PSD-95-TdTomato-FingR (Figure 5.2). The DNA concentration was 1µg/µl and plasmids were electroporated at a 1:3 ratio (GFP: PSD-95-TdTomato-FingR or GFP: Gephyrin-TdTomato-FingR). The aim of this experimental set up was to analyse the density of excitatory and inhibitory synapses in CA1 neurons in Tenm3 mutant mice (homozygous and heterozygous) compared to their

wild type littermates. In an additional experiment, embryos from heterozygous/ heterozygous Tenm3 mutant breedings were electroporated with GFP and Tenm3 at a ratio 1:3. The aim of this experiment was to analyse dendritic spine density in CA1 neurons that overexpress Tenm3 and further, to explore whether any potential aberrations in spine density in Tenm3 mutant mice could be rescued by restoring Tenm3 expression in CA1 neurons.

Unfortunately, these IUEs (n = 15) were largely unsuccessful. Firstly, Tenm3 mutant mice tended to kill their litters shortly after birth, which led to a dramatically low survival rate of 21.6% of embryos (27 out of 125 embryos, 15 litters, Figure 5.2-c-d). Furthermore, only 18.5% (n = 5) of the pups that survived these IUEs had transfected GFP expressing neurons in the brain, out of which only one brain had GFP positive neurons in the DG of the hippocampus.

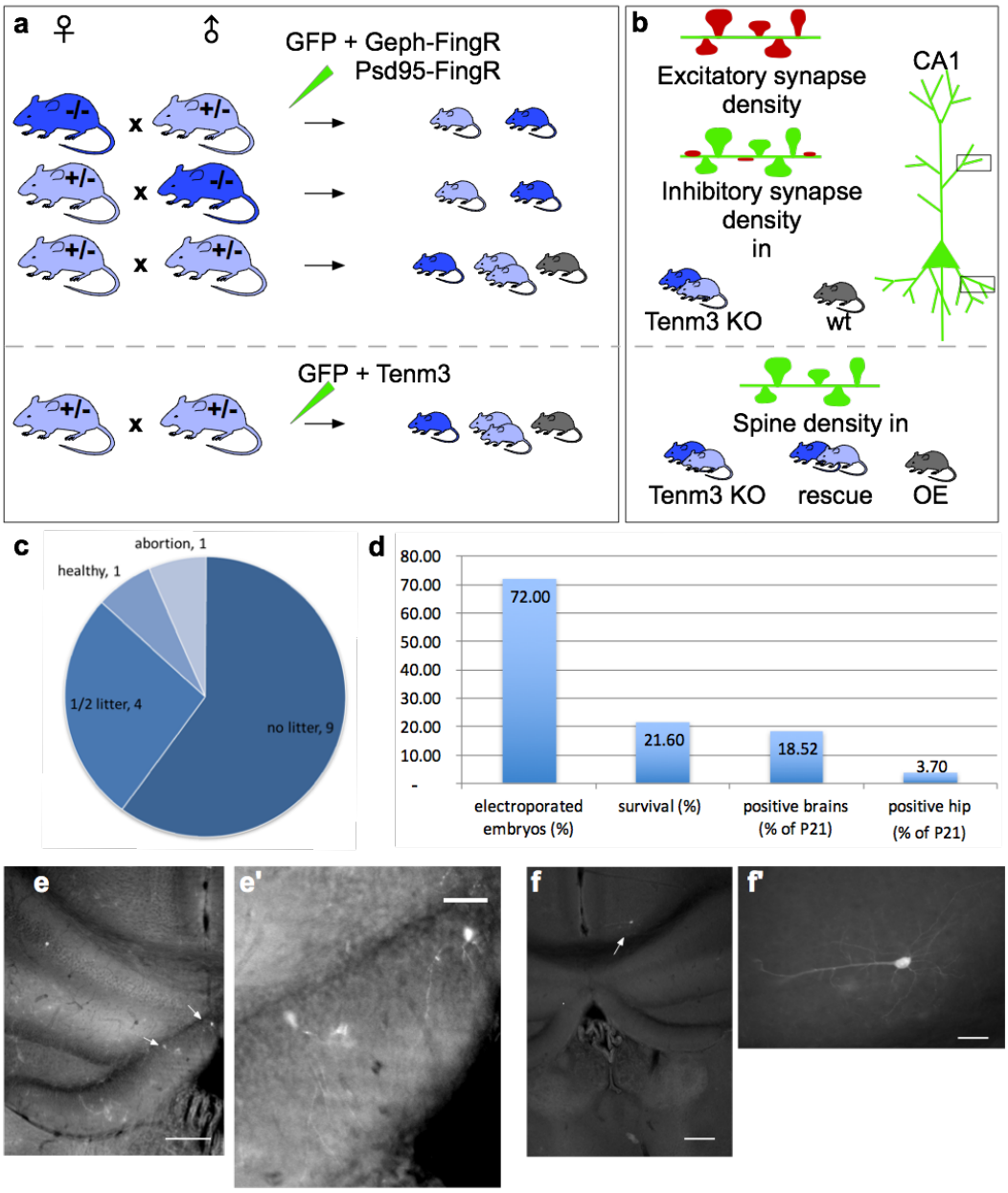

Figure 5.2. First experimental design for investigation of synaptic density in Tenm3 mutant. **a.** Schematic of breedings for IUEs. Surgeries were performed on homo- and heterozygous Tenm3 mutant females and embryos were injected with GFP and either Gephyrin-Td-Tomato-FingR, PSD95-Td-Tomato-FingR or Tenm3. **b.** These experiments were designed to analyse excitatory and inhibitory synapse density in Tenm3 mutants and their wild type littermates, as well as spine density in mice with Tenm3 loss, Tenm3 rescue and Tenm3 overexpression. **c.** Survival of litters (n=15) following IUE. **d.** IUE succes as a measure of: proportion of electroporated embryos per litter, survival rate to age 21 days, proportion of P21 brains with transfected neurons, proportion of P21 brains with transfected neurons in the hippocampus. **e-f.** Examples of transfected neurons. **e.** Transfected DG cells, scale bar 200μm, **e'** scale bar 50μm. **f.** Transfected neuron in the ventral retrosplenial area, scale bar 200μm, **f'** scale bar 50μm.

As mentioned above, homozygous Tenm3 mutant mice (and to a lesser extent heterozygous mutant mice) generally have a higher tendency to kill part of their litters compared to wild type C57BL/6 mice. In an attempt to increase the survival rates of electroporated embryos, I decided to adopt a different breeding strategy. For these experiments, wild type C57BL/6 females were crossed to homozygous and heterozygous Tenm3 mutant males and heterozygous Tenm3 mutant females were crossed to heterozygous Tenm3 mutant males (Figure 5.3-a). As previously, embryos were injected at E14.5 with either GFP and Gephyrin-TdTomato-FingR, GFP and PSD-95-TdTomato-FingR or GFP and Tenm3 and brains were collected at P21. Furthermore, to increase the transfection efficiency, the DNA concentration was used at a concentration of 3µg/µl.

There was a small increase in survival, with 34.5 % (71 out of 206, 23 litters) of embryos surviving to P21 (Figure 5.3-b-c), however the heterozygous mutant mice still had a tendency to kill half their litter shortly after birth and surprisingly some of the wild type mice killed their entire litters immediately after birth (Figure 5.3-b). Unfortunately, the use of foster mothers did not improve the survival rate, as pups still died within the first six days after birth when fostered to CD1 wild type females. The number of abortions increased slightly, possibly because the wild type mice used in these experiments were younger than the Tenm3 mutant mice used previously. When only considering the pups that survived to age 21 days (n = 71), the proportion of mice with GFP fluorescence in the brain increased considerably to 40.85%, the efficiency in targeting the hippocampus improved to 25.35%. Unfortunately, most of the transfected neurons were in the Fasciola Cinerea or in the DG, and only 5.6% of P21 pups had successfully transfected CA1 pyramidal neurons (n = 4). Furthermore, it became apparent that brains coelectroporated with GFP and Tenm3 only expressed GFP in neurons (Figure 5.3-d). Following IHC, no myc-tagged Tenm3 was detected. This suggests that coelectroporated neurons died as a result of Tenm3 overexpression and only neurons expressing GFP survived.

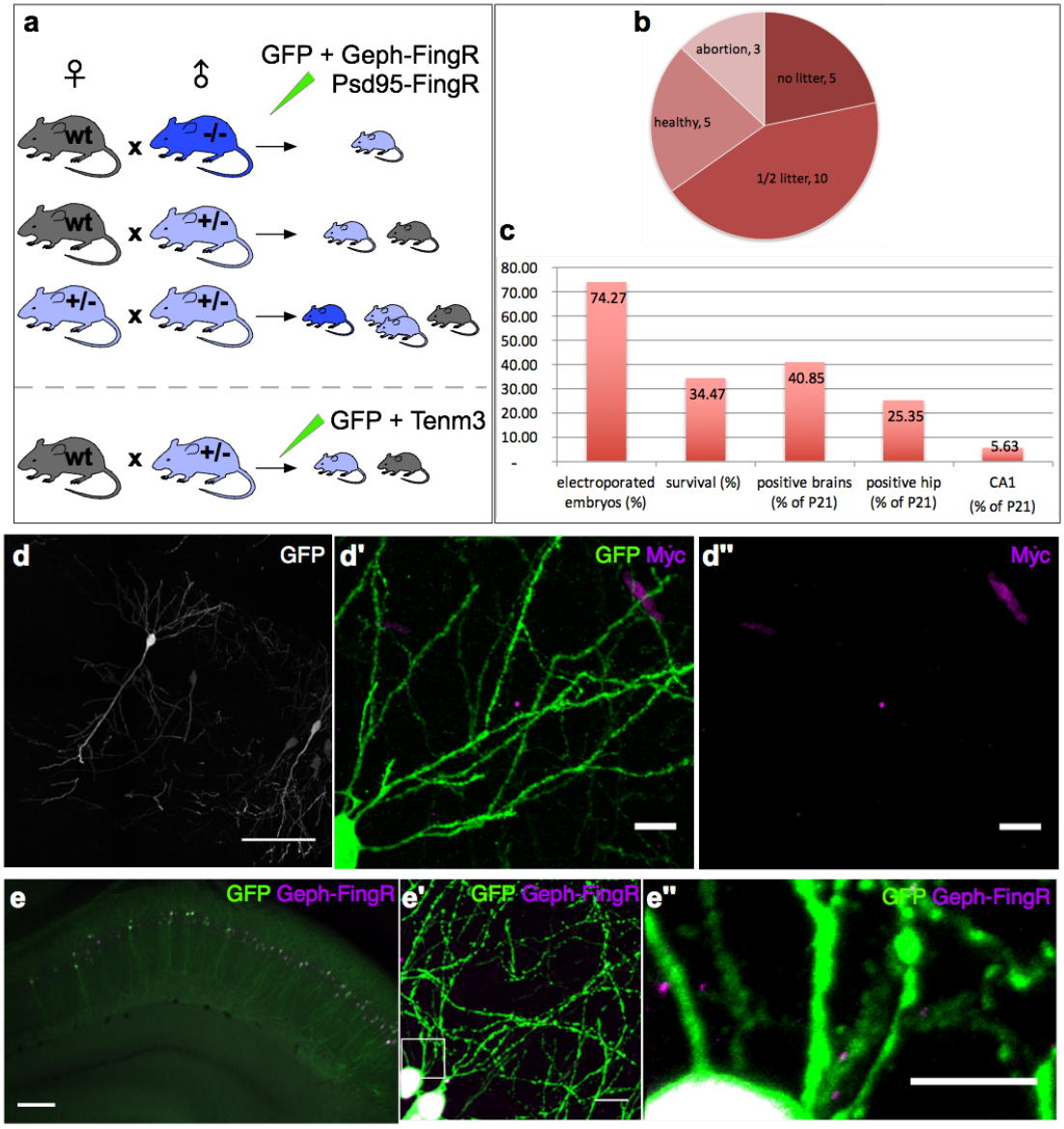

Figure 5.3. Second experimental design for investigation of synaptic density in Tenm3 mutant. **a.** Schematic of breedings for IUEs. Surgeries were performed on mostly wild type females and heterozygous Tenm3 mutant females. Embryos were injected with GFP and either Gephyrin-Td-Tomato-FingR, PSD95-Td-Tomato-FingR or Tenm3-Myc. **b.** Survival of litters (n=23) following IUE. **c.** IUE succes as a measure of: proportion of electroporated embryos per litter, survival rate to age 21 days, proportion of P21 brains with transfected neurons, proportion of P21 brains with transfected neurons in the hippocampus, proportion of P21 brains with transfected CA1 neurons. **d-e.** Examples of transfected neurons. **d.** CA1 pyramidal neurons transfected with GFP and Tenm3-Myc. Scale bar is 100μm. **d'.** There is no detectable Tenm3-Myc expression in neurons, the signal in the Tenm3-Myc channel is background due to the high laser power that was applied to detect Tenm3-Myc (**d''**) scale bar is 10μm. **e.** CA1 neurons of Tenm3-/- mutant transfected with GFP and Gephyrin-Td-Tomato-FingR. **e'**. Basal dendrites. Scale bar is 10μm. **e''.** Gephrin puncta along basal dendrites. Scale bar is 5μm.

In summary, although efficiency and survival improved slightly after performing IUEs on wild type mice crossed to Tenm3 mutants, the transfection efficiency in targeting CA1 pyramidal neurons (when considering all electroporated embryos, n = 153) was only 2.6 % (Figure 5.4-a). Therefore, these experiments were deemed unsustainable and no longer reconcilable with an ethical use of animals for scientific research. Additionally, CA1 neurons from electroporated brains (n = 4) were not analysed, as there was only one successfully transfected brain for each of the following conditions: wild type mouse expressing Gephyrin-TdTomato-FingR and GFP (with only 1 transfected CA1 neuron), homozygous Tenm3 mutant expressing Gephyrin-TdTomato-FingR and GFP (Figure 5.3-e), homozygous Tenm3 mutant expressing PSD-95-TdTomato-FingR and GFP, wild type mouse coelectroporated with Tenm3 and GFP but expressing only GFP (Figure 5.3-d). It is obvious that these sample sizes were too small to perform a sufficiently high powered and reliable analysis. For this reason, the pursuit of these experiments was abandoned. Instead, the alternative approach of crossing Tenm3 mutant mice to a Thy1-GFP reporter mouse line, which allows sparse random GFP labelling of CA1 neurons was adopted (Figure 5.4-b).

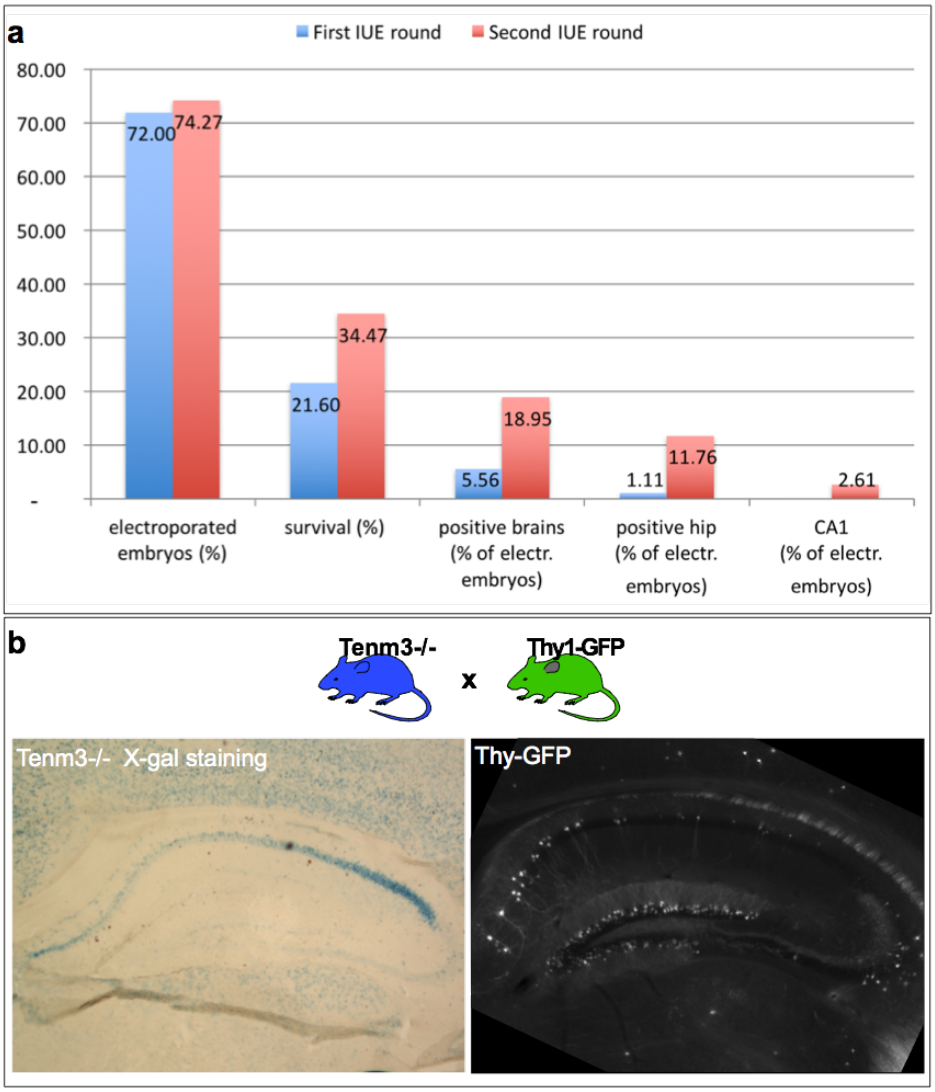

Figure 5.4. a. IUE succes between the first (n = 15,125 embroys) and second experimental round (n = 23, 206 embryos). The proportion of electroporated embryos per litter and survival rate increased. The transfection efficiencies are given as a measure of all electroporated embryos and indicate whether there were any transfected cells in the brain, in the hippocampus and in CA1.
b. The Thy1-GFP reporter mouse line was crossed to the Tenm3 mutant line. Thy1-GFP mice have sparse GFP labeling of CA1 neurons and Tenm3 is knocked out in CA1 in the Tenm3 mutant.

5.3 Changes in excitatory synapse density and morphology in CA1 neurons of Tenm3 mutant mice

In this chapter, the aim was to investigate whether a loss of Tenm3 exerted any effect on the density of excitatory and inhibitory synaptic inputs onto CA1 neurons. However, as IUE to target CA1 neurons with intrabodies and GFP *in vivo* failed, we decided to focus on the density and morphology of dendritic spines in Tenm3 mutant mice. This was investigated using the Tenm3 mutant mice crossed to a Thy1-GFP reporter mouse line (Feng *et al.*, 2000). Mice resulting from this cross are referred to as $Tenm3^{-/-}$/Thy1-GFP, $Tenm3^{+/-}$/Thy1-GFP or $Tenm3^{+/+}$/Thy1-GFP where they have one, both or no mutant Tenm3 alleles respectively, or as RRD180/Thy1-GFP when referring to the crossed mice in general.

5.3.1 Quantitation of dendritic spine density in Tenm3 mutants

Prior to transcardial perfusion at P21, a tissue sample was taken from deeply anaesthetised mice to establish their genotype. Fixed brains of RRD180/Thy1-GFP mice were then coronally sectioned in 100μm slices using a Vibratome and mounted on coverslips with Vectashield. In total, six brains of each phenotype were collected, and two proximal CA1 cells from different sections were imaged per brain. On a confocal microscope, two z-stacks of every CA1 neuron were taken, one of the basal dendritic arbour and one of oblique apical dendrites.

To evaluate whether loss of Tenm3 had an effect on dendritic spine density, z-stacks were reconstructed in Imaris (Figure 5.5). The expression of GFP in CA1 neurons allows for accurate reconstruction of dendrites and spine heads using the diameter function of the filament module in Imaris. Dendrites were traced semi-automatically, dendritic spines were detected automatically followed by manual validation and editing of false-positives. After dendrite tracing and spine detection the diameter of dendrites and spines was automatically reconstructed and the threshold was again manually adjusted. The entire analysis was done blind to genotype. As in Chapter 4, measurements from apical and basal dendrites are reported separately. Data sets were not normally distributed, therefore the non-parametric Kruskal-Wallis test with Dunn's

multiple comparisons test was used to determine significant differences between groups. All statistical values and tests are reported in detail in Appendix 5.

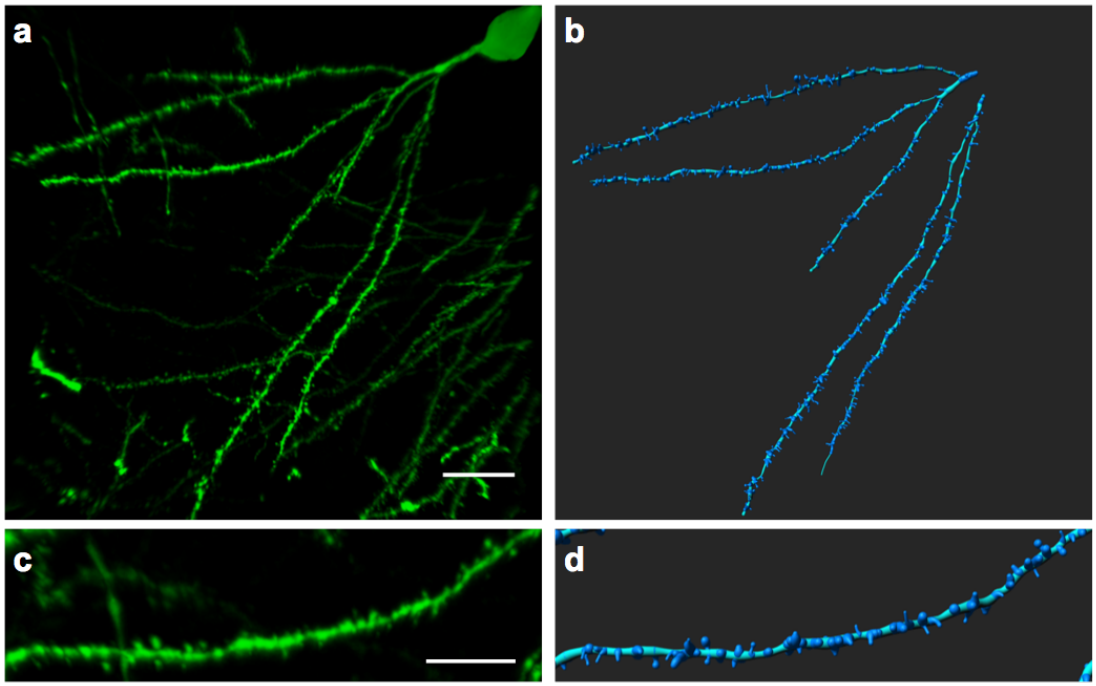

Figure 5.5. Representative image of an Imaris computer rendering of dendrites and spines. **a.** GFP labeled basal dendritic tree of a CA1 neuron from an RRD+/-/Thy1-GFP mouse. Scale bar is 10 µm. **b.** Computer rendering of the dendrites shown in **a**. **c.** GFP labeled dendritic segment. Scale bar is 5 µm. **d.** Computer rendering of the dendritic segment shown in **c**.

After reconstruction of the dendrite diameter, dendritic measurements (Figure 5.6-a) revealed that Tenm3$^{+/-}$/Thy1-GFP mice (n = 61, 0.74 µm ± 0.02 SEM ± 0.17 SD) had significantly thicker basal dendrites compared to both Tenm3$^{-/-}$/Thy1-GFP (n = 49, 0.63 µm ± 0.01 SEM ± 0.10 SD, $p < 0.0017$) and control Tenm3$^{+/+}$/Thy1-GFP mice (n = 50, 0.66 µm ± 0.02 SEM ± 0.16 SD, $p < 0.0448$). Apical dendrites in the heterozygous Tenm3 mutant (n = 55, 0.79 µm ± 0.02 SEM ± 0.19 SD) were also significantly thicker compared to the control (n = 39, 0.67 µm ± 0.03 SEM ± 0.18 SD, $p < 0.0079$) but not the homozygous mutant (n = 28, 0.69 µm ± 0.04 SEM ± 0.21 SD, $p < 0.0831$). To assess further changes in dendritic morphology following Tenm3 loss, the straightness of all analysed dendritic branches was calculated (Figure 5.6-b-c). Neither basal ($p < 0.5729$) nor apical ($p < 0.5854$) dendrite straightness was significantly different between Tenm3$^{-/-}$/Thy1-GFP, Tenm3$^{+/-}$/Thy1-GFP and control Tenm3$^{+/+}$/Thy1-GFP mice.

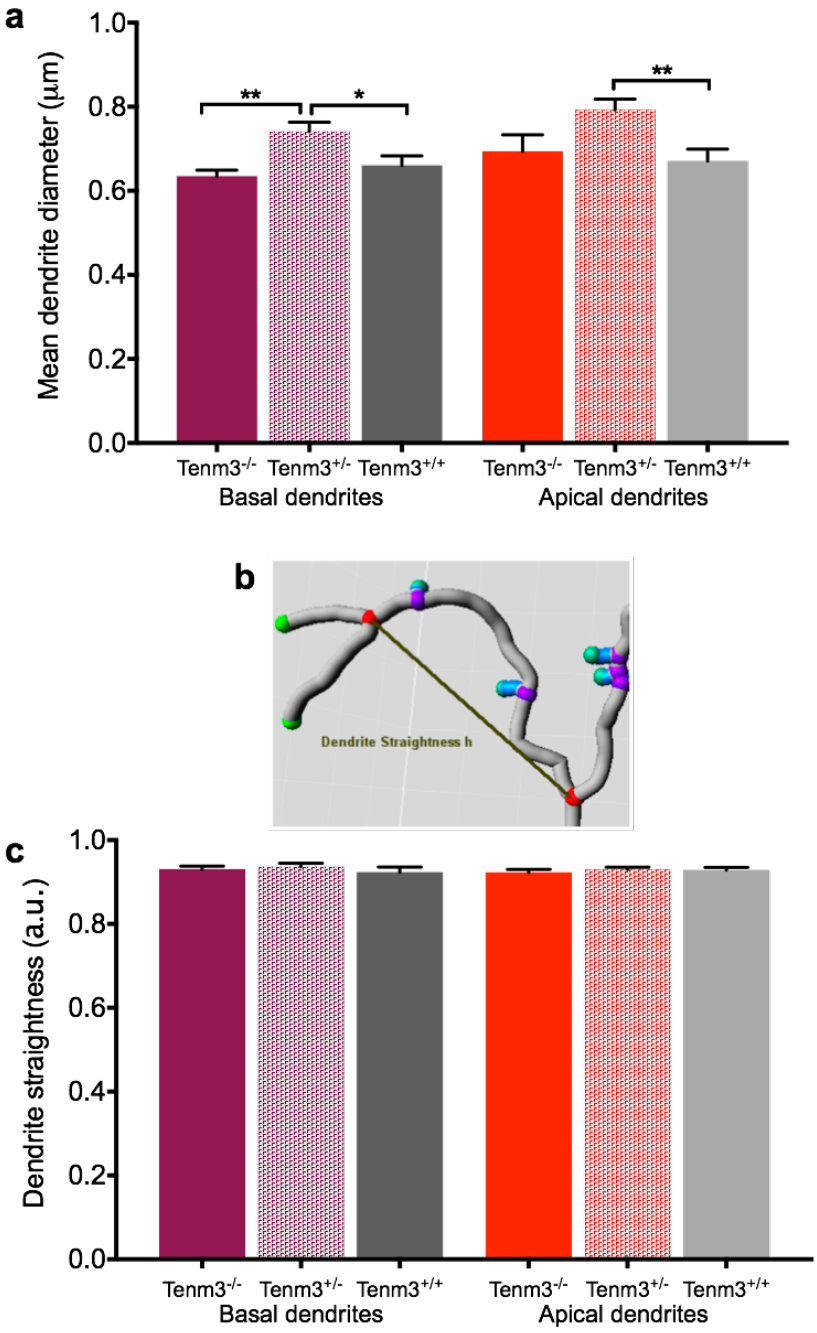

Figure 5.6. Dendritic morphology following Tenm3 perturbation. **a.** Differences in mean dendrite diameter in basal and apical dendrites of Tenm3 homozygous and heterozygous mutants and controls. Kruskal-Wallis test with Dunn's multiple comparisons test. *p<0.05, **p<0.01. **b.** Schematic of calculation of dendrite straightness (from Imaris Reference Manual). h = the distance between two branch points. The dendrite straightness is h per length of dendrite branch. **c.** Differences in basal and apical dendrite straightness of Tenm3 homozygous and heterozygous mutants and controls. Kruskal-Wallis test with Dunn's multiple comparisons test. ns >0.05. Bars represent s.e.m.

Next, dendritic spine density in basal (Figure 5.7) and apical (Figure 5.8) dendrites of CA1 neurons was calculated for every dendritic branch by summing the total number of spines per branch length and given as the average spine density per 10 µm. Surprisingly, spine density in CA1 neurons in Tenm3$^{-/-}$/Thy1-GFP mutant mice was significantly increased in basal (n = 49, 30.79 spines/10 µm ± 1.42 SEM ± 9.96 SD, $p < 0.0163$) and apical dendrites (n = 28, 35.91 spines/10 µm ± 1.7 SEM ± 9.0 SD, $p < 0.0005$) compared to control Tenm3$^{+/+}$/Thy1-GFP animals (basal: n = 50, 26.39 spines/10 µm ± 1.28 SEM ± 9.04 SD, apical: n = 39, 25.83 spines/10 µm ± 2.03 SEM ± 12.7 SD). The same was true for heterozygous Tenm3 mutants (basal: n = 61, 30.99 spines/10 µm ± 1.37 SEM ± 10.7 SD, $p < 0.0299$; apical: n = 51, 37.99 spines/10 µm ± 2.03 SEM ± 15.08 SD, $p < 0.0001$). This means that spine density in basal dendrites increased by 16.67% in homozygous and 17.43% in heterozygous Tenm3 mutants compared to controls. In apical dendrites this effect was stronger with a 39.02% increase in homozygous Tenm3 mutants and a 47.08% increase in heterozygous Tenm3 mutants.

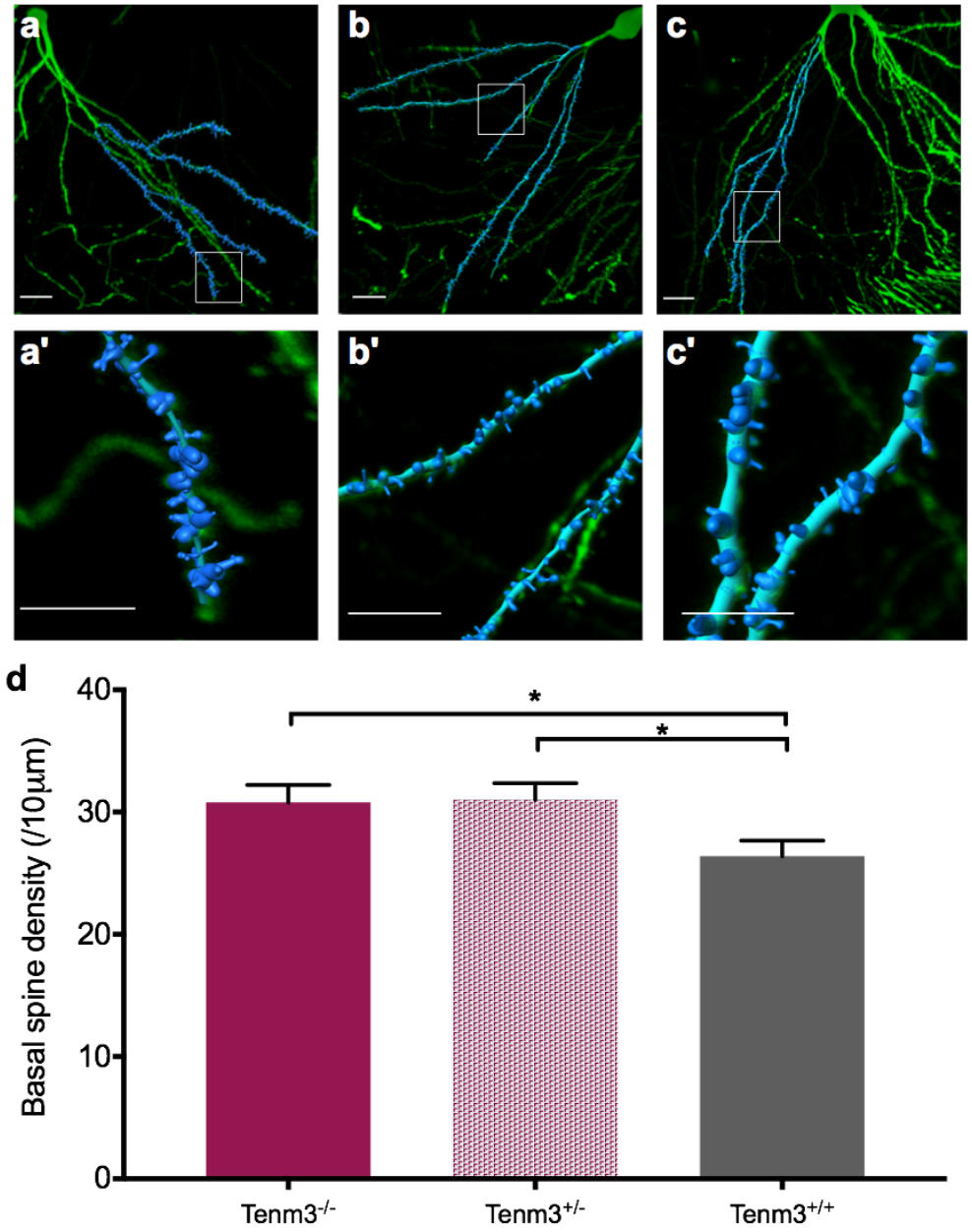

Figure 5.7. Basal dendritic spine density in Tenm3 mutants and control animals. **a-c.** Representative images of computer rendering of basal dendrites of CA1 neurons in Tenm3-/-/Thy1-GFP (**a**), Tenm3+/-/Thy1-GFP (**b**) and control Tenm3+/+/Thy1-GFP (**c**) mice. Scale bar is 10μm. **a'-c'**. Magnified dendritic segments indicated in a-c. Scale bar is 5μm. **d.** Basal dendritic spine density in Tenm3 mutants and control. Kruskal-Wallis test with Dunn's multiple comparisons test. *p<0.05.

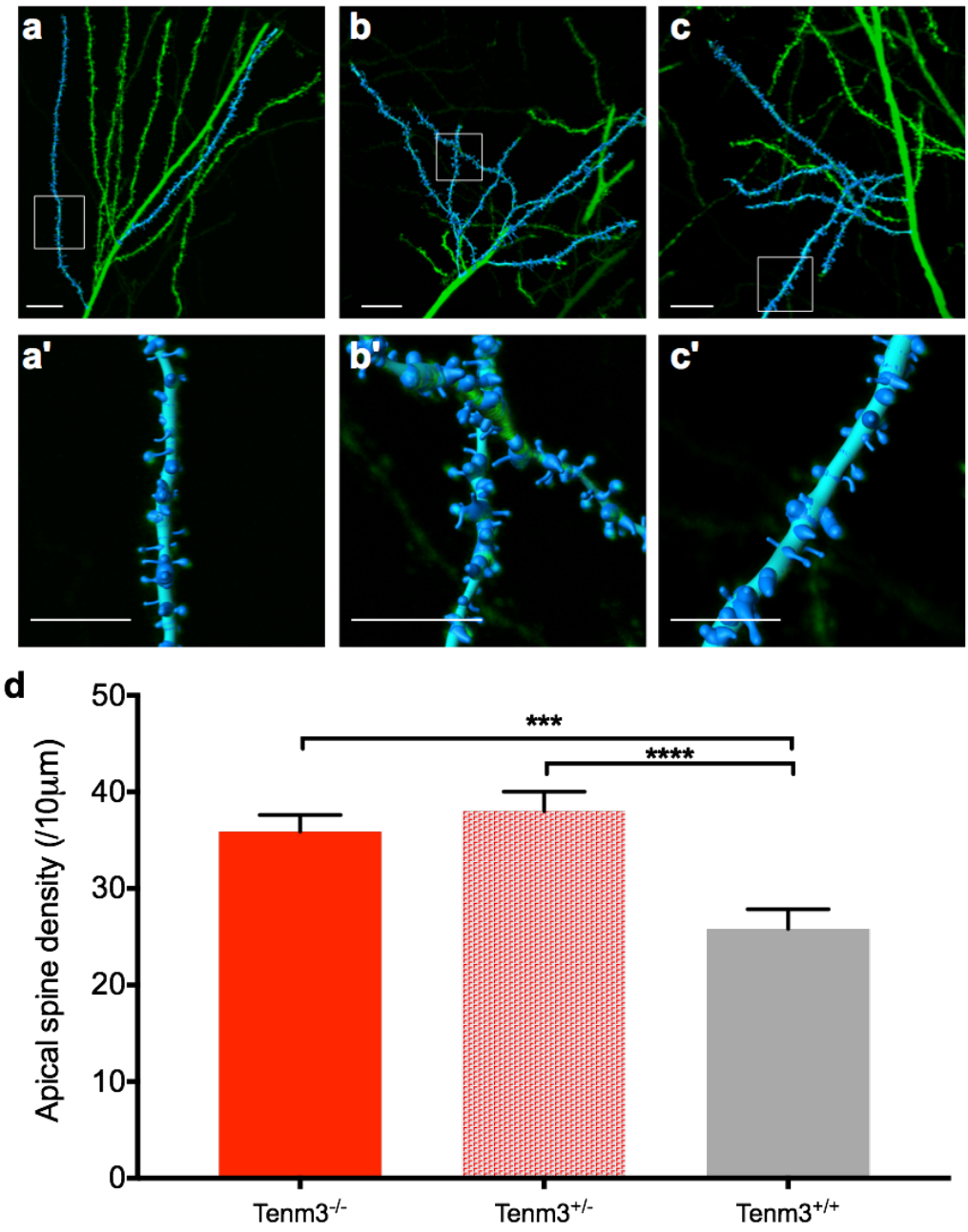

Figure 5.8. Apical dendritic spine density in Tenm3 mutants and control animals. **a-c.** Representative images of computer renderings of apical dendrites of CA1 neurons in Tenm3-/-/Thy1-GFP (**a**), Tenm3+/-/Thy1-GFP (**b**) and control Tenm3+/+/Thy1-GFP (**c**) mice. Scale bar is 10μm. **a'-c'**. Magnified dendritic segments indicated in a-c. Scale bar is 5μm. **d.** Apical dendritic spine density in Tenm3 mutants and control. Kruskal-Wallis test with Dunn's multiple comparisons test. ***p<0.001, ****p<0.0001, bars represent s.e.m.

5.3.2 Quantitation and analysis of dendritic spine morphology and density in Tenm3 mutants

The increase in basal and apical spine density in Tenm3 mutants was contrary to what we expected due to studies in *Drosophila*, which showed that Tenm3 perturbations led to a decrease in the number of synaptic boutons (Mosca *et al.*, 2012). As spine maturity is reflected in the morphology of spines, I proceeded to investigate the density of different spine types. Using the 'Classify Spines Wizard' within Imaris, spines were classified according to the criteria described above and in 2.6.5. In order of increasing maturity, the four spine types were: stubby, sessile, thin and mushroom. Spine classification provided spine subtype density and proportion of the total spine population. All statistical values and tests are reported in detail in Appendix 5.

In CA1 pyramidal neurons, the full or partial loss of Tenm3 in homozygous and heterozygous mutants respectively, tended to increase the density of all spine subtypes in basal (Figure 5.9) and apical dendrites (Figure 5.10), resulting in the increased overall spine density observed above. In basal dendrites, $Tenm3^{+/-}$/Thy1-GFP animals (n = 61, 14.86 spines/10 µm ± 1.21 SEM ± 9.36 SD, $p < 0.0167$, Kruskal-Wallis test) had a significantly higher density of sessile spines compared to $Tenm3^{+/+}$/Thy1-GFP (n = 50, 9.86 spines/10 µm ± 0.72 SEM ± 5.05 SD). The $Tenm3^{-/-}$/Thy1-GFP mutant (n = 49, 13.31 spines/10 µm ± 1.12 SEM ± 7.85 SD, $p > 0.1329$, Kruskal-Wallis test) also tended to have a higher density of sessile spines compared to the control, however this difference was not significant. The strongest difference in spine density was observed in basal mushroom spines, where both the $Tenm3^{-/-}$/Thy1-GFP (n = 49, 1.17 spines/10 µm ± 0.15 SEM ± 1.17 SD, $p < 0.0001$, Kruskal-Wallis test) and $Tenm3^{+/-}$/Thy1-GFP (n = 61, 1.09 spines/10 µm ± 0.15 SEM ± 1.06 SD, $p < 0.0001$, Kruskal-Wallis test) animals had significantly more mushroom spines compared to control $Tenm3^{+/+}$/Thy1-GFP animals (n = 50, 0.48 spines/10 µm ± 0.07 SEM ± 0.38 SD). In apical dendrites, the differences between Tenm3 mutants and the control were more pronounced. $Tenm3^{-/-}$/Thy1-GFP mutants (n = 28, 17.57 spines/10 µm ± 1.24 SEM ± 6.57 SD, $p < 0.0209$, Kruskal-Wallis test) had significantly more stubby spines compared to control $Tenm3^{+/+}$/Thy1-GFP animals (n = 39, 13.39 spines/10 µm ± 0.86 SEM ± 5.44 SD). Sessile spines were also more densely distributed in apical dendrites of $Tenm3^{-/-}$/Thy1-GFP (n = 28, 15.42 spines/10 µm ± 1.14 SEM ± 6.03 SD, $p < 0.0033$, Kruskal-Wallis

test) and Tenm3$^{+/-}$/Thy1-GFP mice (n = 55, 19.78 spines/10 µm ± 1.72 SEM ± 12.73 SD, p < 0.0001, Kruskal-Wallis test) compared to Tenm3$^{+/+}$/Thy1-GFP (n = 39, 10.59 spines/10 µm ± 1.52 SEM ± 9.38 SD) controls. Tenm3$^{+/-}$/Thy1-GFP mice (n = 55, 2.89 spines/10 µm ± 0.3 SEM ± 2.28 SD, p < 0.0014, Kruskal-Wallis test) had more thin spines compared to Tenm3$^{+/+}$/Thy1-GFP (n = 39, 1.54 spines/10 µm ± 0.23 SEM ± 1.47 SD) controls. Finally, a large difference was again observed in mushroom spines, with significantly higher mushroom spine densities in the homozygous (n = 28, 0.94 spines/10 µm ± 0.15 SEM ± 0.73 SD, p < 0.0247, Kruskal-Wallis test) and heterozygous (n = 55, 1.13 spines/10 µm ± 0.14 SEM ± 0.98 SD, p < 0.0001, Kruskal-Wallis test) Tenm3 mutants compared to the control (n = 39, 0.47 spines/10 µm ± 0.08 SEM ± 0.40 SD).

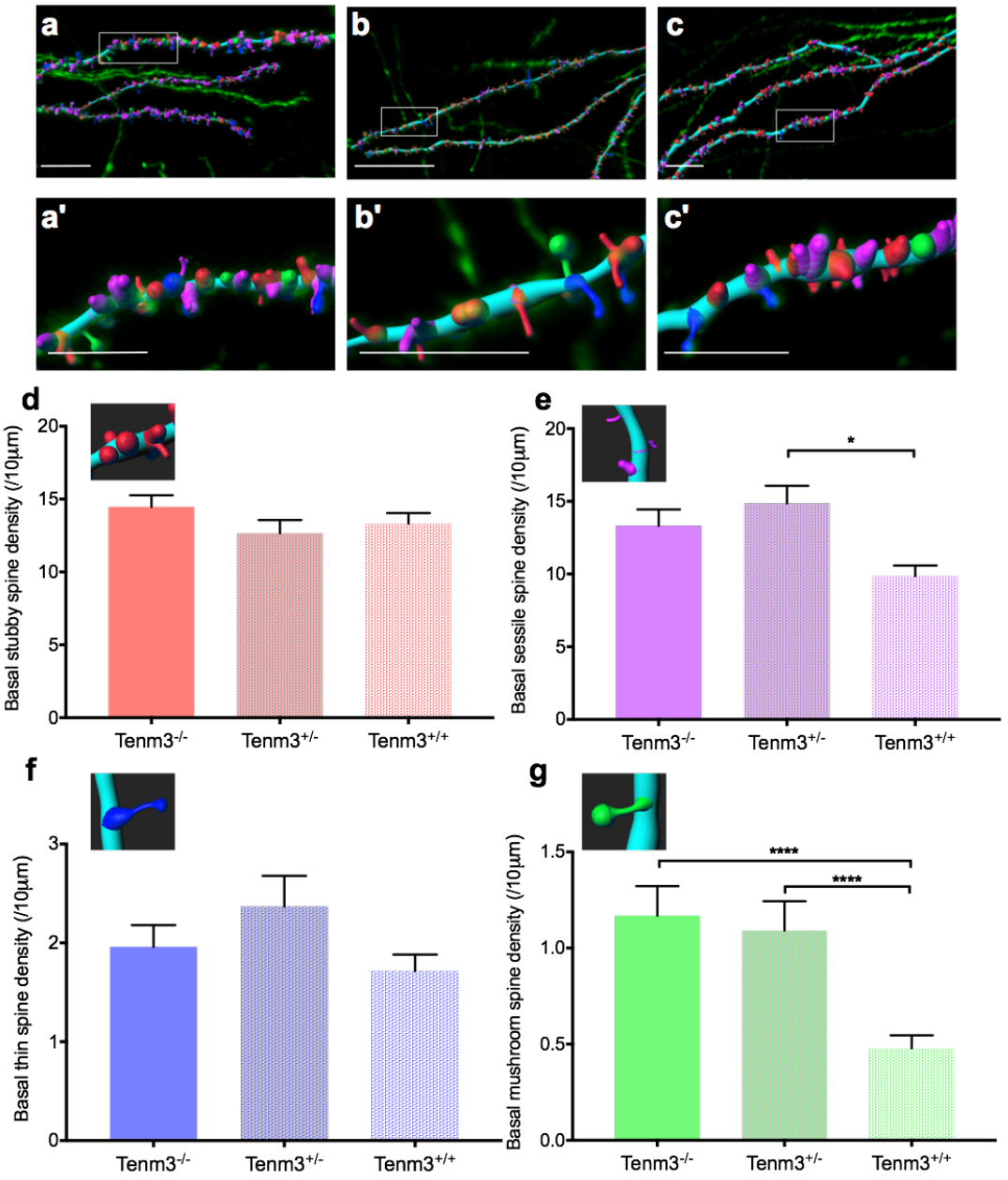

Figure 5.9. Density of basal dendritic spine subtypes in Tenm3 mutants and control animals. **a-c.** Representative images of computer renderings of basal dendrites of CA1 neurons and stubby (red), sessile (purple), thin (blue) and mushroom (green) spines in Tenm3-/-/Thy1-GFP (**a**), Tenm3+/-/Thy1-GFP (**b**) and control Tenm3+/+/Thy1-GFP (**c**) mice. Scale bar is 10μm. **a'-c'**. Magnified dendritic segments indicated in a-c. Scale bar is 5μm. **d-g.** Density of stubby (**d**), sessile (**e**), thin (**f**) and mushroom (**g**) spines in basal CA1 dendrites in Tenm3 mutants and control. Kruskal-Wallis test with Dunn's multiple comparisons test. *p<0.05, ****p<0.0001, bars represent s.e.m.

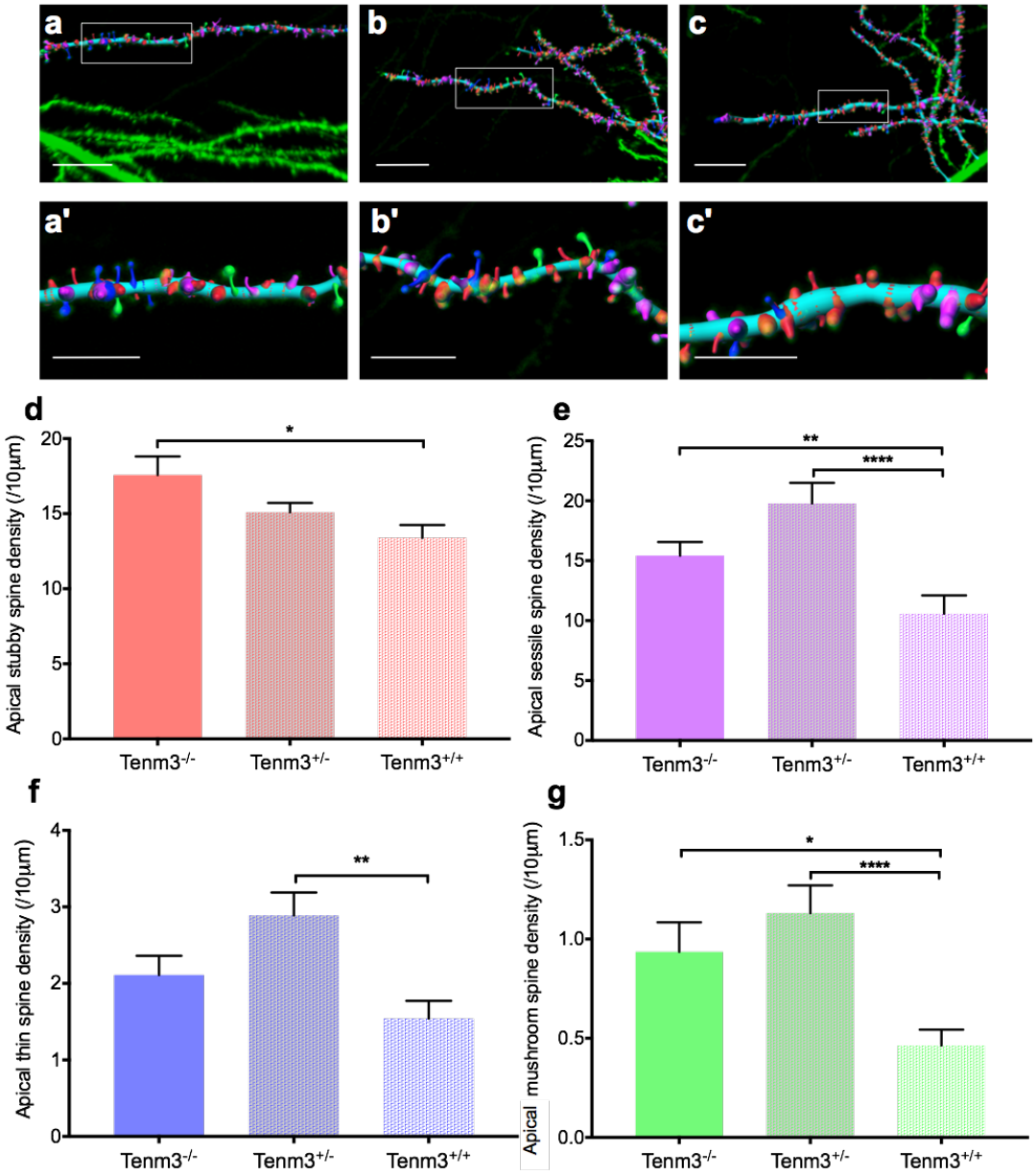

Figure 5.10. Density of apical dendritic spine subtypes in Tenm3 mutants and control animals. **a-c.** Representative images of computer renderings of apical dendrites of CA1 neurons and stubby (red), sessile (purple), thin (blue) and mushroom (green) spines in Tenm3-/-/Thy1-GFP (**a**), Tenm3+/-/Thy1-GFP (**b**) and control Tenm3+/+/Thy1-GFP (**c**) mice. Scale bar is 10μm. **a'-c'**. Magnified dendritic segments indicated in a-c. Scale bar is 5μm. **d-g.** Density of stubby (**d**), sessile (**e**), thin (**f**) and mushroom (**g**) spines in apical CA1 dendrites in Tenm3 mutants and control. Kruskal-Wallis test with Dunn's multiple comparisons test. *p<0.05, **p<0.0021, ****p<0.01, bars represent s.e.m.

This global increase in spine density also significantly altered the proportions of spine subtypes in relation to the total population of spines (Figure 5.11). In particular, mushroom spines constituted a larger proportion of the total spine population in basal dendrites of Tenm3$^{-/-}$/Thy1-GFP (n = 49, 2.62 %± 0.35 SEM ± 2.49 SD, $p < 0.002$, Kruskal-Wallis test) and Tenm3$^{+/-}$/Thy1-GFP mice (n = 61, 2.73 % ± 0.38 SEM ± 3.04 SD, $p < 0.0013$, Kruskal-Wallis test) compared to Tenm3$^{+/+}$/Thy1-GFP (n = 50, 1.04 % ± 0.18 SEM ± 1.24 SD) controls. In apical dendrites, only heterozygous Tenm3 mutants (n = 55, 2.43 % ± 0.27 SEM ± 2.08 SD, $p < 0.0012$, Kruskal-Wallis test) had a significantly larger proportion of mushroom spines compared to controls (n = 39, 1.14 % ± 0.21 SEM ± 1.31 SD). Generally, alterations in spine proportions seemed more pronounced in the heterozygous mutant, which also had a significant increase in the percentage of sessile spines in apical dendrites (n = 55, 49.30 % ± 2.15 SEM ± 16.34 SD, $p < 0.0001$, ANOVA) compared to the control (n = 39, 33.82 % ± 2.98 SEM ± 18.87 SD). The opposite relationship was seen for stubby spines, which constituted a significantly smaller proportion in apical (n = 55, 42.14 %± 2.03 SEM ± 15.46 SD, $p < 0.0001$, ANOVA) and basal dendrites (n = 61, 45.22 % ± 2.62 SEM ± 20.98 SD, $p < 0.0053$, Kruskal-Wallis test) compared to the control (respectively: n = 39, 58.70 % ± 3.09 SEM ± 19.52 SD; n = 50, 54.01 % ± 2.40 SEM ± 16.94 SD). This effect was also observed in homozygous Tenm3 mutants, which had a significantly smaller proportion of apical stubby spines (n = 28, 48.79 % ± 2.56 SEM ± 13.54 SD, $p < 0.0425$, ANOVA).

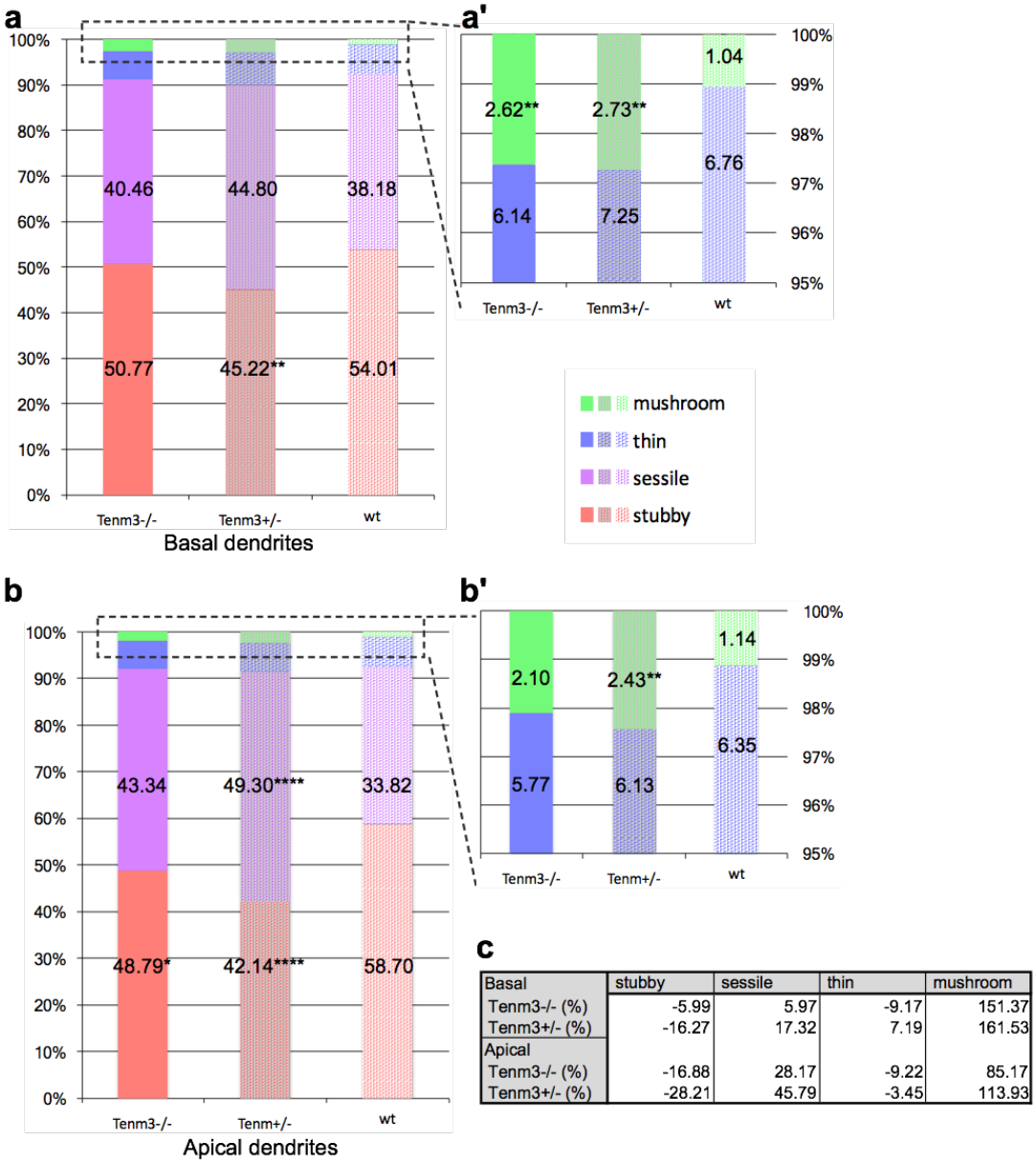

c

Basal	stubby	sessile	thin	mushroom
Tenm3-/- (%)	-5.99	5.97	-9.17	151.37
Tenm3+/- (%)	-16.27	17.32	7.19	161.53
Apical				
Tenm3-/- (%)	-16.88	28.17	-9.22	85.17
Tenm3+/- (%)	-28.21	45.79	-3.45	113.93

Figure 5.11. Proportions of spine subtypes in Tenm3 mutants and control animals. **a.** Proportions of spine subtypes as a percentage of the total spine population in CA1 basal dendrites. **a'.** Magnification of **a** showing proportions of thin and mushroom spines. **b.** Proportions of spine subtypes as a percentage of the total spine population in CA1 apical dendrites. **b'.** Magnification of **b** showing proportions of thin and mushroom spines. Stars indicate significant differences in Tenm3 mutants compared to the control. Kruskal-Wallis test followed by Dunn's multiple comparison, *p<0.05, **p<0.01, ****p<0.0001. **c.** Table showing the direction and percentage of change in spine type proportions in apical and basal dendrites of Tenm3 mutants.

5.4 Summary and discussion

In this chapter I investigated the consequences of a loss of Tenm3 on dendritic spine density and morphology in CA1 neurons. Loss of Tenm3 does not seem to have any significant impact on dendritic morphology as there were no differences in the straightness of dendrites between Tenm3 mutants and controls and the gross morphology of CA1 neurons seemed unaffected. However, Tenm3 loss had a strong effect on spine density. Indeed, Tenm3 mutants had a significantly increased density of dendritic spines compared to control animals. This effect was seen for all four spine classes, which tended to appear in larger numbers in both the homozygous and heterozygous Tenm3 mutants. The most striking increase was seen for mushroom spines, which were consistently more abundant in Tenm3 mutants in basal and apical dendrites. Increases in spine density were generally more pronounced in apical dendrites, where Tenm3 mutants also had significantly larger numbers of stubby, sessile and thin spines. The general increase in spine density also altered the proportions of spine types in relation to the overall spine population. Despite an increase in density, the proportion of stubby spines was significantly lower in basal and apical dendrites of Tenm3 mutants compared to controls (Figure 5.11-c). Conversely, the higher density of mushroom spines also led to a significant increase in their proportion in basal and apical dendrites. The effect on mushroom spines was particularly strong, as their proportion more than doubled in Tenm3 mutants (Figure 5.11-c).

It is important to note, that it was not possible to confirm that Tenm3 was indeed mutated in the analysed CA1 neurons. Whilst the expression of β-galactosidase, which recapitulated the endogenous proximal-to-distal Tenm3 gradient along CA1, was verified using X-gal, this detection method is not compatible with fluorescence imaging. A number of anti-β-galactosidase antibodies were tested unsuccessfully (refer to 2.5.2 and Table 1 for further detail) and therefore it was not possible to confirm β-galactosidase expression in individual GFP-positive CA1 neurons. In order to address this limitation, only CA1 neurons in the proximal area of CA1 (where Tenm3 is most strongly expressed) were analysed, thus increasing the likelihood of selecting neurons in which Tenm3 has been disrupted. Another concern is that we do not know whether the transcribed Tenm3 intracellular domain is still functional or whether it is targeted

for degradation**.** If it does retain some function, a dominant-negative effect cannot be excluded (see Chapter 6).

The findings presented here were entirely unexpected and indeed surprising. The available literature on Teneurins established that these transmembrane proteins regulate wiring specificity and that this is likely to happen via homophilic, transsynaptic interactions (Leamey and Sawatari, 2014). This further led to the suggestion that Teneurins might function similarly to well characterised synaptic cell-adhesion molecules, such as the Neurexin/Neuroligin complex and promote synapse formation through bidirectional signalling. Experimental evidence from work in *Drosophila* provided compelling evidence that Teneurins mediate partner matching and synaptic assembly via transsynaptic interactions (Hong, Mosca and Luo, 2012; Mosca *et al.*, 2012; Mosca and Luo, 2014). In these studies, Teneurin disruption led to a reduction in synapses and a variety of phenotypes consistent with failures in synaptic assembly. Therefore, it seemed a reasonable assumption that Teneurins might be responsible for analogous processes in vertebrates and that disruption of Tenm3 would lead to a reduction in the number of synapses. However, in this project, I found that loss of Tenm3 leads to an increase in synaptic density in the mouse hippocampus. It is possible that Teneurins function differently in vertebrates and invertebrates and thus have different effects on synapse formation.

However, increased synaptic density in Tenm3 mutant mice also seems counterintuitive in light of the suggestion that Teneurins might function similarly to classical cell-adhesion molecules with roles in synapse induction and assembly. Indeed, knockdown of many classical synaptic cell-adhesion molecules results in phenotypes of decreased synaptic density, stability and/ or transmission. For instance, knockdown of Cadherin 9 decreases the number of synapses in *vitro* and in *vivo* (Williams *et al.*, 2011). Disruption of N-Cadherin and αN-Catenin severely reduces dendritic stability and results in aberrant spine morphology (Togashi *et al.*, 2002; Abe *et al.*, 2004). Knockdown of Neuroligins leads to a reduction in synaptic density in hippocampal neurons (Chih, Engelman and Scheiffele, 2005; Shipman *et al.*, 2011), and knockdown of Neurexin abolishes the ability of LRRTM2 to induce presynaptic differentiation (de Wit *et al.*, 2009). Furthermore, triple knockout of α-Neurexin severely disrupts synaptic excitatory synaptic transmission (Missler *et al.*, 2003). However, there are also

examples of cell surface and secreted molecules that exert inhibitory cues to prevent inappropriate formation of synapses. One of the protein families most commonly associated with repulsive cues are the Semaphorins. These ligands, together with their Plexin and Neuropilin receptors, were initially discovered as axon guidance cues but have more recently been found to play key roles in synapse formation and function (Pasterkamp and Giger, 2009). Plexin-A3 and Neuropilin-2 signalling is required for stereotyped pruning of the infrapyramidal bundle (IPB) of the mossy fibre pathway and seems to be mediated by the secreted class 3 Semaphorin ligand Sema3F (Bagri *et al.*, 2003). Pruning of mossy fibre collaterals is intimately associated with the elimination of transient synapses formed onto basal dendrites of CA3 pyramidal neurons. Indeed, in knockout mice, the lack of Plexin-A3 signalling results in a continued maturation of these transient synapses and consequently in a failure of IPB axon pruning (Liu, 2005). Thus, Plexin-A3 signalling triggers axon pruning by promoting synapse elimination. Sema3F was also found to negatively regulate dendritic spine formation in DG neurons and cortical layer V pyramidal neurons (Tran *et al.*, 2009). Indeed, a 3.5-fold increase in dendritic spines in primary dendrites of DG neurons and layer 5 pyramidal neurons was observed in knockout mice lacking Sema3F or its receptor Neuropilin-2. Furthermore, spines on DG neurons were enlarged and harboured perforated PSDs. DG neurons and layer V pyramidal neurons also exhibited increased miniature excitatory postsynaptic currents (Tran *et al.*, 2009) and Sema3F mutant mice exhibit seizures (Sahay, 2005). Treatment of dissociated DG neurons with recombinant Sema3F resulted in a ~40% decrease in excitatory postsynaptic terminals (Tran *et al.*, 2009). Taken together, these results demonstrated that Sema3F-Neuropilin-2 signalling acts as a negative regulator of spine development and growth. The transmembrane class 5 Semaphorin Sema5B was also shown to regulate the elimination of synaptic connections in dissociated hippocampal neurons through its diffusible Semaphorin domain (O'Connor *et al.*, 2009). Since Semaphorins are well known for regulating the rearrangement of the actin-cytoskeleton during growth cone steering (Pasterkamp and Giger, 2009), these findings suggest that Sema3F and Sema5B might exert their inhibitory action on synaptic development through interactions with the cytoskeleton. However, the exact mechanisms that lead to synaptic disassembly during synapse elimination remain largely unknown. Increases in synaptic density can also happen as a compensatory mechanism for reduced synaptic function. Indeed, loss of β-catenin results in a dispersion and reduction of reserved pool synaptic vesicles as well as

impaired responses to synaptic stimulation (Bamji *et al.*, 2003). These conditional β-catenin knockout mice exhibit a ~25% increase in dendritic spines and a 3-fold increase in the number of perforated synapses in CA1 pyramidal neurons. The authors of this study propose that the increase in synaptic density is likely to reflect compensatory changes in response to decreases in synaptic efficacy (Bamji *et al.*, 2003). The present findings establish that Tenm3 plays an important role in the regulation of vertebrate synapses. However, my findings suggest that Tenm3 negatively regulates dendritic spine development in vertebrates, which is at odds with the previously established hypothesis that Teneurins may contribute to the assembly of synapses through the formation of transsynaptic adhesion complexes.

There could be a number of reasons why my findings are not consistent with loss of function studies in *Drosophila*. First, vertebrates have four Teneurin paralogues and the fact that they are all expressed in CA1 suggests a redundancy in function. Therefore, it is possible that compensation is taking place in the Tenm3 mouse mutants. However, this would not account for an increase in synaptic density, unless loss of Tenm3 disrupts synaptic efficacy, which was not investigated. To shed light on the possibility of compensatory mechanisms, it would be interesting to evaluate whether mRNA levels of Tenm1, Tenm2 or Tenm4 are elevated in Tenm3 mutants using quantitative PCR. Second, the vertebrate CNS is more complex than that of *Drosophila* and different Teneurins might have distinct functional mechanisms in mice.

I found that a loss of Tenm3 not only leads to an increase in spine density, but also results in markedly higher proportions of mushroom spines and lower proportions of stubby spines (Figure 5.11-c). Because spine morphology is dependent on synaptic function (Sala and Segal, 2014), my findings suggest that a loss of Tenm3 leads to increased spine plasticity and maturation. Thus, we can speculate that intact Tenm3 function may inhibit spine plasticity and maturation. Teneurins were shown to bind to α-spectrin (an actin binding protein) and perturbations of Teneurins in *Drosophila* lead to disorganisation of the spectrin and microtubule cytoskeleton (Mosca *et al.*, 2012). Since spine plasticity and morphology are determined by the actin cytoskeleton, it is possible that Tenm3 exerts its inhibitory effect on spine plasticity by regulating the dynamics and remodelling of the cytoskeleton. However, more studies are needed to confirm this hypothesis.

It is unclear whether the additional spines observed in the Tenm3 mutant are functional synapses as the achievable resolution in confocal microscopy is insufficient to determine whether spines had synapses. Unfortunately, it was not possible to use FingR intrabodies to visualise excitatory (PSD-95) and inhibitory (Gephyrin) synapses, as IUE to target CA1 neurons with these constructs failed. Consequently, we also do not know whether loss of Tenm3 had an effect on inhibitory synapse density. Electroporation of the hippocampus was achieved when IUE was first described in 2001 (Saito and Nakatsuji, 2001), but reports of targeting the hippocampus were rare in the following years. Despite the great scientific interest in the hippocampus, only two other articles (Nakahira and Yuasa, 2005; Navarro-Quiroga *et al.*, 2007) were published in the six years following the initial description of hippocampal targeting through IUE. This is in stark contrast to the exponential increase in publications that targeted the somatosensory cortex through IUE in the same time span (Appendix 6; dal Maschio *et al.*, 2012). Indeed, hippocampal electroporations are challenging due to the limited physical access to embryos in the amniotic sac and the difficulty in appropriately orientating the electrodes. As described above (section 5.2), considerable efforts were made to transfect CA1 neurons using IUE, however survival rates of electroporated RRD180 mice was not optimal and as a result efficiency in targeting CA1 was very low. To exclude that these low success rates were due to technical errors, two highly skilled operators with years of experience kindly agreed to perform some IUE surgeries for us. However, survival rates of pups from these electroporations were even lower (4% compared to 34.5 %), indicating that this effect was experimenter-independent and not due to a lack of proficiency in performing the IUE surgery. Moreover, prior to starting IUE experiments, considerable time was spent on training to perfect the IUE surgery using wild type CD1 mice, and an acceptable hippocampal transfection efficiency was achieved (~29 % compared to reported average efficiency of ~19 %; dal Maschio *et al.*, 2012), further supporting that low success in RRD180 electroporations was not due to insufficient training and proficiency. A recent study demonstrated significantly higher IUE efficiencies in targeting the hippocampus using a triple electrode (dal Maschio *et al.*, 2012). However, due to time issues, it was not possible to carry out this approach. Thus, opting to cross RRD180 mice with the Thy1-GFP reporter mouse line to achieve sparse fluorescent labeling of CA1 neurons was a reasonable and more ethical alternative.

The classification of spines by their shape has proven useful to determine whether shifts in spine morphology occur with experimental manipulations. In the experiments presented here, using Imaris (Bitplane) software, spines were sequentially classified from stubby to mushroom and to thin according to characteristics described in 2.6.4. Due to this sequential process, stubby, mushroom and thin spines, which have defined criteria, cannot falsely be classified as sessile and there is no overlap in spine categories. Finally, all remaining spines were categorised as "sessile". Because, the maximum spine length was set to 2.5µm, sessile spines had to have no head and a length between 1-2.5µm. However, it is important to note that accurate distinction of dendritic spine shape often depends on dimensions that are beyond the resolution of confocal microscopy. Indeed, mature CA1 dendrites are so densely covered in spines, that profiles of neighbouring spines can overlap one another and interfere with accurate reconstruction of spine shape. Whilst great care was taken in the manual validation process during dendritic spine reconstruction, spine detection and classification was limited to the resolution in confocal microscopy. In order to make subtle distinctions in dendritic spine shape, serial electron microscopy would be necessary. Such an approach would also make it possible to analyse the spine ultrastructure in Tenm3 mutant mice. Alternatively, one could perform super-resolution microscopy such as stimulated emission depletion (STED) imaging, which has been developed more recently and can achieve resolutions beyond the diffraction barrier (Loew and Hell, 2013). STED is based on the use of two lasers, one to excite the fluorophores of interest and the second STED laser to de-excite fluorophores outside the very centre of the point spread function (PSF). In a way, STED microscopy uses a "sharpened" laser to achieve a resolution of about 70nm in biological samples with regular fluorophores. Thus, this technique is well suited to provide a detailed and quantitative analysis of spine morphology in fixed and living samples.

Finally, functional studies should be carried out in the future to assess the physiological consequences of the observed increase in spine density in Tenm3 mutants. Electrophysiological tests such as whole cell voltage-clamp recordings for instance could be performed to measure the frequency of mESPCs in CA1 neurons of Tenm3 mutants. Real-time imaging with calcium indicator dyes could give insight as to whether dendritic spines in Tenm3 mutants receive functional synaptic inputs. To conclude, the findings presented in this chapter show that Tenm3 has important

functions in vertebrate synapse formation and indicate that it negatively regulates dendritic spine development and maturation. The mechanisms underlying the morphological differences in Tenm3 mutants are not known, but we may hypothesise that Tenm3 interacts with the cytoskeleton to inhibit synaptic assembly.

6 General Discussion

In this thesis project, I explored the synaptic role of Teneurins in vertebrates. The aims were first, to address the subcellular localisation pattern of Teneurins and secondly, to address the involvement of Tenm3 in synapse formation and maintenance. I began by investigating whether Teneurins are localised at synapses in hippocampal cultures. This was followed by a thorough investigation of the subcellular localisation pattern of Tenm3 in CA1 neurons using organotypic hippocampal slice cultures. Finally, the functional consequences of a loss of Tenm3 were explored *in vivo* by analysing CA1 dendritic spine density and morphology in a Tenm3 gene trap mutant mouse line. A number of key findings were made; (1) all four Teneurins are localised in punctate fashion in neurons, overlapping in part with synaptic structures, (2) Tenm3 in particular, clusters in a subpopulation of dendritic spine heads and in the shaft at the base of dendritic spines, (3) loss of Tenm3 results in a significant increase in spine density and maturation in CA1 neurons. In this chapter, I start by summarising the main findings of the three results chapters, discuss potential caveats and point to possible alternative methods. I then propose a hypothesis for the cellular mechanisms underlying the observed phenotype in Tenm3 mutants and offer suggestions for future work addressing the role of Teneurins in synapse formation.

6.1 Summary

6.1.1 Teneurins localise in a punctate manner and are partially localised at synapses

In chapter 3, I described the subcellular localisation pattern of all four mouse Teneurin paralogues with the aim of investigating whether these proteins are enriched at synapses. I used dissociated hippocampal neurons for these experiments and due to the lack of Teneurin antibodies, epitope-tagged Teneurin expression vectors were transfected. Overexpression of Teneurins in cultures led to cytotoxicity and after a lengthy transfection optimisation phase it was established that acceptable cell health could be achieved when cultures were transfected at 15DIV and fixed two days later at 17DIV. To analyse whether Teneurins localise at synapses, a colocalisation analysis was performed to quantitate the amount of overlap between Synapsin and Teneurins. Synapsin, a presynaptic protein associated with the membranes of vesicles in excitatory and inhibitory synapses, was used as a general synaptic marker. The key findings made in this chapter were that all four Teneurins formed discrete puncta along both dendrites and axons. About a fifth of Teneurin puncta colocalised with Synapsin. This level of overlap was significantly higher compared to a negative random control, but considerably lower compared to the positive control, in which Synapsin colocalisation with two known pre- and postsynaptic proteins was measured. Indeed, Bassoon, a presynaptic protein, showed ~56% overlap with Synapsin, and Shank2, a postsynaptic protein, showed ~38% overlap. These results suggest that Teneurins are partially localised at synapses, although large amounts of these proteins cluster in non-synaptic puncta along neurites. The nature of non-synaptic Teneurin puncta is unknown.

The use of epitope-tagged expression constructs is a common approach for studying subcellular protein localisation when there are limitations to the application of other methods such as immunohistochemistry. However, there are a number of drawbacks associated with this approach. First, overexpression of proteins is associated with the risk of altering the normal function of neurons and can lead to unwanted functional, structural or cytotoxic effects. Whilst a lot of effort was put into establishing the optimal transfection procedure, some cytotoxicity remained in cultures and functional and/ or structural changes following Teneurin overexpression cannot be entirely excluded.

Such effects were visible in the form of increased cell death, aberrant neuronal morphology, notably with filamentous protrusions emanating from dendrites, engorged cell bodies and fragmented neurites. These adverse effects seemed to be specific to Teneurin overexpression, since control neurons transfected with GFP only exhibited markedly less cell death and no aberrant neuronal morphology. However, even in control cultures, GFP-transfected neurons with bulging cell bodies and fragmented neurites were occasionally observed. Therefore, some cytotoxicity might also have emanated from the cationic lipid-mediated transfection process. Other methods of transfection were not assayed, but future studies might want to consider this. Many different techniques are available for the transfection of nucleic acids into cells, all with their own advantages and limitations concerning efficiency and cell survival. Differentiated neurons are particularly challenging to transfect, because of the difficulty of efficiently introducing and expressing exogenous constructs as well as the fact that these cells tend to be very sensitive to experimental manipulations. Therefore, all available methods to transfect mammalian neurons are associated with some risk regarding the perturbation of cell physiology. Calcium phosphate-mediated transfection has some drawbacks, as it is relatively time consuming and requires optimisation, however it is reported to lead to lower cytotoxicity and higher transfection efficiency compared to lipofection and may thus present a good alternative for the transfection of Teneurins (Karra and Dahm, 2010).

Another concern with the transfection of expression vectors to produce recombinant Teneurins is that the proteins might not be functional and appropriately transported. Whilst many studies report faithful targeting of tagged proteins (El-Husseini, Schnell and Chetkovich, 2000; Ackermann and Matus, 2003; Williams *et al.*, 2011), there have also been cases where overexpressed recombinant proteins failed to localise properly, due to saturation of the targeting machinery. For instance, overexpression of the potassium channel Kv4.2 disrupts its punctate localisation pattern and leads to diffuse expression in the somatodendritic compartment (Chu, Rivera and Arnold, 2006). Protein overexpression can also disrupt normal sorting and transcytosis and drive mistargeting of proteins. For instance overexpression of CRMP-2, a regulator of microtubule dynamics, leads to its mislocalisation in the somatodendritic compartment and can cause aberrant axons to sprout from dendrites (Inagaki *et al.*, 2001). However, as recombinant Teneurins consistently formed puncta along dendrites and axons, it is

likely that these proteins were functional and appropriately transported. This thesis provided a first exploration of the subcellular localisation pattern of Teneurins in hippocampal neurons, but future work should compare the results presented here to the endogenous localisation, which will require the generation of paralogue-specific antibodies.

Subcellular Teneurin localisation was examined in dissociated hippocampal cultures. The majority of neurons in dissociated hippocampal cultures consists of excitatory DG and pyramidal cells from the *cornu ammonis*, whereas a small proportion of the neuronal population is made up of inhibitory interneurons. Whilst in most cases interneurons can be distinguished from spiny excitatory neurons, a distinction between different types of pyramidal neurons and DG cells is not evident in culture. Indeed, due to the dissociated nature of this model system, the structural organisation of neurons is lost, which makes it impossible to distinguish between different pyramidal cell types without the use of cell type-specific markers. The resulting heterogeneity in transfected neurons might have contributed to the variability in Teneurin localisation patterns and overlap with Synapsin. Indeed, it is possible that varying levels of pre-existing endogenous Teneurin in neurons might have differently affected the localisation of recombinant Teneurins and led to higher or lower levels of diffuse localisation, as some diffusely distributed protein was present at low levels along neurites of transfected neurons. Thus, the detection of Teneurin puncta might have varied between different transfected cell types and thereby contributed to increased variability. For this reason, the analysis of subcellular Tenm3 localisation in Chapter 4 was focused on CA1 neurons, which was possible because of the use of organotypic hippocampal slices rather than dissociated cultures.

To summarise, I show that the Teneurins are partially localised at synapses. However, the fact that the majority of Teneurin puncta did not colocalise with Synapsin indicates that these proteins are unlikely to exclusively play a structural role at the synaptic junction. Other known transmembrane molecules with synaptic roles have similar subcellular localisation patterns. Cadherin 9 and αN-Catenin for instance form puncta along axons and dendrites and are enriched at synapses, however they do not show a perfect overlap with synaptic markers such as Synaptophysin and vGlut1 (Uchida *et al.*, 1996; Williams *et al.*, 2011). Interestingly, Teneurin localisation is reminiscent of

that of Sema5B, which has a punctate distribution and only partially colocalises with the synaptic markers PSD-95 and Synapsin (O'Connor *et al.*, 2009). It is well established that the Cadherin-Catenin complex and Semaphorins interact with the cytoskeleton and it is thought that these interactions are crucial for their regulation of synaptic connectivity and axon guidance respectively (Salinas and Price, 2005; Pasterkamp and Giger, 2009; Wang *et al.*, 2012). Because Teneurins are suggested to interact with the cytoskeleton (refer to 1.2.4.1), this further supports a role for Teneurins in contributing to the establishment of synaptic connectivity through similar mechanisms.

6.1.2 Subcellular localisation of Tenm3 in CA1 neurons

Chapter 4 was a continuation of Chapter 3 and dedicated to a more detailed investigation of the subcellular localisation pattern of Tenm3. Tenm3 is endogenously expressed in a strong proximal-to-distal gradient along CA1, which is why organotypic hippocampal slice cultures were chosen to explore the subcellular localisation pattern of Tenm3 in CA1 neurons. The two main advantages of organotypic slice cultures over a dissociated culture system are (1) the preserved architecture of the neural tissue, which enables the identification of CA1 neurons, (2) the preservation of dendritic spines, which decorate pyramidal neurons and represent a morphologically identifiable feature of excitatory synapses. Indeed, organotypic hippocampal slices are cultured from postnatal mice after neuronal development and the initiation of spinogenesis (Yuste and Bonhoeffer, 2004). Similar to the experiments in Chapter 3, cells were transfected with Tenm3, but contrary to dissociated neurons, transfected neurons in slices exhibited markedly fewer signs of cytotoxicity. However, biolistic transfection caused tissue damage and Tenm3-overexpressing CA1 neurons exhibited small "bumps" along dendrites, possibly indicating the initiation of apoptotic mechanisms. The combined effect of Tenm3 overexpression and tissue damage-related cell death resulted in very few Tenm3 and GFP cotransfected CA1 neurons (n=7 from 5 independent cultures). In order to investigate the subcellular localisation pattern of Tenm3 in CA1 neurons, subcellular structures were manually traced in the GFP channel, including dendritic spines and shafts, and Tenm3 fluorescence intensity was subsequently measured in those areas. The main findings from this analysis were that

Tenm3 was localised in about one fifth (19.87 %) of dendritic spines and in about half (55.18 %) of all shafts below spines. Furthermore, Tenm3 puncta in dendritic shafts were spatially restricted to the area directly below the spine and had higher relative intensity compared to spines.

Whilst the work described in chapter 4 enabled a more detailed and specific description of Tenm3 localisation in CA1 neurons, there were some prevailing caveats. Tenm3 localisation had again to be investigated using recombinant Tenm3 transfected into neurons with the associated drawbacks. Firstly, whilst neurites appeared less fragmented and cell bodies less engorged than had been observed in dissociated cultures, it is evident that Tenm3 overexpression still led to some cytotoxicity, since survival of cotransfected neurons was lower than that of GFP-transfected neurons. Moreover, while cotransfected CA1 neurons did not exhibit any major aberrations in their gross morphology, some dendrites appeared "blebby", suggesting latent toxicity from Tenm3 overexpression. Tenm3 overexpression might also have had functional effects, as it is possible that these neurons had fewer dendritic spines compared to control GFP-transfected neurons (Appendix 7). Unfortunately, due to time constraints, it was not possible to quantify dendritic spine density in these neurons. Secondly, it was still not possible to verify that the observed localisation pattern corresponds to the endogenous Tenm3 localisation, due to the unavailability of a specific Tenm3 antibody. Initially, experiments based on organotypic hippocampal slice cultures had been designed to investigate CA1 dendritic spine density in neurons with overexpression or loss of Tenm3. However, following the low number of healthy transfected CA1 neurons obtained in slices, this approach was deemed too inefficient and we decided to investigate dendritic spine density in an intact *in vivo* system instead.

In summary, the results presented in Chapter 4 confirmed that many Tenm3 puncta are not localised at synapses and revealed that large proportions of Tenm3 puncta are found at the shaft. As the shaft is the area where actin filaments branch off microtubules in the dendritic shaft, giving rise to dendritic spines, this finding raises the intriguing possibility of Tenm3 involvement in early spine formation through the regulation of actin dynamics at spine initiation sites. Other proteins have been found to show a similar distribution within dendrites and to have the ability to translocate from shafts to spines. Profilins, which are important regulators of actin polymerisation, are targeted

to spine heads when postsynaptic NMDA receptors are activated. This translocation is thought to block actin dynamics and thus contribute to the stabilisation of dendritic spine structure (Ackermann and Matus, 2003). β-Catenin was found to move from shafts to spines upon depolarisation. This is thought to increase its association with Cadherins at the synaptic junction and contribute to an increase in synaptic size and strength (Murase, Mosser and Schuman, 2002). These are both examples of proteins, which translocate to spines in an activity dependent manner and contribute to the strengthening of synaptic connections. The findings presented in Chapter 5 suggest that Tenm3 acts as a negative regulator of spine formation. Thus, if Tenm3 translocates to spines, it is likely to have an inhibiting effect on spine growth rather than a promoting effect such as the one shown for Profilins and β-Catenin. It is not clear whether Tenm3 actively translocates or whether it gradually accumulates in spines through diffusion and this is a question, which would need to be investigated through time-lapse imaging.

6.1.3 Dendritic spine density following loss of Tenm3

In chapter 5, I examined the synaptic consequences of a loss of Tenm3 *in vivo*. Initially, transfection of CA1 neurons with GFP, PSD-95- and Gephyrin-FingR intrabodies and Tenm3 was attempted in embryonic Tenm3 mutant mice using IUE. However, due to the extremely low efficiency in targeting CA1 neurons and impaired survival of electroporated embryos, these experiments were deemed ethically and scientifically unsustainable. An alternative approach to label CA1 neurons in Tenm3 mutant mice was achieved by crossing this strain to a Thy1-GFP reporter mouse line with random sparse GFP labeling of CA1 neurons in the hippocampus. Brains from RRD180/Thy1-GFP mice were collected at P21 and analysed. The key findings were, that loss of Tenm3 resulted in a significant increase in spine density and altered the proportions of spine types to more mature mushroom spines and fewer stubby spines, which are considered the least mature type (Yuste and Bonhoeffer, 2004). These findings suggest that intact Tenm3 negatively regulates the formation of dendritic spines and may thus contribute to the shaping of neuronal connectivity through synapse elimination or inhibition.

We were surprised to find that the observed phenotypes were equally pronounced in Tenm3$^{+/-}$/Thy1-GFP and Tenm3$^{-/-}$/Thy1-GFP mutants. It is possible that in heterozygous animals, the mutant Tenm3 allele adversely impacts the function of the wild type Tenm3 allele and thus exerts a dominant-negative effect. Given that Teneurins are believed to form homo-dimers in *cis*, one likely scenario is the formation of mixed dimers, composed of a full length and a truncated Tenm3, would disrupt the function of the wild type Tenm3 in the dimer. Such a dominant-negative effect reconciles our findings, because the phenotype resulting from a heterozygous Tenm3$^{+/-}$/Thy1-GFP mutant is equal to that of a homozygous Tenm3$^{-/-}$/Thy1-GFP mutant and thus more severe than haploinsufficiency. This can only be explained in the case where the truncated Tenm3 protein retains some partial function, thus creating the dominant-negative effect. Since the gene trap vector was inserted before the transmembrane domain, the mutant Tenm3 allele is likely hypomorphic. In order to confirm the hypomorphic nature and the dominant-negative effect of the Tenm3 mutation, it is necessary to evaluate the severity of a complete null phenotype, which would be expected to be higher than that of the hypomorphic Tenm3 mutation. This would require a full knockout Tenm3 strain, which is not currently available.

Since the synaptic consequences of a loss of Tenm3 were only assessed by the density and morphology of dendritic spines and the introduction of Gephyrin-FingRs was not possible, we do not know whether inhibitory synapses were also affected. One way in which to determine whether loss of Tenm3 influences inhibitory synapse formation would be through the use of EM. Indeed, using such an approach, excitatory and inhibitory synapses can be distinguished because of their asymmetrical and symmetrical nature, respectively. Such an analysis would require the acquisition of large sets of serial EM samples, but in turn would provide valuable information on the density, ratio and arrangement of excitatory and inhibitory inputs relative to each other, as well as on ultrastructural changes in synapses following loss of Tenm3.

As structural changes in dendritic spines are closely linked to functional changes in the strength of synaptic transmission (Engert and Bonhoeffer, 1999; Sorra and Harris, 2000; Yuste and Bonhoeffer, 2001; Alvarez and Sabatini, 2007; Holtmaat and Svoboda, 2009; Wang and Zhou, 2010; Sala and Segal, 2014), the morphology of dendritic spines in Tenm3 mutants was analysed. In order to determine changes in dendritic spine

morphology, spines were classified into different spine types. As mentioned in Chapter 5, a common criticism of spine classification is that it only captures a static view of highly motile structures. Indeed, whilst the analysis of the density and proportions of different spine types is a good approach to explore the maturation of dendritic spines in fixed tissue samples, it does not give any insights into the dynamics and motility of these spines. Since vertebrate Teneurins are likely to interact with regulators of the actin-cytoskeleton (see 1.2.4.1.) and spine dynamics are regulated by the actin cytoskeleton (Matus, 2000; Bonhoeffer and Yuste, 2002; Ethell and Pasquale, 2005; Hotulainen and Hoogenraad, 2010; Sala and Segal, 2014) it is possible that loss of Tenm3 may affect spine stability and motility, similarly to what has been observed when αN-Catenin and N-Cadherin function was perturbed (Abe *et al.*, 2004). To evaluate possible effects of Tenm3 on spine stability, it would be necessary to perform live-imaging on organotypic hippocampal slices cultured from RRD180/Thy1-GFP mice.

The fact that Tenm3 mutants had increased spine densities suggests that intact Tenm3 is involved in inhibiting the formation and/ or maintenance of spines. However, as spine density in Tenm3 mutants was only analysed in fixed tissue from P21 mice, it is unclear whether the increased numbers of spines are a result of increased synapse formation or a lack of synapse elimination. Dendritic spines are constantly formed and eliminated, however the rates of such turnover change over time, resulting in a net gain during early development, a net reduction in young adulthood and synaptic maintenance in the adult (Holtmaat and Svoboda, 2009; Chen, Lu and Zuo, 2014). In layer 2/3 pyramidal neurons of the rat barrel cortex, spine density continuously increases from early postnatal stages to adolescence (P7 to P24; Lendvai *et al.*, 2000; Chen, Lu and Zuo, 2014). This phase of net spine gain is followed by a period of spine reduction in early adulthood. From P28 to P42, synapse elimination outweighs synapse formation in layer 2/3 pyramidal neurons of the mouse barrel cortex (Zuo *et al.*, 2005; Chen, Lu and Zuo, 2014), thus resulting in a net loss of spines. To determine whether Tenm3 inhibits spine formation or promotes the elimination of spines it would also be necessary to perform live-imaging on organotypic hippocampal slices cultured from RRD180/Thy1-GFP mice, as the rate of synapse elimination and formation could be measured in this system.

To summarise, the results presented in Chapter 5 unexpectedly revealed that loss of Tenm3 in *vivo* leads to an increase in spine density and appears to promote spine maturation. This suggests that intact Tenm3 may function as a negative regulator of synapse formation and maturation. Such a role is also consistent with the observation that Tenm3-overexpressing CA1 neurons had fewer spines than control neurons. However, the cellular mechanisms through which Tenm3 might exert such an effect are unknown and remain an exciting issue for future investigations. Moreover, it is unclear whether Tenm3 negatively regulates spine density by inhibiting spine formation or by promoting spine elimination. The fact that both phenomena persist into adulthood and that Tenm3 is expressed throughout life further suggest its ongoing involvement in the regulation of synaptic connectivity. In the following sections I will propose speculative models for the spine formation- and growth- inhibiting function of Tenm3.

6.2 Speculations and future directions

6.2.1 Possible interactions between Tenm3 and the cytoskeleton in the shaft

Tenm3 localisation in the shaft was an interesting new finding of which the significance is unclear. Tenm3 in shafts below spines is ideally located to play a role at the junction between microtubules and actin filaments in the dendritic shaft. Because actin filaments reside directly on and branch off microtubules in the dendritic shaft, an involvement of microtubule-associated actin-filament nucleators or actin-microtubule cross-linking factors has been suggested in the initiation of spines, the identity of which remains unknown (Hotulainen and Hoogenraad, 2010; Korobova and Svitkina, 2010). Thus, it is plausible that Tenm3 might exert its effect on dendritic spine formation via cytoskeletal interactions at this location. As mentioned in Chapter 1, a direct interaction between vertebrate Teneurins and the cytoskeleton has not yet been shown, but there is evidence in support of such an interaction from invertebrate and *in vitro* studies. In *Drosophila*, disruption of Ten-m and Ten-a results in severe disorganisation of the presynaptic microtubule- and postsynaptic spectrin-cytoskeleton, and Ten-m was shown to bind to α-spectrin and Filamin (Mosca *et al.*, 2012). The same study further showed that Teneurins also regulate the actin-regulating proteins Adducin and Wiskott-Aldrich syndrome protein (WASP), though a direct interaction with actin remains to be shown. Interestingly, WASP is a regulator of the Arp2/3 complex, the main nucleator of actin filaments, and knockout of vertebrate neuronal WASP (N-WASP) was shown to disrupt spine formation (Wegner *et al.*, 2008). Furthermore, Tenm1 was shown to bind to the adapter protein CAP/Ponsin and may form a large signalling complex with the actin-binding protein Vinculin (Nunes *et al.*, 2005). Thus, we can hypothesise that Tenm3 may directly, or indirectly via binding to other Teneurins, interact with the cytoskeleton.

It seems clear that part of the synaptic function of Tenm3 is different from the function of Ten-m and Ten-a in *Drosophila*, since disruption of the latter results in synaptic disassembly, whereas disruption of Tenm3 leads to increased spine formation. However, a common ground can be found in the hypothesised interaction with the cytoskeleton (Mosca *et al.*, 2012; Mosca, 2015). Dendritic filopodia, which are the precursors of dendritic spines, are thought to initiate from patches of actin on the

dendritic shaft (Andersen *et al.*, 2005; Hotulainen and Hoogenraad, 2010; Korobova and Svitkina, 2010). The mechanisms that lead to the formation of dendritic spines are still contested and it remains unclear whether spines are always formed from filopodia or whether they also form from pre-existing shaft synapses (Yuste and Bonhoeffer, 2004; Ethell and Pasquale, 2005; Sala and Segal, 2014). However, it has been shown that transient entry of microtubules into the spine modulates actin dynamics and spine growth (Jaworski *et al.*, 2009). Due to the localisation of Tenm3 in shafts, we can hypothesise that Tenm3 might restrict actin polymerisation at nascent spines and inhibit the movement of microtubules into spines, thereby reducing the maturation and growth of spines. In such a scenario, the loss of Tenm3 would lead to disinhibition of spine initiation, increased stabilisation of transient synaptic contacts and thus result in higher spine density. Such a model of action would be similar to that observed in Plexin-A3 knockout mice, where transient synaptic contacts between IPB axon collaterals and basal dendrites of CA3 neurons, continue to mature and thus fail to be eliminated (Liu, 2005).

6.2.2 Possible contribution of spine-Tenm3 to membrane tension and synapse elimination

As described above, it remains unclear whether Tenm3 inhibits spine formation or promotes spine elimination. In the previous section I proposed a model whereby Tenm3 in the shaft might inhibit spine formation through the restriction of actin and microtubule dynamics. However, it is also conceivable that Tenm3 might promote the elimination of spines. Tenm3 in the spinehead is ideally located to engage in cell-surface interactions with other ligands (see below) to trigger the disassembly of synapses. A similar mechanism has been described for Sema5B (O'Connor *et al.*, 2009). It is thought that after proteolytic cleavage, the release of the bioactive Semaphorin domain from postsynaptic cells triggers the destabilisation of presynaptic terminals and thus contributes to synapse elimination. Since Teneurins can be proteolitically cleaved and release their ECDs (Vysokov *et al.*, 2016), one possible scenario would be that Tenm3 is cleaved at the spine and that the secreted Tenm3 ECD induces the disassembly of contacting axons. Alternatively, Tenm3 might

transsynaptically interact with presynaptic ligands and bidirectionally initiate the elimination of synaptic contacts.

In the spine head, Tenm3 might further be involved in linking the cytoskeleton to the cell membrane. Indeed, different groups have previously proposed that Teneurins may anchor the cytoskeleton via their intracellular domain and thus link it to the cell-membrane (Mosca *et al.*, 2012; Beckmann *et al.*, 2013; Mosca and Luo, 2014; Mosca, 2015). One model for cell motility suggests that movement is generated by the tension that the cytoskeleton exerts on the membrane (Sheetz, 2001). According to this model, which is based on biophysical observations, the loss of cohesion between the cell membrane and the cytoskeleton generates cell "blebs", where the membrane protrudes into the extracellular space. The actin cytoskeleton rapidly assembles beneath blebs and thus the membrane surface area is adjusted to the volume of the cell. It has been proposed that a similar phenomenon could account for the swelling of spines (Richards *et al.*, 2004). As the results presented in this thesis suggest that intact Tenm3 inhibits spine maturation and growth, one plausible model would be that Tenm3 might regulate membrane tension and cohesion with the cytoskeleton. In such a model, Tenm3 might create tight cohesion between the membrane and the cytoskeleton and thus exert a restrictive force on spine head expansion.

6.2.3 Different functions for homophilic and heterophilic Tenm3 interactions?

As described in the introduction, a number of in *vivo* studies have shown that Tenm3 is expressed in interconnected regions of the visual system in zebrafish, mice and wallaby (Leamey *et al.*, 2007; Dharmaratne *et al.*, 2012; Antinucci *et al.*, 2013, 2016, Carr *et al.*, 2013, 2014). Moreover, in mice and wallaby, Tenm3 expression follows topographically corresponding gradients (Leamey *et al.*, 2007; Dharmaratne *et al.*, 2012; Carr *et al.*, 2013, 2014). This, together with loss and gain of function studies, which demonstrated alterations in ipsilateral retinocollicular projections and RGC stratification defects, led to the suggestion that Tenm3 contributes to neuronal wiring specificity (Leamey *et al.*, 2007; Dharmaratne *et al.*, 2012; Antinucci *et al.*, 2013, 2016, Carr *et al.*, 2013, 2014). Indeed, these studies support a Tenm3 role of homophilic attraction between appropriate pre- and postsynaptic partners. This is somewhat at odds

with the findings presented in this thesis, which are more in keeping with a Tenm3 role as a repellent molecule that shapes specificity by inhibiting synaptic connections. However, both functions can be reconciled in a model, whereby homophilic Tenm3 interactions regulate neuronal wiring and cellular specificity, whereas heterophilic interactions regulate subcellular specificity and synaptic assembly. A similar model has previously been proposed for Ten-a and Ten-m interactions in *Drosophila* (Mosca, 2015). Indeed, my findings suggest that the synaptic role of Tenm3 is mediated via heterophilic interactions in *trans*, since the analysed basal and apical dendrites of CA1 pyramidal neurons receive inputs from CA3 pyramidal neurons (Figure 1.6), which do not express Tenm3. Vertebrate Teneurins have been shown to have the ability to heterophilically interact in *trans* with other Teneurins as well as Latrophilins (Silva *et al.*, 2011; Boucard, Maxeiner and Südhof, 2013; O'Sullivan *et al.*, 2014). Additionally, Latrophilin 1 (de Wit and Ghosh, 2014), Tenm2 and Tenm4 (Figure 3.1; Zhou *et al.*, 2003; Li, Bishop and O'Leary, 2006) are expressed in CA3. Thus, according to the proposed model, these molecules are possible transsynaptic ligands of Tenm3 in an interaction that might inhibit spine formation and growth or contribute to synapse elimination.

6.2.4 Future directions

The present investigation positions Tenm3 as a critical player in the regulation of appropriate synaptic connectivity in vertebrates. However, further studies are needed to better understand the function of Tenm3 in synapse elimination and to assess whether the models proposed here are viable. An important direction for future studies will be to examine whether Tenm3 inhibits spine formation or promotes synaptic elimination using time-lapse imaging. Future work should also be careful to determine how Tenm3 is transported in neurons. Live-imaging studies could be performed to investigate Tenm3 dynamics and establish whether Tenm3 is first localised at the spine or at the shaft and whether translocation occurs in response to certain stimuli. Another question of great importance is whether Tenm3 directly, or indirectly, interacts with the cytoskeleton. Exciting new insights could be gained through platinum replica EM studies (Korobova and Svitkina, 2010), which would enable the analysis of the cytoskeletal ultrastructure of dendritic spines following loss of Tenm3. Serial section

EM studies could be performed to identify whether changes in other subcellular components are involved and to explore whether loss of Tenm3 affects inhibitory synapses. Furthermore, future work is needed to identify Tenm3 ligands and dissect downstream effectors and signalling cascades. Finally, the functional implications of the observed abnormalities in spine density and morphology in Tenm3 mutants are not clear, and it remains to be investigated whether they have an impact on the regulation of activity levels. Future studies using electrophysiological methods should address these questions. Notably, it will be interesting to see whether the intrinsic properties of CA1 neurons in Tenm3 mutants are altered and how these neurons respond to patterns of electrical activity that induce LTP/LTD. Follow up *in vivo* studies may deliver useful insights as to the behavioural phenotypes of Tenm3 mutant mice. These open questions reveal that the quest to understand how Tenm3 is processed *in vivo* and contributes to synaptic connectivity remains an exciting area of future study.

6.2.5 Conclusion

Since the discovery of dendritic spines over a century ago, a wealth of evidence has accumulated, indicating that spine remodelling is required for synaptic modification and forms the basis of memory. However, the cellular mechanisms underlying the formation and elimination of synapses and spines remain unclear. A multitude of molecules and sophisticated signalling pathways have been implicated in the regulation of synaptic connectivity, but our understanding of the identity of these molecules is incomplete. The findings presented in this thesis identify, for the first time, Tenm3 as a novel, critical regulator of vertebrate synapse development *in vivo*. Our results indicate that Tenm3 regulates spine morphogenesis in CA1 neurons, serving to constrain overall spine number and size. The present investigation emphasises the importance of Tenm3 in the process of synapse development and provides a starting point for future studies, which will enhance our understanding of the molecular mechanisms underlying neural connectivity.

Bibliography

Abe, K., Chisaka, O., Van Roy, F. and Takeichi, M. (2004) 'Stability of dendritic spines and synaptic contacts is controlled by alpha N-catenin.', *Nature neuroscience*, 7(4), pp. 357–363. doi: 10.1038/nn1212.

Abuelo, D. N., Ahsanuddin, A. N. and Mark, H. F. (2000) 'Distal 5q trisomy resulting from an X;5 translocation detected by chromosome painting.', *American journal of medical genetics*. United States, 94(5), pp. 392–399.

Ackermann, M. and Matus, A. (2003) 'Activity-induced targeting of profilin and stabilization of dendritic spine morphology.', *Nature neuroscience*, 6(11), pp. 1194–200. doi: 10.1038/nn1135.

Aldahmesh, M. a, Mohammed, J. Y., Al-Hazzaa, S. and Alkuraya, F. S. (2012) 'Homozygous null mutation in ODZ3 causes microphthalmia in humans.', *Genetics in medicine : official journal of the American College of Medical Genetics*, 14(11), pp. 900–4. doi: 10.1038/gim.2012.71.

Allison, D. W., Gelfand, V. I., Spector, I. and Craig, A. M. (1998) 'Role of Actin in Anchoring Postsynaptic Receptors in Cultured Hippocampal Neurons: Differential Attachment of NMDA versus AMPA Receptors', *J. Neurosci.*, 18(7), pp. 2423–2436. doi: 10.1038/385439a0.

Alvarez, V. a and Sabatini, B. L. (2007) 'Anatomical and Physiological Plasticity of Dendritic Spines', *Annual Review of Neruoscience*, 30, pp. 79–97. doi: 10.1146/annurev.neuro.30.051606.094222.

Amaral, D. G. (1993) 'Emerging principles of intrinsic hippocampal organization', *Current Opinion in Neurobiology*, pp. 225–229. doi: 10.1016/0959-4388(93)90214-J.

Andersen, P. (2007) *The hippocampus book*. Oxford university press.

Andersen, P., Bliss, T. V, Lomo, T., Olsen, L. I. and Skrede, K. K. (1971) 'Lamellar organization of hippocampal excitatory pathways.', *Acta physiologica Scandinavica*. England, 76(1), p. 4A–5A.

Andersen, R., Li, Y., Resseguie, M. and Brenman, J. E. (2005) 'Calcium/Calmodulin-Dependent Protein Kinase II Alters Structural Plasticity and Cytoskeletal Dynamics in Drosophila', *J. Neurosci.*, 25(39), pp. 8878–8888. doi: 10.1523/JNEUROSCI.2005-05.2005.

Antinucci, P., Nikolaou, N., Meyer, M. P. and Hindges, R. (2013) 'Teneurin-3 Specifies Morphological and Functional Connectivity of Retinal Ganglion Cells in the Vertebrate Visual System.', *Cell reports*, 5(3), pp. 582–592. doi: 10.1016/j.celrep.2013.09.045.

Antinucci, P., Suleyman, O., Monfries, C. and Hindges, R. (2016) 'Neural Mechanisms Generating Orientation Selectivity in the Retina', *Current Biology*, pp. 1–14. doi: 10.1016/j.cub.2016.05.035.

Arnold, D. B. and Clapham, D. E. (1999) 'Molecular determinants for subcellular localization of PSD-95 with an interacting K+ channel', *Neuron*, 23(1), pp. 149–157. doi: 10.1016/S0896-6273(00)80761-8.

Ashrafi, S., Betley, J. N., Comer, J. D., Brenner-Morton, S., Bar, V., Shimoda, Y., Watanabe, K., Peles, E., Jessell, T. M. and Kaltschmidt, J. A. (2014) 'Neuronal Ig/Caspr Recognition Promotes the Formation of Axoaxonic Synapses in Mouse Spinal Cord', *Neuron*, 81(1), pp. 120–129. doi: 10.1016/j.neuron.2013.10.060.

Bagri, A., Cheng, H. J., Yaron, A., Pleasure, S. J. and Tessier-Lavigne, M. (2003) 'Stereotyped pruning of long hippocampal axon branches triggered by retraction inducers of the semaphorin family', *Cell*, 113(3), pp. 285–299. doi: 10.1016/S0092-8674(03)00267-8.

Bagutti, C., Forro, G., Ferralli, J., Rubin, B. and Chiquet-Ehrismann, R. (2003) 'The intracellular domain of teneurin-2 has a nuclear function and represses zic-1-mediated transcription.', *Journal of cell science*, 116(Pt 14), pp. 2957–66. doi: 10.1242/jcs.00603.

Bamji, S. X., Shimazu, K., Kimes, N., Huelsken, J., Birchmeier, W., Lu, B. and Reichardt, L. F. (2003) 'Role of β-catenin in synaptic vesicle localization and presynaptic assembly', *Neuron*, 40(4), pp. 719–731. doi: 10.1016/S0896-6273(03)00718-9.

Banker, G. A. and Cowan, W. M. (1977) 'Rat hippocampal neurons in dispersed cell culture', *Brain Research*, 126(3), pp. 397–425. doi: 10.1016/0006-8993(77)90594-7.

Bannister, N. J. and Larkman, A. U. (1995) 'Dendritic morphology of CA1 pyramidal neurones from the rat hippocampus: I. Branching patterns.', *The Journal of comparative neurology*, 360(1), pp. 150–60. doi: 10.1002/cne.903600111.

Bartlett, W. P. and Banker, G. a (1984) 'An electron microscopic study of the development of axons and dendrites by hippocampal neurons in culture. II. Synaptic relationships.', *The Journal of neuroscience : the official journal of the Society for Neuroscience*, 4(8), pp. 1954–65.

Baumann, C. a, Ribon, V., Kanzaki, M., Thurmond, D. C., Mora, S., Shigematsu, S., Bickel, P. E., Pessin, J. E. and Saltiel, a R. (2000) 'CAP defines a second signalling pathway required for insulin-stimulated glucose transport.', *Nature*, 407(6801), pp. 202–207. doi: 10.1038/35025089.

Baumgartner, S. and Chiquet-Ehrismann, R. (1993) 'Tena, a Drosophila gene related to tenascin, shows selective transcript localization', *Mechanisms of Development*,

40(3), pp. 165–176. doi: 10.1016/0925-4773(93)90074-8.

Baumgartner, S., Martin, D., Hagios, C. and Chiquet-ehrismann, R. (1994) 'tenm, a Drosophila gene related to tenascin, is a new pair-rule gene', *EMBO Journal*, 13(16), pp. 3728–3740.

Beckmann, J., Schubert, R., Chiquet-Ehrismann, R. and Müller, D. J. (2013) 'Deciphering teneurin domains that facilitate cellular recognition, cell-cell adhesion, and neurite outgrowth using atomic force microscopy-based single-cell force spectroscopy.', *Nano letters*, 13(6), pp. 2937–46. doi: 10.1021/nl4013248.

Ben-Zur, T., Feige, E., Motro, B. and Wides, R. (2000) 'The mammalian Odz gene family: homologs of a Drosophila pair-rule gene with expression implying distinct yet overlapping developmental roles.', *Developmental biology*, 217(1), pp. 107–20. doi: 10.1006/dbio.1999.9532.

Benson, D. L. and Tanaka, H. (1998) 'N-Cadherin Redistribution during Synaptogenesis in Hippocampal Neurons', *Journal of Neuroscience*, 18(17), pp. 6892–6904.

Biederer, T., Sara, Y., Mozhayeva, M., Atasoy, D., Liu, X., Kavalali, E. T. and Südhof, T. C. (2002) 'SynCAM, a synaptic adhesion molecule that drives synapse assembly.', *Science (New York, N.Y.)*, 297(5586), pp. 1525–31. doi: 10.1126/science.1072356.

Biederer, T. and Scheiffele, P. (2007) 'Mixed-culture assays for analyzing neuronal synapse formation.', *Nature protocols*, 2(3), pp. 670–6. doi: 10.1038/nprot.2007.92.

Boeckers, T. M., Kreutz, M. R., Winter, C., Zuschratter, W., Smalla, K. H., Sanmarti-Vila, L., Wex, H., Langnaese, K., Bockmann, J., Garner, C. C. and Gundelfinger, E. D. (2001) 'Proline-rich synapse-associated protein-1/cortactin binding protein 1 (ProSAP1/CortBP1) is a PDZ-domain protein highly enriched in the postsynaptic density', *Annals of Anatomy*, 183(2), p. 101. doi: 10.1016/S0940-9602(01)80024-8.

Bolte, S. and Cordelières, F. P. (2006) 'A guided tour into subcellular colocalization analysis in light microscopy.', *Journal of microscopy*, 224(Pt 3), pp. 213–32. doi: 10.1111/j.1365-2818.2006.01706.x.

Bonhoeffer, T. and Yuste, R. (2002) 'Spine motility: phenomenology, mechanisms, and function', *Neuron*, 35(6), pp. 1019–1027. doi: 10.1016/s0896-6273(02)00906-6.

Boucard, A. a, Chubykin, A. a, Comoletti, D., Taylor, P. and Südhof, T. C. (2005) 'A splice code for trans-synaptic cell adhesion mediated by binding of neuroligin 1 to alpha- and beta-neurexins.', *Neuron*, 48(2), pp. 229–36. doi: 10.1016/j.neuron.2005.08.026.

Boucard, A. a, Ko, J. and Südhof, T. C. (2012) 'High affinity neurexin binding to cell adhesion G-protein-coupled receptor CIRL1/latrophilin-1 produces an intercellular

adhesion complex.', *The Journal of biological chemistry*, 287(12), pp. 9399–413. doi: 10.1074/jbc.M111.318659.

Boucard, A. a, Maxeiner, S. and Südhof, T. C. (2013) 'Latrophilins Function as Heterophilic Cell-Adhesion Molecules by Binding to Teneurins: Regulation by Alternative Splicing.', *The Journal of biological chemistry*. doi: 10.1074/jbc.M113.504779.

Bozdagi, O., Shan, W., Tanaka, H., Benson, D. L. and Huntley, G. W. (2000) 'Increasing Numbers of Synaptic Puncta during Late-Phase LTP', *Neuron*, 28(1), pp. 245–259. doi: 10.1016/S0896-6273(00)00100-8.

Bresler, T. (2004) 'Postsynaptic Density Assembly Is Fundamentally Different from Presynaptic Active Zone Assembly', *Journal of Neuroscience*, 24(6), pp. 1507–1520. doi: 10.1523/JNEUROSCI.3819-03.2004.

Bresler, T., Ramati, Y., Zamorano, P. L., Zhai, R., Garner, C. C. and Ziv, N. E. (2001) 'The dynamics of SAP90/PSD-95 recruitment to new synaptic junctions.', *Molecular and cellular neurosciences*, 18(2), pp. 149–67. doi: 10.1006/mcne.2001.1012.

Brown, M. S., Ye, J., Rawson, R. B. and Goldstein, J. L. (2000) 'Regulated intramembrane proteolysis: a control mechanism conserved from bacteria to humans.', *Cell*, 100(4), pp. 391–398. doi: 10.1016/S0092-8674(00)80675-3.

Burack, M. a, Silverman, M. a and Banker, G. (2000) 'The role of selective transport in neuronal protein sorting.', *Neuron*, 26(2), pp. 465–472. doi: 10.1016/S0896-6273(00)81178-2.

Carr, O. P., Glendining, K. A., Leamey, C. A. and Marotte, L. R. (2013) 'Overexpression of Ten-m3 in the retina alters ipsilateral retinocollicular projections in the wallaby (Macropus eugenii)', *International Journal of Developmental Neuroscience*. International Society for Developmental Neuroscience, 31(7), pp. 496–504. doi: 10.1016/j.ijdevneu.2013.05.011.

Carr, O. P., Glendining, K. a, Leamey, C. a and Marotte, L. R. (2014) 'Retinal overexpression of Ten-m3 alters ipsilateral retinogeniculate projections in the wallaby (Macropus eugenii).', *Neuroscience letters*. Elsevier Ireland Ltd, 566, pp. 167–71. doi: 10.1016/j.neulet.2014.02.048.

Al Chawaf, A., Amant, K. ST., Belsham, D. and Lovejoy, D. A. (2007) 'Regulation of neurite growth in immortalized mouse hypothalamic neurons and rat hippocampal primary cultures by teneurin C-terminal-associated peptide-1', *Neuroscience*, 144(4), pp. 1241–1254. doi: 10.1016/j.neuroscience.2006.09.062.

Al Chawaf, A., Xu, K., Tan, L., Vaccarino, F. J., Lovejoy, D. A. and Rotzinger, S. (2007) 'Corticotropin-releasing factor (CRF)-induced behaviors are modulated by intravenous administration of teneurin C-terminal associated peptide-1 (TCAP-1)',

Peptides, 28(7), pp. 1406–1415. doi: 10.1016/j.peptides.2007.05.014.

Chen, B. E., Kondo, M., Garnier, A., Watson, F. L., Püettmann-Holgado, R., Lamar, D. R. and Schmucker, D. (2006) 'The Molecular Diversity of Dscam Is Functionally Required for Neuronal Wiring Specificity in Drosophila', *Cell*, 125(3), pp. 607–620. doi: 10.1016/j.cell.2006.03.034.

Chen, C.-C., Lu, J. and Zuo, Y. (2014) 'Spatiotemporal dynamics of dendritic spines in the living brain', *Frontiers in Neuroanatomy*, 8(May), pp. 1–7. doi: 10.3389/fnana.2014.00028.

Cheng, L., Ziegelhoffer, P. R. and Yang, N. S. (1993) 'In vivo promoter activity and transgene expression in mammalian somatic tissues evaluated by using particle bombardment.', *Proceedings of the National Academy of Sciences*, 90(10), pp. 4455–4459. doi: 10.1073/pnas.90.10.4455.

Chevaleyre, V. and Siegelbaum, S. A. (2010) 'Strong CA2 pyramidal neuron synapses define a powerful disynaptic cortico-hippocampal loop', *Neuron*. Elsevier Ltd, 66(4), pp. 560–572. doi: 10.1016/j.neuron.2010.04.013.

Chia, P. H., Li, P. and Shen, K. (2013) 'Cellular and molecular mechanisms underlying presynapse formation', *Journal of Cell Biology*, 203(1), pp. 11–22. doi: 10.1083/jcb.201307020.

Chih, B., Engelman, H. and Scheiffele, P. (2005) 'Control of excitatory and inhibitory synapse formation by neuroligins.', *Science (New York, N.Y.)*, 307(5713), pp. 1324–8. doi: 10.1126/science.1107470.

Chu, P. J., Rivera, J. F. and Arnold, D. B. (2006) 'A role for Kif17 in transport of Kv4.2', *Journal of Biological Chemistry*, 281(1), pp. 365–373. doi: 10.1074/jbc.M508897200.

Chubykin, A. a, Atasoy, D., Etherton, M. R., Brose, N., Kavalali, E. T., Gibson, J. R. and Südhof, T. C. (2007) 'Activity-dependent validation of excitatory versus inhibitory synapses by neuroligin-1 versus neuroligin-2.', *Neuron*, 54(6), pp. 919–31. doi: 10.1016/j.neuron.2007.05.029.

Cingolani, L. a and Goda, Y. (2008) 'Actin in action: the interplay between the actin cytoskeleton and synaptic efficacy', *Nature Reviews Neuroscience*, 9(5), pp. 344–356. doi: 10.1038/nrn2373.

Collins, M. O., Husi, H., Yu, L., Brandon, J. M., Anderson, C. N. G., Blackstock, W. P., Choudhary, J. S. and Grant, S. G. N. (2006) 'Molecular characterization and comparison of the components and multiprotein complexes in the postsynaptic proteome.', *Journal of neurochemistry*, 97 Suppl 1(m), pp. 16–23. doi: 10.1111/j.1471-4159.2005.03507.x.

Costes, S. V, Daelemans, D., Cho, E. H., Dobbin, Z., Pavlakis, G. and Lockett, S. (2004) 'Automatic and quantitative measurement of protein-protein colocalization in live cells.', *Biophysical journal*, 86(6), pp. 3993–4003. doi: 10.1529/biophysj.103.038422.

Craig, A. M., Graf, E. R. and Linhoff, M. W. (2006) 'How to build a central synapse: Clues from cell culture', *Trends in Neurosciences*, 29(1), pp. 8–20. doi: 10.1016/j.tins.2005.11.002.

Craig, a M. and Banker, G. (1994) 'Neuronal polarity.', *Annual review of neuroscience*, 17(1991), pp. 267–310. doi: 10.1146/annurev.ne.17.030194.001411.

Craig, M. T. and McBain, C. J. (2015) 'Fast Gamma Oscillations Are Generated Intrinsically in CA1 without the Involvement of Fast-Spiking Basket Cells', *The Journal of Neuroscience*, 35(8), pp. 3616–3624. doi: 10.1523/jneurosci.4166-14.2015.

Craven, S. E., El-Husseini, A. E. and Bredt, D. S. (1999) 'Synaptic targeting of the postsynaptic density protein PSD-95 mediated by a tyrosine-based trafficking signal', *Neuron*, 22, pp. 497–509. doi: 10.1074/jbc.M910153199.

Cutsuridis, V., Graham, B., Cobb, S. and Vida, I. (eds) (2010) *Hippocampal microcircuits: A computational modeler's resource book.* New York: Springer.

Dahlhaus, R., Hines, R. M., Eadie, B. D., Kannangara, T. S., Hines, D. J., Brown, C. E., Christie, B. R. and El-Hussefini, A. (2010) 'Overexpression of the cell adhesion protein neuroligin-1 induces learning deficits and impairs synaptic plasticity by altering the ratio of excitation to inhibition in the hippocampus', *Hippocampus*, 20(2), pp. 305–322. doi: 10.1002/hipo.20630.

dal Maschio, M., Ghezzi, D., Bony, G., Alabastri, A., Deidda, G., Brondi, M., Sato, S. S., Zaccaria, R. P., Di Fabrizio, E., Ratto, G. M. and Cancedda, L. (2012) 'High-performance and site-directed in utero electroporation by a triple-electrode probe', *Nature Communications*. Nature Publishing Group, 3, p. 960. doi: 10.1038/ncomms1961.

Dalva, M. B., McClelland, A. C. and Kayser, M. S. (2007) 'Cell adhesion molecules: signalling functions at the synapse.', *Nature reviews. Neuroscience*, 8(3), pp. 206–220. doi: 10.1038/nrn2075.

Davletov, B. a, Shamotienko, O. G., Lelianova, V. G., Grishin, E. V and Ushkaryov, Y. a (1996) 'Isolation and Biochemical Characterization of a Ca 2+-independent Latrotoxin-binding Protein', *The Journal of Biochemical Chemistry*, 271(38), pp. 23239–23245.

Dean, C., Scholl, F. G., Choih, J., DeMaria, S., Berger, J., Isacoff, E. and Scheiffele, P. (2003) 'Neurexin mediates the assembly of presynaptic terminals', *Nature Neuroscience*, 6(7), pp. 708–716. doi: 10.1038/nn1074.

Desmond, N. L. and Levy, W. B. (1986) 'Changes in the postsynaptic density with long-term potentiation in the dentate gyrus', *Journal of Comparative Neurology*, 253(4), pp. 476–482. doi: 10.1002/cne.902530405.

Dharmaratne, N., Glendining, K. a, Young, T. R., Tran, H., Sawatari, A. and Leamey, C. A. (2012) 'Ten-m3 is required for the development of topography in the ipsilateral retinocollicular pathway.', *PloS one*, 7(9), p. e43083. doi: 10.1371/journal.pone.0043083.

Dotti, C. G., Sullivan, C. a and Banker, G. a (1988) 'The establishment of polarity by hippocampal neurons in culture.', *The Journal of neuroscience : the official journal of the Society for Neuroscience*, 8(4), pp. 1454–1468. doi: 10.1016/0012-1606(89)90269-8.

Drabikowski, K., Trzebiatowska, A. and Chiquet-Ehrismann, R. (2005) 'ten-1, an essential gene for germ cell development, epidermal morphogenesis, gonad migration, and neuronal pathfinding in Caenorhabditis elegans', *Developmental Biology*, 282(1), pp. 27–38. doi: 10.1016/j.ydbio.2005.02.017.

Le Duigou, C., Simonnet, J., Teleñczuk, M. T., Fricker, D. and Miles, R. (2014) 'Recurrent synapses and circuits in the CA3 region of the hippocampus: an associative network.', *Frontiers in cellular neuroscience*, 7(January), p. 262. doi: 10.3389/fncel.2013.00262.

Dunaevsky, A., Blazeski, R., Yuste, R. and Mason, C. (2001) 'Spine motility with synaptic contact', *Nature Neuroscience*, 4(7), pp. 685–686. doi: 10.1038/89460.

Dunaevsky, a, Tashiro, a, Majewska, a, Mason, C. and Yuste, R. (1999) 'Developmental regulation of spine motility in the mammalian central nervous system.', *Proceedings of the National Academy of Sciences of the United States of America*, 96(23), pp. 13438–43. doi: 10.1073/PNAS.96.23.13438.

Edwards, T. a, Wilkinson, B. D., Wharton, R. P. and Aggarwal, A. K. (2003) 'Model of the Brain Tumor – Pumilio translation repressor complex', pp. 2508–2513. doi: 10.1101/gad.1119403.In.

El-Husseini, A., Schnell, E. and Chetkovich, D. (2000) 'PSD-95 involvement in maturation of excitatory synapses', *Science*, 290(5495), pp. 1364–8. doi: 10.1126/science.290.5495.1364.

Engert, F. and Bonhoeffer, T. (1999) 'Dendritic spine changes associated with hippocampal long-term plasticity', *Nature*, 399(May).

Erb, S., McPhee, M., Brown, Z. J., Kupferschmidt, D. A., Song, L. and Lovejoy, D. A. (2014) 'Repeated intravenous administrations of teneurin-C terminal associated peptide (TCAP)-1 attenuates reinstatement of cocaine seeking by corticotropin-releasing factor (CRF) in rats', *Behavioural Brain Research*. Elsevier B.V., 269, pp. 1–5. doi:

10.1016/j.bbr.2014.04.013.

Ethell, I. M. and Pasquale, E. B. (2005) 'Molecular mechanisms of dendritic spine development and remodeling', *Progress in Neurobiology*, 75(3), pp. 161–205. doi: 10.1016/j.pneurobio.2005.02.003.

Feng, G., Mellor, R. H., Bernstein, M., Keller-Peck, C., Nguyen, Q. T., Wallace, M., Nerbonne, J. M., Lichtman, J. W. and Sanes, J. R. (2000) 'Imaging neuronal subsets in transgenic mice expressing multiple spectral variants of GFP.', *Neuron*, 28(1), pp. 41–51.

Feng, K., Zhou, X. H., Oohashi, T., Mörgelin, M., Lustig, A., Hirakawa, S., Ninomiya, Y., Engel, J., Rauch, U. and Fässler, R. (2002) 'All four members of the Ten-m/Odz family of transmembrane proteins form dimers', *Journal of Biological Chemistry*, 277(29), pp. 26128–26135. doi: 10.1074/jbc.M203722200.

Feng, W. and Zhang, M. (2009) 'Organization and dynamics of PDZ-domain-related supramodules in the postsynaptic density', *Nature Reviews Neuroscience*, 10(2), pp. 87–99. doi: 10.1038/nrn2540.

Fiala, J. C., Feinberg, M., Popov, V. and Harris, K. M. (1998) 'Synaptogenesis via dendritic filopodia in developing hippocampal area CA1', *J Neurosci*, 18(21), pp. 8900–8911.

Fifková, E. and Anderson, C. L. (1981) 'Stimulation-induced changes in dimensions of stalks of dendritic spines in the dentate molecular layer', *Experimental Neurology*, 74(2), pp. 621–627. doi: 10.1016/0014-4886(81)90197-7.

Fischer, M., Kaech, S., Knutti, D. and Matus, A. (1998) 'Rapid actin-based plasticity in dendritic spines', *Neuron*, 20(5), pp. 847–854. doi: 10.1016/S0896-6273(00)80467-5.

Fletcher, T. L., De Camilli, P. and Banker, G. (1994) 'Synaptogenesis in hippocampal cultures: evidence indicating that axons and dendrites become competent to form synapses at different stages of neuronal development.', *The Journal of neuroscience : the official journal of the Society for Neuroscience*, 14(November), pp. 6695–6706.

Fogel, A. I., Stagi, M., Perez de Arce, K. and Biederer, T. (2011) 'Lateral assembly of the immunoglobulin protein SynCAM 1 controls its adhesive function and instructs synapse formation', *The EMBO Journal*. Nature Publishing Group, 30(23), pp. 4728–4738. doi: 10.1038/emboj.2011.336.

Friedman, H. V., Bresler, T., Garner, C. C. and Ziv, N. E. (2000) 'Assembly of New Individual Excitatory Synapses: Time Course and Temporal Order of Synaptic Molecule Recruitment', *Neuron*, 27(1), pp. 57–69. doi: 10.1016/S0896-6273(00)00009-X.

Garner, C. C., Waites, C. L. and Ziv, N. E. (2006) 'Synapse development: Still looking for the forest, still lost in the trees', *Cell and Tissue Research*, 326(2), pp. 249–262. doi: 10.1007/s00441-006-0278-1.

Gasparini, S., Migliore, M. and Magee, J. C. (2004) 'On the Initiation and Propagation of Dendritic Spikes in CA1 Pyramidal Neurons', *Journal of Neuroscience*, 24(49), pp. 11046–11056. doi: 10.1523/JNEUROSCI.2520-04.2004.

Geinisman, Y., deToledo-Morrell, L. and Morrell, F. (1991) 'Induction of long-term potentiation is associated with an increase in the number of axospinous synapses with segmented postsynaptic densities', *Brain Research*, 566(1–2), pp. 77–88. doi: 10.1016/0006-8993(91)91683-R.

Gerrow, K., Romorini, S., Nabi, S. M., Colicos, M. a., Sala, C. and El-Husseini, A. (2006) 'A preformed complex of postsynaptic proteins is involved in excitatory synapse development', *Neuron*, 49(4), pp. 547–562. doi: 10.1016/j.neuron.2006.01.015.

Gitler, D., Takagishi, Y., Feng, J., Ren, Y., Rodriguiz, R. M., Wetsel, W. C., Greengard, P. and Augustine, G. J. (2004) 'Different Presynaptic Roles of Synapsins at Excitatory and Inhibitory Synapses', 24(50), pp. 11368–11380. doi: 10.1523/JNEUROSCI.3795-04.2004.

Grabrucker, A., Vaida, B., Bockmann, J. and Boeckers, T. M. (2009) 'Synaptogenesis of hippocampal neurons in primary cell culture.', *Cell and tissue research*, 338(3), pp. 333–41. doi: 10.1007/s00441-009-0881-z.

Graf, E. R., Zhang, X., Jin, S.-X., Linhoff, M. W. and Craig, A. M. (2004) 'Neurexins induce differentiation of GABA and glutamate postsynaptic specializations via neuroligins.', *Cell*. United States, 119(7), pp. 1013–1026. doi: 10.1016/j.cell.2004.11.035.

Grant, S. G. N. (2012) 'Synaptopathies: Diseases of the synaptome', *Current Opinion in Neurobiology*. Elsevier Ltd, 22(3), pp. 522–529. doi: 10.1016/j.conb.2012.02.002.

Gray, E. G. (1957) 'Axo-somatic and Axo-Dendritic Synapses of the Cerebral Cortex: an Electron Microscope Study', *J Anat*.

Gross, G. G., Junge, J. a, Mora, R. J., Kwon, H.-B., Olson, C. A., Takahashi, T. T., Liman, E. R., Ellis-Davies, G. C. R., McGee, A. W., Sabatini, B. L., Roberts, R. W. and Arnold, D. B. (2013) 'Recombinant probes for visualizing endogenous synaptic proteins in living neurons.', *Neuron*. Elsevier Inc., 78(6), pp. 971–85. doi: 10.1016/j.neuron.2013.04.017.

Grutzendler, J., Kasthuri, N. and Gan, W.-B. (2002) 'Long-term dendritic spine stability in the adult cortex', *Nature*, 420(6917), pp. 812–816. doi: 10.1038/nature01276.

Gupta, S. C., Yadav, R., Pavuluri, R., Morley, B. J., Stairs, D. J. and Dravid, S. M. (2015) 'Essential role of GluD1 in dendritic spine development and GluN2B to GluN2A NMDAR subunit switch in the cortex and hippocampus reveals ability of GluN2B inhibition in correcting hyperconnectivity', *Neuropharmacology*. Elsevier Ltd, 93, pp. 274–284. doi: 10.1016/j.neuropharm.2015.02.013.

Halpain, S. (2000) 'Actin and the agile spine: How and why do dendritic spines dance?', *Trends in Neurosciences*, 23(4), pp. 141–146. doi: 10.1016/S0166-2236(00)01576-9.

Hamos, J. E., Van Horn, S. C., Raczkowski, D. and Sherman, S. M. (1987) 'Synaptic circuits involving an individual retinogeniculate axon in the cat', *Journal of Comparative Neurology*, 259(2), pp. 165–192. doi: 10.1002/cne.902590202.

Van Harreveld, A. and Fifkova, E. (1975) 'Swelling of dendritic spines in the fascia dentata after stimulation of the perforant fibers as a mechanism of post-tetanic potentiation', *Experimental Neurology*, 49(3), pp. 736–749. doi: 10.1016/0014-4886(75)90055-2.

Harris, K. M. and Stevens, J. K. (1989) 'Dendritic spines of CA 1 pyramidal cells in the rat hippocampus: serial electron microscopy with reference to their biophysical characteristics.', *The Journal of neuroscience : the official journal of the Society for Neuroscience*, 9(8), pp. 2982–2997.

Harris, M., Jensen, F. E. and Tsao, B. (1992) 'Three-Dimensional Structure of Dendritic Spines and Synapses Rat Hippocampus (CAI) at Postnatal Day 15 and Adult Ages : Implications for the Maturation of Synaptic Physiology and Long-term Potentiation', *The Journal of Neuroscience*, 12(7), pp. 2685–2705.

Heinrich, A., Lourdusamy, A., Tzschoppe, J., Vollstädt-Klein, S., Bühler, M., Steiner, S., Bach, C., Poustka, L., Banaschewski, T., Barker, G., Büchel, C., Conrod, P., Garavan, H., Gallinat, J., Heinz, A., Ittermann, B., Loth, E., Mann, K., Martinot, J. L., Paus, T., Pausova, Z., Smolka, M., Ströhle, A., Struve, M., Witt, S., Flor, H., Schumann, G., Rietschel, M. and Nees, F. (2013) 'The risk variant in ODZ4 for bipolar disorder impacts on amygdala activation during reward processing', *Bipolar Disorders*, 15(4), pp. 440–445. doi: 10.1111/bdi.12068.

Hering, H. and Sheng, M. (2001) 'Dendritic spines: structure, dynamics and regulation.', *Nature reviews. Neuroscience*, 2(12), pp. 880–888. doi: 10.1038/35104061.

Hermans, E. and Challiss, R. A. (2001) 'Structural, signalling and regulatory properties of the group I metabotropic glutamate receptors: prototypic family C G-protein-coupled receptors.', *The Biochemical journal*. England, 359(Pt 3), pp. 465–484.

Holtmaat, A. J. G. D., Trachtenberg, J. T., Wilbrecht, L., Shepherd, G. M., Zhang, X., Knott, G. W. and Svoboda, K. (2005) 'Transient and persistent dendritic spines in the

neocortex in vivo', *Neuron*, 45(2), pp. 279–291. doi: 10.1016/j.neuron.2005.01.003.

Holtmaat, A. and Svoboda, K. (2009) 'Experience-dependent structural synaptic plasticity in the mammalian brain.', *Nature reviews. Neuroscience*, 10(9), pp. 647–658. doi: 10.1038/nrn2721.

Hong, W., Mosca, T. J. and Luo, L. (2012) 'Teneurins instruct synaptic partner matching in an olfactory map', *Nature*. Nature Publishing Group, 484(7393), pp. 201–207. doi: 10.1038/nature10926.

Honkura, N., Matsuzaki, M., Noguchi, J., Ellis-Davies, G. C. R. and Kasai, H. (2008) 'The Subspine Organization of Actin Fibers Regulates the Structure and Plasticity of Dendritic Spines', *Neuron*, 57(5), pp. 719–729. doi: 10.1016/j.neuron.2008.01.013.

Hor, H., Francescatto, L., Bartesaghi, L., Ortega-Cubero, S., Kousi, M., Lorenzo-Betancor, O., Jiménez-Jiménez, F. J., Gironell, A., Clarimón, J., Drechsel, O., Agúndez, J. a. G., Kenzelmann Broz, D., Chiquet-Ehrismann, R., Lleó, A., Coria, F., García-Martin, E., Alonso-Navarro, H., Martí, M. J., Kulisevsky, J., Hor, C. N., Ossowski, S., Chrast, R., Katsanis, N., Pastor, P. and Estivill, X. (2015) 'Missense mutations in *TENM4* , a regulator of axon guidance and central myelination, cause essential tremor', *Human Molecular Genetics*, (July), p. ddv281. doi: 10.1093/hmg/ddv281.

Hortopan, G. a, Dinday, M. T. and Baraban, S. C. (2010) 'Zebrafish as a model for studying genetic aspects of epilepsy.', *Disease models & mechanisms*, 3(3–4), pp. 144–8. doi: 10.1242/dmm.002139.

Hotulainen, P. and Hoogenraad, C. C. (2010) 'Actin in dendritic spines: Connecting dynamics to function', *Journal of Cell Biology*, 189(4), pp. 619–629. doi: 10.1083/jcb.201003008.

Huberman, A. D., Clandinin, T. R. and Baier, H. (2010) 'Molecular and cellular mechanisms of lamina-specific axon targeting.', *Cold Spring Harbor perspectives in biology*, 2(3), pp. 1–17. doi: 10.1101/cshperspect.a001743.

Humeau, Y., Herry, C., Kemp, N., Shaban, H., Fourcaudot, E., Bissière, S. and Lüthi, A. (2005) 'Dendritic spine heterogeneity determines afferent-specific Hebbian plasticity in the amygdala', *Neuron*, 45(1), pp. 119–131. doi: 10.1016/j.neuron.2004.12.019.

Humpel, C. (2015) 'Neuroscience forefront review organotypic brain slice cultures: A review', *Neuroscience*. IBRO, 305, pp. 86–98. doi: 10.1016/j.neuroscience.2015.07.086.

Inagaki, N., Chihara, K., Arimura, N., Ménager, C., Kawano, Y., Matsuo, N., Nishimura, T., Amano, M. and Kaibuchi, K. (2001) 'CRMP-2 induces axons in cultured hippocampal neurons.', *Nature neuroscience*, 4(8), pp. 781–782. doi: 10.1038/90476.

Ippolito, D. M. and Eroglu, C. (2010) 'Quantifying synapses: an immunocytochemistry-based assay to quantify synapse number.', *Journal of visualized experiments : JoVE*, (45), pp. 2–9. doi: 10.3791/2270.

Ishizuka, N., Weber, J. and Amaral, D. G. (1990) 'Organization of intrahippocampal projections originating from CA3 pyramidal cells in the rat', *Journal of Comparative Neurology*, 295(4), pp. 580–623. doi: 10.1002/cne.902950407.

Janssen, B. J. C., Robinson, R. A., Pérez-Brangulí, F., Bell, C. H., Mitchell, K. J., Siebold, C. and Jones, E. Y. (2010) 'Structural basis of semaphorin–plexin signalling', *Nature*, 467(7319), pp. 1118–1122. doi: 10.1038/nature09468.

Jaworski, J., Kapitein, L. C., Gouveia, S. M., Dortland, B. R., Wulf, P. S., Grigoriev, I., Camera, P., Spangler, S. A., Di Stefano, P., Demmers, J., Krugers, H., Defilippi, P., Akhmanova, A. and Hoogenraad, C. C. (2009) 'Dynamic Microtubules Regulate Dendritic Spine Morphology and Synaptic Plasticity', *Neuron*. Elsevier Inc., 61(1), pp. 85–100. doi: 10.1016/j.neuron.2008.11.013.

Jensen, C. S., Watanabe, S., Rasmussen, H. B., Schmitt, N., Olesen, S. P., Frost, N. a., Blanpied, T. a. and Misonou, H. (2014) 'Specific sorting and post-golgi trafficking of dendritic potassium channels in living neurons', *Journal of Biological Chemistry*, 289(15), pp. 10566–10581. doi: 10.1074/jbc.M113.534495.

Jones, E. G. and Powell, T. P. S. (1969) 'Morphological Variations in the Dendritic Spines of the Neocortex', *J. Cell Sci. s*, 529, pp. 509–529.

Jung, Y., Mulholland, P. J., Wiseman, S. L., Judson Chandler, L. and Picciotto, M. R. (2013) 'Constitutive knockout of the membrane cytoskeleton protein beta adducin decreases mushroom spine density in the nucleus accumbens but does not prevent spine remodeling in response to cocaine', *European Journal of Neuroscience*, 37(1), pp. 1–9. doi: 10.1111/ejn.12037.

Jüngling, K., Eulenburg, V., Moore, R., Kemler, R., Lessmann, V. and Gottmann, K. (2006) 'N-cadherin transsynaptically regulates short-term plasticity at glutamatergic synapses in embryonic stem cell-derived neurons.', *The Journal of neuroscience : the official journal of the Society for Neuroscience*, 26(26), pp. 6968–78. doi: 10.1523/JNEUROSCI.1013-06.2006.

Kaech, S. and Banker, G. (2006) 'Culturing hippocampal neurons.', *Nature protocols*, 1(5), pp. 2406–15. doi: 10.1038/nprot.2006.356.

Karra, D. and Dahm, R. (2010) 'Transfection techniques for neuronal cells.', *The Journal of neuroscience : the official journal of the Society for Neuroscience*. United States, 30(18), pp. 6171–6177. doi: 10.1523/JNEUROSCI.0183-10.2010.

Kater, S. B. and Harris, K. M. (1994) 'Dendritic spines : Cellular specializations', *Annual review of neuroscience*, 17, pp. 341–371.

Kenzelmann, D., Chiquet-Ehrismann, R., Leachman, N. T. and Tucker, R. P. (2008) 'Teneurin-1 is expressed in interconnected regions of the developing brain and is processed in vivo.', *BMC developmental biology*, 8(1), p. 30. doi: 10.1186/1471-213X-8-30.

Kinel-Tahan, Y., Weiss, H., Dgany, O., Levine, A. and Wides, R. (2007) 'Drosophila odz gene is required for multiple cell types in the compound retina', *Developmental Dynamics*, 236(9), pp. 2541–2554. doi: 10.1002/dvdy.21284.

Klein, T. M., Wolf, E. D., Wu, R. and Sanford, J. C. (1987) 'High-velocity microprojectiles for delivering nucleic acids into living cells', *Nature biotechnology*, 327(7).

Ko, J., Soler-Llavina, G. J., Fuccillo, M. V, Malenka, R. C. and Südhof, T. C. (2011) 'Neuroligins/LRRTMs prevent activity- and Ca2+/calmodulin-dependent synapse elimination in cultured neurons.', *The Journal of cell biology*, 194(2), pp. 323–34. doi: 10.1083/jcb.201101072.

Korkotian, E. and Segal, M. (2001) 'Regulation of dendritic spine motility in cultured hippocampal neurons.', *The Journal of neuroscience : the official journal of the Society for Neuroscience*, 21(16), pp. 6115–6124. doi: 21/16/6115 [pii].

Korobova, F. and Svitkina, T. (2010) 'Molecular Architecture of Synaptic Actin Cytoskeleton in Hippocampal Neurons Reveals a Mechnism of Dendritic Spine Morphogenesis', *Molecular Biology of the Cell*, 21(22), pp. 4042–4056. doi: 10.1091/mbc.E09.

Kostadinov, D. and Sanes, J. R. (2015) 'Protocadherin-dependent dendritic selfavoidance regulates neural connectivity and circuit function', *eLife*, 4(JULY2015), pp. 1–23. doi: 10.7554/eLife.08964.

Kurita, S., Ogita, H. and Takai, Y. (2011) 'Cooperative role of nectin-nectin and nectin-afadin interactions in formation of nectin-based cell-cell adhesion', *Journal of Biological Chemistry*, 286(42), pp. 36297–36303. doi: 10.1074/jbc.M111.261768.

Kuriu, T., Inoue, A., Bito, H., Sobue, K. and Okabe, S. (2006) 'Differential control of postsynaptic density scaffolds via actin-dependent and -independent mechanisms', *J Neurosci*, 26(29), pp. 7693–7706. doi: 26/29/7693 [pii]\n10.1523/JNEUROSCI.0522-06.2006.

Lagache, T., Meas-Yedid, V. and Olivo-Marin, J.-C. (2013) 'A statistical analysis of spatial colocalization using Ripley's K function', *wordpress*, (1).

Lang, C., Barco, A., Zablow, L., Kandel, E. R., Siegelbaum, S. a and Zakharenko, S. S. (2004) 'Transient expansion of synaptically connected dendritic spines upon induction of hippocampal long-term potentiation.', *Proceedings of the National Academy of Sciences of the United States of America*, 101(47), pp. 16665–16670. doi:

10.1073/pnas.0407581101.

Langley, J. N. (1895) ‘Note on regeneration of prae-ganglionic fibres of the sympathetic.’, *J. Physiol.*, 18.

Leamey, C. A., Glendining, K. a, Kreiman, G., Kang, N.-D., Wang, K. H., Fassler, R., Sawatari, A., Tonegawa, S. and Sur, M. (2008) ‘Differential gene expression between sensory neocortical areas: potential roles for Ten_m3 and Bcl6 in patterning visual and somatosensory pathways.’, *Cerebral cortex (New York, N.Y. : 1991)*, 18(1), pp. 53–66. doi: 10.1093/cercor/bhm031.

Leamey, C. A., Merlin, S., Lattouf, P., Sawatari, A., Zhou, X., Demel, N., Glendining, K. A., Oohashi, T., Sur, M. and Fässler, R. (2007) ‘Ten_m3 regulates eye-specific patterning in the mammalian visual pathway and is required for binocular vision.’, *PLoS biology*. Edited by W. A. Harris. Public Library of Science, 5(9), p. e241. doi: 10.1371/journal.pbio.0050241.

Leamey, C. a and Sawatari, A. (2014) ‘The teneurins: New players in the generation of visual topography.’, *Seminars in cell & developmental biology*. Elsevier Ltd, 35C, pp. 173–179. doi: 10.1016/j.semcdb.2014.08.007.

Lefebvre, J. L., Kostadinov, D., Chen, W. V., Maniatis, T. and Sanes, J. R. (2012) ‘Protocadherins mediate dendritic self-avoidance in the mammalian nervous system’, *Nature*. Nature Publishing Group, 488(7412), pp. 517–521. doi: 10.1038/nature11305.

Lendvai, B., Stern, E. a, Chen, B. and Svoboda, K. (2000) ‘Experience-dependent plasticity of dendritic spines in the developing rat barrel cortex in vivo.’, *Nature*, 404(6780), pp. 876–881. doi: 10.1038/35009107.

Levine, A., Bashan-Ahrend, A., Budai-Hadrian, O., Gartenberg, D., Menasherow, S. and Wides, R. (1994) ‘odd Oz: A novel Drosophila pair rule gene’, *Cell*, 77(4), pp. 587–598. doi: 10.1016/0092-8674(94)90220-8.

Li, H., Bishop, K. M. and O’Leary, D. D. M. (2006) ‘Potential target genes of EMX2 include Odz/Ten-M and other gene families with implications for cortical patterning.’, *Molecular and cellular neurosciences*, 33(2), pp. 136–49. doi: 10.1016/j.mcn.2006.06.012.

Li, X. G., Somogyi, P., Ylinen, A. and Buzsaki, G. (1994) ‘The hippocampal CA3 network: An in vivo intracellular labeling study’, *Journal of Comparative Neurology*, 339(2), pp. 181–208. doi: 10.1002/cne.903390204.

Linhoff, M. W., Lauren, J., Cassidy, R. M., Dobie, F. A., Takahashi, H., Nygaard, H. B., Airaksinen, M. S., Strittmatter, S. M. and Craig, A. M. (2009) ‘An unbiased expression screen for synaptogenic proteins identifies the LRRTM protein family as synaptic organizers.’, *Neuron*. United States, 61(5), pp. 734–749. doi: 10.1016/j.neuron.2009.01.017.

Liu, H., Juo, Z. S., Shim, A. H. R., Focia, P. J., Chen, X., Garcia, K. C. and He, X. (2010) 'Structural Basis of Semaphorin-Plexin Recognition and Viral Mimicry from Sema7A and A39R Complexes with PlexinC1', *Cell*. Elsevier Ltd, 142(5), pp. 749–761. doi: 10.1016/j.cell.2010.07.040.

Liu, X.-B. (2005) 'Stereotyped Axon Pruning via Plexin Signaling Is Associated with Synaptic Complex Elimination in the Hippocampus', *Journal of Neuroscience*, 25(40), pp. 9124–9134. doi: 10.1523/JNEUROSCI.2648-05.2005.

Loew, L. M. and Hell, S. W. (2013) 'Superresolving dendritic spines.', *Biophysical journal*. Biophysical Society, 104(4), pp. 741–3. doi: 10.1016/j.bpj.2013.01.011.

Losonczy, A. and Magee, J. C. (2006) 'Integrative Properties of Radial Oblique Dendrites in Hippocampal CA1 Pyramidal Neurons', *Neuron*, 50(2), pp. 291–307. doi: 10.1016/j.neuron.2006.03.016.

Lovejoy, D. A., Rotzinger, S. and Barsyte-Lovejoy, D. (2009) 'Evolution of complementary peptide systems: teneurin C-terminal-associated peptides and corticotropin-releasing factor superfamilies.', *Annals of the New York Academy of Sciences*, 1163, pp. 215–20. doi: 10.1111/j.1749-6632.2008.03629.x.

Lučić, V., Yang, T., Schweikert, G., Förster, F. and Baumeister, W. (2005) 'Morphological characterization of molecular complexes present in the synaptic cleft', *Structure*, 13(3), pp. 423–434. doi: 10.1016/j.str.2005.02.005.

Lukacs, G. L., Haggie, P., Seksek, O., Lechardeur, D., Freedman, N. and Verkman, A. S. (2000) 'Size-dependent DNA mobility in cytoplasm and nucleus', *Journal of Biological Chemistry*, 275(3), pp. 1625–1629. doi: 10.1074/jbc.275.3.1625.

Majewska, A. and Sur, M. (2003) 'Motility of dendritic spines in visual cortex in vivo: changes during the critical period and effects of visual deprivation.', *Proceedings of the National Academy of Sciences of the United States of America*, 100(26), pp. 16024–16029. doi: 10.1073/pnas.2636949100.

Malenka, R. C. and Nicoll, R. A. (1997) 'Silent synapses speak up', *Neuron*, 19(3), pp. 473–476. doi: 10.1016/S0896-6273(00)80362-1.

Malmgren, H., Sundvall, M., Dahl, N., Gustavson, K. H., Anneren, G., Wadelius, C., Steenbondeson, M. L. and Pettersson, U. (1993) 'Linkage Mapping of a Severe X-Linked Mental-Retardation Syndrome', *American Journal of Human Genetics*, 52, pp. 1046–1052.

Manabe, T., Togashi, H., Uchida, N., Suzuki, S. C., Hayakawa, Y., Yamamoto, M., Yoda, H., Miyakawa, T., Takeichi, M. and Chisaka, O. (2000) 'Loss of Cadherin-11 Adhesion Receptor Enhances Plastic Changes in Hippocampal Synapses and Modifies Behavioral Responses', *Molecular and Cellular Neuroscience*, 15(6), pp. 534–546. doi: 10.1006/mcne.2000.0849.

Mandai, K., Nakanishi, H., Satoh, A., Takahashi, K., Satoh, K., Nishioka, H., Mizoguchi, A. and Takai, Y. (1999) 'Ponsin / SH3P12 : An l-Afadin – and Vinculin-binding Protein Localized at', *The Journal of Cell Biology*, 144(5), pp. 1001–1018.

Margeta, M. A., Shen, K. and Grill, B. (2008) 'Building a synapse: lessons on synaptic specificity and presynaptic assembly from the nematode C. elegans', *Current Opinion in Neurobiology*, 18(1), pp. 69–76. doi: 10.1016/j.conb.2008.04.003.

Mast, J. D., Prakash, S., Chen, P. L. and Clandinin, T. R. (2006) 'The mechanisms and molecules that connect photoreceptor axons to their targets in Drosophila', *Seminars in Cell and Developmental Biology*, 17(1), pp. 42–49. doi: 10.1016/j.semcdb.2005.11.004.

Matsuzaki, M., Ellis-Davies, G. C., Nemoto, T., Miyashita, Y., Iino, M. and Kasai, H. (2001) 'Dendritic spine geometry is critical for AMPA receptor expression in hippocampal CA1 pyramidal neurons.', *Nature neuroscience*, 4(11), pp. 1086–92. doi: 10.1038/nn736.

Matsuzaki, M., Honkura, N., Ellis-Davies, G. C. R. and Kasai, H. (2004) 'Structural basis of long-term potentiation in single dendritic spines', *Nature*, 429(June), pp. 761–766. doi: 10.1038/nature02594.1.

Matus, A. (2000) 'Actin-based plasticity in dendritic spines.', *Science (New York, N.Y.)*. United States, 290(5492), pp. 754–758.

Matus, a, Ackermann, M., Pehling, G., Byers, H. R. and Fujiwara, K. (1982) 'High actin concentrations in brain dendritic spines and postsynaptic densities.', *Proceedings of the National Academy of Sciences of the United States of America*, 79(23), pp. 7590–7594. doi: 10.1073/pnas.79.23.7590.

Mcallister, a K. (2007) 'Dynamic Aspects of Synapse Formation', *Annual review of neuroscience*, 30(530), pp. 425–450. doi: 10.1146/annurev.neuro.29.051605.112830.Dynamic.

McKinney, R. a, Capogna, M., Dürr, R., Gähwiler, B. H. and Thompson, S. M. (1999) 'Miniature synaptic events maintain dendritic spines via AMPA receptor activation.', *Nature neuroscience*, 2(1), pp. 44–49.

McLenachan, S., Sarsero, J. P. and Ioannou, P. a. (2007) 'Flow-cytometric analysis of mouse embryonic stem cell lipofection using small and large DNA constructs', *Genomics*, 89(6), pp. 708–720. doi: 10.1016/j.ygeno.2007.02.006.

Megías, M., Emri, Z. S., Freund, T. F. and Gulyás, A. I. (2001) 'Total number and distribution of inhibitory and excitatory synapses on hippocampal CA1 pyramidal cells', *Neuroscience*, 102(3), pp. 527–540. doi: 10.1016/S0306-4522(00)00496-6.

Mendez, P., De Roo, M., Poglia, L., Klauser, P. and Muller, D. (2010) 'N-cadherin

mediates plasticity-induced long-term spine stabilization', *Journal of Cell Biology*, 189(3), pp. 589–600. doi: 10.1083/jcb.201003007.

Merlin, S., Horng, S., Marotte, L. R., Sur, M., Sawatari, A. and Leamey, C. A. (2013) 'Deletion of Ten-m3 induces the formation of eye dominance domains in mouse visual cortex.', *Cerebral cortex (New York, N.Y. : 1991)*, 23(4), pp. 763–74. doi: 10.1093/cercor/bhs030.

Miles, R., Tóth, K., Gulyás, A. I., Hájos, N. and Freund, T. F. (1996) 'Differences between somatic and dendritic inhibition in the hippocampus', *Neuron*, 16(4), pp. 815–823. doi: 10.1016/S0896-6273(00)80101-4.

Minet, A. D. and Chiquet-Ehrismann, R. (2000) 'Phylogenetic analysis of teneurin genes and comparison to the rearrangement hot spot elements of E. coli', *Gene*, 257(1), pp. 87–97. doi: 10.1016/S0378-1119(00)00388-7.

Minet, A. D., Rubin, B. P., Tucker, R. P., Baumgartner, S. and Chiquet-ehrismann, R. (1999) 'Teneurin-1 , a vertebrate homologue of the Drosophila pair-rule gene Ten-m , is a neuronal protein with a novel type of heparin-binding domain', 2032, pp. 2019–2032.

Missler, M., Südhof, T. C. and Biederer, T. (2012) 'Synaptic cell adhesion.', *Cold Spring Harbor perspectives in biology*, 4(4), p. a005694. doi: 10.1101/cshperspect.a005694.

Missler, M., Zhang, W., Rohlmann, A., Kattenstroth, G., Hammer, R. E., Gottmann, K. and Südhof, T. C. (2003) 'Alpha-neurexins couple Ca2+ channels to synaptic vesicle exocytosis.', *Nature*, 423, pp. 939–948. doi: 10.1038/nature01755.

Mosca, T. J. (2015) 'On the Teneurin track: a new synaptic organization molecule emerges', *Frontiers in Cellular Neuroscience*, 9(May), pp. 1–14. doi: 10.3389/fncel.2015.00204.

Mosca, T. J., Hong, W., Dani, V. S., Favaloro, V. and Luo, L. (2012) 'Trans-synaptic Teneurin signalling in neuromuscular synapse organization and target choice', *Nature*. Nature Publishing Group, 484(7393), pp. 237–241. doi: 10.1038/nature10923.

Mosca, T. J. and Luo, L. (2014) 'Synaptic organization of the Drosophila antennal lobe and its regulation by the Teneurins', *eLife*, 3, pp. 1–29. doi: 10.7554/eLife.03726.

Müller, D. J., Helenius, J., Alsteens, D. and Dufrêne, Y. F. (2009) 'Force probing surfaces of living cells to molecular resolution', *Nature Chemical Biology*, 5(6), pp. 383–390. doi: 10.1038/nchembio.181.

Murase, S., Mosser, E. and Schuman, E. M. (2002) 'Depolarization drives beta-catenin into neuronal spines promoting changes in synaptic structure and function', *Neuron*, 35(1), pp. 91–105. doi: 10.1016/S0896-6273(02)00764-X.

Na, U. V., Eberhorn, N., Cambridge, S. B., Bonhoeffer, T., Nägerl, U. V., Eberhorn, N., Cambridge, S. B. and Bonhoeffer, T. (2004) 'Bidirectional activity-dependent morphological plasticity in hippocampal neurons.', *Neuron*, 44(5), pp. 759–67. doi: 10.1016/j.neuron.2004.11.016.

Naber, P. A., Lopes Da Silva, F. H. and Witter, M. P. (2001) 'Reciprocal connections between the entorhinal cortex and hippocampal fields CA1 and the subiculum are in register with the projections from CA1 to the subiculum', *Hippocampus*, 11(2), pp. 99–104. doi: 10.1002/hipo.1028.

Nägerl, U. V., Willig, K. I., Hein, B., Hell, S. W. and Bonhoeffer, T. (2008) 'Live-cell imaging of dendritic spines by STED microscopy.', *Proceedings of the National Academy of Sciences of the United States of America*, 105(48), pp. 18982–7. doi: 10.1073/pnas.0810028105.

Naisbitt, S., Eunjoon, K., Tu, J. C., Xiao, B., Sala, C., Valtschanoff, J., Weinberg, R. J., Worley, P. F. and Sheng, M. (1999) 'Shank, a novel family of postsynaptic density proteins that binds to the NMDA receptor/PSD-95/GKAP complex and cortactin', *Neuron*, 23(3), pp. 569–582. doi: 10.1016/S0896-6273(00)80809-0.

Nakahira, E. and Yuasa, S. (2005) 'Neuronal generation, migration, and differentiation in the mouse hippocampal primoridium as revealed by enhanced green fluorescent protein gene transfer by means of in utero electroporation', *The Journal of Comparative Neurology*, 483(3), pp. 329–340. doi: 10.1002/cne.20441.

Nakaya, N., Sultana, A., Munasinghe, J., Cheng, A., Mattson, M. P. and Tomarev, S. I. (2013) 'Deletion in the N-terminal half of olfactomedin 1 modifies its interaction with synaptic proteins and causes brain dystrophy and abnormal behavior in mice', *Experimental Neurology*, 250, pp. 205–218. doi: 10.1016/j.expneurol.2013.09.019.

Nava, C., Lamari, F., Héron, D., Mignot, C., Rastetter, a, Keren, B., Cohen, D., Faudet, a, Bouteiller, D., Gilleron, M., Jacquette, a, Whalen, S., Afenjar, a, Périsse, D., Laurent, C., Dupuits, C., Gautier, C., Gérard, M., Huguet, G., Caillet, S., Leheup, B., Leboyer, M., Gillberg, C., Delorme, R., Bourgeron, T., Brice, a and Depienne, C. (2012) 'Analysis of the chromosome X exome in patients with autism spectrum disorders identified novel candidate genes, including TMLHE', *Translational Psychiatry*, 2(10), p. e179. doi: 10.1038/tp.2012.102.

Navarro-Quiroga, I., Chittajallu, R., Gallo, V. and Haydar, T. F. (2007) 'Long-term, selective gene expression in developing and adult hippocampal pyramidal neurons using focal in utero electroporation', *J Neurosci*, 27(19), pp. 5007–5011. doi: 10.1523/JNEUROSCI.0867-07.2007.

Neves, G., Zucker, J., Daly, M. and Chess, A. (2004) 'Stochastic yet biased expression of multiple Dscam splice variants by individual cells.', *Nature genetics*. United States, 36(3), pp. 240–246. doi: 10.1038/ng1299.

Nicholson, D. A., Trana, R., Katz, Y., Kath, W. L., Spruston, N. and Geinisman, Y. (2006) 'Distance-Dependent Differences in Synapse Number and AMPA Receptor Expression in Hippocampal CA1 Pyramidal Neurons', *Neuron*, 50(3), pp. 431–442. doi: 10.1016/j.neuron.2006.03.022.

Nimchinsky, E. a, Sabatini, B. L. and Svoboda, K. (2001) 'Structure and function of dendritic spines', *Annual review of physiology*, 64, pp. 313–353. doi: 10.1146/annurev.physiol.64.081501.160008.

Nunes, S. M., Ferralli, J., Choi, K., Brown-Luedi, M., Minet, A. D. and Chiquet-Ehrismann, R. (2005) 'The intracellular domain of teneurin-1 interacts with MBD1 and CAP/ponsin resulting in subcellular codistribution and translocation to the nuclear matrix.', *Experimental cell research*, 305(1), pp. 122–32. doi: 10.1016/j.yexcr.2004.12.020.

Nuriya, M. and Huganir, R. L. (2006) 'Regulation of AMPA receptor trafficking by N-cadherin', *Journal of Neurochemistry*, 97(3), pp. 652–661. doi: 10.1111/j.1471-4159.2006.03740.x.

Nusser, Z., Lujan, R., Laube, G., Roberts, J. D. B., Molnar, E. and Somogyi, P. (1998) 'Cell type and pathway dependence of synaptic AMPA receptor number and variability in the hippocampus', *Neuron*, 21(3), pp. 545–559. doi: 10.1016/S0896-6273(00)80565-6.

O'Connor, T. P., Cockburn, K., Wang, W., Tapia, L., Currie, E. and Bamji, S. X. (2009) 'Semaphorin 5B mediates synapse elimination in hippocampal neurons', *Neural Development*, 4(1), p. 18. doi: 10.1186/1749-8104-4-18.

O'Sullivan, M. L., Martini, F., von Daake, S., Comoletti, D. and Ghosh, A. (2014) 'LPHN3, a presynaptic adhesion-GPCR implicated in ADHD, regulates the strength of neocortical layer 2/3 synaptic input to layer 5.', *Neural development*, 9(7), pp. 1–11. doi: 10.1186/1749-8104-9-7.

O'Sullivan, M. L., de Wit, J., Savas, J. N., Comoletti, D., Otto-Hitt, S., Yates, J. R. and Ghosh, A. (2012) 'FLRT Proteins Are Endogenous Latrophilin Ligands and Regulate Excitatory Synapse Development', *Neuron*, 73(5), pp. 903–910. doi: 10.1016/j.neuron.2012.01.018.

Okamoto, K.-I., Nagai, T., Miyawaki, A. and Hayashi, Y. (2004) 'Rapid and persistent modulation of actin dynamics regulates postsynaptic reorganization underlying bidirectional plasticity.', *Nature neuroscience*, 7(10), pp. 1104–12. doi: 10.1038/nn1311.

Oohashi, T., Zhou, X. H., Feng, K., Richter, B., Mörgelin, M., Perez, M. T., Su, W. D., Chiquet-Ehrismann, R., Rauch, U. and Fässler, R. (1999) 'Mouse ten-m/Odz is a new family of dimeric type II transmembrane proteins expressed in many tissues.', *The Journal of cell biology*, 145(3), pp. 563–77.

Oray, S., Majewska, A. and Sur, M. (2004) 'Dendritic spine dynamics are regulated by monocular deprivation and extracellular matrix degradation', *Neuron*, 44(6), pp. 1021–1030. doi: 10.1016/j.neuron.2004.12.001.

Passafaro, M., Nakagawa, T., Sala, C. and Sheng, M. (2003) 'Induction of dendritic spines by an extracellular domain of AMPA receptor subunit GluR2.', *Nature*, 424(6949), pp. 677–681. doi: 10.1038/nature01781.

Pasterkamp, R. J. and Giger, R. J. (2009) 'Semaphorin function in neural plasticity and disease', *Current Opinion in Neurobiology*, 19(3), pp. 263–274. doi: 10.1016/j.conb.2009.06.001.

Peng, J., Kim, M. J., Cheng, D., Duong, D. M., Gygi, S. P. and Sheng, M. (2004) 'Semiquantitative Proteomic Analysis of Rat Forebrain Postsynaptic Density Fractions by Mass Spectrometry', *Journal of Biological Chemistry*, 279(20), pp. 21003–21011. doi: 10.1074/jbc.M400103200.

Perestenko, P. V and Henley, J. M. (2003) 'Characterization of the intracellular transport of GluR1 and GluR2 alpha-amino-3-hydroxy-5-methyl-4-isoxazole propionic acid receptor subunits in hippocampal neurons.', *The Journal of biological chemistry*. United States, 278(44), pp. 43525–43532. doi: 10.1074/jbc.M306206200.

Peters, A. and Kaiserman-Abramof, I. R. (1970) 'The small pyramidal neuron of the rat cerebral cortex. The perikaryon, dendrites and spines', *American Journal of Anatomy*, 127(4), pp. 321–355. doi: 10.1002/aja.1001270402.

Pokutta, S. and Weis, W. I. (2007) 'Structure and mechanism of cadherins and catenins in cell-cell contacts.', *Annual review of cell and developmental biology*, 23, pp. 237–61. doi: 10.1146/annurev.cellbio.22.010305.104241.

Popov, V. I., Davies, H. a., Rogachevsky, V. V., Patrushev, I. V., Errington, M. L., Gabbott, P. L. a, Bliss, T. V. P. and Stewart, M. G. (2004) 'Remodelling of synaptic morphology but unchanged synaptic density during late phase long-term potentiation (LTP): A serial section electron micrograph study in the dentate gyrus in the anaesthetised rat', *Neuroscience*, 128(2), pp. 251–262. doi: 10.1016/j.neuroscience.2004.06.029.

Qian, X., Barsyte-Lovejoy, D., Wang, L., Chewpoy, B., Gautam, N., Al Chawaf, A. and Lovejoy, D. A. (2004) 'Cloning and characterization of teneurin C-terminus associated peptide (TCAP)-3 from the hypothalamus of an adult rainbow trout (Oncorhynchus mykiss)', *General and Comparative Endocrinology*, 137(2), pp. 205–216. doi: 10.1016/j.ygcen.2004.02.007.

Ramon y Cajal, S. (1893) 'New findings about the histological structure of the central nervous system', *Archiv fur Anatomie und Physiologie (Anatomie)*, 17, pp. 319–428.

Ribon, V., Herrera, R., Kay, B. K. and Saltiel, A. R. (1998) 'A role for CAP, a novel,

multifunctional Src homology 3 domain- containing protein in formation of actin stress fibers and focal adhesions', *Journal of Biological Chemistry*, 273(7), pp. 4073–4080. doi: 10.1074/jbc.273.7.4073.

Richards, D. a, De Paola, V., Caroni, P., Gähwiler, B. H. and McKinney, R. a (2004) 'AMPA-receptor activation regulates the diffusion of a membrane marker in parallel with dendritic spine motility in the mouse hippocampus.', *The Journal of physiology*, 558(Pt 2), pp. 503–12. doi: 10.1113/jphysiol.2004.062091.

Richter, K., Langnaese, K., Kreutz, M. R., Olias, G., Zhai, R., Scheich, H., Garner, C. C. and Gundelfinger, E. D. (1999) 'Presynaptic cytomatrix protein bassoon is localized at both excitatory and inhibitory synapses of rat brain.', *The Journal of comparative neurology*. United States, 408(3), pp. 437–448.

Rubin, B. P., Tucker, R. P., Brown-Luedi, M., Martin, D. and Chiquet-Ehrismann, R. (2002) 'Teneurin 2 is expressed by the neurons of the thalamofugal visual system in situ and promotes homophilic cell-cell adhesion in vitro.', *Development (Cambridge, England)*, 129(20), pp. 4697–705.

Rubin, B. P., Tucker, R. P., Martin, D. and Chiquet-Ehrismann, R. (1999) 'Teneurins: a novel family of neuronal cell surface proteins in vertebrates, homologous to the Drosophila pair-rule gene product Ten-m.', *Developmental biology*, 216(1), pp. 195–209. doi: 10.1006/dbio.1999.9503.

Sahay, A. (2005) 'Secreted Semaphorins Modulate Synaptic Transmission in the Adult Hippocampus', *Journal of Neuroscience*, 25(14), pp. 3613–3620. doi: 10.1523/JNEUROSCI.5255-04.2005.

Saito, T. (2006) 'In vivo electroporation in the embryonic mouse central nervous system', *Nature Protocols*, 1(3), pp. 1552–1558. doi: 10.1038/nprot.2006.276.

Saito, T. and Nakatsuji, N. (2001) 'Efficient gene transfer into the embryonic mouse brain using in vivo electroporation.', *Developmental biology*, 240(1), pp. 237–46. doi: 10.1006/dbio.2001.0439.

Sala, C. and Segal, M. (2014) 'Dendritic Spines: The Locus of Structural and Functional Plasticity', *Physiological Reviews*, 94(1), pp. 141–188. doi: 10.1152/physrev.00012.2013.

Salinas, P. C. and Price, S. R. (2005) 'Cadherins and catenins in synapse development', *Current Opinion in Neurobiology*, 15(1), pp. 73–80. doi: 10.1016/j.conb.2005.01.001.

San Antonio, A., Liban, K., Ikrar, T., Tsyganovskiy, E. and Xu, X. (2014) 'Distinct physiological and developmental properties of hippocampal CA2 subfield revealed by using anti-Purkinje cell protein 4 (PCP4) immunostaining', *Journal of Comparative Neurology*, 522(6), pp. 1333–1354. doi: 10.1002/cne.23486.

Sanes, J.R. & Yamagata, M. (1999) 'Formation of lamina-specific synaptic connections', *Current opinion in neurobiology*, pp. 79–87.

Sanes, J. R. and Yamagata, M. (2009) 'Many paths to synaptic specificity.', *Annual review of cell and developmental biology*, 25, pp. 161–195. doi: 10.1146/annurev.cellbio.24.110707.175402.

Sara, Y., Biederer, T., Atasoy, D., Chubykin, A., Mozhayeva, M. G., Südhof, T. C. and Kavalali, E. T. (2005) 'Selective Capability of SynCAM and Neuroligin for Functional Synapse Assembly', *Journal of Neuroscience*, 25(1), pp. 260–270. doi: 10.1523/JNEUROSCI.3165-04.2005.

Scheiffele, P., Fan, J., Choih, J., Fetter, R. and Serafini, T. (2000) 'Neuroligin expressed in nonneuronal cells triggers presynaptic development in contacting axons.', *Cell*, 101(6), pp. 657–69. doi: 10.1016/S0092-8674(00)80877-6.

Schikorski, T. and Stevens, C. F. (1997) 'Quantitative ultrastructural analysis of hippocampal excitatory synapses.', *The Journal of neuroscience : the official journal of the Society for Neuroscience*, 17(15), pp. 5858–5867.

Segal, M. (2005) 'Dendritic spines and long-term plasticity', *Nat Rev Neurosci*, 6(4), pp. 277–284. doi: 10.1038/nrn1649.

Shapira, M., Zhai, R. G., Dresbach, T., Bresler, T., Torres, V. I., Gundelfinger, E. D., Ziv, N. E. and Garner, C. C. (2003) 'Unitary assembly of presynaptic active zones from Piccolo-Bassoon transport vesicles', *Neuron*, 38(2), pp. 237–252. doi: 10.1016/S0896-6273(03)00207-1.

Sheetz, M. P. (2001) 'Cell control by membrane-cytoskeleton adhesion.', *Nature reviews. Molecular cell biology*, 2(5), pp. 392–396. doi: 10.1038/35073095.

Shen, K. and Scheiffele, P. (2010) 'Genetics and Cell Biology of Building Specific Synaptic Connectivity', *Annual review of neuroscience*, 33, pp. 473–507. doi: 10.1146/annurev.neuro.051508.135302.

Sheng, M. and Kim, E. (2011) 'The postsynaptic organization of synapses', *Cold Spring Harbor perspectives in biology*, 3, p. a005678. doi: 10.1101/cshperspect.a005678.

Shi, Y., Ikrar, T., Olivas, N. D. and Xu, X. (2014) 'Bidirectional global spontaneous network activity precedes the canonical unidirectional circuit organization in the developing hippocampus', *Journal of Comparative Neurology*, 522(9), pp. 2191–2208. doi: 10.1002/cne.23528.

Shipman, S. L., Schnell, E., Hirai, T., Chen, B.-S., Roche, K. W. and Nicoll, R. A. (2011) 'Functional dependence of neuroligin on a new non-PDZ intracellular domain', *Nature Neuroscience*, 14(6), pp. 718–726. doi: 10.1038/nn.2825.

Siddiqui, T. J. and Craig, A. M. (2011) 'Synaptic organizing complexes', *Current Opinion in Neurobiology*. Elsevier Ltd, 21(1), pp. 132–143. doi: 10.1016/j.conb.2010.08.016.

Silva, J.-P., Lelianova, V. G., Ermolyuk, Y. S., Vysokov, N., Hitchen, P. G., Berninghausen, O., Rahman, M. A., Zangrandi, A., Fidalgo, S., Tonevitsky, A. G., Dell, A., Volynski, K. E. and Ushkaryov, Y. a (2011) 'Latrophilin 1 and its endogenous ligand Lasso/teneurin-2 form a high-affinity transsynaptic receptor pair with signaling capabilities.', *Proceedings of the National Academy of Sciences of the United States of America*, 108(29), pp. 12113–8. doi: 10.1073/pnas.1019434108.

Sklar, P. and Group, P. G. C. B. D. W. (2011) 'Large-scale genome-wide association analysis of bipolar disorder identifies a new susceptibility locus near ODZ4', 43(10). doi: 10.1038/ng.943.

Soler-llavina, G. J., Fuccillo, M. V, Ko, J., Südhof, T. C. and Malenka, R. C. (2011) 'The neurexin ligands, neuroligins and leucine-rich repeat transmembrane proteins, perform confergent and divergent synaptic functions in vivo', *Proceedings of the National Academy of Sciences*, 108(40), pp. 16502–16509. doi: 10.1073/pnas.1114028108/.

Sorra, K. E. and Harris, K. M. (1998) 'Stability in Synapse Number and Size at 2 Hr after Long-Term Potentiation in Hippocampal Area CA1', *The Journal of Neuroscience*, 18(2), pp. 658–671. doi: 0270-6474/98/180658-14$05.00/0.

Sorra, K. E. and Harris, K. M. (2000) 'Overview on the structure, composition, function, development, and plasticity of hippocampal dendritic spines', *Hippocampus*, 10(5), pp. 501–511. doi: 10.1002/1098-1063(2000)10:5<501::AID-HIPO1>3.0.CO;2-T.

Spacek, J. and Harris, K. M. (1997) 'Three-Dimensional Organization of Smooth Endoplasmic Reticulum in Hippocampal CA1 Dendrites and Dendritic Spines of the Immature and Mature Rat', 17(1), pp. 190–203.

Sperry, R. W. (1963) 'Chemoaffinity in the orderly growth of nerve fiber patterns and connections.', *Proceedings of the National Academy of Sciences*, 50, pp. 703–710.

Spruston, N. (2008) 'Pyramidal neurons: dendritic structure and synaptic integration.', *Nature reviews. Neuroscience*, 9(3), pp. 206–221. doi: 10.1038/nrn2286.

Staffend, N. A., Loftus, C. M. and Meisel, R. L. (2011) 'Estradiol reduces dendritic spine density in the ventral striatum of female syrian hamsters', *Brain Structure and Function*, 215(3–4), pp. 187–194. doi: 10.1007/s00429-010-0284-7.

Stanford, W. L., Cohn, J. B., Cordes, S. P. and Lunenfeld, S. (2001) 'Gene-trap mutagenesis: past, present and beyond', 2(October), pp. 756–768.

Star, E. N., Kwiatkowski, D. J. and Murthy, V. N. (2002) ‘Rapid turnover of actin in dendritic spines and its regulation by activity’, *Nat Neurosci*, 5(3), p. 239–46. doi: 10.1038/nn811\nnn811 [pii].

Stoppini, L., Buchs, P. a. and Muller, D. (1991) ‘A simple method for organotypic cultures of nervous tissue’, *Journal of Neuroscience Methods*, 37(2), pp. 173–182. doi: 10.1016/0165-0270(91)90128-M.

Storey, E., Bahlo, M., Fahey, M., Sisson, O., Lueck, C. J. and Gardner, R. J. M. (2009) ‘A new dominantly inherited pure cerebellar ataxia, SCA 30.’, *Journal of neurology, neurosurgery, and psychiatry*, 80(4), pp. 408–11. doi: 10.1136/jnnp.2008.159459.

Südhof, T. C. (2008) ‘Neuroligins and neurexins link synaptic function to cognitive disease.’, *Nature*, 455(7215), pp. 903–11. doi: 10.1038/nature07456.

Sugita, S., Saito, F., Tang, J., Satz, J., Campbell, K. and Südhof, T. C. (2001) ‘A stoichiometric complex of neurexins and dystroglycan in brain’, *Journal of Cell Biology*, 154(2), pp. 435–445. doi: 10.1083/jcb.200105003.

Sun, L. O., Jiang, Z., Rivlin-Etzion, M., Hand, R., Brady, C. M., Matsuoka, R. L., Yau, K.-W., Feller, M. B. and Kolodkin, A. L. (2013) ‘On and off retinal circuit assembly by divergent molecular mechanisms.’, *Science (New York, N.Y.)*. United States, 342(6158), p. 1241974. doi: 10.1126/science.1241974.

Sun, Y., Nguyen, A. Q., Nguyen, J. P., Le, L., Saur, D., Choi, J., Callaway, E. M. and Xu, X. (2014) ‘Cell-type-specific circuit connectivity of hippocampal CA1 revealed through cre-dependent rabies tracing’, *Cell Reports*, 7(1), pp. 269–280. doi: 10.1016/j.celrep.2014.02.030.

Suzuki, N., Numakawa, T., Chou, J., de Vega, S., Mizuniwa, C., Sekimoto, K., Adachi, N., Kunugi, H., Arikawa-Hirasawa, E., Yamada, Y. and Akazawa, C. (2014) ‘Teneurin-4 promotes cellular protrusion formation and neurite outgrowth through focal adhesion kinase signaling.’, *FASEB journal : official publication of the Federation of American Societies for Experimental Biology*, 28(3), pp. 1386–97. doi: 10.1096/fj.13-241034.

Tada, T. and Sheng, M. (2006) ‘Molecular mechanisms of dendritic spine morphogenesis’, *Current Opinion in Neurobiology*, 16(1), pp. 95–101. doi: 10.1016/j.conb.2005.12.001.

Tan, L. A., Xu, K., Vaccarino, F. J., Lovejoy, D. A. and Rotzinger, S. (2009) ‘Teneurin C-terminal associated peptide (TCAP)-1 attenuates corticotropin-releasing factor (CRF)-induced c-Fos expression in the limbic system and modulates anxiety behavior in male Wistar rats’, *Behavioural Brain Research*, 201(1), pp. 198–206. doi: 10.1016/j.bbr.2009.02.013.

Tanaka, H., Shan, W., Phillips, G. R., Arndt, K., Bozdagi, O., Shapiro, L., Huntley, G. W., Benson, D. L. and Colman, D. R. (2000) ‘Molecular modification of N-cadherin in

response to synaptic activity.', *Neuron*, 25, pp. 93–107. doi: 10.1016/S0896-6273(00)80874-0.

Togashi, H., Abe, K., Mizoguchi, A., Takaoka, K., Chisaka, O. and Takeichi, M. (2002) 'Cadherin regulates dendritic spine morphogenesis', *Neuron*, 35(1), pp. 77–89. doi: 10.1016/S0896-6273(02)00748-1.

tom Dieck, S., Sanmartí-Vila, L., Langnaese, K., Richter, K., Kindler, S., Soyke, A., Wex, H., Smalla, K. H., Kämpf, U., Fränzer, J. T., Stumm, M., Garner, C. C. and Gundelfinger, E. D. (1998) 'Bassoon, a novel zinc-finger CAG/glutamine-repeat protein selectively localized at the active zone of presynaptic nerve terminals', *Journal of Cell Biology*, 142(2), pp. 499–509. doi: 10.1083/jcb.142.2.499.

Toni, N., Buchs, P. a, Nikonenko, I., Bron, C. R. and Muller, D. (1999) 'LTP promotes formation of multiple spine synapses between a single axon terminal and a dendrite.', *Nature*, 402(6760), pp. 421–425. doi: 10.1038/46574.

Trachtenberg, J. T., Chen, B. E., Knott, G. W., Feng, G., Sanes, J. R., Welker, E. and Svoboda, K. (2002) 'Long-term in vivo imaging of experience-dependent synaptic plasticity in adult cortex', *Nature*, 420(6917), pp. 788–794. doi: 10.1038/nature01273.

Tran, H., Sawatari, A. and Leamey, C. a (2014) 'The glycoprotein Ten-m3 mediates topography and patterning of thalamostriatal projections from the parafascicular nucleus in mice.', *The European journal of neuroscience*, (July), pp. 1–14. doi: 10.1111/ejn.12767.

Tran, T. S., Rubio, M. E., Clem, R. L., Johnson, D., Case, L., Tessier-Lavigne, M., Huganir, R. L., Ginty, D. D. and Kolodkin, A. L. (2009) 'Secreted semaphorins control spine distribution and morphogenesis in the postnatal CNS.', *Nature*. Nature Publishing Group, 462(7276), pp. 1065–9. doi: 10.1038/nature08628.

Traynelis, S. F., Wollmuth, L. P., McBain, C. J., Menniti, F. S., Vance, K. M., Ogden, K. K., Hansen, K. B., Yuan, H., Myers, S. J. and Dingledine, R. (2010) 'Glutamate receptor ion channels: structure, regulation, and function.', *Pharmacological reviews*. United States, 62(3), pp. 405–496. doi: 10.1124/pr.109.002451.

Trzebiatowska, A., Topf, U., Sauder, U., Drabikowski, K. and Chiquet-Ehrismann, R. (2008) 'Caenorhabditis elegans Teneurin, ten-1, Is Required for Gonadal and Pharyngeal Basement Membrane Integrity and Acts Redundantly with Integrin ina-1 and Dystroglycan dgn-1', *Molecular Biology of the Cell*, 19, pp. 3898–3908. doi: 10.1091/mbc.E08.

Tu, J. C., Xiao, B., Naisbitt, S., Yuan, J. P., Petralia, R. S., Brakeman, P., Doan, A., Aakalu, V. K., Lanahan, A. A., Sheng, M. and Worley, P. F. (1999) 'Coupling of mGluR / Homer and PSD-95 Complexes by the Shank Family of Postsynaptic Density Proteins', 23, pp. 583–592.

Tucker, R. P., Beckmann, J., Leachman, N. T., Schöler, J. and Chiquet-Ehrismann, R. (2012) 'Phylogenetic analysis of the teneurins: conserved features and premetazoan ancestry.', *Molecular biology and evolution*, 29(3), pp. 1019–29. doi: 10.1093/molbev/msr271.

Tucker, R. P., Chiquet-Ehrismann, R., Chevron, M. P., Martin, D., Hall, R. J. and Rubin, B. P. (2001) 'Teneurin-2 is expressed in tissues that regulate limb and somite pattern formation and is induced in vitro and in situ by FGF8', *Developmental Dynamics*, 220(1), pp. 27–39. doi: 10.1002/1097-0177(2000)9999:9999<::AID-DVDY1084>3.0.CO;2-B.

Uchida, N., Honjo, Y., Johnson, K. R., Wheelock, M. J. and Takeichi, M. (1996) 'The catenin/cadherin adhesion system is localized in synaptic junctions bordering transmitter release zones.', *The Journal of cell biology*, 135(3), pp. 767–79.

Ushkaryov, Y. A., Petrenko, A. G., Geppert, M. and Sudhof, T. C. (1992) 'Neurexins: synaptic cell surface proteins related to the alpha-latrotoxin receptor and laminin.', *Science (New York, N.Y.)*. United States, 257(5066), pp. 50–56.

Varoqueaux, F., Aramuni, G., Rawson, R. L., Mohrmann, R., Missler, M., Gottmann, K., Zhang, W., Sudhof, T. C. and Brose, N. (2006) 'Neuroligins determine synapse maturation and function.', *Neuron*. United States, 51(6), pp. 741–754. doi: 10.1016/j.neuron.2006.09.003.

Voronin, L. L. and Cherubini, E. (2004) '"Deaf, mute and whispering" silent synapses: their role in synaptic plasticity.', *The Journal of physiology*, 557, pp. 3–12. doi: 10.1113/jphysiol.2003.058966.

Vysokov, N. V., Silva, J.-P., Lelianova, V. G., Ho, C., Djamgoz, M. B., Tonevitsky, A. G. and Ushkaryov, Y. a. (2016) 'The Mechanism of Regulated Release of Lasso/Teneurin-2', *Frontiers in Molecular Neuroscience*, 9(July), pp. 1–17. doi: 10.3389/fnmol.2016.00059.

Wade, P. A. (2001) 'Methyl CpG-binding proteins and transcriptional repression', *BioEssays*, 23(12), pp. 1131–1137. doi: 10.1002/bies.10008.

Waites, C. L., Craig, A. M. and Garner, C. C. (2005) 'Mechanisms of Vertebrate Synaptogenesis', *Annual Review of Neuroscience*, 28(1), pp. 251–274. doi: 10.1146/annurev.neuro.27.070203.144336.

Wang, L., Rotzinger, S., Al Chawaf, A., Elias, C. F., Baršyte-Lovejoy, D., Qian, X., Wang, N. C., De Cristofaro, A., Belsham, D., Bittencourt, J. C., Vaccarino, F. and Lovejoy, D. A. (2005) 'Teneurin proteins possess a carboxy terminal sequence with neuromodulatory activity', *Molecular Brain Research*, 133(2), pp. 253–265. doi: 10.1016/j.molbrainres.2004.10.019.

Wang, X. Bin and Zhou, Q. (2010) 'Spine remodeling and synaptic modification',

Molecular Neurobiology, 41(1), pp. 29–41. doi: 10.1007/s12035-009-8093-9.

Wang, Y., He, H., Srivastava, N., Vikarunnessa, S., Chen, Y., Jiang, J., Cowan, C. W. and Zhang, X. (2012) 'Plexins Are GTPase-Activating Proteins for Rap and Are Activated by Induced Dimerization', *Science Signaling*, 5(207), p. ra6-ra6. doi: 10.1126/scisignal.2002636.

Washbourne, P., Dityatev, A., Scheiffele, P., Biederer, T., Weiner, J. a, Christopherson, K. S. and El-Husseini, A. (2004) 'Cell adhesion molecules in synapse formation.', *The Journal of neuroscience : the official journal of the Society for Neuroscience*, 24(42), pp. 9244–9. doi: 10.1523/JNEUROSCI.3339-04.2004.

Wegner, A. M., Nebhan, C. A., Hu, L., Majumdar, D., Meier, K. M., Weaver, A. M. and Webb, D. J. (2008) 'N-WASP and the Arp2/3 complex are critical regulators of actin in the development of dendritic spines and synapses', *Journal of Biological Chemistry*, 283(23), pp. 15912–15920. doi: 10.1074/jbc.M801555200.

Williams, M. E., Wilke, S. a, Daggett, A., Davis, E., Otto, S., Ravi, D., Ripley, B., Bushong, E. a, Ellisman, M. H., Klein, G. and Ghosh, A. (2011) 'Cadherin-9 regulates synapse-specific differentiation in the developing hippocampus.', *Neuron*. Elsevier Inc., 71(4), pp. 640–55. doi: 10.1016/j.neuron.2011.06.019.

Williams, M. E., de Wit, J. and Ghosh, A. (2010) 'Molecular mechanisms of synaptic specificity in developing neural circuits.', *Neuron*, 68(1), pp. 9–18. doi: 10.1016/j.neuron.2010.09.007.

de Wit, J. and Ghosh, A. (2014) 'Control of neural circuit formation by leucine-rich repeat proteins.', *Trends in neurosciences*, 37(10), pp. 539–50. doi: 10.1016/j.tins.2014.07.004.

de Wit, J. and Ghosh, A. (2015) 'Specification of synaptic connectivity by cell surface interactions', *Nature Reviews Neuroscience*, 17(1), pp. 22–35. doi: 10.1038/nrn.2015.3.

de Wit, J., O'Sullivan, M., Savas, J., Condomitti, G., Caccese, M., Vennekens, K., Yates, J. and Ghosh, A. (2013) 'Unbiased discovery of Glypican as a receptor for LRRTM4 in regulating excitatory synapse development', *Neuron*, 79(4), pp. 696–711. doi: 10.1016/j.neuron.2013.06.049.

de Wit, J., Sylwestrak, E., O'Sullivan, M. L., Otto, S., Tiglio, K., Savas, J. N., Yates, J. R., Comoletti, D., Taylor, P. and Ghosh, A. (2009) 'LRRTM2 Interacts with Neurexin1 and Regulates Excitatory Synapse Formation', *Neuron*, 64(6), pp. 799–806. doi: 10.1016/j.neuron.2009.12.019.

Xu, X., Sun, Y., Holmes, T. C. and Lopez, A. J. (2016) 'Noncanonical connections between the subiculum and hippocampal CA1', *Journal of Comparative Neurology*, 524(17), pp. 3666–3673. doi: 10.1002/cne.24024.

Yamagata, M. and Sanes, J. R. (2008) 'Dscam and Sidekick proteins direct lamina-specific synaptic connections in vertebrate retina', *Nature*, 451(7177), pp. 465–469. doi: 10.1038/nature06469.

Yamagata, M. and Sanes, J. R. (2012) 'Expanding the Ig superfamily code for laminar specificity in retina: expression and role of contactins.', *The Journal of neuroscience : the official journal of the Society for Neuroscience*, 32(41), pp. 14402–14. doi: 10.1523/JNEUROSCI.3193-12.2012.

Yang, Y., Wang, X.-B., Frerking, M. and Zhou, Q. (2008) 'Spine Expansion and Stabilization Associated with Long- Term Potentiation', *Journal of Neuroscience*, 28(22), pp. 5740–5751. doi: 10.1523/JNEUROSCI.3998-07.2008.

Yankova, M., Hart, S. a and Woolley, C. S. (2001) 'Estrogen increases synaptic connectivity between single presynaptic inputs and multiple postsynaptic CA1 pyramidal cells: a serial electron-microscopic study.', *Proceedings of the National Academy of Sciences of the United States of America*, 98(6), pp. 3525–30. doi: 10.1073/pnas.051624598.

Yogev, S. and Shen, K. (2014) 'Cellular and molecular mechanisms of synaptic specificity', *Annu Rev Cell Dev Biol*, 30, pp. 417–437. doi: 10.1146/annurev-cellbio-100913-012953.

Young, T. R., Bourke, M., Zhou, X., Oohashi, T., Sawatari, A., Fässler, R. and Leamey, C. A. (2013) 'Ten-m2 is required for the generation of binocular visual circuits.', *The Journal of neuroscience : the official journal of the Society for Neuroscience*, 33(30), pp. 12490–509. doi: 10.1523/JNEUROSCI.4708-12.2013.

Yuste, R. and Bonhoeffer, T. (2001) 'Morphological changes in dendritic spines associated with long-term synaptic plasticity.', *Annual Review of Neuroscience*, 24, pp. 1071–89.

Yuste, R. and Bonhoeffer, T. (2004) 'Genesis of dendritic spines: insights from ultrastructural and imaging studies.', *Nature reviews. Neuroscience*, 5(1), pp. 24–34. doi: 10.1038/nrn1300.

Zhang, Y., Cudmore, R. H., Lin, D.-T., Linden, D. J. and Huganir, R. L. (2015) 'Visualization of NMDA receptor–dependent AMPA receptor synaptic plasticity in vivo', *Nature Neuroscience*, 18(3), pp. 402–407. doi: 10.1038/nn.3936.

Zheng, L., Michelson, Y., Freger, V., Avraham, Z., Venken, K. J. T., Bellen, H. J., Justice, M. J. and Wides, R. (2011) 'Drosophila Ten-m and filamin affect motor neuron growth cone guidance.', *PloS one*, 6(8), p. e22956. doi: 10.1371/journal.pone.0022956.

Zhong, S., Salomoni, P. and Pandolfi, P. P. (2000) 'The transcriptional role of PML and the nuclear body.', *Nature cell biology*, 2(May), pp. E85–E90. doi: 10.1038/35010583.

Zhou, Q., Homma, K. J. and Poo, M. M. (2004) 'Shrinkage of dendritic spines associated with long-term depression of hippocampal synapses', *Neuron*, 44(5), pp. 749–757. doi: 10.1016/j.neuron.2004.11.011.

Zhou, X. H., Brandau, O., Feng, K., Oohashi, T., Ninomiya, Y., Rauch, U. and Fässler, R. (2003) 'The murine Ten-m/Odz genes show distinct but overlapping expression patterns during development and in adult brain', *Gene Expression Patterns*, 3(4), pp. 397–405. doi: 10.1016/S1567-133X(03)00087-5.

Zimmer, J. and Gähwiler, B. H. (1984) 'Cellular and connective organization of slice cultures of the rat hippocampus and fascia dentata.', *The Journal of comparative neurology*, 228(3), pp. 432–446. doi: 10.1002/cne.902280310.

Zipursky, S. L. and Sanes, J. R. (2010) 'Chemoaffinity revisited: dscams, protocadherins, and neural circuit assembly.', *Cell*, 143(3), pp. 343–53. doi: 10.1016/j.cell.2010.10.009.

Zuber, B., Nikonenko, I., Klauser, P., Muller, D. and Dubochet, J. (2005) 'The mammalian central nervous synaptic cleft contains a high density of periodically organized complexes.', *Proceedings of the National Academy of Sciences of the United States of America*, 102(52), pp. 19192–7. doi: 10.1073/pnas.0509527102.

van Zundert, B., Alvarez, F. J., Tapia, J. C., Yeh, H. H., Diaz, E. and Aguayo, L. G. (2004) 'Developmental-dependent action of microtubule depolymerization on the function and structure of synaptic glycine receptor clusters in spinal neurons', *J Neurophysiol*, 91(2), pp. 1036–1049. doi: 10.1152/jn.00364.2003\r00364.2003 [pii].

Zuo, Y., Yang, G., Kwon, E. and Gan, W.-B. (2005) 'Long-term sensory deprivation prevents dendritic spine loss in primary somatosensory cortex', *Nature*, 436(7048), pp. 261–265. doi: 10.1038/nature03715.

Appendix

Appendix 1

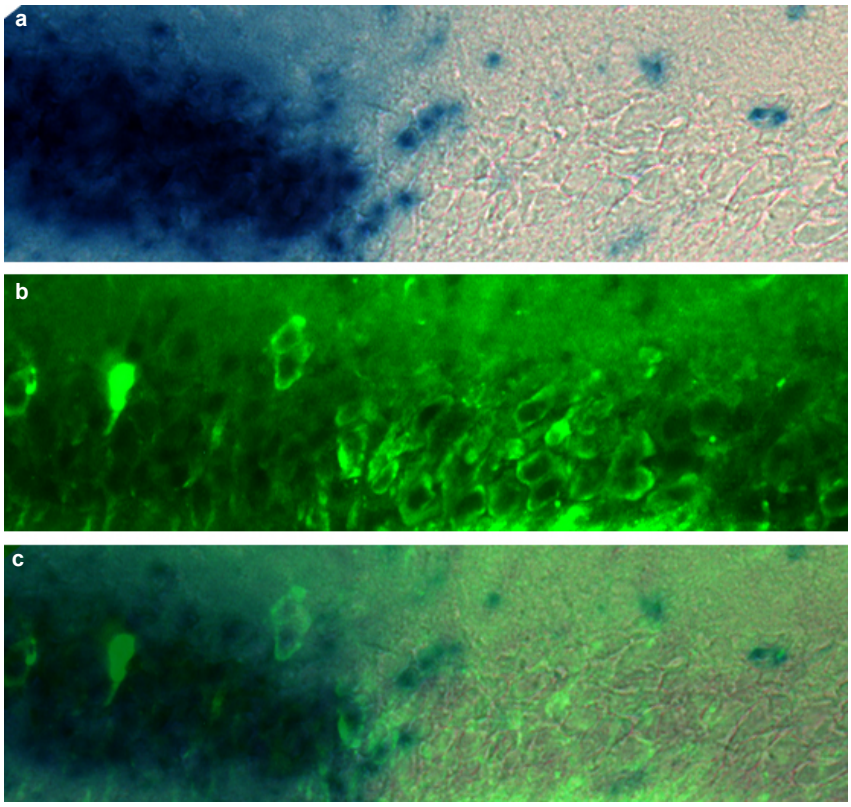

Tenm3 expression in CA1. **a**. **β**-galactosidase expression in a Tenm3-/- mutant mouse evidenced by X-gal staining. **β**-galactosidase reports the expression of endogenous Tenm3 in this gene trap mutant line. **b.** PCP4 staining for the identification of the CA1/CA2 boundary. **c.** Merge of X-gal and PCP4 staining shows that X-gal expression is restricted to CA1. These images were obtained by Alexander Hinton (Hindges Lab).

Appendix 2

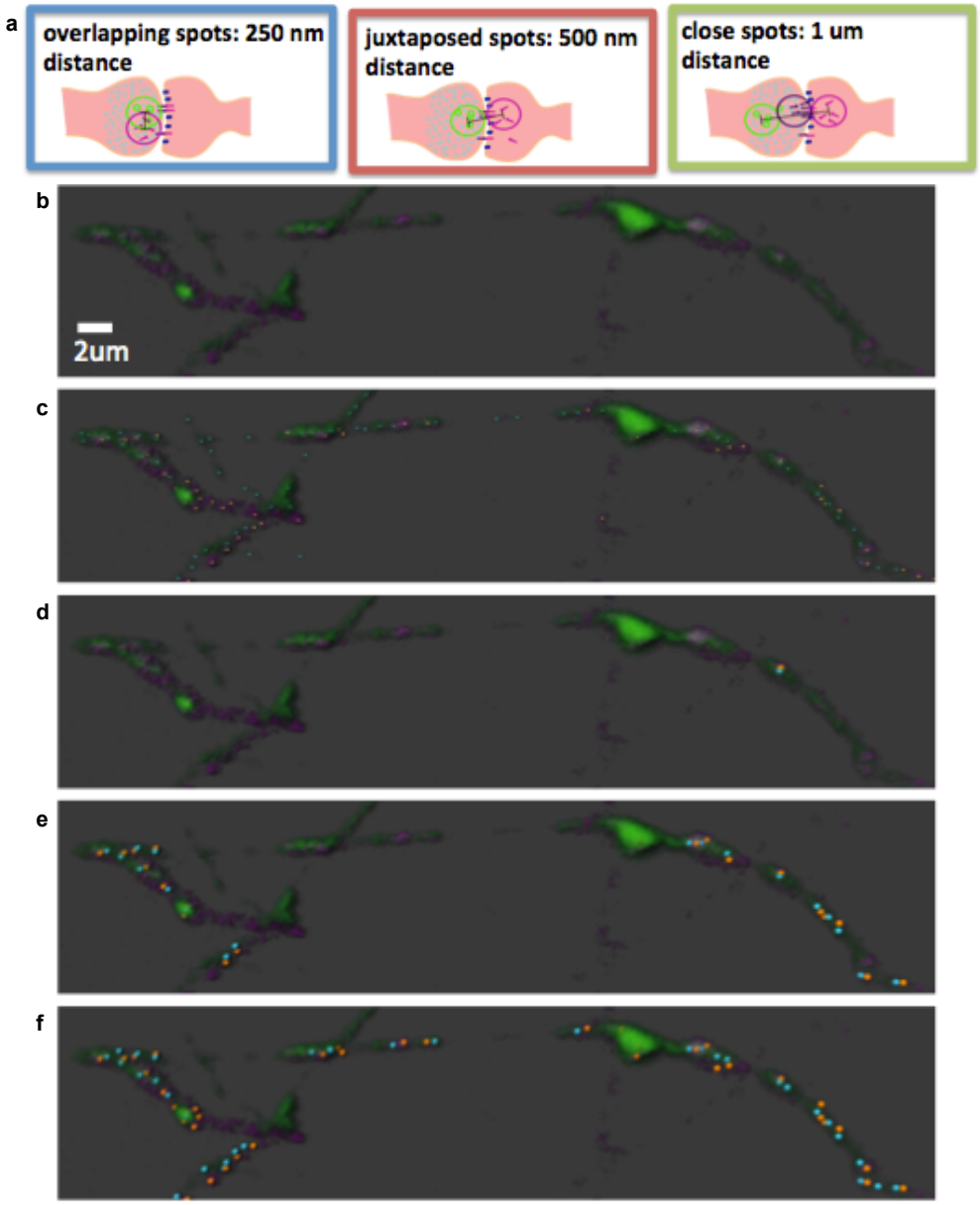

Colocalisation analysis with spot detection function in Imaris. In Imaris, the spot detection function allows the automated detection of protein puncta, which are represented as spots with a defined diameter. Many different spots diameter were assayed. In this example, spots were set to a diameter of 500nm. After spot detection, the colocalisation analysis in Imaris automatically detects spots, whose centres are within a predefined distance of each other. In this example, three distances were chosen: 250nm, 500nm and 1µm. **a.** Schematic representation of the different settings for colocalisation analysis. Spots were considered to *overlap* if there centres were separated by a distance of <250nm, *juxtapposed* when the distance was < 500nm and *close* when the distance was < 1µm. **b**. Example of Tenm1 (magenta) and synapsin (green) localisation in a hippocampal neuron. **c.** Representation of automatically detected Teneurin (orange) and Synapsin (cyan) spots (only the centre of the spot, not the full diameter is represented). **d.** Overlapping Tenm1 and Synapsin spots. **e.** Juxtaposed Tenm1 and Synapsin spots. **f.** Close Tenm1 and Synapsin spots.

Appendix 3

Genomic region and validated and predicted transcripts of mouse Tenm3, displayed in NCBI's sequence viewer. This annotation can be accessed via https://www.ncbi.nlm.nih.gov/gene/23965

The red line represents the insertion site of the gene trap vector in intron 3-4 and which leads to the disruption of all Tenm3 transcripts.

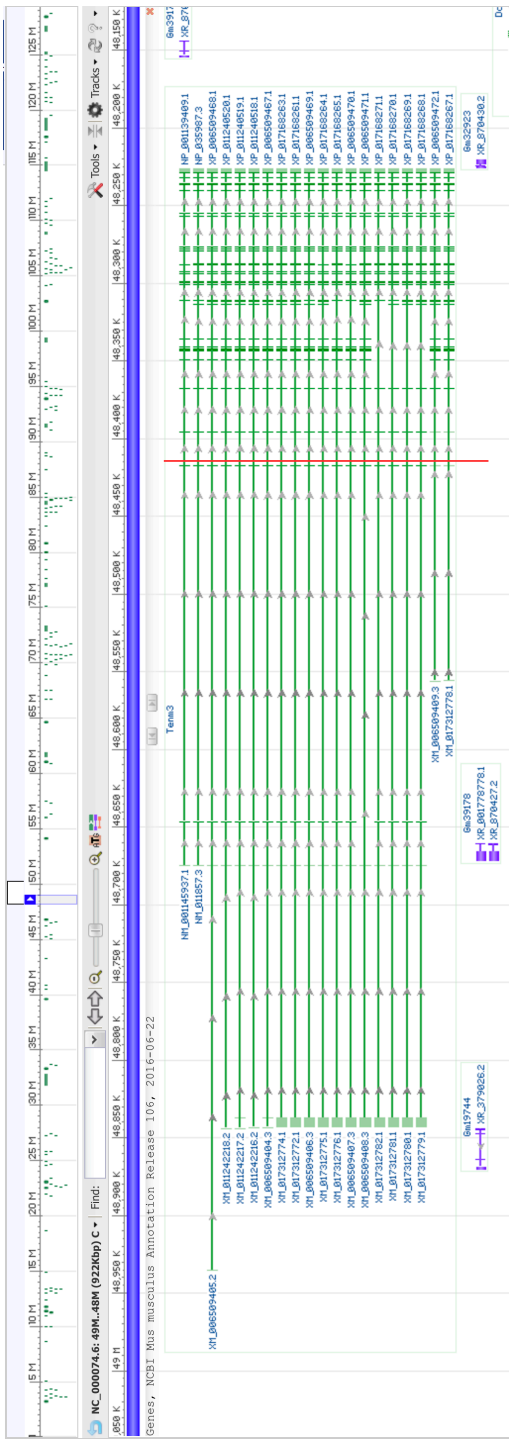

Appendix 4

Gene annotation of Tenm3 from Ensembl. This annotation can be accessed via http://www.ensembl.org/Mus_musculus/Gene/Summary?g=ENSMUSG00000031561;r=8:48227682-48843951

The red line represents the insertion site of the gene trap vector in intron 3-4 and which leads to the disruption of seven Tenm3 transcripts.

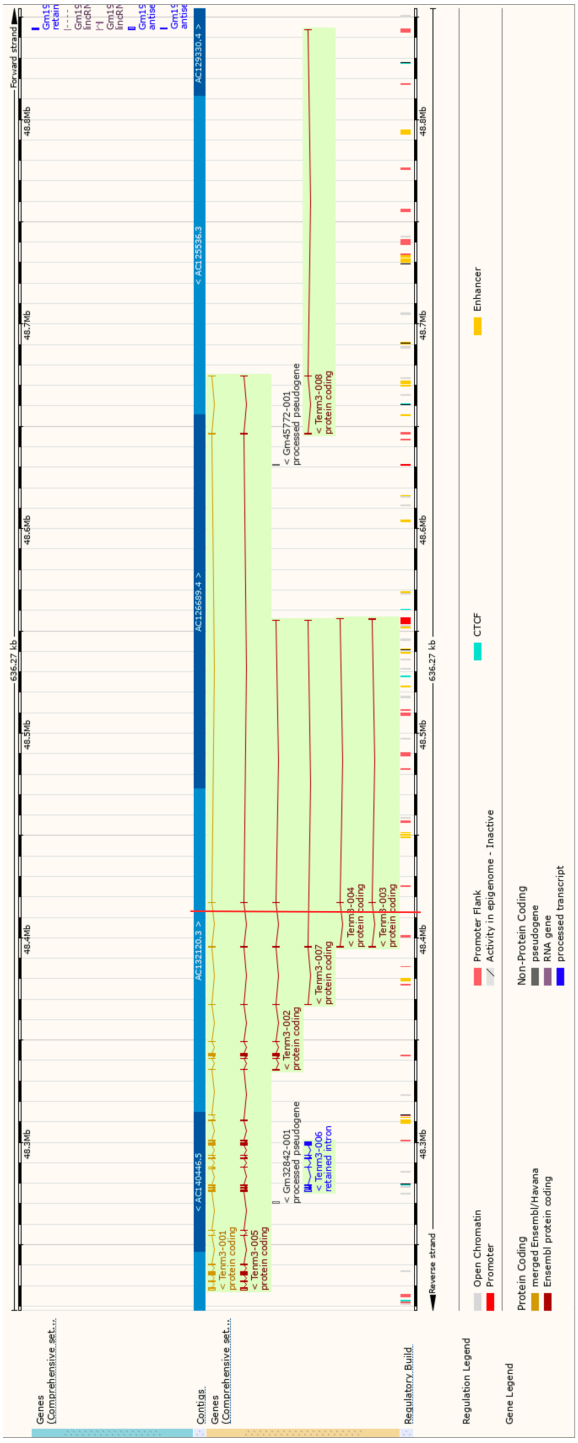

Appendix 5

Quantification of spine density and spine type proportions in Tenm3 mutants and control littermates.

Data	n	Gaussian	D'Agostino & Pearson p value	Mean	SD	SEM	Stats test	ANOVA/ Kruskal-Wallis p value	significance		comparison	significance	Multiple comparison adjusted p value
Apical dendrite mean diameter Figure 5.6													
Tenm3-/-	28	no	0.0023	0.69	0.21	0.04	KW	0.0056	**		Tenm3-/- vs Tenm3+/-	ns	0.0831
Tenm3+/-	55	yes	0.2078	0.79	0.19	0.03	KW	0.0056	**		Tenm3-/- vs Tenm3+/+	ns	> 0.9999
Tenm3+/+	39	yes	0.1168	0.67	0.18	0.03	KW	0.0056	**		Tenm3+/- vs Tenm3+/+	**	0.0079
Basal dendrite mean diameter Figure 5.6													
Tenm3-/-	49	yes	0.1512	0.63	0.10	0.01	KW	0.0016	**		Tenm3-/- vs Tenm3+/-	**	0.0017
Tenm3+/-	61	no	0.6535	0.74	0.17	0.02	KW	0.0016	**		Tenm3-/- vs Tenm3+/+	ns	0.7949
Tenm3+/+	50	no	0.016	0.66	0.16	0.02	KW	0.0016	**		Tenm3+/- vs Tenm3+/+	*	0.0448
Apical dendrite straightness Figure 5.6													
Tenm3-/-	28	no	0.0424	0.92	0.04	0.01	KW	0.5854	ns		Tenm3-/- vs Tenm3+/-	ns	0.903
Tenm3+/-	55	yes	0.1196	0.93	0.04	0.01	KW	0.5854	ns		Tenm3-/- vs Tenm3+/+	ns	> 0.9999
Tenm3+/+	39	yes	0.3388	0.93	0.04	0.01	KW	0.5854	ns		Tenm3+/- vs Tenm3+/+	ns	> 0.9999
Basal dendrite straightness Figure 5.6													
Tenm3-/-	49	no	0.0003	0.93	0.05	0.01	KW	0.5729	ns		Tenm3-/- vs Tenm3+/-	ns	> 0.9999
Tenm3+/-	61	no	<0.0001	0.94	0.06	0.01	KW	0.5729	ns		Tenm3-/- vs Tenm3+/+	ns	> 0.9999
Tenm3+/+	50	no	<0.0001	0.92	0.09	0.01	KW	0.5729	ns		Tenm3+/- vs Tenm3+/+	ns	0.9696
Apical spine density Figure 5.8													
Tenm3-/-	28	yes	0.2102	35.91	9.00	1.70	KW	< 0.0001	****		Tenm3-/- vs Tenm3+/-	ns	> 0.9999
Tenm3+/-	55	yes	0.1146	37.99	15.08	2.03	KW	< 0.0001	****		Tenm3-/- vs Tenm3+/+	***	0.0005
Tenm3+/+	39	no	0.0009	25.83	12.70	2.03	KW	< 0.0001	****		Tenm3+/- vs Tenm3+/+	****	< 0.0001
Basal spine density Figure 5.7													
Tenm3-/-	49	yes	0.7411	30.79	9.96	1.42	KW	0.0320	*		Tenm3-/- vs Tenm3+/-	ns	0.9186
Tenm3+/-	61	yes	0.0863	30.99	10.70	1.37	KW	0.0320	*		Tenm3-/- vs Tenm3+/+	*	0.0163
Tenm3+/+	50	no	0.0063	26.39	9.04	1.28	KW	0.0320	*		Tenm3+/- vs Tenm3+/+	*	0.0299
Apical stubby spine density Figure 5.10													
Tenm3-/-	28	yes	0.4589	17.57	6.57	1.24	KW	0.0248	*		Tenm3-/- vs Tenm3+/-	ns	0.4555
Tenm3+/-	55	no	0.0103	15.09	4.73	0.62	KW	0.0248	*		Tenm3-/- vs Tenm3+/+	*	0.0209
Tenm3+/+	39	yes	0.3339	13.39	5.44	0.86	KW	0.0248	*		Tenm3+/- vs Tenm3+/+	ns	0.3094
Basal stubby spine density Figure 5.9													
Tenm3-/-	49	no	0.0261	14.46	5.64	0.80	KW	0.1126	ns		Tenm3-/- vs Tenm3+/-	ns	0.1765
Tenm3+/-	61	no	<0.0001	12.67	7.30	0.90	KW	0.1126	ns		Tenm3-/- vs Tenm3+/+	ns	> 0.9999
Tenm3+/+	50	yes	0.1006	13.32	5.13	0.72	KW	0.1126	ns		Tenm3+/- vs Tenm3+/+	ns	0.3133
Apical sessile spine density Figure 5.10													
Tenm3-/-	28	no	0.0016	15.42	6.03	1.14	KW	< 0.0001	****		Tenm3-/- vs Tenm3+/-	ns	> 0.9999
Tenm3+/-	55	yes	0.0604	19.78	12.73	1.72	KW	< 0.0001	****		Tenm3-/- vs Tenm3+/+	**	0.0033
Tenm3+/+	39	no	<0.0001	10.59	9.38	1.52	KW	< 0.0001	****		Tenm3+/- vs Tenm3+/+	****	< 0.0001
Basal sessile spine density Figure 5.9													
Tenm3-/-	49	no	0.0496	13.32	7.85	1.12	KW	0.0173	*		Tenm3-/- vs Tenm3+/-	ns	> 0.9999
Tenm3+/-	61	no	0.0434	14.86	9.36	1.21	KW	0.0173	*		Tenm3-/- vs Tenm3+/+	ns	0.1329
Tenm3+/+	50	no	0.0295	9.86	5.05	0.72	KW	0.0173	*		Tenm3+/- vs Tenm3+/+	*	0.0167
Apical thin spine density Figure 5.10													
Tenm3-/-	28	yes	0.6298	2.11	1.33	0.25	KW	0.0021	**		Tenm3-/- vs Tenm3+/-	ns	0.7447
Tenm3+/-	55	no	<0.0001	2.89	2.28	0.30	KW	0.0021	**		Tenm3-/- vs Tenm3+/+	ns	0.195
Tenm3+/+	39	no	<0.0001	1.54	1.47	0.23	KW	0.0021	**		Tenm3+/- vs Tenm3+/+	**	0.0014
Basal thin spine density Figure 5.9													
Tenm3-/-	49	no	0.0004	1.96	1.55	0.22	KW	0.3883	ns		Tenm3-/- vs Tenm3+/-	ns	> 0.9999
Tenm3+/-	61	no	<0.0001	2.37	2.53	0.31	KW	0.3883	ns		Tenm3-/- vs Tenm3+/+	ns	> 0.9999
Tenm3+/+	50	no	0.0072	1.72	1.19	0.17	KW	0.3883	ns		Tenm3+/- vs Tenm3+/+	ns	0.5316
Apical mushroom spine density Figure 5.10													
Tenm3-/-	28	yes	0.1508	0.94	0.73	0.15	KW	< 0.0001	****		Tenm3-/- vs Tenm3+/-	ns	0.6989
Tenm3+/-	55	no	<0.0001	1.13	0.98	0.14	KW	< 0.0001	****		Tenm3-/- vs Tenm3+/+	*	0.0247
Tenm3+/+	39	no	<0.0001	0.47	0.40	0.08	KW	< 0.0001	****		Tenm3+/- vs Tenm3+/+	****	< 0.0001
Basal mushroom spine density Figure 5.9													
Tenm3-/-	49	no	<0.0001	1.17	0.95	0.15	KW	< 0.0001	****		Tenm3-/- vs Tenm3+/-	ns	> 0.9999
Tenm3+/-	61	no	<0.0001	1.09	1.06	0.15	KW	< 0.0001	****		Tenm3-/- vs Tenm3+/+	****	< 0.0001
Tenm3+/+	50	no	<0.0001	0.48	0.38	0.07	KW	< 0.0001	****		Tenm3+/- vs Tenm3+/+	****	< 0.0001
Apical stubby spine proportion (%) Figure 5.11													
Tenm3-/-	28	yes	0.3638	48.79	13.54	2.56	ANOVA	<0.0001	****		Tenm3-/- vs Tenm3+/-	ns	0.1898
Tenm3+/-	55	yes	0.944	42.14	15.46	2.03	ANOVA	<0.0001	****		Tenm3-/- vs Tenm3+/+	*	0.0425
Tenm3+/+	39	yes	0.9949	58.70	19.52	3.09	ANOVA	<0.0001	****		Tenm3+/- vs Tenm3+/+	****	<0.0001
Basal stubby spine proportion (%) Figure 5.11													
Tenm3-/-	49	Yes	0.7737	50.77	18.02	2.55	KW	0.0061	**		Tenm3-/- vs Tenm3+/-	ns	0.1488
Tenm3+/-	61	No	0.0126	45.22	20.98	2.62	KW	0.0061	**		Tenm3-/- vs Tenm3+/+	ns	0.8176
Tenm3+/+	50	No	0.0321	54.01	16.94	2.40	KW	0.0061	**		Tenm3+/- vs Tenm3+/+	**	0.0053
Apical sessile spine proportion (%) Figure 5.11													
Tenm3-/-	28	Yes	0.9068	43.34	12.65	2.39	ANOVA	<0.0001	****		Tenm3-/- vs Tenm3+/-	ns	0.2621
Tenm3+/-	55	Yes	0.4084	49.30	16.34	2.15	ANOVA	<0.0001	****		Tenm3-/- vs Tenm3+/+	ns	0.0534
Tenm3+/+	39	Yes	0.7726	33.82	18.87	2.98	ANOVA	<0.0001	****		Tenm3+/- vs Tenm3+/+	****	<0.0001
Basal sessile spine proportion (%) Figure 5.11													
Tenm3-/-	49	Yes	0.8051	40.46	15.88	2.25	KW	0.0775	ns		Tenm3-/- vs Tenm3+/-	ns	0.7304

Data	n	Gaussian	D'Agostino & Pearson p value	Mean	SD	SEM	Stats test	ANOVA/ Kruskal-Wallis p value	significance		comparison	significance	Multiple comparison adjusted p value
Tenm3+/-	61	Yes	0.8536	44.80	20.81	2.60	KW	0.0775	ns		Tenm3-/- vs Tenm3+/+	ns	0.9153
Tenm3+/+	50	No	<0.0001	38.18	16.43	2.32	KW	0.0775	ns		Tenm3+/- vs Tenm3+/+	ns	0.0728
Apical thin spine proportion (%) Figure 5.11													
Tenm3-/-	28	Yes	0.8215	5.77	3.33	0.63	KW	0.3371	ns		Tenm3-/- vs Tenm3+/-	ns	>0.9999
Tenm3+/-	55	Yes	0.4652	6.13	3.92	0.51	KW	0.3371	ns		Tenm3-/- vs Tenm3+/+	ns	>0.9999
Tenm3+/+	39	No	<0.0001	6.35	7.47	1.18	KW	0.3371	ns		Tenm3+/- vs Tenm3+/+	ns	0.423
Basal thin spine proportion (%) Figure 5.11													
Tenm3-/-	49	Yes	0.3096	6.14	4.04	0.57	ANOVA	0.4083	ns		Tenm3-/- vs Tenm3+/-	ns	0.374
Tenm3+/-	61	yes	0.1043	7.25	4.89	0.61	ANOVA	0.4083	ns		Tenm3-/- vs Tenm3+/+	ns	0.758
Tenm3+/+	50	Yes	0.4031	6.76	3.97	0.56	ANOVA	0.4083	ns		Tenm3+/- vs Tenm3+/+	ns	0.8257
Apical mushroom spine proportion (%) Figure 5.11													
Tenm3-/-	28	Yes	0.1231	2.10	1.82	0.34	KW	0.0015	**		Tenm3-/- vs Tenm3+/-	ns	>0.9999
Tenm3+/-	55	No	0.0008	2.43	2.08	0.27	KW	0.0015	**		Tenm3-/- vs Tenm3+/+	ns	0.0554
Tenm3+/+	39	No	<0.0001	1.14	1.31	0.21	KW	0.0015	**		Tenm3+/- vs Tenm3+/+	**	0.0012
Basal mushroom spine proportion (%) Figure 5.11													
Tenm3-/-	49	No	0.0061	2.62	2.49	0.35	KW	0.0004	****		Tenm3-/- vs Tenm3+/-	ns	>0.9999
Tenm3+/-	61	No	<0.0001	2.73	3.04	0.38	KW	0.0004	****		Tenm3-/- vs Tenm3+/+	**	0.002
Tenm3+/+	50	No	<0.0001	1.04	1.24	0.18	KW	0.0004	****		Tenm3+/- vs Tenm3+/+	**	0.0013

Appendix 6

Cumulative distribution of the number of publications per year with description of in utero electroporation targeting somatosensory cortex, hippocampus or visual cortex. Reproduced from dal Maschio *et al.*, 2012. The number of publications on IUE targeting the hippocampus and visual cortex stand in stark contrast to the exponential increase in publications targeting the somatosensory cortex. This indicates technical difficulties in electroporating certain brain areas using IUE.

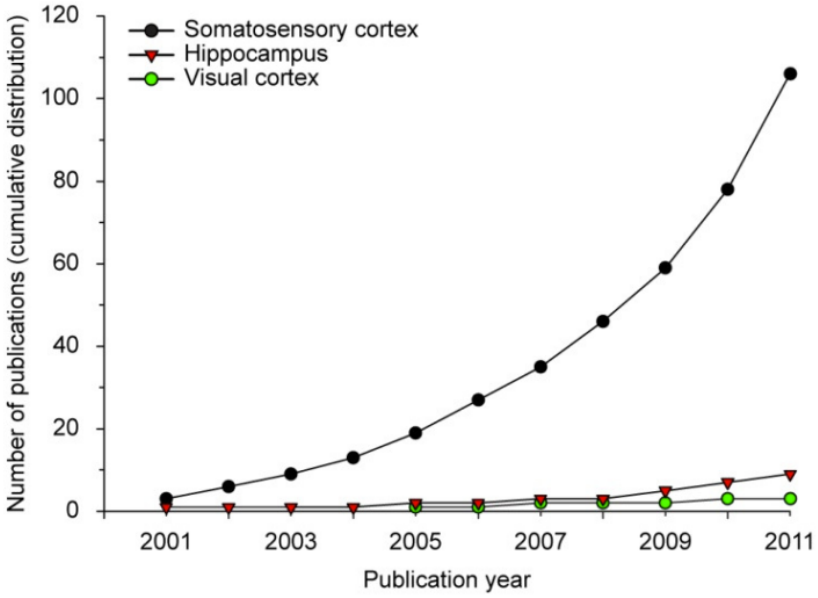

Appendix 7

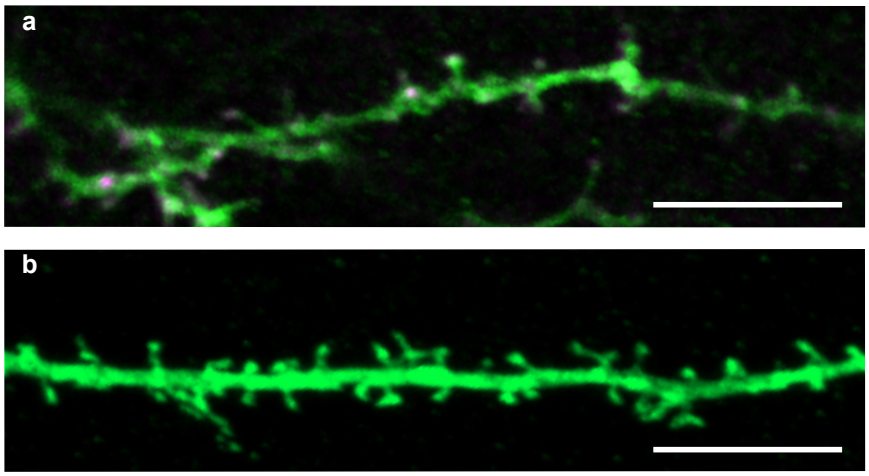

Dendritic spine density following overexpression of Tenm3. **a.** Basal dendritic segment of a CA1 neuron cotransfected with Tenm3 (magenta) and GFP (green). **b.** Basal dendritic segment of control CA1 neuron transfected with GFP only. Both images are of CA1 neurons in organotypic hippocampal slices. The scale bar is 10μm. Note the increased levels of background fluorescence due to staining with anti-Myc in **a.** compared to **b.** Higher background levels rendered the identification of spines more challenging, however it does appear as though there is a decrease in synaptic spine density in Tenm3-overexpressing neurons. This observation was not quantified.